

Electronic Theses and Dissertations, 2004-2019

2017

An Assessment of Trace Elements Distribution in Teeth Utilizing a Sample Group from Postclassic Lamanai: The Application of LA-ICP-MS in Bioarchaeology and Forensics

Michelle Hawkins
University of Central Florida

 Part of the [Archaeological Anthropology Commons](#), and the [Biological and Physical Anthropology Commons](#)

Find similar works at: <https://stars.library.ucf.edu/etd>
University of Central Florida Libraries <http://library.ucf.edu>

This Masters Thesis (Open Access) is brought to you for free and open access by STARS. It has been accepted for inclusion in Electronic Theses and Dissertations, 2004-2019 by an authorized administrator of STARS. For more information, please contact STARS@ucf.edu.

STARS Citation

Hawkins, Michelle, "An Assessment of Trace Elements Distribution in Teeth Utilizing a Sample Group from Postclassic Lamanai: The Application of LA-ICP-MS in Bioarchaeology and Forensics" (2017). *Electronic Theses and Dissertations, 2004-2019*. 5738.
<https://stars.library.ucf.edu/etd/5738>

AN ASSESSMENT OF TRACE ELEMENTS DISTRIBUTION IN TEETH UTILIZING
A SAMPLE GROUP FROM POSTCLASSIC LAMANAI: THE APPLICATION OF
LA-ICP-MS IN BIOARCHAEOLOGY AND FORENSICS

by

MICHELLE MARIE HAWKINS
B.S. Southeastern Louisiana University, 2012

A thesis submitted in partial fulfillment of the requirements
for the degree of Master of Arts
in the Department of Anthropology
in the College of Sciences
at University of Central Florida
Orlando, Florida

Fall Term
2017

© 2017 Michelle M. Hawkins

ABSTRACT

Trace element analysis of skeletal remains and teeth is a common research technique in biological and forensic anthropology. In particular, LA-ICP-MS has become a widely-accepted tool for analyzing and mapping the distribution of trace elements in teeth. Investigation into the relative spectral intensities and spatial distribution of thirteen trace isotopes (^{13}C , ^{24}Mg , ^{27}Al , ^{31}P , ^{44}Ca , ^{47}Ti , ^{52}Cr , ^{55}Mn , ^{56}Fe , ^{66}Zn , ^{88}Sr , ^{138}Ba , ^{208}Pb) within teeth was undertaken using LA-ICP-MS. The total archaeological sample of teeth (N=26) was comprised of four tooth types (UCI, ULI, UPM1, and UPM2) and 18 individuals from a Postclassic Lamanai site. In preparation for analysis, teeth sectioned down the center using a low-speed saw. Maps were created using the laser ablation system and MATLAB® software. The frequency of each isotope detected at low, moderate, and high intensities at each of the six defined tooth locations was calculated. The inner dentine and the outer root border were the two areas that most commonly exhibited the highest intensities of isotopes. Detection of major structural isotopes (^{44}Ca and ^{31}P) was similar in both spatial locations and relative intensity across all teeth. In comparison, detection of more minor isotopes, while similar in spatial locations across all teeth, varied in relative intensity per individual sample. The frequency that each isotope was detected also varied by tooth type. These findings demonstrate the disparities between different types of dental tissue for retaining trace elements and serve to illuminate possible sources of external exposure and internal bioavailability influencing interindividual variation within the Lamanai sample population. Variation in isotope frequency based on tooth type may be due to developmental properties and/or changes in

diet during early life. Ultimately, teeth act as storehouses of trace elements, and maps of isotopic distribution in teeth help reveal how individuals are influenced by both biological processes and cultural activities.

ACKNOWLEDGMENTS

While graduate school has certainly been challenging, there are several individuals whom I would like to thank for making this thesis project a possibility and my experience as a graduate student an incredibly rewarding one. Firstly, I would like to thank my advisor and mentor, Dr. John Schultz, who has always been a great voice of wisdom and guidance throughout this journey and who has given me many amazing opportunities to practice being a forensic anthropologist. I would also like to thank the two other members of my committee. Thank you to Dr. Lana Williams for always speaking the truth with graciousness and for helping a former biologist learn to think more like a bioarchaeologist. And thank you to Dr. Matthieu Baudalet for dedicating your time, resources, and insight to this project.

I would also like to thank the National Center for Forensic Science for supplying the space and equipment necessary to conduct this research. In particular, I am grateful to Dr. Mauro Labrador for his patient instruction and invaluable assistance with the data collection and mapping processes.

I also thank the faculty, staff members, and my fellow colleagues of the Department of Anthropology at UCF, who have all helped equip and develop me as an anthropologist through coursework and discussion. I am especially grateful for Allison Apland and Emily Herrington, whose friendship and support these past two years have meant the world to me. Finally, thank you to my parents, family, and friends near and far, for your continual prayers and unconditional love. I could never have done this without you. And I could not have finished the race without Him.

TABLE OF CONTENTS

LIST OF FIGURES	xiii
LIST OF TABLES	xvii
LIST OF ACRONYMS/ABBREVIATIONS	xxi
CHAPTER ONE: INTRODUCTION	1
CHAPTER TWO: LITERATURE REVIEW	6
Human Dentition	6
Tooth Anatomy	6
Tooth Development	9
Tooth Chemical Composition.....	11
Properties of Enamel	11
Properties of Dentine	12
Properties of Pulp Cavity	12
Trace Elements in Teeth	12
Bioavailability of Trace Elements	16
Bioavailability of Mg	17
Bioavailability of Al.....	17
Bioavailability of P	18
Bioavailability of Ca	18

Bioavailability of Ti.....	19
Bioavailability of Cr.....	19
Bioavailability of Mn	19
Bioavailability of Fe.....	20
Bioavailability of Zn	20
Bioavailability of Sr	21
Bioavailability of Ba	21
Bioavailability of Pb	22
LA-ICP-MS and Trace Element Analysis	22
Trace Element Analysis in Dentistry	26
Trace Element Analysis in Bioarchaeology	26
Trace Element Analysis in Forensics.....	28
Archaeological Background.....	31
Lamanai Location and Setting.....	31
N10/1 Structure.....	33
N10/2 Structure.....	33
N10/4 Structure.....	33
Postclassic Maya Diet	34
CHAPTER THREE: MATERIALS AND METHODS	35

Materials.....	35
Teeth Preparation.....	39
Cleaning	39
Embedding.....	39
Sectioning.....	41
LA-ICP-MS Elemental Analysis	43
Individual Tooth Sample Parameters.....	45
Mapping	49
Statistical Analysis	54
CHAPTER FOUR: RESULTS	55
Overall Detection and Distribution of Isotopes.....	55
Total Frequency of Detection.....	57
Frequency of Detection by Tooth Location	58
Enamel Surface	58
Inner Enamel.....	59
Inner Dentine	59
EDJ.....	61
DPB.....	61
Outer Root Border.....	62

Detection of Isotopes by Tooth Type	63
Upper Central Incisor.....	63
Carbon (¹³ C)	66
Magnesium (²⁴ Mg).....	66
Aluminum (²⁷ Al).....	67
Phosphorus (³¹ P).....	67
Calcium (⁴⁴ Ca)	68
Titanium (⁴⁷ Ti).....	68
Chromium (⁵² Cr).....	69
Manganese (⁵⁵ Mn)	69
Iron (⁵⁶ Fe).....	70
Zinc (⁶⁶ Zn).....	70
Strontium (⁸⁸ Sr)	71
Barium (¹³⁸ Ba)	71
Lead (²⁰⁸ Pb)	72
Upper Lateral Incisor	72
Carbon (¹³ C)	74
Magnesium (²⁴ Mg).....	75
Aluminum (²⁷ Al).....	75

Phosphorus (^{31}P)	76
Calcium (^{44}Ca)	76
Titanium (^{47}Ti)	77
Chromium (^{52}Cr)	77
Manganese (^{55}Mn)	77
Iron (^{56}Fe)	78
Zinc (^{66}Zn)	78
Strontium (^{88}Sr)	78
Barium (^{138}Ba)	79
Lead (^{208}Pb)	79
Upper First Premolar	80
Carbon (^{13}C)	82
Magnesium (^{24}Mg)	83
Aluminum (^{27}Al)	83
Phosphorus (^{31}P)	83
Calcium (^{44}Ca)	84
Titanium (^{47}Ti)	84
Chromium (^{52}Cr)	85
Manganese (^{55}Mn)	85

Iron (^{56}Fe)	86
Zinc (^{66}Zn)	86
Strontium (^{88}Sr)	87
Barium (^{138}Ba)	87
Lead (^{208}Pb)	88
Upper Second Premolar	88
Carbon (^{13}C)	88
Magnesium (^{24}Mg).....	91
Aluminum (^{27}Al).....	91
Phosphorus (^{31}P).....	92
Calcium (^{44}Ca).....	92
Titanium (^{47}Ti).....	93
Chromium (^{52}Cr).....	93
Manganese (^{55}Mn)	94
Iron (^{56}Fe)	94
Zinc (^{66}Zn)	95
Strontium (^{88}Sr)	95
Barium (^{138}Ba)	96
Lead (^{208}Pb)	96

Frequency of Detection by Tooth Type	97
CHAPTER FIVE: DISCUSSION	103
Relative Intensities of Isotopes by Tooth Location	103
Relative Intensities Compared to Other Studies	109
Relative Intensities of Isotopes by Tooth Type	116
Relative Intensities Through Time	120
Intentionally Modified Teeth.....	127
Unique Tooth.....	128
Exposure and Bioavailability	130
CHAPTER SIX: CONCLUSION	138
Implications	138
Limitations	140
Future Directions	140
APPENDIX A: ELEMENTAL MAPS	145
APPENDIX B: RELATIVE INTENSITY DATA TABLES	189
LIST OF REFERENCES	216

LIST OF FIGURES

Figure 1: Cross-sectional anatomy of a single tooth and its respective features.	8
Figure 2: A simplified schematic of the overall process of LA-ICP-MS.	24
Figure 3: Map of Belize depicting location of Lamanai archaeological site. Map created using Google Maps.	32
Figure 4: Two test teeth embedded in hardened epoxy resin (left) and the silicone mold previously containing resin with teeth (right).	40
Figure 5: Example of a tooth embedded in resin attached to the support arm that has already been sliced down the center in the lingual-labial direction.	42
Figure 6: Example of a tooth slice from tooth sample N10-4/33 UPM2.	42
Figure 7: Example of stitching from tooth sample N10-4/10 UPM2. Note the boxes representing separate frames that have been stitched together.	47
Figure 8: Photo of pattern settings on Screen 1, including pattern icon and raster pattern (circled), pattern dimensions (bottom two arrows), and number of lines (top arrow).	48
Figure 9: Screenshot of overall coding parameters for creating maps.	50
Figure 10: Screenshot of coding for figure (1) map, which is the figure for ¹³ Carbon.	51
Figure 11: Example of relative spectral intensity scale with assigned qualitative values. ...	53
Figure 12: Average detection of intensities of each isotope across entire tooth sample for all teeth (N=26). N/A=0, Low=1, Mod=2, and High=3.	58
Figure 13: Frequency of isotopes detected at low, moderate, and high intensities at enamel surface for all teeth (N=26).	59

Figure 14: Frequency of isotopes detected at low, moderate, and high intensities at inner enamel for all teeth (N=26).....	60
Figure 15: Frequency of isotopes detected at low, moderate, and high intensities at inner dentine for all teeth (N=26).....	60
Figure 16: Frequency of isotopes detected at low, moderate, and high intensities at EDJ for all teeth (N=26).....	61
Figure 17: Frequency of isotopes detected at low, moderate, and high intensities at DPB for all teeth (N=26).....	62
Figure 18: Frequency of isotopes detected at low, moderate, and high intensities at outer root border for all teeth (N=26).....	63
Figure 19: Example of low or poor isotopic detection (^{55}Mn) within UCI sample.	65
Figure 20: Example of moderate isotopic detection (^{13}C) within UCI sample.	65
Figure 21: Example of high or good isotopic detection (^{44}Ca) within UCI sample.	65
Figure 22: Example of low or poor isotopic detection (^{55}Mn) within ULI sample.....	73
Figure 23: Example of moderate isotopic detection (^{66}Zn) within ULI sample.	74
Figure 24: Example of high or good isotopic detection (^{31}P) within ULI sample.	74
Figure 25: Example of low or poor isotopic detection (^{47}Ti) within UPM1 sample.....	80
Figure 26: Example of moderate isotopic detection (^{24}Mg) within UPM1 sample.....	80
Figure 27: Example of high or good isotopic detection (^{88}Sr) within UPM1 sample.	82
Figure 28: Example of low or poor isotopic detection (^{208}Pb) within UPM2 sample.....	89
Figure 29: Example of moderate isotopic detection (^{24}Mg) within UPM2 sample.....	89
Figure 30: Example of high or good isotopic detection (^{44}Ca) within UPM2 sample.	91

Figure 31: Total frequency of all isotopes detected based on tooth type. This included detection of low, moderate, and high intensities per tooth.	97
Figure 32: Frequency of all isotopes detected based on tooth type. This included detection of only moderate and high intensities per tooth.	100
Figure 33: Frequencies of isotopes detected at only moderate and high intensities at each tooth location across entire sample (N=26).	104
Figure 34: Example of ^{138}Ba distribution in the tooth (sample N10-4/46C Large UCI), showing highest relative intensity occurring at the inner dentine and outer root border.	105
Figure 35: Example of ^{66}Zn distribution in the tooth (sample N10-4/46C Large UCI), showing highest relative intensity occurring at the enamel surface.	106
Figure 36: Average isotope intensities varying across time in individual N10-1/02.	121
Figure 37: Average isotope intensities varying across time in individual N10-2/20A or B.	121
Figure 38: Average isotope intensities varying across time in individual N10-2/21.	122
Figure 39: Average isotope intensities varying across time in individual N10-2/21A. ..	123
Figure 40: Average isotope intensities varying across time in individual N10-2/42B....	124
Figure 41: Average isotope intensities varying across time in individual N10-4/01.	124
Figure 42: Average isotope intensities varying across time in individual N10-4/43.	125
Figure 43: Average isotope intensities varying across time in individual N10-4/46C Large.	126
Figure 44: Frequency of detection of moderate and high intensities between all teeth associated with modified UCI (n=10) and all teeth associated with unmodified UCI (n=16).	128

Figure 45: Example of ^{27}Al distribution in tooth sample N10-2/21 UCI. Note the high intensity of ^{27}Al outlining where the jade piece is located. 129

Figure 46: Possible external sources of exposure and internal bioavailability influencing the presence of certain trace elements in teeth..... 131

LIST OF TABLES

Table 1: Summary of previous relevant literature comparing trace element concentrations found at inner enamel and inner dentine.....	15
Table 2: Summary of sample group (N=26) from a Postclassic Lamanai site, containing teeth deemed suitable for this research and belonging to one of the four assigned groups. Data for individual determined sex obtained from Williams and White (2006) and White (1986).....	36
Table 3: Four groups (G1 through G4) of 18 individuals sorted based on tooth availability.....	39
Table 4: Operating parameters and conditions for elemental analysis by LA-ICP-MS....	44
Table 5: Abbreviations of selected elements for mapping, their corresponding isotopes, and the minimum number selected for the map spectral intensity.	52
Table 6: Summary of isotopes detected at moderate and high intensities only at each defined tooth location.	56
Table 7: Average frequencies of isotopes detected and highest detection locations across all teeth (N=26). This included moderate and high intensities only.	57
Table 8: Summary of relative signal intensities of isotopes observed at each defined tooth location in the UCI sample (n=12).	64
Table 9: Summary of relative signal intensities of isotopes observed at each tooth location in the ULI sample (n=1).	73
Table 10: Summary of relative signal intensities of isotopes observed at each tooth location in the UPM1 sample (n=6).	81

Table 11: Summary of relative signal intensities of isotopes observed at each tooth location in the UPM2 sample (n=7).	90
Table 12: Calculated averages and ranges of frequencies of isotope detection across all teeth (N=26) for low, moderate, and high intensities.	99
Table 13: Calculated averages and ranges of frequencies of isotope detection across all teeth (N=26) for moderate and high intensities only.	102
Table 14: Summary of tooth types exhibiting the highest frequency of detection of each isotope. Bold text indicates that this tooth type had the highest frequency of detection of the isotope in both categories	102
Table 15: Biologically essential isotope intensities by tooth location and tooth type in comparison with previous studies.	110
Table 16: Nonessential isotope intensities by tooth location and tooth type in comparison with previous studies.	111
Table 17: Summary of observed isotope intensities in relationship to one another and possible bioavailability and exposure influences.	132
Table 18: Relative intensities of isotopes observed in N10-1/02 UCI at each tooth location.....	190
Table 19: Relative intensities of isotopes observed in N10-1/02 UPM1 at each tooth location.....	191
Table 20: Relative intensities of isotopes observed in N10-2/20A or B UCI at each tooth location.....	192
Table 21: Relative intensities of isotopes observed in N10-2/20A or B UPM2 at each tooth location.....	193

Table 22: Relative intensities of isotopes observed in N10-2/21 UCI at each tooth location.....	194
Table 23: Relative intensities of isotopes observed in N10-2/21 UPM2 at each tooth location.....	195
Table 24: Relative intensities of isotopes observed in N10-2/21A UCI at each tooth location.....	196
Table 25: Relative intensities of isotopes observed in N10-2/21A UPM1 at each tooth location.....	197
Table 26: Relative intensities of isotopes observed in N10-2/42B UCI at each tooth location.....	198
Table 27: Relative intensities of isotopes observed in N10-2/42B UPM1 at each tooth location.....	199
Table 28: Relative intensities of isotopes observed in N10-4/01 UCI at each tooth location.....	200
Table 29: Relative intensities of isotopes observed in N10-4/01 UPM2 at each tooth location.....	201
Table 30: Relative intensities of isotopes observed in N10-4/43 UCI at each tooth location.....	202
Table 31: Relative intensities of isotopes observed in N10-4/43 UPM1 at each tooth location.....	203
Table 32: Relative intensities of isotopes observed in N10-4/4C Large UCI at each tooth location.....	204

Table 33: Relative intensities of isotopes observed in N10-4/4C Large UPM2 at each tooth location.....	205
Table 34: Relative intensities of isotopes observed in N10-4/19 UCI at each tooth location.....	206
Table 35: Relative intensities of isotopes observed in N10-4/31 UCI at each tooth location.....	207
Table 36: Relative intensities of isotopes observed in N10-4/35 UCI at each tooth location.....	208
Table 37: Relative intensities of isotopes observed in N10-4/46A UCI at each tooth location.....	209
Table 38: Relative intensities of isotopes observed in N10-2/49 ULI at each tooth location.....	210
Table 39: Relative intensities of isotopes observed in N10-2/22 UPM1 at each tooth location.....	211
Table 40: Relative intensities of isotopes observed in N10-2/40 UPM1 at each tooth location.....	212
Table 41: Relative intensities of isotopes observed in N10-4/10 UPM2 at each tooth location.....	213
Table 42: Relative intensities of isotopes observed in N10-4/33 UPM2 at each tooth location.....	214
Table 43: Relative intensities of isotopes observed in N10-4/46C Small UPM2 at each tooth location.....	215

LIST OF ACRONYMS/ABBREVIATIONS

Al	Aluminum
Ar	Argon
Ba	Barium
C	Carbon
Ca	Calcium
Cd	Cadmium
Cr	Chromium
Cu	Copper
DPB	Dentine-Pulp Border
EDJ	Enamel-Dentine Junction
F	Fluorine
Fe	Iron
He	Helium
Hg	Mercury
Kr	Krypton
LA-ICP-MS	Laser Ablation Inductively-Coupled Plasma Mass Spectrometry
Mg	Magnesium
Mn	Manganese
Na	Sodium
NCFS	National Center for Forensic Science
Ni	Nickel

NIST	National Institute of Standards
P	Phosphorus
Pb	Lead
Rb	Rubidium
S	Sulfur
Sr	Strontium
Sn	Tin
Ti	Titanium
UCF	University of Central Florida
UCI	Upper Central Incisor
ULI	Upper Lateral Incisor
UPM1	Upper First Premolar
UPM2	Upper Second Premolar
V	Vanadium
Zn	Zinc

CHAPTER ONE: INTRODUCTION

Under the discipline of biological anthropology, bioarchaeology is considered to be the study of ancient and historic human remains with a biocultural perspective and often involves the holistic interpretation of life history, culture, and environmental factors influencing a group of individuals from the past (Martin et al., 2013). In comparison, forensic anthropology is focused on the analysis of human remains from the very recent past and within a legal context, often for the purpose of interpreting manner of death or making an identification (Christensen et al., 2014). In both of these fields of study, it has become an increasingly common research practice to conduct trace element analyses of skeletal materials, including bone and teeth.

Trace element analysis has multiple applications and can illuminate various avenues within biological anthropological research, including diet and dietary changes (Dolphin et al., 2005; Kohn et al., 2013; Reynard and Balter, 2014), residence and mobility patterns (Cucina et al., 2011; Galiová et al., 2013), environmental influence on health (Asaduzzaman et al., 2017; Budd et al., 1998; Shepherd et al., 2012), impact of diagenesis on buried remains (Kohn et al., 1999; Martin et al., 2007), discrimination between ages and sexes (Castro et al., 2010; Kumagai et al., 2012), and manner of death (Fortes et al., 2015). Due to their highly calcified tissue and higher level of preservation than bone (Kang et al., 2004), teeth have become a valuable biological material utilized within a variety of chemical analyses, such as trace element analyses and stable isotope analyses (Balasse, 2002; Humphrey, 2016).

In recent years, there has been a steady technological advancement in the fields of analytical chemistry and forensic science, from highly destructive to minimally destructive or completely nondestructive techniques, with the purpose of increasing measurement precision and preserving the sample. One such minimally destructive technology that has emerged as a prominent instrument in analytical chemistry is Laser Ablation Inductively Coupled Plasma Mass Spectrometry (LA-ICP-MS), as this instrument allows for more precise measuring, via a highly sensitive ICP-MS, and requires minimal sample preparation (Pozebon et al., 2017). Thus, LA-ICP-MS yields maximum information with minimal destruction of the material itself (Speakman and Neff, 2005). LA-ICP-MS has become a widely-accepted method for studying minor trace elements present within solid samples in geochemistry, environmental sciences, archaeology, biology, and medicine (Fricker and Günther, 2016; Limbeck et al., 2015; Pozebon et al., 2017). In particular, LA-ICP-MS has been demonstrated useful as a method for chemically characterizing and mapping the distribution of minor trace elements present in human tissues and in particular teeth (Arora et al., 2011; Becker et al., 2010; Farrell et al., 2013; Hare et al., 2011; Guede et al., 2017; Pozebon et al., 2017).

In both clinical and bioarchaeological literature, trace elements found in teeth have been reported to be a valuable indicator of the natural bioavailability and environmental history of exposure to individuals and populations (Brown et al., 2004; Dolphin and Goodman, 2009; Shepherd et al., 2012). Research has demonstrated that teeth serve as a useful source of measuring and comparing the abundance of biologically essential trace elements needed to sustain homeostasis and overall health, such as calcium (Ca), magnesium (Mg), and zinc (Zn), with the abundance of functionally nonessential

trace elements, such aluminum (Al), barium (Ba), and lead (Pb) (Brown et al., 2004; Fraga, 2005; Reynard and Balter, 2014). Thus, it is expected that essential trace elements would appear more abundantly within teeth relative to nonessential trace elements. Circumstances in which nonessential trace elements exhibit an unnaturally high presence in teeth could indicate a prolonged exposure or toxicity (Fraga, 2005; Humphrey, 2016). Fluctuations in levels of certain trace elements can also illuminate bioavailability and potentially inform the biocultural influences on diet and health of a past population (Dolphin and Goodman, 2009).

It is important to note, however, that trace element presence and abundance can vary naturally, based on tooth location in the oral cavity and location within the tooth structure itself (Arnold and Gaengler, 2007; Fischer et al., 2009). Teeth are heterogenous in structure, comprised of an exposed, highly mineralized tissue called enamel and an internal, less mineralized tissue called dentine. Since the processes which allow for elemental absorption and retention differ between enamel and dentine (Antoine and Hillson, 2016; Tang et al., 2016), it is also expected that trace element detection and distribution will vary based on whether the elements are found in the enamel or the dentine.

Previous research examining elemental distribution in human teeth has largely focused on deciduous (juvenile) teeth (Arora et al., 2011; Austin et al., 2013; de Souza Guerra et al., 2010; Dolphin and Goodman, 2009; Farrell et al., 2013; Hare et al., 2011). However, currently, there are limited studies examining elemental distribution in permanent (adult) teeth (Arruda-Neto et al., 2010; Fortes et al., 2015; Guede et al., 2017; Tacail et al., 2017). In addition, while many studies in bioarchaeology, chemistry, and

dentistry have produced two-dimensional distribution maps of various trace elements in teeth, these studies are often limited by one or multiple factors, including small sample size (Duval et al., 2011; Galiová et al., 2013; Hare et al., 2011), limited number of trace elements selected (i.e. less than ten elements) (Arora et al., 2011; Austin et al., 2013; Hare et al., 2011), and/or producing maps that are focused on just one tooth location, rather than mapping an entire cross-sectional area of the tooth (Tacail et al., 2017; Willmes et al., 2016).

The purpose of this study is to evaluate the relative spectral intensity and spatial distribution of selected trace elements within an archaeological sample of human teeth. This study will also involve an assessment of the viability in utilizing human teeth as a source material when conducting a trace elemental analysis using LA-ICP-MS. The levels of certain trace elements detected within the harder and softer teeth tissues may infer environmental influences on tooth physiology. Data obtained from this research may serve to illuminate some biocultural context of a sample group of individuals recovered from the archaeological site of Lamanai, Belize (Maya Postclassic 900-1521 CE) (Dormon, 2007), as well as generate information on how LA-ICP-MS may best be applied in future anthropological study. The research questions addressed in this study include the following:

- (1) What are the relative spectral intensities of selected trace elements/isotopes at defined locations in the tooth?
- (2) How do the relative spectral intensities and distributions of selected trace elements/isotopes compare and contrast across four tooth types?

- (3) How does the presence and distribution of essential and nonessential trace elements/isotopes inform the bioavailability and environmental exposure of a Maya sample group from Postclassic Lamanai?

The following chapters will assess these research questions. A sample group of 26 adult teeth (N=26), comprised of 18 individuals, will be analyzed using LA-ICP-MS as a method. It is important to note that only eight of the individuals (10 teeth) acquired for this study came from individuals in which the biological sex was known; thus, it was not possible to use this demographic indicator as a means of further analysis in this study.

Chapter Two provides a review of relevant literature pertaining to tooth anatomy, development, and chemistry; trace elements found in teeth; the bioavailability of trace elements examined; previous research applying LA-ICP-MS trace element analysis on teeth; and a brief archaeological background of the sample group being used in this study. Chapter Three outlines the materials and methods used in this study. Chapter Four presents the results of LA-ICP-MS mapping for each trace element/isotope examined at each tooth location for each tooth type, as well as relative frequencies of each trace element/isotope detected. Chapter Five examines the similarities and differences of the trace element/isotope data according to defined tooth locations, tooth types, and essentiality and nonessentiality. Chapter Five also includes a discussion regarding how patterns of these trace elements/isotopes identified in the teeth may inform environmental exposure and bioavailability of a Postclassic Lamanai sample population. Finally, Chapter Six summarizes the analysis and provides a conclusion, as well implications, limitations, and future research directions of this study.

CHAPTER TWO: LITERATURE REVIEW

With increasing precision and calibration improvements in chemical and analytical methods, trace element analysis has become more prominent, and sample materials have expanded to include various biological tissues, such as teeth. Since this research relies on human teeth as the sample material, it is important to understand the basic biological components and chemical properties of human teeth and the method being used to conduct the trace element analysis. This chapter includes four major sections: an overview of relevant human tooth anatomy, physiology, and chemical properties; an examination of trace elements commonly found in teeth and their bioavailability; a review of current LA-ICP-MS applications, with a focus on trace elemental analysis of teeth in the disciplines of dentistry, bioarchaeology, and forensics; and a brief archaeological background of the sample group being used in this study.

Human Dentition

Tooth Anatomy

In humans, a complete, permanent or adult dentition is comprised of 32 heterodont (or morphologically mixed) teeth in total, with a dental formula of 2123/2123 (Harris, 2016). As indicated by this dental formula, there are four different classes of teeth contained within each quadrant of an adult human: two incisors, one canine, two premolars, and three molars. Each tooth type is comprised of a different structure and serves a different function in the breakdown of food to provide nutrition (Harris, 2016).

For example, incisors are the most anterior of the teeth, are generally flat and spatula-shaped, and are used for guiding and gnawing food particles into finer pieces that may more easily fit into the mouth and lead to further chewing by other teeth (Hillson, 2005; White and Folkens, 2005). There are two types of incisors, central incisors and lateral incisors. Central incisors are larger than lateral incisors and are the most “central” (most anterior) of all the teeth. Canines are also located in the anterior portion of the mouth but are also distal in relation to the incisors; canines bear a distinct tusk-like shape, used for gripping and puncturing food (Hillson, 2005; White and Folkens, 2005). Premolars are considered cheek teeth, as they are located towards the cheek (distal to the canines, mesial to the molars). There are two types of premolars, first (or third) premolars and second (or fourth) premolars. Premolars are round in shape and usually have two cusps. First premolars have a larger buccal cusp compared to a smaller lingual cusp, whereas second premolars have cusps of fairly equal size (White and Folkens, 2005). And upper first premolars often have two roots, whereas upper second premolars have one root (White and Folkens, 2005). Due to their shape, premolars allow for slicing food into smaller particles to aid in the digestive process (Hillson, 2005). Finally, molars are the largest of human teeth and bear a more square-like shape and contain multiple cusps. Molars are used for crushing or grinding purposes in food digestion (Hillson, 2005).

A single tooth is also a heterogenous structure within itself, containing multiple structures. Each tooth is comprised of two distinct structures: the crown and the root(s) (see Figure 1). The crown of the tooth is covered by a layer of a hard, primarily mineralized and avascular substance called enamel, while the internal core of the tooth is composed primarily of dentine, and living, avascular and mineralized tissue, though not

as mineralized as enamel (White and Folkens, 2005). Within the inner dentine at the center of the tooth lies the pulp cavity, which supplies blood and nutrients necessary for sustaining the living dentine tissue during life (Legge and Hardin, 2016). Covering the outside of the tooth root is the cementum, which is a layer of calcified tissue that helps anchor the roots via the periodontal ligament (White and Folkens, 2005; Tang et al., 2016). Finally, the distal end of the tooth root contains an opening called the apical foramen, or apex, to funnel blood vessels and nerves into the pulp cavity (White and Folkens, 2005). The boundary between the enamel and the dentine is referred to as the enamel-dentine junction (EDJ). In addition, the boundary between the inner dentine and the pulp cavity is referred to as the dentine-pulp border (DPB).

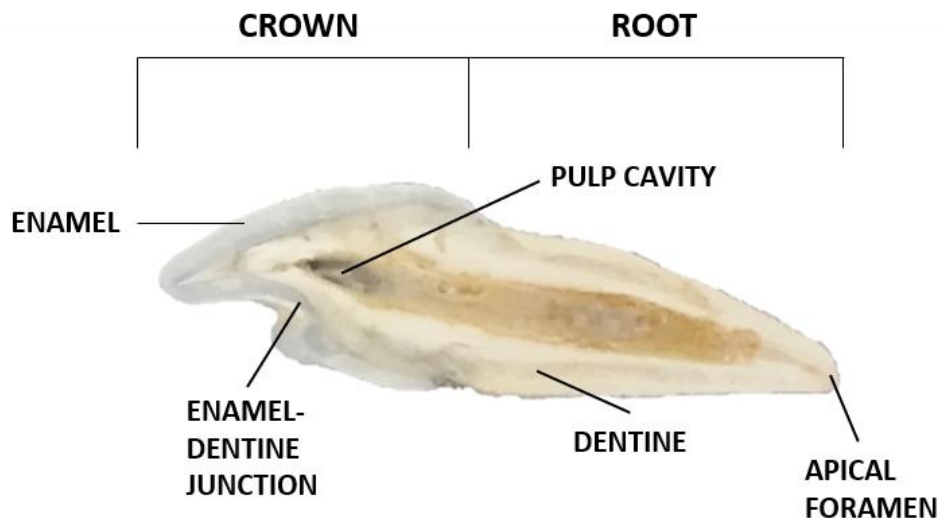


Figure 1: Cross-sectional anatomy of a single tooth and its respective features.

Tooth Development

Teeth undergo formation, development, and eruption in a continuous, sequential manner. Although the first set of primary (deciduous) teeth do not initially begin to emerge until around seven to eight months, initial teeth soft tissue formation and mineralization can begin as early as week five in utero (Harris, 2016). The morphological stages of tooth development include bud, cap and bell. The crown template forms first, followed by the root formation. During the first stage of initiation, the oral ectoderm induces the mesenchyme within the dental lamina to form the enamel organ and the dental papilla, called the tooth germ (Harris, 2016). A dental sac then forms from the ectomesenchyme, creating the first appearance of a tooth bud in the bud stage (Harris, 2016). During the next stage, the cap stage, the tissues undergo condensation and cell proliferation, in which ectomesenchymal cells arrange in a cluster and eventually differentiate into odontoblasts to begin forming the crown matrix during the bell stage and later the dentine (Harris, 2016).

Cuboidal cells differentiate into ameloblasts to deposit the enamel, moving from the EDJ to the enamel surface over time, producing microstructures along the way that are referred to as enamel rods (or enamel prisms) (Guatelli-Steinberg, 2016; Harris, 2016). Ameloblasts secrete cross-striations of the enamel matrix in daily circadian rhythmic, metabolic activity, creating short-period lines (Antoine and Hillson, 2016; Guatelli-Steinberg, 2016). At regular intervals throughout all developing teeth within the individual, the enamel-forming matrix simultaneously slow their secretion, creating a series of growth planes called the planes or striae of Retzius (Guatelli-Steinberg, 2016; Hillson, 2005). These striae are referred to as long-period lines and contain layers of

short-term period lines interspaced between throughout the growth layers of the enamel up to the occlusal (biting) surface (Guatelli-Steinberg, 2016). At the occlusal surface, long-period lines overlap one another and so become hidden, whereas on the lateral (side) enamel, long-period lines manifest as perikymata, appearing as waves and troughs along the surface (Hillson, 2005). Once the enamel crown has form completely, the enamel organ terminates in its growth.

In association with enamel apposition, the inner dentine fills the space between the growing enamel cap and the pulp cavity, by continuously increasing its surface area at the horn tip, followed by expanding apically in order to complete the tooth root and filling in all the fringes of the tooth root(s) with odontoblasts (Harris, 2016; Tang et al., 2016). Dentine is formed through the mixed deposit of both inorganic and organic layers (Tang et al., 2016). During growth, two types of dentine are commonly formed via odontoblasts (primary dentine and secondary dentine), and these structurally similar tissues are secreted in incremental striae (Tang et al., 2016). Primary dentine rapidly forms first along the border of the enamel, located along the EDJ, while also forming around the pulp cavity as well (Shepherd et al., 2012; Zilberman and Smith, 2000). Secondary dentine results from the continual yet slowed apposition of primary dentine (Zilberman and Smith, 2000); secondary dentine may form alongside primary dentine, though its formation is more uneven around the pulp cavity (Shepherd et al., 2012). However, according to previous research, there appears to be a substantial time delay between primary dentine secretion completion and the onset of second dentine secretion, as some research has suggested that root formation is completed prior to the formation of secondary dentine (Shepherd et al., 2012). Tertiary dentine usually only forms as a repair

mechanism in response to a health condition or trauma, such as dental caries or attrition (Shepherd et al., 2012).

While there can be some variation, the development and eruption of maxillary teeth per quadrant generally follows this pattern: Molar 1 → Central Incisor → Lateral Incisor → Premolar 1 → Canine → Premolar 2 → Molar 2 → Molar 3 (Harris, 2016). The first upper tooth to erupt is the first molar, occurring around six years of age, followed by the central incisor erupting at around seven years of age (Ubelaker, 1989). The next tooth to erupt is the lateral incisor at eight years of age, followed by the first premolar at ten years of age and the second premolar at eleven years of age (Ubelaker, 1989). The canine also erupts around eleven to twelve years of age (Ubelaker, 1989). Finally, the second molar erupts at 12 years of age, and the third molar erupts at around 16 to 21 years of age (Ubelaker, 1989).

Tooth Chemical Composition

Properties of Enamel

Tooth enamel is a highly inorganic material. Because enamel has a higher mineral content and tissue preservation than bone, enamel is susceptible to the same chemical processes that impact and decompose bone content so easily (Burton et al., 2003; Hollund et al., 2015; Scott, 2008). Tooth enamel is approximately 96-97% mineralized (inorganic), containing mostly hydroxyapatite (composed mainly of calcium and phosphorus) (Antoine and Hillson, 2016; Hillson, 2005). These types of tissue do not undergo the same level of remodeling or turnover that bone does (Balasse, 2002); thus, elemental signatures found within these tissues reflect more accurately the local

environmental composition and are therefore more suitable for chemical characterization studies (Balasse, 2002; Cucina et al., 2007).

Properties of Dentine

Tooth dentine is also mineralized, though less mineralized than enamel, is richer in organic content, containing approximately 80% mineralization (80% inorganic, 20% organic) (Asaduzzaman et al., 2017; Hillson, 2005; Tang et al., 2016). Throughout life, odontoblasts aligned along the pulp cavity within the dentine continually produce more dentine until that tooth is lost (Asaduzzaman et al., 2017). In addition, because dentine is encased within the enamel, it does not come into contact with the oral environment in the way enamel does (Asaduzzaman et al., 2017).

Properties of Pulp Cavity

During life, the pulp cavity serves to maintain proper functioning of the living dental tissues with proper blood supply and other nutrients (Legge and Hardin, 2016). The number of roots in the tooth (e.g. one, two, or three) indicates the number of canals leading into the pulp chamber (Legge and Hardin, 2016). For example, an upper central incisor would have a single pulp canal leading into the pulp chamber, whereas an upper first premolar may have two pulp canals leading into the pulp chamber.

Trace Elements in Teeth

There are two different classes of elements that can accumulate within a living system: major elements and minor or trace elements. Of the 50 known elements that can

occur in measurable quantities within living systems, only about a dozen of these elements are considered to be trace elements (Fraga, 2005). Examples of major elements commonly found in enamel are phosphorus (P), calcium (Ca), sodium (Na), magnesium (Mg), and chlorine (Cl) (Reitznerová et al., 2000). In contrast to major elements, which are measured in higher concentrations in analytical chemistry, trace elements are elements that are detected at low concentrations, including parts per million (ppm) or even parts per billion (ppb) level.

Generally, trace elements have been considered to occur in two forms, as functionally or nutritionally essential (bioessential) elements and as nonessential elements. Although some nonessential elements may not be biologically necessary, they can be viewed as essential from an analytical perspective (e.g. minor, trace elements that are often found in comparatively larger quantities, even though these elements have no known biological function).

In optimal quantities, biologically essential elements are vital for supporting proper reactions, growth, and development in their interactions with enzymes and proteins in biological systems (Mertz, 1981). Thus, essential elements are maintained within tightly regulated concentration thresholds (Reynard and Balter, 2014). It is important to note that although nonessential elements are considered innately toxic, essential may become toxic to living systems when their concentrations surpass what is necessary to maintain biological function (Fraga, 2005). Some essential trace elements include iron (Fe), copper (Cu), zinc (Zn), and manganese (Mn) (Fraga, 2005; Mertz, 1981; Reynard and Balter, 2014).

In comparison, nonessential elements can often mimic the reactivity and chemical metabolism of essential elements and can even be detected in unusually high quantities depending on the exposure. Thus, their distribution and concentrations are best understood in comparison to essential elements, most commonly Ca (Reynard and Balter, 2014). Examples of nonessential trace elements include aluminum (Al), chromium (Cr), strontium (Sr), barium (Ba), titanium (Ti), and lead (Pb) (Brown et al., 2004; Reynard and Balter, 2014). Due to their calcified tissues, bones and teeth in particular have a high affinity for accumulating metals and heavy metals (Asaduzzaman et al., 2017). During life, alkaline-earth elements such as Mg, Sr, and Ba can enter and become incorporated within the body at high levels, while divalent, heavier metals such as Zn, Cu, and Fe become incorporated at lower levels, since these elements cannot easily enter the body (Reynard and Balter, 2014; Wright, 1999).

Previous chemical and bioarchaeological studies have demonstrated that trace elements vary both in distribution and concentration depending on the specific dental tissue type being examined (Arnold and Gaengler, 2007; Guede et al., 2017; Kang et al., 2004; Tanaka et al., 2004). In particular, major differences have been observed in number of elements detected, types of elements detected, and their concentrations between enamel and dentine (Table 1). For example, using LA-ICP-MS, Farrell et al. (2013) found that trace element Zn had the highest concentration in the pulp, the next highest concentration in the enamel, and the lowest concentration in the dentine; in comparison, Pb increased in concentration from the outer to the inner tooth, with the enamel being the lowest in concentration and the pulp being the highest in concentration.

Table 1: Summary of previous relevant literature comparing trace element concentrations found at inner enamel and inner dentine.

Inner Enamel > Inner Dentine	Inner Dentine > Inner Enamel	Enamel = Dentine	Source
Ca, P	C		Arnold and Gaengler, 2007
	Mn		Arora et al., 2011
	Pb		Budd et al., 1998
P, Ca, Fe, Zn, Cu	Mg, S		de Dios Teruel et al., 2015
Ca			de Souza Guerra et al., 2010
	Pb, Zn		Farell et al., 2013
Na, Mg, Al, Cr, Mn,	Ti, V, Zn, Sr, Ba, Pb	Fe, Cu	Guede et al., 2017
Ca	Al, Sr, Ba		Hanć et al., 2013
	Sr, Zn, Pb	Cd	Hare et al., 2011
P, Ca, Sr	Ba, Pb		Liu et al., 2013
Al			Tanaka et al., 2004

Increased age (i.e. prolonged exposure time) leads to increased concentration levels of most heavy trace elements or metals (Asaduzzaman et al., 2017). For example, in more contemporary populations, Pb appears to be the most commonly noted element that exhibited significant increases in concentrations over large age brackets (Asaduzzaman et al., 2017; Budd et al., 1998). Current research on some trace elements provides various and sometimes opposing information about the same trace elements, depending on the geographical location and age of the humans remains. For example, previous studies have demonstrated that enamel accumulates more zinc especially on the outer surfaces, which come into contact with saliva (Asaduzzaman et al., 2017; Castro et al., 2010). However, other studies have reported increasing zinc from the upper enamel

surface to the area of the pulp region, with the pulp exhibited the highest content of zinc (Anjos et al., 2004).

While carbon (C), Ca, P, and Mg are generally referred to as major elements in other fields of study, for the purposes of this study, all elements selected for analysis were classified as trace elements and were grouped according to whether or not the element has a known biological or nutritional function (i.e. essential and nonessential).

Bioavailability of Trace Elements

The bioavailability of a trace element can directly affect the presence and distribution of that element found within a tooth (Brown et al., 2004). Bioavailability refers to the amount of a micronutrient (e.g. trace element) that is ingested and absorbed into the body and then used in regular physiological processes. This phenomenon helps explain how elements can interact with one another, as bioavailability influences which minerals are available for use within the body, based on the interplay of diet, other elements present, and molecular inhibitors and enhancers, such as enzymes (Dolphin and Goodman, 2009; Mertz, 1981). Several intrinsic factors influencing the bioavailability of trace elements include age, sex, pregnancy, trauma, gastrointestinal infections, and the occurrence of other diseases or illnesses (Freeland-Graves et al., 2015). Extrinsic factors influencing bioavailability include geographical location and biocultural practices, such as food preparation and processing (Freeland-Graves et al., 2015).

Bioavailability of Mg

The functional and nutritional essential trace element and heavy metal Mg is prevalent throughout nature and in the human body, with about 53% of Mg content present in the skeleton (Rude, 2014). Mg binds to ribosomes and other macromolecules, most especially serving to bind to substrates and interacting with enzymes (Rude, 2014). Some of the reactions Mg is involved in include amino acid activation, protein kinases, and lipid metabolism, (Rude, 2014). Mg is widely distributed among various plant and animal food sources, and thus is usually prevalent within the diet (Rude, 2014). Studies have shown that Mg absorption and retention is not significantly affected by Ca intake; however, increasing Zn intake does significantly lower Mg absorption and retention (Rude, 2014; Spencer et al., 1994).

Bioavailability of Al

The nonessential element and heavy metal Al is an abundant element often found within the earth's crust; however, it is only detected in very small amounts in living organisms (Tanaka et al., 2004). Al has been associated with dental caries prevalence in dental studies, while other studies have noted that Al salts may inhibit the growth of oral bacteria (Tanaka et al., 2004). Additionally, previous studies have detected the presence of Al in trace amounts in Maya ceramics and pottery dating from the Classic and Postclassic periods (Little et al., 2004). Thus, it is possible for individuals to become exposed to Al through manufacturing and dietary processes.

Bioavailability of P

Considered a major element, P is uniquely essential to maintaining human life, as P is a component within the DNA structure (O'Brien et al., 2014). This element is also key part the body's energy source, integrated with sugar, protein, and enzyme reactions (O'Brien et al., 2014). P is a foundational component to the mineralized structure within the human skeleton, as well as in teeth, forming a portion of hydroxyapatite ($\text{Ca}_5(\text{PO}_4)_3(\text{OH})$) (O'Brien et al., 2014). Sources of P for dietary intake include milk, meat, poultry, fish, eggs, nuts, and grains (O'Brien et al., 2014). P absorption may be affected by the presence of other minerals, such as Ca, Mg, and Al (O'Brien et al., 2014).

Bioavailability of Ca

Also considered a major element, Ca is an abundant mineral and pivotal to the mass of the body, including the strength of bones and teeth (Wolinsky and Altchuler, 1983; Wright, 1999). Ca is present throughout nature, found in various minerals and rocks, such as limestone and marble, as well as pearls, eggs shells, and animal antlers (Weaver and Heaney, 2014). Ca is also the other major component of hydroxyapatite found in bone and teeth (Weaver and Heaney, 2014). Ca absorption occurs in the small intestine and can be affected by multiple dietary factors, mainly milk and other dairy products serving as a major source of Ca (Cashman, 2002), as well as vegetables (Fairweather-Tait and Hurrell, 1996). Deficiency in Ca can lead to various health issues, such as osteoporosis (loss of bone mass) (Cashman, 2002; Weaver and Heaney, 2014).

Bioavailability of Ti

Ti is a nonessential element and heavy metal toxicant, generally associated with environmental pollution and dental implants in more contemporary studies (Asaduzzaman et al., 2017; Bosshardt et al., 2017). Previous studies have detected the presence of Ti in trace amounts in Maya ceramics and pottery dating from the Classic and Postclassic periods (Jadot et al., 2016; Little et al., 2004). Thus, it is possible for individuals to become exposed to Ti through manufacturing and dietary processes.

Bioavailability of Cr

Cr is a nonessential trace element and heavy metal, available through various dietary sources, such as peppers, mushrooms, nuts and a few vegetables, including corn and maize (Fairweather-Tait and Hurrell, 1996). Regardless of dose amount, Cr intestinal absorption is generally less than 3% (Fairweather-Tait and Hurrell, 1996). While higher compounds of Cr are toxic, Cr deficiency can also cause glucose intolerance in the body by increasing insulin activity (Fairweather-Tait and Hurrell, 1996). Cr interacts with various other metals, such as Zn, Fe, Ca, and vanadium (V); in particular, because Fe and Cr share a common gastrointestinal transport mechanism, the presence of Fe can inhibit the absorption of Cr in the small intestine (Fairweather-Tait and Hurrell, 1996).

Bioavailability of Mn

Though a heavy metal, Mn is considered to be a functionally essential trace element and is necessary for maintaining neuronal functions (Asaduzzaman et al., 2017). This element is used in amino acid, lipid, and carbohydrate metabolism, particularly as an

enzyme activator (Buchman, 2014; Fraga, 2005). Mn has also been associated with bone development, and some sources of dietary intake for Mn include tea, rice, nuts, and grains (Fraga, 2005). Mn deficiency has not been well documented, but some studies suggest that deficiency in Mn can lead to unnatural blood clotting neurological issues, since it can cross the blood-brain barrier (Aschner, 2000; Keen et al., 1999).

Bioavailability of Fe

The functionally essential trace element Fe is important for supporting various metabolic functions, including red blood cell production, oxygen supply, and energy metabolism (Wessling-Resnick, 2014). Fe is found within several classes of protein, including proteins for storage and transport (Fraga, 2005). Sources of Fe include vegetables, fruits, and various dairy products (Fraga, 2005; Hare et al., 2015). Fe is also highly disrupted within meat (Fairweather-Tait and Hurrell, 1996). While Fe deficiency can cause anemia, an overload of Fe can also lead to Fe poisoning (Fraga, 2005); older individuals especially are more susceptible to these two phenomena (Wessling-Resnick, 2014). Fe and Zn have varying affects depending on the food source carrying these micronutrients; for example, high quantities of Zn within aqueous solutions will impair Fe absorption, while solid Zn does not impact Fe absorption (Sandström, 2001).

Bioavailability of Zn

The functional and nutritional essential trace element and heavy metal Zn serves multiple catalytic functions, including binding to enzymes, lending structural support, and helping regulate functions (Fraga, 2005; King and Cousins, 2014). Zn helps support

growth and development from prenatal through adolescence (Fraga, 2005). Generally, Zn seems to be found in higher quantities within meat-source foods and less within vegetation, eggs, or dairy (Dolphin and Goodman, 2009; Fraga, 2005). Zn interacts with Cu and Fe at the level of absorption between tissues, while Zn availability and absorption are not impeded by the presence of Ca (Sandström, 2001).

Bioavailability of Sr

Also a heavy metal, Sr has been debated on its essentiality to the human body. While Sr has no known biological function, many anthropological studies consider Sr to be an essential trace element, since it is found in such high quantities in human remains (Brown et al., 2004; Guede et al., 2017; Reynard and Balter, 2014). Plants contain a higher level of strontium than animals; thus, individuals that are primarily vegetarian will exhibit higher levels of strontium in teeth than carnivores (Asaduzzaman et al., 2017).

Bioavailability of Ba

Ba is a nonessential trace element for terrestrial organisms and is potentially toxic at higher concentrations (Brown et al., 2004; Lamb et al., 2013). Although Ba is functionally nonessential, this element has become increasingly studied in anthropology in comparison to Sr and Ca (Austin et al., 2013; Dolphin et al., 2005). Divalent cations of Ba and Sr can interact with and replace isovalent Ca sites within the dentine and enamel matrix hydroxyapatite (Asaduzzaman et al., 2017). Ba absorption in humans (especially those that are chronically ill) is still not well understood, though animal studies reveal that Ba levels can influence every biological system in the body (Kravchenko et al.,

2014). Ba has been found generally within soil, with elevated levels documented due to nearby mining activities and modern sources of contamination (Kravchenko et al., 2014; Lamb et al., 2013).

Bioavailability of Pb

Pb is a nonessential trace element and one of the more abundant heavy metals (Amr, 2011; Brown et al., 2004). Pb is the most common heavy metal toxicant, generally associated with environmental pollution in more contemporary studies (Asaduzzaman et al., 2017). However, in more recent years, Pb uptake by crops and aquatic animals may also introduce lead into the food chain and thus introduce lead exposure to human bodies (Asaduzzaman et al., 2017). Additionally, previous studies have detected the presence of Pb in trace amounts in Maya ceramics, pottery, and structures dating from the Classic and Postclassic periods (LeCount et al., 2016; Little et al., 2004). Thus, it is possible for individuals to become exposed to Pb through manufacturing and dietary processes.

LA-ICP-MS and Trace Element Analysis

Due to the instrument's high sensitivity and multidata acquisition within a single analysis, mapping of elemental distribution and bioimaging at the μm level has become a common technique for analyzing various living tissues, including individual cells, blood, hair samples, proteins, skeletal elements, dental tissues, vegetation tissues, and shells (Pozebon et al., 2017). In comparison to traditional mass spectrometry, the combination of laser ablation with inductively-coupled-plasma and mass spectrometry allows for more precise data collection and ease of replicability of study. LA-ICP-MS also allows for

detection beyond other nondestructive chemical analyses, such as X-Ray Fluorescence, can measure elements in parts per billion (ppb) or even part per trillion (ppt), whereas X-Ray Fluorescence can only provide trace element analysis at the parts per million (ppm) level. In this way, due to its precise sample extraction and measurement and minimal destruction of sample, LA-ICP-MS can be seen as beneficial to bioarchaeology and forensic anthropology studies, particularly in cases involving highly fragmented artifacts or skeletal remains that need to be chemically analyzed.

Overall, LA-ICP-MS is a precise, minimally destructive method that can be applied to both solid and liquid sample analysis (Figure 2) (Limbeck et al., 2015; Speakman and Neff, 2005). The three major stages of this method include (a) ablation of the sample surface generating aerosols, (b) generated aerosol transport, and (c) atomization, vaporization, and ionization. To begin, the analyst places a small sample inside the first chamber, a holder cell (which is approximately 2 cm by 5 cm in size), and then uses the small mounted video camera inside the cell to identify areas of interest to be ablated by the laser (Speakman and Neff, 2005). By using the image projected on the computer screen, the analyst may also superimpose spots, lines, and/or rectangular scanning patterns known as raster patterns onto the targeted area to assist with making the ablation more precise (Speakman and Neff, 2005).

During analysis, the pulsed laser beam first ablates (vaporizes) a small portion of the top, surface layer on the sample with intense heat, and the ablated material is then transported via flowing argon (Ar) gas into an ICP-MS torch system, containing plasma (Speakman and Neff, 2005).

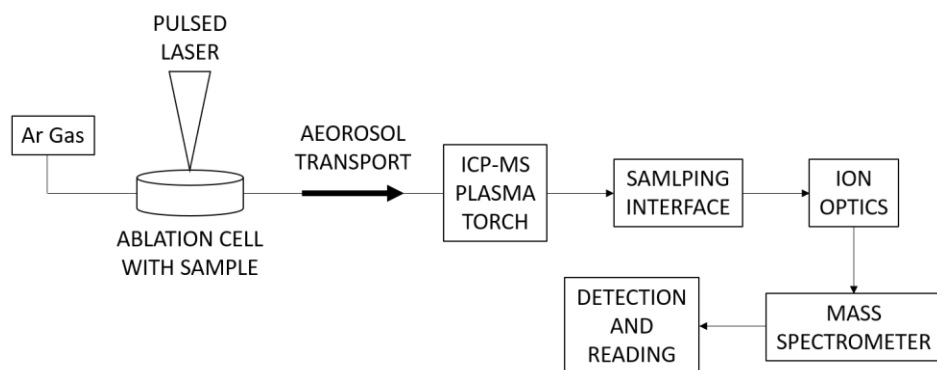


Figure 2: A simplified schematic of the overall process of LA-ICP-MS.

In the first chamber, a high-intensity laser beam focuses on the sample surface, removing the top layer of the surface sample (Delmdahl and von Oldershausen, 2005; Speakman and Neff, 2005). This produces vaporized plasma that is then transported to a second chamber, where sample becomes ionized, before being transported to a mass spectrometer for analysis (Limbeck et al., 2015; Speakman and Neff, 2005). When the vaporized sample is carried into the plasma, the plasma ionizes the sample, and these newly-formed ions transition from atmospheric pressure to the vacuum chamber of the ICP-MS system (Speakman and Neff, 2005). Through high voltage acceleration, ions produced in plasma are drawn into the mass spectrometer and then separated according to their individual mass/charge ratios, due to the varying strength of a magnet within the mass spectrometer (Speakman and Neff, 2005). Although the detector can only record a small atomic mass range at a given time, the use of the magnet allows an entire mass range to be scanned in a relatively short period of time, thus accelerating and analytical process (Speakman and Neff, 2005). In this way, this method is an improvement over traditional mass spectrometry, because LA-ICP-MS machinery involves direct

vaporization of a solid sample, thus reducing preparation time and destruction of the sample material itself (Speakman and Neff, 2005).

Regardless of machine model, some parameters that the analyst may control and adjust according to the specificity of the sample itself include the following: the amount of power applied to the sample (i.e. laser energy or intensity), how many pulses or shots the laser will fire per second (i.e. laser pulse rate, measured in Hz), and how fast the laser will scan across sample surface area (i.e. scan speed or scan mode) (Speakman and Neff, 2005). Although laser ablation creates a small crater (approximately 50 μ m in diameter and 80 μ m in depth) on the surface of the sample, the process is still considerably nondestructive, as compared to other chemical analyses that visibly alter the overall state of sample composition beyond repair, such as stable isotope analysis (Cucina et al., 2007). A solid state laser (Nd:YAG) with a wavelength of emitted energy of 266nm emits a short light wavelength with low energy output and quadrupled frequency (as compared to a laser with 230nm), thus generating more complete vaporization within the plasma (Fricker and Günher, 2016).

There have been a number of studies which have utilized LA-ICP-MS to determine the distribution and concentration levels of various biologically essential and nonessential trace elements present within human dental tissues (Table 1). In a recent review published in the Journal of Analytical Atomic Spectrometry, Pozebon et al. (2017) provide an overview of current applications and mapping strategies for elemental analysis within biological tissues utilizing the LA-ICP-MS system. Two currently emerging applications of LA-ICP-MS involve mapping elemental distribution and determining elemental migration within the teeth (Pozebon et al., 2017).

Trace Element Analysis in Dentistry

In the field of dentistry, LA-ICP-MS is being applied as a novel laboratory method for two-dimension mapping of trace elements present across the whole tooth structure. For example, one study found that the concentrations of Sr, Zn and Pb varied based on different types of tissue that were produced at different growth stages in juvenile incisors (Hare et al., 2011). Thus, this technique may allow researchers in dentistry to further understand how certain elements found in teeth are related to the structural development and timing of eruption of teeth.

Trace Element Analysis in Bioarchaeology

According to Shepherd et al. (2012), the use of dental tissue as a source material for LA-ICP-MS analysis has become a widely-accepted technique. In order to properly ablate teeth and for analysis results to be considered accurate, the specimen being analyzed must be homogenous and uncontaminated (Cucina et al., 2007). In this case, a homogeneous sample refers to a sample that contains an even, flat surface. Surface homogeneity is important. Even minute variation in surface topography can introduce unwanted variation regarding how laser beam interacts with the sample surface, which could potentially cause changes in vaporization and transportation process through the mass spectrometer, thus altering one's results (Cucina et al., 2007). To create this homogeneity and expose the inner dentine tissue, teeth must be thin-sectioned using a low-speed metallic blade, which does minimize the damage to the inner surface of the tooth (Cucina et al., 2007). Thus, while the application of laser ablation itself is

minimally destructive to the sample, the protocol required to prepare a tooth for analysis via LA-ICP-MS is somewhat destructive to the tooth (Cucina et al., 2007).

The use of LA-ICP-MS has grown within archaeological research as a tool for characterizing and thus contextualizing material artifacts, from obsidian to ceramics (Speakman and Neff, 2005). The instrument configurations of LA-ICP-MS are able to produce a large quantity of trace element and isotopic data within a relatively short period of time (Simonetti et al., 2008). In the more specific subfield of osteoarchaeology, dental information can be especially valuable in order to answer questions concerning diagenetic changes, movement, lifestyle, and identity of ancient and modern populations (Budd et al., 1998; Cucina et al., 2007; Kohn et al., 2013; Willmes et al., 2016). Data provided from LA-ICP-MS also provide insight into how diagenesis affects bone/teeth composition (Galiová et al., 2013; Kohn et al., 2013). Over time, trace elements such as Ba and Sr can substitute for natural Ca in developing bone and dental tissues (Reynard and Balter, 2014). Dental tissues (e.g. dentine) representing different life stages may exhibit different ratios of trace elements to calcium (Tang et al., 2016). In addition, dentine may reflect temporally toxic exposure patterns (Tang et al., 2016). Thus, an abnormal abundance of one type of metal (such as Pb) may serve as a biomarker, allowing researchers to infer a life history of exposure to certain chemicals (Budd et al., 1998; Shepherd et al., 2012).

Previous studies using LA-ICP-MS have focused on geochemistry, environmental sciences, and extinct species dietary history (Galiová et al., 2013; Limbeck et al., 2015). In current bioarchaeological research, areas of application utilizing LA-ICP-MS include the following. As an analytical tool, LA-ICP-MS has been used to detect element

concentrations within a variety of archaeology-related studies, including ceramic analysis, obsidian sourcing, and other chemical characterization studies (Cucina et al., 2007; Speakman and Neff, 2005). In bioarchaeological studies, LA-ICP-MS can be used as a method to examine preservation and long-term exposure of elements and isotopes in human tissues, including the inorganic content of bone, inorganic dental enamel tissue, and organic primary and secondary dentine tissue (Budd et al., 1998; Cucina et al., 2007; Kohn et al., 2013). LA-ICP-MS may also be useful in bioarchaeological studies at the population level to address issues of health, frailty and survivability (Stojanowski et al., 2007; Smith and Tafforeau, 2008). Additionally, LA-ICP-MS may be used to reconstruct paleodiet from archaeological bone (Djingova et al., 2004). This method may also aid bioarchaeologists in understanding heterogeneity of trace elements as biomarkers corresponding to specific structural and development features within teeth (Hare et al., 2011). In addition, this technique can be used to evaluate environmental history and reconstruct dietary changes based isotopic analysis of tooth enamel (Balasse, 2002). One study in particular noted that variation in breastfeeding diets during their first year of life resulted in concentration and spatial distribution variation of Ba in juvenile incisors (Austin et al., 2013). Thus, this technique may allow researchers to further understand how dietary exposure influences the structure and physiology of teeth during early childhood development.

Trace Element Analysis in Forensics

For trace element analyses, studies have demonstrated that the presence and distribution of Sr in skeletal materials can tie human and faunal remains to a specific

region (Jones, 2014). Current studies in this field have demonstrated the value in measuring trace element concentrations among paleo teeth found in Idaho (Kohn et al., 2013). In addition, trace elemental analysis comparisons have been made at burial sites (Martin et al., 2007). Previous research has involved trace element analysis and elemental mapping of enamel, primary dentine, and secondary dentine contained in the tooth crown and roots respectively (Cucina et al., 2007; Galiová et al., 2013; Kohn et al., 2013).

Previous research involving the use of LA-ICP-MS and teeth has also demonstrated that it is possible to distinguish primary human dentine as a biomarker and examine lead exposure throughout life (Budd et al., 1998). This information can then be utilized to ascertain temporal and spatial distribution information regarding pre- and neonatal periods (Beaumont et al., 2015). LA-ICP-MS provides information regarding paleodiet and weaning, thus lending insight in past biocultural phenomena (Beaumont et al., 2015; Dijngova et al., 2004). When considering the impact of diet and diagenesis, the use of laser ablation on teeth has been considered a viable means of investigation, as teeth are less susceptible to the process of diagenesis as compared to bone elements (Hollund et al., 2015). LA-ICP-MS can also be used in forensics to analyze concentrations of metals present in bone, teeth, and hair, aiding researchers in determining the origin and possible identification of the remains (Stadlbauer et al., 2007). Finally, this method can also be used to answer questions concerning biodistance and hominid evolutionary history, as patterns of development may correlate with social stress, weaning, and ecological variables (Beaumont et al., 2015; Smith and Tafforeau, 2008).

In addition to bioarchaeological studies, LA-ICP-MS has been applied in forensic contexts in order to investigate the spatial distribution of metals in specific layers of

growth-related tissues in the dentine and the enamel (Kang et al., 2004). In current forensic and forensic anthropological research, other areas of application utilizing LA-ICP-MS include the standardization of glass as a homogeneous substance and analyses of heterogeneous elements such as soil, bone, and teeth (Almirall and Trejos, 2016). Forensic anthropological researchers have utilized LA-ICP-MS as a method for identifying key trace elements at a very small scale of detection among individuals and within populations to differentiate between osseous and nonosseous material and sort commingled remains (Castro et al., 2010). The tool LA-ICP-MS may also be used for discrimination purposes, such as sorting individuals within commingled contexts based on unique chemical signatures (Castro et al., 2010). Additionally, previous clinical-based research has involved the use of two-dimensional imaging of trace elements to help dentists better understand the chemical nature of enamel, dentine, and pulp (Hare et al., 2011; Kang et al., 2004).

In addition, recent technological improvements in LA-ICP-MS methodology have allowed researchers to recognize diagenetic changes in fossilized human teeth through stable isotope analysis. This method may possibly allow researchers to recognize trends in mobility and dietary patterns bioarchaeologically without having to consider as heavily the potential long-term effects of taphonomy on skeletal remains (Willmes et al., 2016). Additional research in this area is warranted in order to address issues concerning calibration techniques used and replicability of forensic data produced.

Other mapping using a similar method called Laser Induced Breakdown Spectroscopy has also allowed researchers interpret manner of death. For example, in

study by Fortes et al. (2015), individuals who had drowned exhibited a comparatively higher abundance of Sr distribution within their inner dentine.

Archaeological Background

Lamanai Location and Setting

The sample population analyzed within this project originated from the archaeological site Lamanai, which is located approximately 80km northeast of Pacbitun, in the Orange Walk District of Belize, and on the western shore of the New River Lagoon (Figure 3) (Coyston, 1995; Pendergast, 1981a). Recorded history of Lamanai indicates a length, unbroken occupation that spans almost two millennia, from Middle Preclassic Period (1250-400 BCE) to the Historical Period (1520-1625 CE) (Coyston, 1995). The individuals to be analyzed in this study are associated with structures that have been dated to the Pre-Columbian, Postclassic time period (900-1521 CE) (Coyston, 1995; Dormon, 2007).

This sample of individuals was also selected based on their collective association with the following structures: N10/1, N10/2, and N10/4, which are a cluster of associated structures located in the southern area of the site (Lang, 1990; Pendergast, 1981a). The longevity and stability of Lamanai is credited to its pivotal location near the New River for trade and transport and its political and social ties to other Maya centers (Coyston, 1995). According to previous research, (Coyston, 1995; Lang, 1990; Pendergast, 1981a), there is sufficient structural and grave good evidence indicating that the sample group derived from the three structures listed above comprises a relatively homogenous, high status group of individuals from the Postclassic period.



Figure 3: Map of Belize depicting location of Lamanai archaeological site. Map created using Google Maps.

One example of this fact is that some of the teeth used in this study have evidence of intentional dental modification, which is likely a symbol indicative of social or political importance (Williams and White, 2006). Another example of high status evidence is the fact that artifacts found in association with structure N10/1 were also found in some of the burials within structure N10/2 (Lang, 1990). In addition, artifacts likely attributed to wealth (i.e. gold sheet and copper objects) recovered in associated with N10/2 burials were also found in some of the N10/4 burials (Lang, 1990). Pendergast (1981a, 1981b, and 1984) also asserts that grave goods from all three of these structures reflect individuals of high social status at Lamanai.

N10/1 Structure

The N10/1 structure has been described as a small platform at the center of the plaza, containing two total recovered burials, recovered ceramic samples that correspond to the early Postclassic period (12th century), and locally manufactured ceramics from a later, unspecified time period (Lang, 1990; Pendergast, 1981a; Pendergast, 1986). One individual from this structure is included in this study (see Table 2 in Materials and Methods chapter).

N10/2 Structure

The N10/2 structure has been described as a small, ceremonial building containing a total of 50 recovered burials, as well as ceramic vessels that correspond to the early and late Postclassic period (Lang, 1990; Pendergast, 1981a; White, 1986). A total of seven individuals from this structure are included in this study (see Table 2).

N10/4 Structure

The N10/4 structure contained 47 recovered burials and has been described as an acting graveyard during the Postclassic period (Lang, 1990; White, 1986). Based on associated grave goods, the burials at this structure appear to correspond to the late 15th or early 16th century (Lang, 1990; Pendergast, 1981a). A total of 12 individuals from this structure are included in this study (see Table 2).

Postclassic Maya Diet

At the height of the Postclassic period, (11-12th century CE) (Pendergast, 1981a), the diet of the ancient Maya heavily involved maize consumption (White, 1986). Although, stable isotope and paleobotanical research also suggests that, following the Late Classic period, other plant resources still remained a major source of carbon as well (Coyston, 1995; Lentz, 1999). Stable isotope research also suggests that, due to enriched carbon levels, the Lamanai Maya diet during the Postclassic period may have involved greater incorporation of lipids and meats as food resources, as compared to the previous periods (Coyston, 1995; Emery, 1999). In particular, zooarchaeological evidence suggests that marine resources (e.g. fish and shellfish) were an important source of protein at Lamanai during the Postclassic period, with this increasing dependence on marine produces likely influenced by new trading systems along the coast and improved fishing technologies (Coyston et al., 1999; Emery, 1999). Stable isotope data of bone apatite and collagen support the interpretation of an increased dependence on marine foods during the Postclassic period, particularly among the most elite members of the Lamanai community (Coyston, 1995; Coyston et al., 1999).

CHAPTER THREE: MATERIALS AND METHODS

The following protocol were undertaken for sample selection and preparation, data collection, and data analysis.

Materials

A population sample of 18 individuals was selected based on their collective association with a cluster of structures (including N10-01, N10-02, and N10-04) and located in the southern area of the Lamanai site (Lang, 1990) (Table 2). The total sample of teeth (N=26) was then divided based on tooth type. Upper central incisors are abbreviated as UCI (n=12); upper lateral incisors are abbreviated as ULI (n=1); upper first premolars are abbreviated as UPM1 (n=6); and upper second premolars are abbreviated as UPM2 (n=7).

The sample used in this research was determined by a number of factors. The first criterion used in selection was that all individuals in this study should come from the same time period (i.e. Postclassic) and relatively the same social status, as indicated by previous archaeological and bioarchaeological findings at Lamanai (Lang, 1990; Pendergast, 1981a; Pendergast, 1981b; Williams and White, 2006). According to previous research (Lang, 1990), there is sufficient evidence indicating individuals belonging to the N/10 structures comprise a relatively homogenous and potentially high-status population from the Postclassic era, as described in the previous chapter.

Table 2: Summary of sample group (N=26) from a Postclassic Lamanai site, containing teeth deemed suitable for this research and belonging to one of the four assigned groups. Data for individual determined sex obtained from Williams and White (2006) and White (1986).

Group Number	Individual Number	Individual ID Number	Sex*	Tooth Types	Dental Modification
1	1	N10-1/2	M	UCI + UPM1	Present
1	2	N10-2/20A or B	U	UCI + UPM2	Present
1	3	N10-2/21	U	UCI + UPM2	Absent
1	4	N10-2/21A	U	UCI + UPM1	Absent
1	5	N10-2/42B	I	UCI + UPM1	Present
1	6	N10-4/01	U	UCI + UPM2	Present
1	7	N10-4/43	M	UCI + UPM1	Absent
1	8	N10-4/46C Large	U	UCI + UPM2	Absent
2	9	N10-4/19	I	UCI	Present
2	10	N10-4/31	F	UCI	Present
2	11	N10-4/35	U	UCI	Absent
2	12	N10-4/46A	M	UCI	Absent
3	13	N10-2/49	U	ULI	Absent
4	14	N10-2/22	M	UPM1	Absent
4	15	N10-2/40	F	UPM1	Absent
4	16	N10-4/10	M	UPM2	Absent
4	17	N10-4/33	F	UPM2	Absent
4	18	N10-4/46C Small	U	UPM2	Absent

*M=Male; F=Female; U=Unknown; I=Indeterminate

Because the individuals within these structures share a common geographic location, as well as a similar social status, it is expected that the chemicals exhibited in teeth from these three structures should exhibit similar elemental patterns as well.

The second criterion used in selection was relative age, which was consistently determined by the presence of multiple adult (i.e. permanent, non-deciduous) teeth in the individual. The third criterion was that individuals selected should exhibit the same tooth

types in both location and dental growth progression. In order for the data collected through this project to be consistent and comparable with other bioarchaeological and forensic literature (e.g., Austin et al., 2013; Castro et al., 2010; Dolphin et al., 2005; Dolphin and Goodman, 2009; Hare et al., 2011; Kang et al., 2004), only permanent (adult) maxillary (upper) teeth were selected for use.

In addition, to maintain as close a consistency in age range as possible, based on average development of maxillary teeth, only upper central incisors (UCI), upper lateral incisors (ULI) and upper premolars (UPM) were selected for use. These four types of teeth were selected for use in this project, since these were the teeth most available across all individuals. Permanent upper central incisors have a crown formation completion time of 4-5 years of age and an eruption time of 7-8 years of age (Logan and Kronfeld, 1933; Ubelaker, 1989). Permanent upper lateral incisors have a crown formation completion time of 4-5 years and an eruption time of 8-9 years (Logan and Kronfeld, 1933; Ubelaker, 1989). Permanent upper first (third) premolars have a crown formation completion time of 5-6 years and an eruption time of 10-11 years (Logan and Kronfeld, 1933; Liversidge, 2016). Finally, permanent upper second (fourth) premolars have a crown formation completion time of 6-7 years and an eruption time of 10-12 years (Logan and Kronfeld, 1933; Liversidge, 2016). Thus, for this study, the maximum age range of dental tissues observed was 4-7 years for the crown portions and 7-12 years for the root portions.

The final criterion used in selection was evaluating the teeth for any signs of cracks or trauma. The purpose in using teeth with few or no cracks present was to minimize the potential influence of diagenesis on the tooth preservation and consequential elemental distribution (Kohn et al., 1999; Willmes et al., 2016). It is

important to note that only highly visible cracks or trauma (i.e. broken teeth or cracks that could be seen with the naked eye or through magnification using a magnifying lens) were discounted. It is possible that some teeth exhibited microcracks which the observer could not recognize.

Teeth exhibiting prominent pathological conditions (e.g. dental caries) were also excluded. However, teeth containing visible dental calculus deposits but maintaining an overall preserved shape were still considered viable for use in this project, as built-up calcified plaque is considered to be a pathological condition that primarily occupies the surface of the tooth enamel and dentine during its early stages (Hillson, 2005; Lieverse, 1999). Only teeth containing surface calculus deposits that showed no clear evidence of penetrating into the dentine or enamel were utilized in this project. All dental calculus observed on teeth used in this project were scored following the Brothwell method (1981), prior to being removed through the cleaning process.

In addition, following the same criteria listed above, three test teeth were also selected from a group of unprovenanced teeth from Lamanai. These teeth included one upper canine, one upper central incisor, and one upper premolar and were designated usable as test teeth for comparative purposes only, as they were not associated with a particular individual or group.

Sample size consisted of 26 teeth (N=26) selected from 18 individuals. Some of the individuals selected still maintained teeth embedded within complete or mostly complete alveolar maxillary bone. Thus, to remove teeth as needed, dental picks were used to gently break away the alveolar bone until the tooth was able to be extracted without damage to the tooth root. Once removed, teeth were placed into small plastic

bags, separated and labeled according to their individual identification number. The teeth were then sorted into four groups based on availability and development (Table 3).

Table 3: Four groups (G1 through G4) of 18 individuals sorted based on tooth availability.

Group 1 (G1)	Individual contains both usable UCI and UPM.
Group 2 (G2)	Individual contains usable UCI.
Group 3 (G3)	Individual contains usable ULI.
Group 4 (G4)	Individual contains usable UPM.

Teeth Preparation

Cleaning

Selected and sorted teeth were cleaned in order to remove any excessive, adhered dirt or dried clay, as well as any adhered remnants of alveolar bone. All teeth (N=26) were cleaned using soft bristle toothbrushes and distilled deionized (DDI) water. After they were clean, teeth were left to dry overnight on brown masking paper before being placed back into sterile, air-tight plastic bags. Each tooth was placed into a separate sterile plastic bag, marked, and stored in the air-conditioned Anthropology Laboratory at the National Center for Forensic Science (NCFS) until embedding.

Embedding

In order to keep individual teeth mounted and to prevent cracking during the thin-sectioning process, teeth were embedded in cold-setting epoxy resin. Materials included Epofix™ Cold-Setting Embedding Resin (Electron Microscopy Sciences, 1232-R),

Epofix™ Cold-Setting Embedding Hardener (Electron Microscopy Sciences, 1232-H), disposable paper cups, small wooden spatulas (tongue depressors), circular silicone molds (approximately 5cm diameter), a digital weight scale, and a depression chamber.

During the embedding process, teeth were initially placed inside round silicone mold containers (two teeth per container). Each container was labeled with the individual's identification number. The epoxy cold-setting resin mixture was made by combining 25 parts by weight epoxy resin with 3 parts by weight epoxy hardener. The two liquids were combined within a sterile paper cup and stirred for approximately two minutes until air bubbles could be seen within the mixture.

The epoxy resin mixture was then poured into the embedding container until the top of the teeth were completely covered by the mixture. In order to reduce the number of air bubbles and speed up the hardening process, the epoxy-filled containers were placed inside a pressure chamber, set at approximately 20-25 psi, for 24 hours, and then removed after releasing the pressure from the container (Figure 4).



Figure 4: Two test teeth embedded in hardened epoxy resin (left) and the silicone mold previously containing resin with teeth (right).

Sectioning

After embedding teeth in hardened resin, the teeth inside resin molds were mounted and sectioned in order to create thin, homogenously flat slices, as suitable for analysis via LA-ICP-MS. Sectioning materials included Buehler IsoMet® Low Speed Saw (Isomet™ 230V), Buehler 8” 15HC diamond wafering blade (0.5in or 12.7mm arbor size), Buehler counter-balance weights, and distilled water (Buehler, 1992). During all sectioning, the wafering blade was lubricated in a distilled water bath to prevent overheating and to ensure effective, clean cutting each time. Counter-balance weights (totaling 100g) were also used to keep the level (arm) holding each embedded tooth sample steady during the cutting process.

Prior to making sample cuts, the wafering blade was dressed using a dressing stick to expose the abrasive grain on the blade and to prevent contamination (dressed five times prior to using a new blade, dressed twice prior to using a previously used blade and twice between every two samples).

Teeth within the same epoxy mold were first separated from each other by cutting the circular mold near the center, creating two semicircle pieces of resin, each containing one tooth. Afterward, each semicircle section containing one tooth was sliced down around the edges until the blade could be positioned in such a way as to cut the whole tooth (crown and root) directly in half down the center of the tooth, in the anterior-posterior or lingual-labial direction (Figure 5).

Once the tooth was cut in half down the center, an additional thin slice is cut across the top of each center half. For each tooth, two or three approximately two 1½-2mm longitudinal sections were removed from the center, using 200-300 rpm speed

(Figure 6). After being cut, each tooth slice was placed and sealed into a new 50mm by 100mm sterile plastic bag for storage and to prevent contamination prior to the elemental analysis.

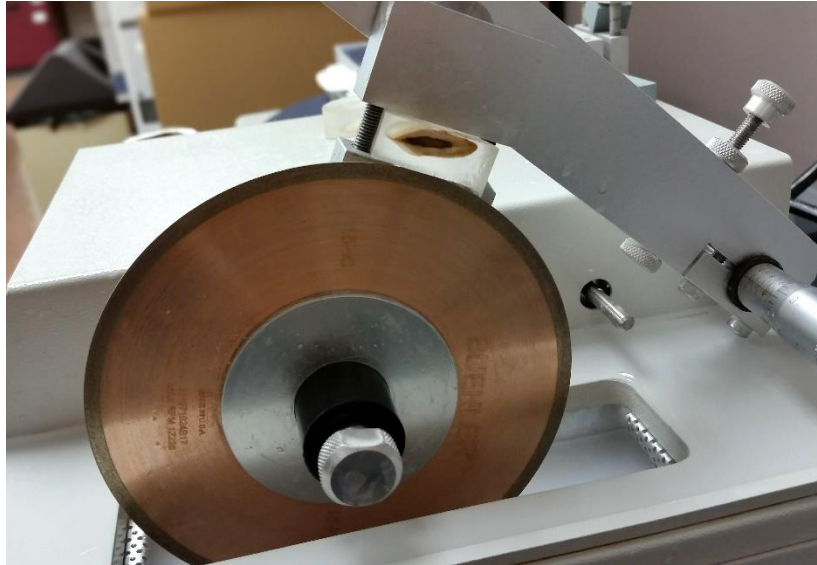


Figure 5: Example of a tooth embedded in resin attached to the support arm that has already been sliced down the center in the lingual-labial direction.



Figure 6: Example of a tooth slice from tooth sample N10-4/33 UPM2.

LA-ICP-MS Elemental Analysis

The analysis of elements was performed using a 266nm (Nd:YAG) J200 Femtosecond Laser Ablation Instrument, located at NCFS near the University of Central Florida (UCF) main campus. Instrument parameters were established during the analysis of the initial three test teeth (Table 4).

After these method parameters had been selected, they were saved under the first method file name "170615-Teeth1.mswn" Worksheet and maintained as the method throughout the remaining teeth sample analyses in order to promote the highest degree of accuracy for future quantitative analysis, while also reducing analysis time. Each new elemental analysis of a different tooth sample involved using the established protocol saved on the computer file and simply editing the file name with the corresponding date and/or tooth number and saving the new, edited file each time.

Analyses were carried out with the focused laser ablation spot size at 100 μ m, maintaining a laser repetition rate of 10Hz, and maintaining a carrier gas flow rate of 0.6L/min and a make-up gas flow rate of 0.58L/min.

Following general LA-ICP-MS operating procedures, each morning the instrument underwent a startup procedure, first by turning on the cooling unit (vacuum system) and then waiting a few minutes before starting the ICP-MS plasma. It took approximately 15 minutes to warm the plasma. After the plasma had warmed, the system was brought online and the sample chamber was purged to minimize contamination of gases in the chamber.

Table 4: Operating parameters and conditions for elemental analysis by LA-ICP-MS.

Parameters	Values
<i>Laser Ablation</i>	
Laser type	Nd:YAG
Wavelength	266nm
Carrier gas (He) flow rate	0.6L/min
Make-up gas (Ar) flow rate	0.58L/min
Spot size	100 μ m
Velocity	0.1mm/s
Laser repetition rate	10Hz
Sampling scheme	Rastering (horizontal line pattern)
Distance between ablation lines	~0.111 μ m (varied by sample)
<i>Pre-ablation</i>	
Pre-ablation time	11.00s
Laser delay	11.00s
Spot size	100 μ m
<i>ICP-MS</i>	
Plasma flow rate	9.0L/min
Auxiliary gas flow rate	1.20L/min
Nebulizer gas flow rate	1.12L/min
Torch alignment sampling depth	5.0mm
Plasma RF power	1.25kW
Pump rate	10rpm
Stabilization delay	10s
Isotopes measured	^{12,13} C, ¹⁹ F, ²⁴ Mg, ²⁷ Al, ³¹ P, ³² S, ⁴⁴ Ca, ⁴⁷ Ti, ⁵¹ V, ^{52,53} Cr, ⁵⁵ Mn, ⁵⁶ Fe, ⁶⁰ Ni, ⁶³ Cu, ⁶⁶ Zn, ⁸³ Kr, ⁸⁵ Rb, ^{86,87,88} Sr, ¹¹⁶ Sn, ^{137,138} Ba, ^{206,207,208} Pb
<i>Ion Optics</i>	
First extraction lens	-82volts
Second extraction lens	-525volts
Third extraction lens	-525volts
Corner lens	-450volts
Mirror lens left	93volts
Mirror lens right	63volts
Mirror lens bottom	37volts
Entrance lens	5volts
Fringe bias	-2.5volts
Entrance plate	-90volts
Pole bias	-2.0volts

After warm up, daily tuning or optimization was also conducted using the National Institute of Standards (NIST) Glass 610, as is standard when conducting optimization techniques (Lin et al., 2016). Prior to each tooth analysis that took place in the morning, the optimization would scan for approximately 30 minutes to prepare to the instrument. In addition, prior to each tooth sample being loaded into the sample chamber, the system glass chamber slot was also cleaned with a contamination wipe and a small amount of ethyl alcohol, and the gases in the chamber were also purged (approximately a five-minute process) to prevent contamination.

Individual Tooth Sample Parameters

Each tooth slice sample was mounted to a black loading disc (approximately 5.5cm in diameter); to prevent movement during the laser ablation process, the tooth slice was also mounted to the loading disc, with the corners of the resin slice tapped to the disc to prevent the sample from shifting during the laser ablation process. Once secured to a disc, the tooth sample was then inserted into the platform disc space within the center of the loading stage, leaving a small depression/margin between the level of the tooth and the level of the top of the platform (approximately 5mm space). This was determined to be the best distance from the laser to the tooth to allow for optimal scanning and maintain minimal damage to the tooth surface itself during the scanning process. The disc was also rotated in order to keep the tooth slice parallel relative to the scanner. The loading stage was then inserted into the scanning platform.

Two computer monitors were used to conduct each elemental analysis. The first computer screen (Screen 1) contained all controls for sample loading, pattern creation,

and other manual laser parameters. The second computer screen (Screen 2) contained all automatic protocols of the elemental analysis method and was also the screen where each elemental analysis was recorded and stored.

After a sample was inserted into the sample chamber, on Screen 1, the “Load Sample” button was enabled, which brought the center of the platform (and the approximate center of the tooth) in line with the laser overhead. Once loaded into the sampling chamber, the chamber was “purged” of possible gas contaminants using the “Purge” button located under the “Gas” tab on Screen 1. This process took approximately five minutes. Meanwhile, as the system was purging, a screenshot was taken using the macrocamera lens via the camera icon located under the “Operations” tab on the laser screen main page.

The camera was then switched to the microcamera lens and refocused either using the “autofocus” button or using the scrollbar located on the left-hand side of the screen to manually focus the lens in microcamera mode. Stitching protocol was then implemented using the “Stitching” tab located under Operations. Stitching was set to either 14 or 15 parallel lines, depending on the size of the tooth slice. The result of the stitching protocol produced a cross-lattice image (see Figure 7), which allowed for more precise placement of the pattern lines.

After stitching, a pattern was established for each tooth using the pattern settings available under the “Operation” tab (Figure 8). Patterns were created by first constructing a diagonal line between two points, one point being the top left corner of the stitching pattern, just above the tooth slice, and the other point being the bottom right corner of the stitching pattern, just below the tooth slice.

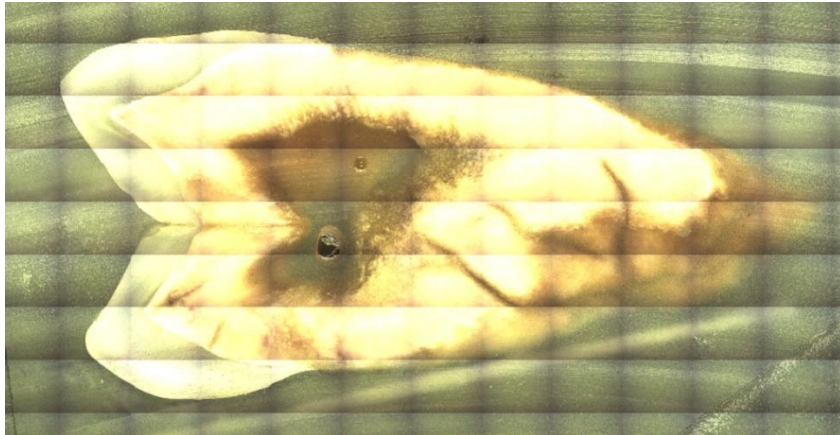


Figure 7: Example of stitching from tooth sample N10-4/10 UPM2. Note the boxes representing separate frames that have been stitched together.

The number of lines of the pattern was then typed into the corresponding box, with this number varying depending on the size of the tooth. It is important to note that the number of lines per tooth sample was determined when the distance between each pattern line reached as close to $0.111\mu\text{m}$ as possible, as this spacing was determined optimal for generating optimal, consistent resolution across all samples and to reduce fractionation during ablation (Becker et al., 2010).

For each laser pattern, a box or rectangular shape was constructed, one that covered the entire span of the tooth size. The pattern button of horizontal bars ($\overline{\text{---}}$) was always implemented (see Figure 8). After a large enough pattern had been established, vertical (y-axis) and horizontal (x-axis) dimensions and the number of lines per sample were recorded, as these numbers would later be used to create the two-dimensional maps. Finally, the microcamera was directed to the approximate center of the tooth and a final “autofocus” was enabled to ensure all lasering occurred in focus.

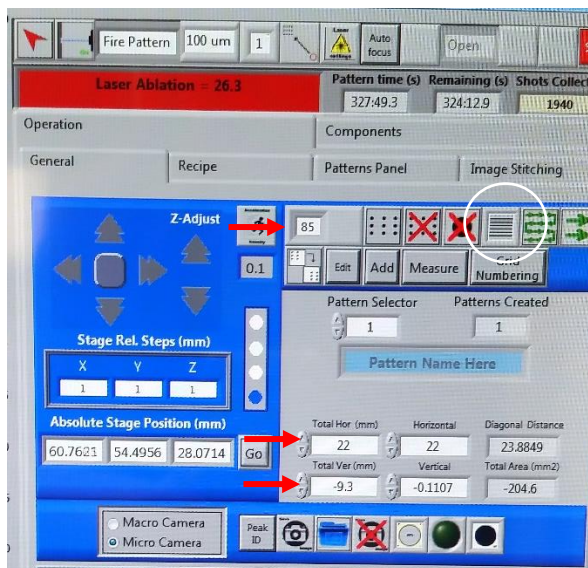


Figure 8: Photo of pattern settings on Screen 1, including pattern icon and raster pattern (circled), pattern dimensions (bottom two arrows), and number of lines (top arrow).

Laser ablation pattern lines count and dimensions varied relative to tooth size. In general, premolar slices exhibited larger dimensions and required more ablation lines than incisor slices, and thus premolars generally took about an hour longer to complete the elemental analysis than incisors.

After a pattern had been established, the analytical method was edited using the “Edit Method” button located on Screen 2. In order to ensure that each elemental analysis incorporated the entire laser pattern each time a new scan occurred, the method was edited to adjust the elemental scanning time to match each sample’s laser Array Completion Time. This updated method was then saved using the date of the analysis and tooth number’s identity in the file name.

When the purging was completed and it was time to commence with the elemental analysis, on Screen 2, the “Run” button was enabled, followed by “Read.”

These buttons began the ICP-MS data collection, including initial background elemental scanning. After about 30 seconds of background scanning, the “Fire in Pattern” button on Screen 1 was then selected. A laser delay of 11s was enabled (laser parameters, Table 3). After the laser delay of 11s and stabilization delay of 10s (laser parameters, Table 3), the laser then began firing in the established pattern for the allotted time, while the second monitor recorded all elemental intensities in the mass spectrometer.

After each laser and elemental analysis was completed, the text file containing the element data was automatically saved. The tooth sample was then removed from the loading chamber and the glass platform was cleaned with a contamination wipe and a small amount of ethyl alcohol to prevent contamination.

Mapping

Maps were generated using MATLAB® software, which is an array-based coding language, used primarily within mathematical and engineering applications in order to create and process variables. The MATLAB® 2015a software was made available through the UCF license at the NCFS laboratory. In this project, all maps were generated within the Image Processing application, with maps created using matrices as variables and square brackets used to construct arrays. All coding was input into the Command Window located on the home screen.

In the MATLAB® software, an overall code for reading and generating maps was first established in the Command Window, which could then be edited each time a new tooth file needed to be read, adjusting only the parameters specific to that tooth file, including dimensions, number of lines, and color saturation (Figure 9).

```

1 - clear all
2 - %Read the file from LAICPMS data, is delimited by one space
3 - data = readtable('170519-Teeth2.txt', 'Delimiter',' ');
4 - %data = dlmread('./170615-Teeth1.txt', '\t', 4, 0);
5
6 - %data.Properties.VariableNames;
7 - %Now the name of teh isotopes measures and the possible in interest to work
8 - %patern characteristics
9 - xL = 22; %x length
10 - yL = 7.7; %y length
11 - lines = 71; %number of lines
12
13 - %obtained parameters to data cut and build map
14 - smth_MIsotope = smooth(data.M13,10,'sgolay',2); %smooth process for the sample
15 - dy=diff(smth_MIsotope) ./diff(data.Scan);
16 - dx2=data.Scan(2:end);
17 - [~,locsP] = findpeaks(dy,'MinPeakHeight',3000);

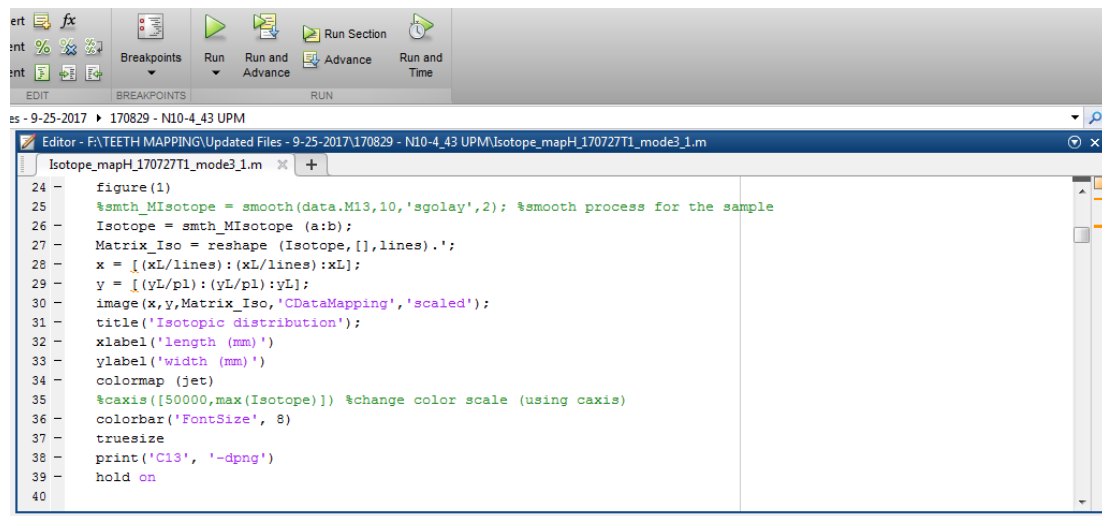
17 - [~,locsP] = findpeaks(dy,'MinPeakHeight',3000);
18 - dy_inverted = -dy;
19 - [~,locsN] = findpeaks(dy_inverted,'MinPeakHeight',3000);
20 - p1 = round((locsN(end) - locsP(1))/lines); %number of points by line
21 - a = (locsN(end) - (p1*lines))+1; %first point in the raster
22 - b = locsN(end); %last point in the raster
23

```

Figure 9: Screenshot of overall coding parameters for creating maps.

The command for data analysis was set to “data = readtable,” which allowed the software to read the specific text file that was uploaded and typed into the code (line 3 in Figure 9). The matrix for each map was established using x and y boundaries that matched the dimensions of the pattern created during the laser ablation process. For example, lines 9 through 11 of code were manually changed to match the specific parameters (i.e. dimensions) of the laser ablation each time a new tooth file was uploaded and run. Line 9 refers contained the xL input and corresponded to the x-axis dimension (i.e. horizontal length of the pattern). Line 10 contained the yL input and corresponded to the y-axis dimension (i.e. the vertical length of the pattern). Line 11 contained the number of lines and corresponded to the number of lines scanned by the laser of the whole tooth.

To generate a map corresponding to each desired isotope measured via the LA-ICP-MS instrument, each isotope scan number was input into the program under “print” and generated a corresponding figure number (see Figure 10). For example, figure(1) had a print of ‘C13’ corresponding to the .M13 data from the text file, which is the isotope ¹³Carbon). Every color map background was set to jet (blue) by default in order to maximize the color diversity seen inside the tooth and within the growth lines.



```
24 - figure(1)
25 - %smth_Misotope = smooth(data.M13,10,'sgolay',2); %smooth process for the sample
26 - Isotope = smth_Misotope (a:b);
27 - Matrix_Iso = reshape (Isotope,[],lines).';
28 - x = [(xL/lines):(xL/lines):xL];
29 - y = [(yL/pl):(yL/pl):yL];
30 - image(x,y,Matrix_Iso,'CDataMapping','scaled');
31 - title('Isotopic distribution');
32 - xlabel('length (mm)')
33 - ylabel('width (mm)')
34 - colormap (jet)
35 - %caxis([50000,max(Isotope)]) %change color scale (using caxis)
36 - colorbar('FontSize', 8)
37 - truesize
38 - print('C13', '-dpng')
39 - hold on
40
```

Figure 10: Screenshot of coding for figure (1) map, which is the figure for ¹³Carbon.

Although many isotopes were analyzed and stored via LA-ICP-MS, only a portion of isotopes were selected for mapping. Elements selected for mapping of teeth were chosen due to many of these elements being biologically essential within dental tissues (Fraga, 2005; Reynard and Balter, 2014) and potentially informative for answering research questions, in comparison with previous dental and anthropological research (e.g., Arora et al., 2011; Austin et al., 2013; Guede et al., 2017; Hare et al., 2011;

Humphrey, 2016; Tanaka et al., 2004). Of the trace elements selected, one stable isotope that is naturally occurring and generally abundant was also chosen per element to use for the mapping portion of this research. In addition, the stable isotopes of Ca and P, while they comprised the matrix of the tooth, were also mapped for comparative purposes.

These selected stable isotopes are presented in Table 5.

Table 5: Abbreviations of selected elements for mapping, their corresponding isotopes, and the minimum number selected for the map spectral intensity.

ICP-MS Scan Number	Isotope	Minimum Starting Spectral Intensity
M13	¹³ Carbon (¹³ C)	50000
M24	²⁴ Magnesium (²⁴ Mg)	5000
M27	²⁷ Aluminium (²⁷ Al)	5000
M31	³¹ Phosphorus (³¹ P)	50000
M44	⁴⁴ Calcium (⁴⁴ Ca)	50000
M47	⁴⁷ Titanium (⁴⁷ Ti)	5000
M52	⁵² Chromium (⁵² Cr)	50000
M55	⁵⁵ Manganese (⁵⁵ Mn)	50000
M56	⁵⁶ Iron (⁵⁶ Fe)	130000
M66	⁶⁶ Zinc (⁶⁶ Zn)	10000
M88	⁸⁸ Strontium (⁸⁸ Sr)	50000
M138	¹³⁸ Barium (¹³⁸ Ba)	50000
M208	²⁰⁸ Lead (²⁰⁸ Pb)	500

After the text file was uploaded to the MATLAB® program and parameters were adjusted according to the specific tooth dimension, the “Run” icon was pushed, generating a map corresponding to each scan number.

Mapping parameters were adjusted, and maps were rerun as needed. For example, the saturation of color in the map (i.e. the color scheme scale seen on the right-hand side of the map) was adjusted at the %caxis code line (e.g. line 35 in Figure 10) in order to

maximize color diversity depicted inside the tooth. Each isotope was given a minimum spectral intensity level (or saturation level), varying depending on the expected levels of intensity to be seen (according to previous chemical and anthropological research) and in relationship to the background intensity level. It is important to note that the minimum and maximum spectral intensity numbers were adjusted according to the relative intensities exhibited per individual tooth slice (see Table 5). All generated maps (338 images in total) were saved as .png files and are available in the Appendix.

Maps were scored according to the relative spectral intensity of the sample background and the color spectrum scale made available on the right-hand margin for each individual map. The relative intensity of each isotope at each defined tooth location for all teeth (N=26) was recorded using the following four-point qualitative scale: no intensity detection (N/A), low intensity (LOW), moderate intensity (MOD), and high intensity (HIGH). These descriptive values were assigned according to where on the relative scale the detection occurred (Figure 11).

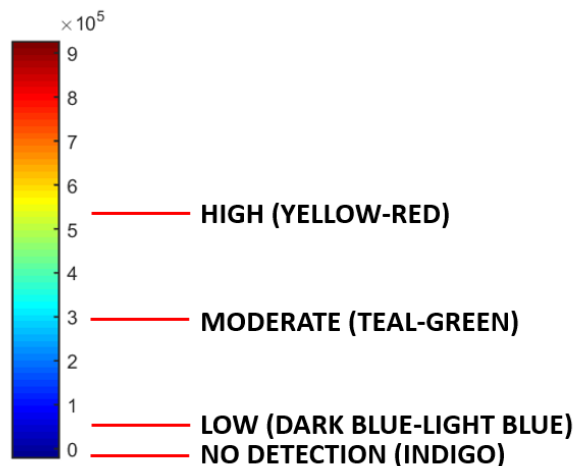


Figure 11: Example of relative spectral intensity scale with assigned qualitative values.

No detection was defined at 0 or as matching the background indigo color. Low was defined between the dark blue and light blue region. Moderate was defined between the teal and green region. And high was defined from yellow up to the red region.

Statistical Analysis

Using Microsoft® Excel 2016, frequencies were calculated of relative intensities of each isotope observed at each tooth location. For statistical purposes, the four-point scale was also converted to the following ordinal values: no intensity detection (N/A)=0, low intensity=1, moderate intensity=2, and high intensity=3. Relative frequencies of each isotope observed at all tooth locations for all teeth was calculated by adding up the total number of times the isotope was detected (whether low, moderate, or high) and dividing by the maximum number of times an isotope could be detected. Total frequencies of isotope occurrences based on tooth location and tooth type were also calculated.

CHAPTER FOUR: RESULTS

Results consist of four main sections focusing on tooth location and tooth type (UCI, ULI, UPM1 and UPM2). Results are presented in the following summary tables (Tables 6 through 14), a scatter plot (Figure 12), and example image maps (Figures 19 through 30). Relative frequency data is also presented in Figures 13 through 18, while total frequency data is also presented in Figures 31 and 32. Results for the detection of relative intensities of each isotope will be presented in the following order: ^{13}C , ^{24}Mg , ^{27}Al , ^{31}P , ^{44}Ca , ^{47}Ti , ^{52}Cr , ^{55}Mn , ^{56}Fe , ^{66}Zn , ^{88}Sr , ^{138}Ba , and ^{208}Pb . Results for isotopic detections at each tooth location will be presented in the following order: Enamel Surface, Inner Enamel, Inner Dentine, EDJ, DPB, and Outer Root Border.

Overall Detection and Distribution of Isotopes

All 13 isotopes selected for analysis and mapping using the LA-ICP-MS were detected throughout the entire sample of teeth (N=26) at some capacity, whether at low, moderate, and/or high intensity and with the majority of isotopic detection being at low intensity. However, at only moderate and high intensities, the overall detection and distribution of isotopes in teeth was more limited (Table 6).

Isotopes ^{44}Ca and ^{31}P , which help comprise the fundamental chemical composition of teeth, were detected at the highest frequency of all isotopes and were commonly distributed throughout the entire cross-sectional area of the tooth (Table 7). In addition, ^{44}Ca and ^{31}P exhibited more consistent, homogeneous distributions throughout the tooth, with overall moderate-to-high intensity detection occurring at all defined tooth locations. The isotope ^{47}Ti also exhibited a generally homogeneous distribution

throughout the tooth but had an overall low intensity detection. In comparison, the remaining 10 isotopes exhibited more heterogeneous distributions, with the two most common locations for low, moderate, and/high intensity detection being the enamel surface and the outer root border (Table 7).

Table 6: Summary of isotopes detected at moderate and high intensities only at each defined tooth location.

Location	Isotopes Detected
<i>Crown</i>	
Enamel Surface	^{13}C , ^{24}Mg , ^{31}P , ^{44}Ca , ^{47}Ti , ^{55}Mn , ^{56}Fe , ^{66}Zn , ^{208}Pb
Inner Enamel	^{24}Mg , ^{31}P , ^{44}Ca , ^{47}Ti , ^{55}Mn , ^{88}Sr
EDJ	^{13}C , ^{24}Mg , ^{31}P , ^{44}Ca , ^{55}Mn , ^{88}Sr , ^{138}Ba
<i>Root</i>	
Inner Dentine	^{13}C , ^{24}Mg , ^{31}P , ^{44}Ca , ^{47}Ti , ^{52}Cr , ^{55}Mn , ^{66}Zn , ^{88}Sr , ^{138}Ba
DPB	^{13}C , ^{24}Mg , ^{27}Al , ^{31}P , ^{44}Ca , ^{52}Cr , ^{55}Mn , ^{56}Fe , ^{66}Zn , ^{88}Sr , ^{138}Ba , ^{208}Pb
Outer Root Border	^{13}C , ^{24}Mg , ^{27}Al , ^{31}P , ^{44}Ca , ^{47}Ti , ^{52}Cr , ^{55}Mn , ^{56}Fe , ^{66}Zn , ^{88}Sr , ^{138}Ba , ^{208}Pb

Table 7: Average frequencies of isotopes detected and highest detection locations across all teeth (N=26). This included moderate and high intensities only.

Isotope	Detection	Highest Detection Location	Classification
⁴⁴ Ca	69%	Inner Dentine	Essential
³¹ P	67%	Inner Dentine	Essential
⁸⁸ Sr	54%	Inner Dentine / Outer Root Border	Nonessential
¹³⁸ Ba	53%	Inner Dentine / Outer Root Border	Nonessential
⁵⁶ Fe	38%	Outer Root Border	Essential
⁶⁶ Zn	36%	Enamel Surface	Essential
²⁴ Mg	28%	Inner Dentine	Essential
²⁰⁸ Pb	24%	Outer Root Border	Nonessential
¹³ C	21%	Inner Dentine / Outer Root Border	Essential
⁵⁵ Mn	16%	Outer Root Border	Essential
²⁷ Al	8%	Outer Root Border	Nonessential
⁵² Cr	7%	Outer Root Border	Nonessential
⁴⁷ Ti	4%	Outer Root Border	Nonessential

Total Frequency of Detection

Overall, all of the teeth exhibited some level of each isotope at varying intensities. The average of ⁴⁴Ca displayed the most moderate to high frequency of detection with 69%, followed by ³¹P with 67% detection and ⁸⁸Sr with 54% detection (Table 7). ⁵²Cr and ⁴⁷Ti had the lowest frequency of detection with 7% and 4% respectively (Table 7). In addition, Figure 12 presents a scatter plot that shows the average frequency detection for the majority of isotopes lies in the low to moderate intensity range.

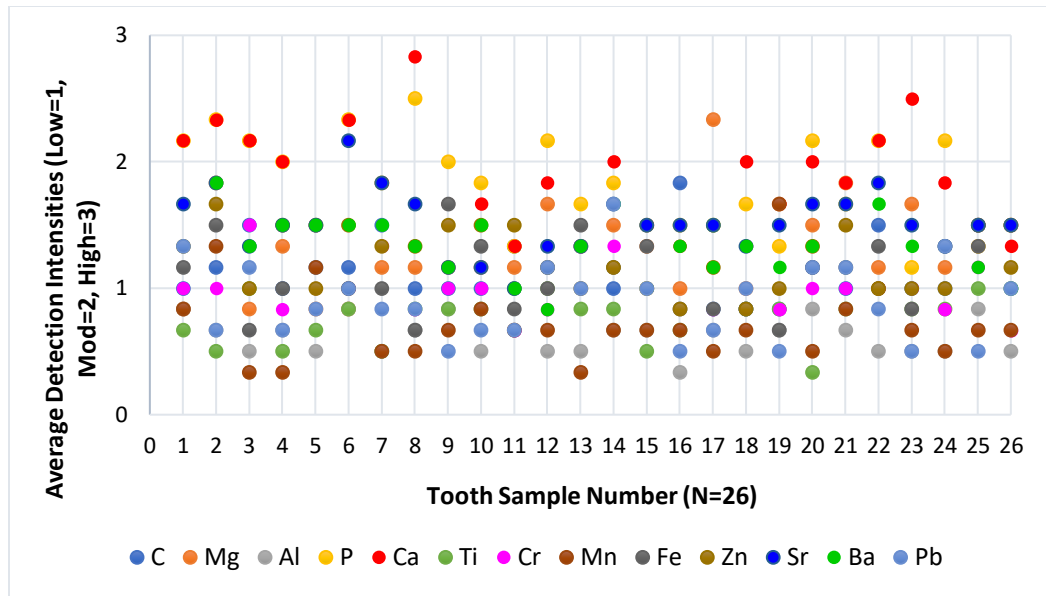


Figure 12: Average detection of intensities of each isotope across entire tooth sample for all teeth (N=26). N/A=0, Low=1, Mod=2, and High=3.

Frequency of Detection by Tooth Location

Enamel Surface

At the enamel surface, all isotopes were detected at low intensity, nine isotopes were detected at moderate intensity, and five isotopes were detected at high intensity (Figure 13). Isotopes that exhibited the most detection (including low, moderate, and high intensity detection) at the enamel surface are ^{31}P , ^{44}Ca , ^{55}Mn , ^{56}Fe , and ^{66}Zn .

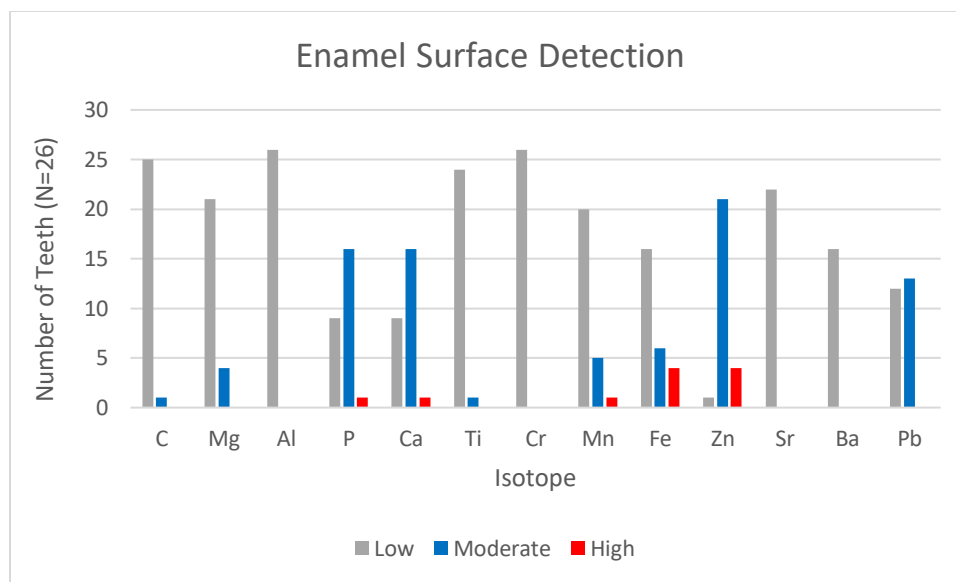


Figure 13: Frequency of isotopes detected at low, moderate, and high intensities at enamel surface for all teeth (N=26).

Inner Enamel

At the inner enamel, 10 of the 13 isotopes were detected in total, with 10 isotopes detected in low intensity, six isotopes detected at moderate intensity, and two isotopes detected at high intensity (Figure 14). Isotopes that exhibited the most detection (including low, moderate, and high intensity detection) at the inner enamel are ^{31}P and ^{44}Ca .

Inner Dentine

At the inner dentine, 11 isotopes were detected at low intensity, 10 isotopes were detected at moderate intensity, and five isotopes were detected at high intensity (Figure 15). Isotopes that exhibited the most detection (including low, moderate, and high intensity detection) at the inner dentine are ^{24}Mg , ^{31}P , ^{44}Ca , ^{88}Sr , and ^{138}Ba .

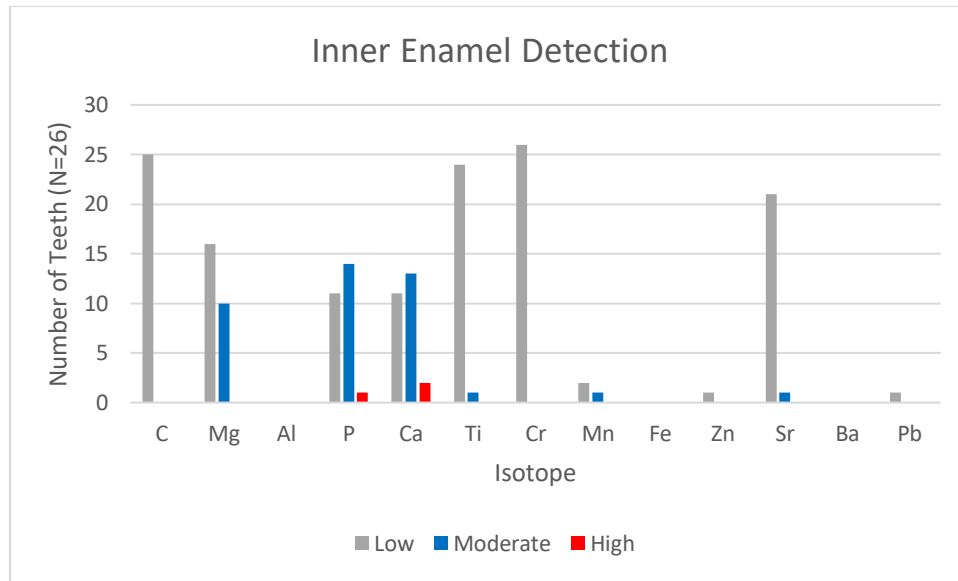


Figure 14: Frequency of isotopes detected at low, moderate, and high intensities at inner enamel for all teeth (N=26).

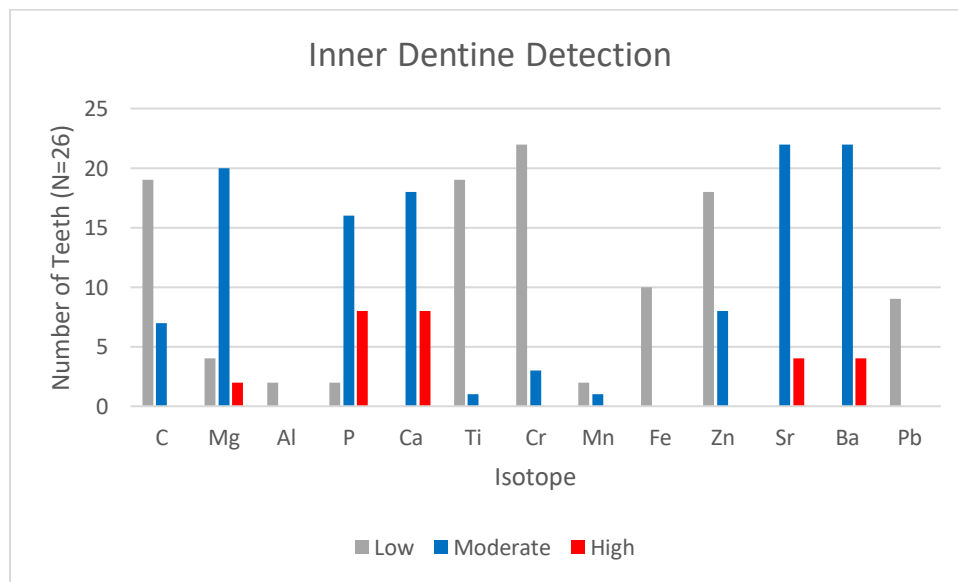


Figure 15: Frequency of isotopes detected at low, moderate, and high intensities at inner dentine for all teeth (N=26).

EDJ

At the EDJ, 12 of the 13 isotopes were detected in total, with 12 isotopes detected at low intensity, seven isotopes detected at moderate intensity, and five isotopes were detected at high intensity (Figure 16). Isotopes that exhibited the most detection (including low, moderate, and high intensity detection) at the EDJ are ^{24}Mg , ^{31}P , ^{44}Ca , ^{88}Sr , and ^{138}Ba .

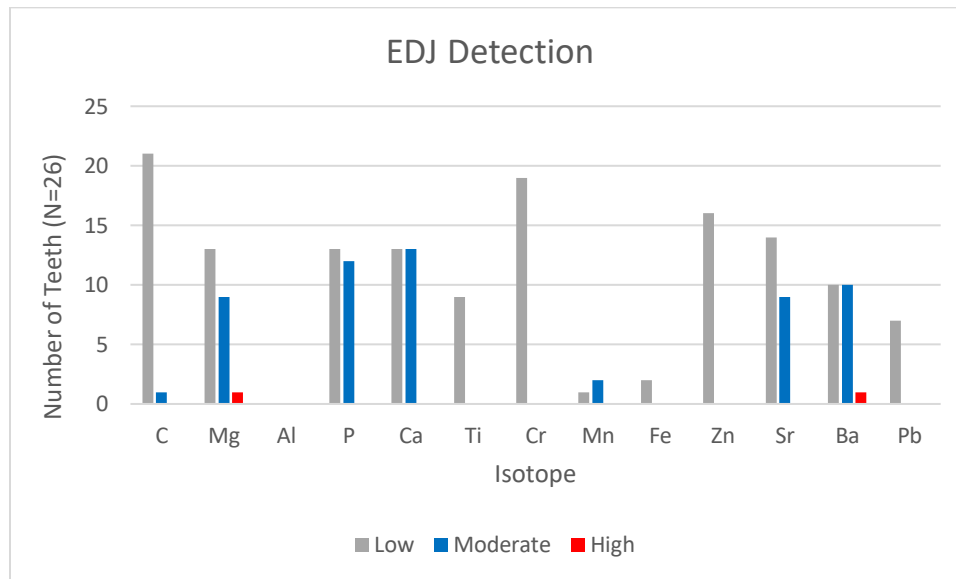


Figure 16: Frequency of isotopes detected at low, moderate, and high intensities at EDJ for all teeth (N=26).

DPB

At the DPB, all, all isotopes were detected at low intensity, 12 isotopes were detected at moderate intensity, and eight isotopes were detected at high intensity (Figure

17). Isotopes that exhibited the most detection (including low, moderate, and high intensity detection) at the DPB are ^{24}Mg , ^{31}P , ^{44}Ca , ^{56}Fe , ^{66}Zn , ^{88}Sr , and ^{138}Ba .

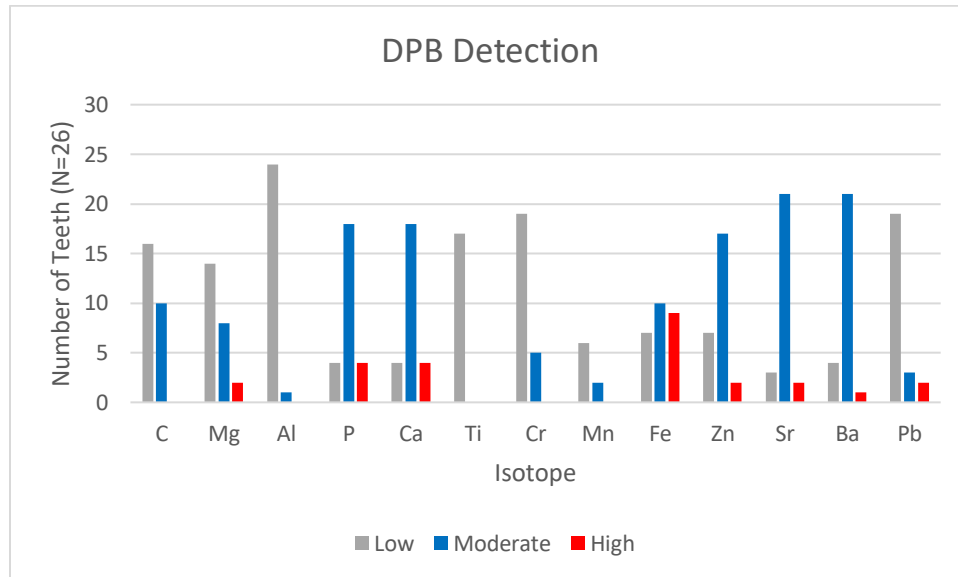


Figure 17: Frequency of isotopes detected at low, moderate, and high intensities at DPB for all teeth (N=26).

Outer Root Border

At the outer root border, all isotopes were detected, with 11 isotopes detected at low intensity, all isotopes detected at moderate intensity, and seven isotopes detected at high intensity (Figure 18). Isotopes that exhibited the most detection (including low, moderate, and high intensity detection) at the outer root border are ^{44}Ca , ^{55}Mn , ^{56}Fe , and ^{208}Pb .

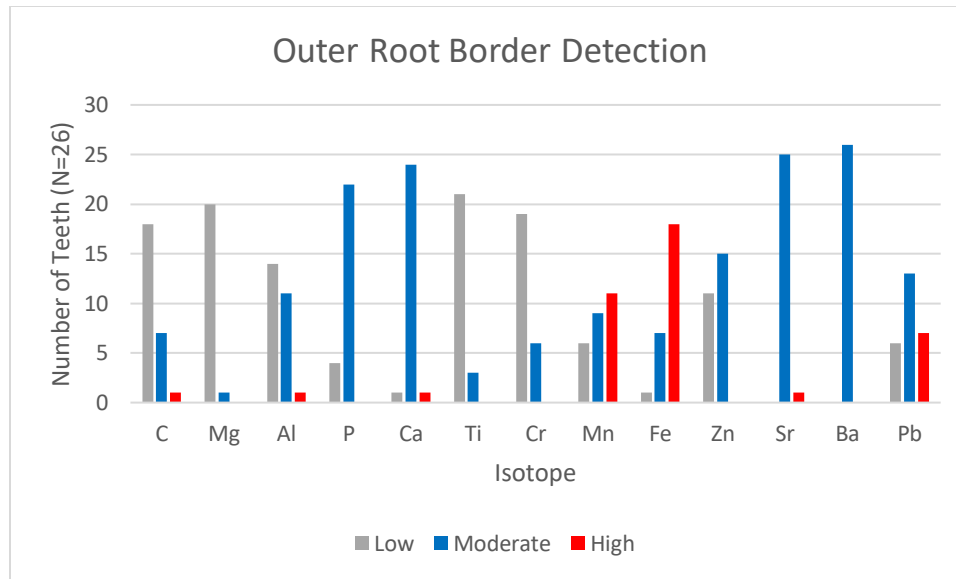


Figure 18: Frequency of isotopes detected at low, moderate, and high intensities at outer root border for all teeth (N=26).

Detection of Isotopes by Tooth Type

Upper Central Incisor

All thirteen elements were observed at various locations and in varying relative intensities in the UCI sample (n=12, refer to Table 2 in Materials and Methods section for tooth identification numbers). Table 8 provides a summary of relative intensities of isotopes detected for this tooth type. Figures 19, 20, and 21 depict examples of isotopic detection and distribution for this tooth type.

Table 8: Summary of relative signal intensities of isotopes observed at each defined tooth location in the UCI sample (n=12).

Isotope	Enamel Surface	Inner Enamel	Inner Dentine	EDJ	DPB	Outer Root Border
¹³ C	LOW	LOW	LOW-MOD	LOW	LOW-MOD	LOW-MOD
²⁴ Mg	LOW-MOD	LOW-MOD	MOD	N/A-LOW	LOW-MOD	N/A-LOW
²⁷ Al	LOW-MOD	N/A	N/A	N/A	LOW-MOD	LOW-HIGH
³¹ P	LOW-MOD	LOW-MOD	MOD-HIGH	LOW-MOD	LOW-HIGH	MOD-HIGH
⁴⁴ Ca	LOW-MOD	LOW-MOD	MOD-HIGH	LOW-MOD	LOW-HIGH	MOD-HIGH
⁴⁷ Ti	LOW	LOW	N/A-LOW	N/A-LOW	N/A-LOW	N/A-MOD
⁵² Cr	LOW	LOW	LOW-MOD	N/A-LOW	LOW-MOD	LOW-MOD
⁵⁵ Mn	LOW-MOD	N/A	N/A-LOW	N/A-MOD	N/A-MOD	MOD-HIGH
⁵⁶ Fe	LOW-MOD	N/A	N/A-LOW	N/A-LOW	LOW-HIGH	MOD-HIGH
⁶⁶ Zn	MOD-HIGH	N/A-LOW	LOW-MOD	N/A-LOW	LOW-MOD	LOW-MOD
⁸⁸ Sr	N/A-LOW	N/A-LOW	MOD-HIGH	N/A-MOD	LOW-HIGH	MOD-HIGH
¹³⁸ Ba	N/A-LOW	N/A	MOD-HIGH	LOW-MOD	LOW-HIGH	MOD
²⁰⁸ Pb	LOW-MOD	N/A-LOW	N/A-LOW	N/A-LOW	N/A-MOD	LOW-HIGH

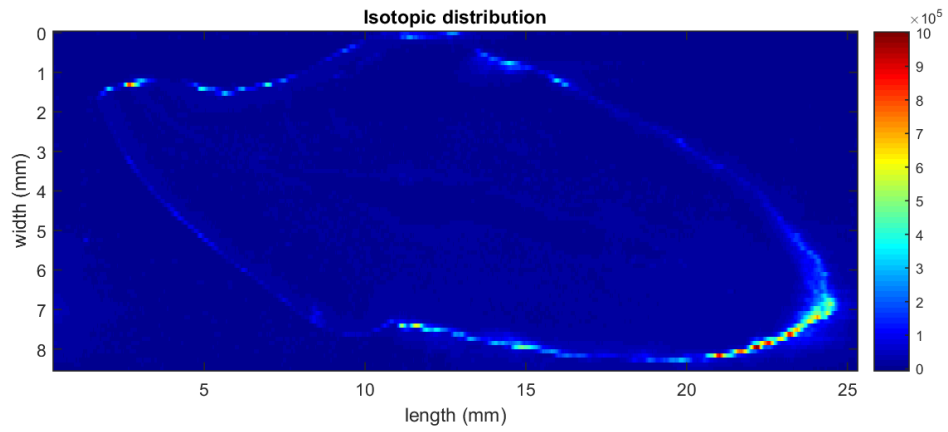


Figure 19: Example of low or poor isotopic detection (^{55}Mn) within UCI sample.

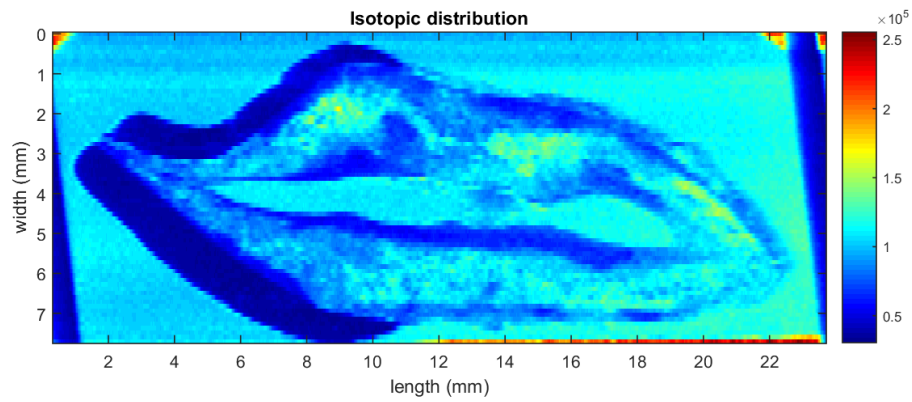


Figure 20: Example of moderate isotopic detection (^{13}C) within UCI sample.

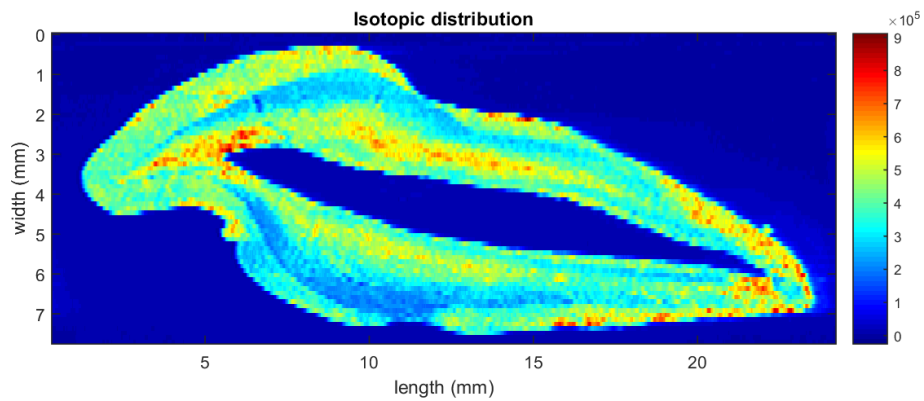


Figure 21: Example of high or good isotopic detection (^{44}Ca) within UCI sample.

Carbon (^{13}C)

The relative intensity of isotope carbon-13 (^{13}C) varied within the UCI sample, depending on the tooth location (Table 8, Figure 20). Both the enamel surface and within the inner enamel exhibited low intensity of ^{13}C detection. The inner dentine exhibited low-to-moderate intensity of ^{13}C detection. The EDJ exhibited either no detection for the presence of ^{13}C or low intensity of ^{13}C detection, depending on the individual tooth scale. The DPB exhibited low-to-moderate intensity of ^{13}C detection. And the outer root border exhibited low-to-high intensity of ^{13}C detection, depending on the individual tooth scale. Overall, the dentine surrounding the pulp border (i.e. near the DPB) and the dentine near the root apex exhibited the highest relative intensity of ^{13}C detection, whereas the enamel exhibited the lowest relative intensity of ^{13}C detection for this tooth type.

Magnesium (^{24}Mg)

The relative intensity of isotope magnesium-24 (^{24}Mg) varied within the UCI sample, depending on the tooth location (Table 8). The enamel surface, the inner enamel, and the inner dentine exhibited low-to-moderate intensity of ^{24}Mg detection. Both the EDJ and the DPB exhibited low-to-high intensity of ^{24}Mg detection, depending on the individual tooth scale. And the outer root border exhibited either no detection for the presence of ^{24}Mg or low intensity of ^{24}Mg detection, depending on the individual tooth scale. Overall, the dentine space surrounding the pulp border (i.e. near the DPB, but not the DPB itself) exhibited the highest relative intensity of ^{24}Mg detection, whereas the outer root border exhibited the lowest relative intensity of ^{24}Mg detection for this tooth type.

Aluminum (^{27}Al)

The relative intensity of isotope aluminum-27 (^{27}Al) varied within the UCI sample, depending on the tooth location (Table 8). The enamel surface exhibited low intensity of ^{27}Al detection. The inner enamel exhibited no detection for the presence of ^{27}Al . The inner dentine exhibited either no detection for the presence of ^{27}Al or low intensity of ^{27}Al detection, depending on the individual tooth scale. The EDJ also exhibited no detection for the presence of ^{27}Al . The DPB exhibited low-to-moderate intensity of ^{27}Al detection. And the outer root border exhibited low-to-high intensity of ^{27}Al detection, depending on the individual tooth scale. Overall, the outer root border exhibited the highest relative intensity of ^{27}Al detection for this tooth type.

Phosphorus (^{31}P)

The relative intensity of isotope phosphorus-31 (^{31}P) varied within the UCI sample, depending on the tooth location (Table 8). The enamel surface and the inner enamel exhibited low-to-moderate intensity of ^{31}P detection. The inner dentine exhibited moderate-to-high intensity of ^{31}P detection. The EDJ exhibited a range from no detection for the presence of ^{31}P to moderate intensity of ^{31}P detection, depending on the individual tooth scale. The DPB exhibited moderate intensity of ^{31}P detection. And the outer root border exhibited low-to-moderate intensity of ^{31}P detection. Overall, the dentine space surrounding the pulp border (i.e. near the DPB) and some dentine closer to the root apex exhibited the highest relative intensity of ^{31}P detection, whereas the dentine space near or at the EDJ exhibited the lowest relative intensity of ^{31}P detection for this tooth type.

Calcium (^{44}Ca)

The relative intensity of isotope calcium-44 (^{44}Ca) varied within the UCI sample, depending on the tooth location (Table 8, Figure 21). The enamel surface exhibited low-to-moderate intensity of ^{44}Ca detection. The inner enamel exhibited low-to-high intensity of ^{44}Ca detection, depending on the individual tooth scale. The inner dentine exhibited moderate-to-high intensity of ^{44}Ca detection. The EDJ exhibited low-to-moderate intensity of ^{44}Ca detection. The DPB exhibited low-to-high intensity of ^{44}Ca detection, depending on the individual tooth scale. And the outer root border exhibited moderate intensity of ^{44}Ca detection. Overall, the dentine space surrounding the pulp border (i.e. near the DPB) and some dentine closer to the root apex exhibited the highest relative intensity of ^{44}Ca detection, whereas the dentine space near or at the EDJ exhibited the lowest relative intensity of ^{44}Ca detection for this tooth type.

Titanium (^{47}Ti)

When detected, the relative intensity of isotope titanium-47 (^{47}Ti) remained at a generally consistent level of intensity within each tooth in the UCI sample (Table 8). The enamel surface exhibited low intensity of ^{47}Ti detection. The inner enamel, the inner dentine, the EDJ, and the DPB all exhibited either no detection for the presence of ^{47}Ti or low intensity of ^{47}Ti detection, depending on the individual tooth scale. And the outer root border exhibited low intensity of ^{47}Ti detection for this tooth type.

Chromium (^{52}Cr)

The relative intensity of isotope chromium-52 (^{52}Cr) within the UCI sample, depending on the tooth location (Table 8). The enamel surface and inner enamel exhibited low intensity of ^{52}Cr detection. The inner dentine, the EDJ, and the DPB exhibited either no detection for the presence of ^{52}Cr or low intensity of ^{52}Cr detection, depending on the individual tooth scale. And the outer root border exhibited low-to-moderate intensity of ^{52}Cr detection. Overall, the dentine space near the root apex exhibited the highest relative intensity of ^{52}Cr detection, whereas the enamel exhibited the lowest relative intensity of ^{52}Cr detection for this tooth type.

Manganese (^{55}Mn)

The relative intensity of isotope manganese-55 (^{55}Mn) varied within the UCI sample, depending on the tooth location (Table 8, Figure 19). The enamel surface exhibited low-to-high intensity of ^{55}Mn detection, depending on the individual tooth scale. The inner enamel, the inner dentine, the EDJ, and the DPB all exhibited either no detection for the presence of ^{55}Mn or low intensity of ^{55}Mn detection, depending on the individual tooth scale. And the outer root border exhibited moderate-to-high intensity of ^{55}Mn detection. Overall, the outer root border exhibited the highest relative intensity of ^{55}Mn detection for this tooth type.

Iron (^{56}Fe)

The relative intensity of isotope iron-56 (^{56}Fe) varied within the UCI sample, depending on the tooth location (Table 8). The enamel surface exhibited low-to-high intensity of ^{56}Fe detection, depending on the individual tooth scale. The inner enamel exhibited no detection for the presence of ^{56}Fe . The inner dentine exhibited either no detection for the presence of ^{56}Fe or low intensity of ^{56}Fe detection, depending on the individual tooth scale. The EDJ exhibited no detection for the presence of ^{56}Fe . The DPB exhibited low-to-high intensity of ^{56}Fe detection, depending on the individual tooth scale. And the outer exhibited moderate-to-high intensity of ^{56}Fe detection for this tooth type.

Zinc (^{66}Zn)

The relative intensity of isotope zinc-66 (^{66}Zn) varied within the UCI sample, depending on the tooth location (Table 8). The enamel surface exhibited moderate-to-high intensity of ^{66}Zn detection. The inner enamel exhibited no detection for the presence of ^{66}Zn . The inner dentine exhibited low-to-moderate intensity of ^{66}Zn detection. The EDJ exhibited either no detection for the presence of ^{66}Zn or low intensity of ^{66}Zn detection, depending on the individual tooth scale. The DPB exhibited low-to-high intensity of ^{66}Zn detection, depending on the individual tooth scale. And the outer root border exhibited low-to-moderate intensity of ^{66}Zn detection. Overall, dentine space surrounding near and at the DPB exhibited the highest relative intensity of ^{66}Zn detection for this tooth type

Strontium (^{88}Sr)

The relative intensity of isotope strontium-88 (^{88}Sr) varied within the UCI sample, depending on the tooth location (Table 8). The enamel surface and inner enamel exhibited either no detection for the presence of ^{88}Sr or low intensity of ^{88}Sr detection, depending on the individual tooth scale. The inner dentine exhibited moderate-to-high intensity of ^{88}Sr detection. The EDJ exhibited low-to-moderate intensity of ^{88}Sr detection. Both the DPB and the outer root border exhibited moderate intensity of ^{88}Sr detection. Overall, the dentine space surrounding the pulp border (i.e. near the DPB) and some dentine closer to the root apex exhibited the highest relative intensity of ^{88}Sr detection, whereas the enamel exhibited the lowest relative intensity of ^{88}Sr detection for this tooth type.

Barium (^{138}Ba)

The relative intensity of isotope barium-138 (^{138}Ba) varied within the UCI sample, depending on the tooth location (Table 8). The enamel surface exhibited either no detection for the presence ^{138}Ba or low intensity of ^{138}Ba detection, depending on the individual tooth scale. The inner enamel exhibited no detection for the presence of ^{138}Ba . The inner dentine exhibited moderate-to-high intensity of ^{138}Ba detection. The EDJ exhibited a range of either no detection for the presence ^{138}Ba up to moderate intensity of ^{138}Ba detection, depending on the individual tooth scale. Both the EDJ and the outer root border exhibited moderate intensity of ^{138}Ba detection. Overall, the dentine space surrounding the pulp border (i.e. near the DPB) and some dentine closer to the root apex

exhibited the highest relative intensity of ^{138}Ba detection, whereas the enamel exhibited the lowest relative intensity of ^{138}Ba detection for this tooth type.

Lead (^{208}Pb)

The relative intensity of isotope lead-208 (^{208}Pb) varied within the UCI sample, depending on the tooth location (Table 8). The enamel surface exhibited low-to-moderate intensity of ^{208}Pb detection. The inner enamel exhibited no detection for the presence of ^{208}Pb . The inner dentine and the EDJ exhibited either no detection for the presence ^{208}Pb or low intensity of ^{208}Pb detection, depending on the individual tooth scale. The DPB exhibited low-to-high intensity of ^{208}Pb detection, depending on the individual tooth scale. And the outer root border exhibited moderate-to-high intensity of ^{208}Pb detection. Overall, the outer root border highest relative intensity of ^{208}Pb detection, whereas the inner enamel exhibited the lowest relative intensity of ^{208}Pb detection for this tooth type.

Upper Lateral Incisor

All thirteen elements were observed at various locations and in varying relative intensities in the UCI sample (n=1, refer to Table 2 in Materials and Methods section for tooth identification number). Table 9 provides a summary of relative intensities of elements detected for this tooth type. Figures 22, 23, and 24 depict examples of isotopic detection and distribution for this tooth type.

Table 9: Summary of relative signal intensities of isotopes observed at each tooth location in the ULI sample (n=1).

Isotope	Enamel Surface	Inner Enamel	Inner Dentine	EDJ	DPB	Outer Root Border
^{13}C	LOW	LOW	MOD	LOW	MOD	LOW-MOD
^{24}Mg	LOW	LOW-MOD	MOD	MOD	LOW	LOW
^{27}Al	LOW	N/A	N/A	N/A	LOW	LOW-MOD
^{31}P	MOD	MOD	MOD	LOW	LOW-MOD	MOD
^{44}Ca	MOD	LOW-MOD	MOD	LOW	LOW-MOD	MOD
^{47}Ti	LOW	LOW	N/A-LOW	LOW	LOW	LOW
^{52}Cr	LOW	LOW	LOW-MOD	LOW	LOW	LOW-MOD
^{55}Mn	LOW	N/A	N/A	N/A	N/A	LOW
^{56}Fe	HIGH	N/A	N/A	N/A	HIGH	HIGH
^{66}Zn	MOD-HIGH	N/A	LOW-MOD	LOW	LOW	LOW
^{88}Sr	LOW	LOW	MOD	N/A	MOD	MOD
^{138}Ba	LOW	N/A	MOD-HIGH	LOW	MOD	MOD
^{208}Pb	MOD	N/A	LOW	LOW	LOW	LOW

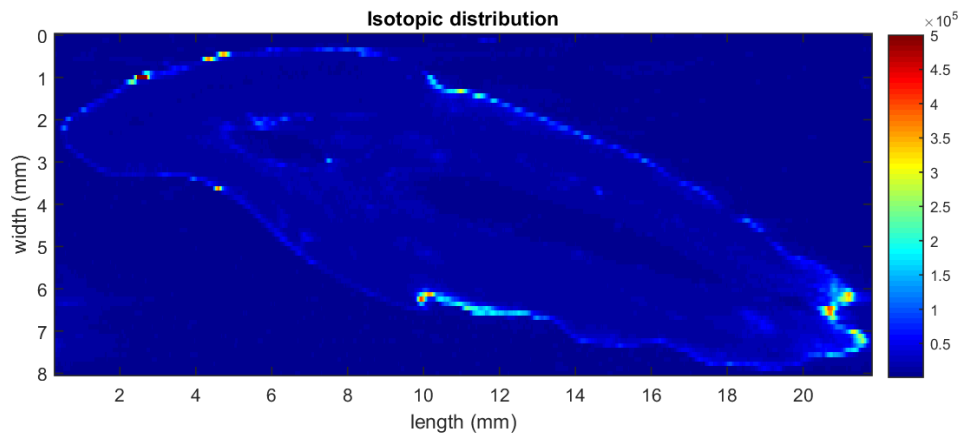


Figure 22: Example of low or poor isotopic detection (^{55}Mn) within ULI sample.

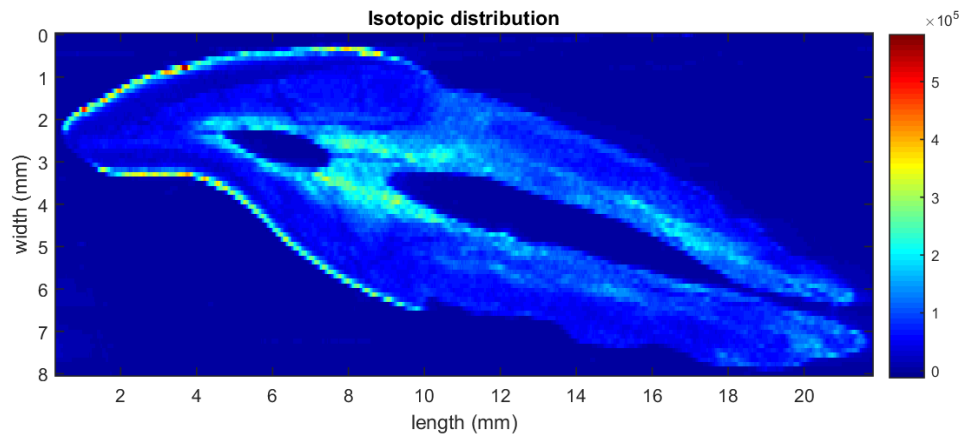


Figure 23: Example of moderate isotopic detection (^{66}Zn) within ULI sample.

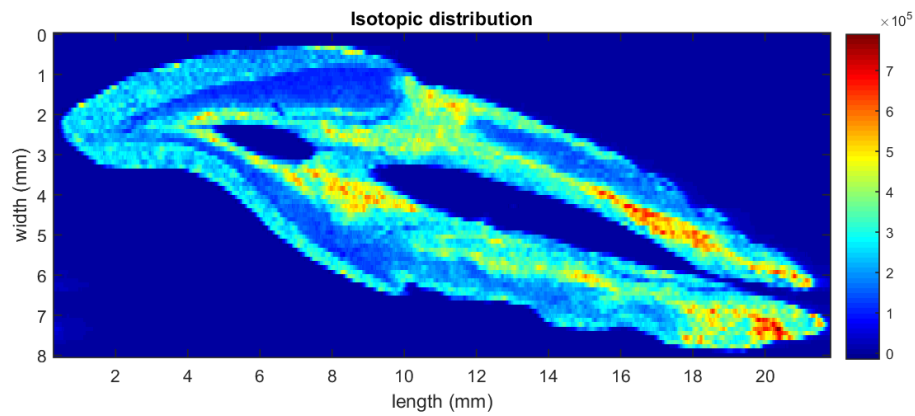


Figure 24: Example of high or good isotopic detection (^{31}P) within ULI sample.

Carbon (^{13}C)

The relative intensity of ^{13}C varied within the ULI sample, depending on the tooth location (Table 9). Both the enamel surface and within the inner enamel exhibited low intensity of ^{13}C detection. The inner dentine exhibited moderate intensity of ^{13}C detection. The EDJ exhibited low intensity of ^{13}C detection. The DPB exhibited moderate intensity of ^{13}C detection. And the outer root border exhibited low-to-moderate intensity of ^{13}C detection. Overall, the dentine surrounding both pulp borders (i.e. near the DPB)

and the dentine near the root apex exhibited the highest relative intensity of ^{13}C detection, whereas the enamel exhibited the lowest relative intensity of ^{13}C detection for this tooth type.

Magnesium (^{24}Mg)

The relative intensity of ^{24}Mg varied within the ULI sample, depending on the tooth location (Table 9). The enamel surface exhibited low intensity of ^{24}Mg detection. The inner enamel exhibited low-to-moderate intensity ^{24}Mg detection. Both the inner dentine and the EDJ exhibited moderate intensity of ^{24}Mg detection. And both the DPB and the outer root border exhibited low intensity of ^{24}Mg detection. Overall, the small area of dentine in between the two pulp borders (i.e. near the DPB) exhibited the highest relative intensity of ^{24}Mg detection, whereas the dentine near the EDJ and near the outer root border exhibited the lowest relative intensity of ^{24}Mg detection for this tooth type.

Aluminum (^{27}Al)

The relative intensity of ^{27}Al varied within the ULI sample, depending on the tooth location (Table 9). The enamel surface exhibited low intensity of ^{27}Al detection. The inner enamel, the inner dentine, and the EDJ exhibited no detection for the presence of ^{27}Al . The DPB exhibited low intensity of ^{27}Al detection. And the outer root border exhibited low-to-moderate intensity of ^{27}Al detection. Overall, the outer root border exhibited the highest relative intensity of ^{27}Al detection for this tooth type.

Phosphorus (^{31}P)

The relative intensity of ^{31}P varied within the ULI sample, depending on the tooth location (Table 9, Figure 24). The enamel surface, the inner enamel, and the inner dentine exhibited moderate intensity of ^{31}P detection. The EDJ exhibited low intensity of ^{31}P detection. The DPB exhibited low-to-moderate intensity of ^{31}P detection. And the outer root border exhibited moderate intensity of ^{31}P detection. Overall, the dentine surrounding both pulp borders (i.e. near the DPB) and some dentine near the root apex exhibited the highest relative intensity of ^{31}P detection, whereas the dentine close to the EDJ exhibited the lowest relative intensity of ^{31}P detection for this tooth type.

Calcium (^{44}Ca)

The relative intensity of ^{44}Ca varied within the ULI sample, depending on the tooth location (Table 9). The enamel surface exhibited moderate intensity of ^{44}Ca detection. The inner enamel exhibited low-to-moderate intensity of ^{44}Ca detection. The inner dentine exhibited moderate intensity of ^{44}Ca detection. The EDJ exhibited low intensity of ^{44}Ca detection. The DPB exhibited low-to-moderate intensity of ^{44}Ca detection. And the outer root border exhibited moderate intensity of ^{44}Ca detection. Overall, the dentine surrounding both pulp borders (i.e. near the DPB) and some dentine near the root apex exhibited the highest relative intensity of ^{44}Ca detection, whereas the dentine close to the EDJ exhibited the lowest relative intensity of ^{44}Ca detection for this tooth type.

Titanium (^{47}Ti)

When detected, the relative intensity of ^{47}Ti remained at a generally consistent level of intensity within the ULI sample (Table 9). The enamel surface and inner enamel exhibited low intensity of ^{47}Ti detection. The inner dentine exhibited low intensity of ^{47}Ti detection near the DPB, and there was no detection for the presence of ^{47}Ti within the inner dentine near the EDJ and outer root border. The EDJ, the DPB, and the outer root border exhibited low intensity of ^{47}Ti detection for this tooth type.

Chromium (^{52}Cr)

The relative intensity of ^{52}Cr within the ULI sample, depending on the tooth location (Table 9). The enamel surface and inner enamel exhibited low intensity of ^{52}Cr detection. The inner dentine exhibited low-to-moderate intensity of ^{52}Cr detection. Both the EDJ and the DPB exhibited low intensity of ^{52}Cr detection. And the outer root border exhibited low-to-moderate intensity of ^{52}Cr detection. Overall, the dentine near the root apex exhibited the highest relative intensity of ^{52}Cr detection, whereas the enamel exhibited the lowest relative intensity of ^{52}Cr detection for this tooth type.

Manganese (^{55}Mn)

The relative intensity of ^{55}Mn varied within the ULI sample, depending on the tooth location (Table 9, Figure 22). The enamel surface exhibited low intensity of ^{55}Mn detection. The inner enamel, the inner dentine, the EDJ, and the DPB exhibited no detection for the presence of ^{55}Mn . And the outer root border exhibited low intensity of

^{55}Mn detection. Overall, the outer root border exhibited the highest relative intensity of ^{55}Mn detection for this tooth type.

Iron (^{56}Fe)

When detected, the relative intensity of ^{56}Fe was generally consistent within the ULI sample (Table 9). The enamel surface exhibited high intensity of ^{56}Fe detection. The inner enamel, the inner dentine, and the EDJ exhibited no detection for the presence of ^{56}Fe . Both the DPB and the outer root border exhibited high intensity of ^{56}Fe detection for this tooth type.

Zinc (^{66}Zn)

The relative intensity of ^{66}Zn varied within the ULI sample, depending on the tooth location (Table 9, Figure 23). The enamel surface exhibited moderate-to-high intensity of ^{66}Zn detection. The inner enamel exhibited no detection for the presence of ^{66}Zn . The inner dentine exhibited low-to-moderate intensity of ^{66}Zn detection. The EDJ, DPB, and the outer root border exhibited low intensity of ^{66}Zn detection. Overall, enamel surface exhibited the highest relative intensity of ^{66}Zn detection for this tooth type.

Strontium (^{88}Sr)

The relative intensity of ^{88}Sr varied within the ULI sample, depending on the tooth location (Table 9). The enamel surface and inner enamel exhibited low intensity of ^{88}Sr detection. The inner dentine exhibited moderate intensity of ^{88}Sr detection. The EDJ exhibited no detection for the presence of ^{88}Sr . Both the DPB and the outer root border

exhibited moderate intensity of ^{88}Sr detection. Overall, the dentine surrounding both pulp borders (i.e. near the DPB) and some dentine near the root apex exhibited the highest relative intensity of ^{88}Sr detection, whereas the enamel exhibited the lowest relative intensity of ^{88}Sr detection for this tooth type.

Barium (^{138}Ba)

The relative intensity of ^{138}Ba varied within the ULI sample, depending on the tooth location (Table 9). The enamel surface exhibited low intensity of ^{138}Ba detection. The inner enamel exhibited no detection for the presence of ^{138}Ba . The inner dentine exhibited moderate-to-high intensity of ^{138}Ba detection. The EDJ exhibited low intensity of ^{138}Ba detection. Both the EDJ and the outer root border exhibited moderate intensity of ^{138}Ba detection. Overall, the dentine surrounding both pulp borders (i.e. near the DPB) and dentine near the root apex exhibited the highest relative intensity of ^{138}Ba detection, whereas the enamel exhibited the lowest relative intensity of ^{138}Ba detection for this tooth type.

Lead (^{208}Pb)

The relative intensity of ^{208}Pb varied within the ULI sample, depending on the tooth location (Table 9). The enamel surface exhibited moderate intensity of ^{208}Pb detection. The inner enamel exhibited no detection for the presence of ^{208}Pb . The inner dentine, the EDJ, the DPB, and the outer root border exhibited low intensity of ^{208}Pb detection. Overall, the enamel surface exhibited the highest relative intensity of ^{208}Pb detection for this tooth type.

Upper First Premolar

All thirteen elements were observed at various locations and in varying relative intensities in the UPM1 sample (n=6, refer to Table 2 in Materials and Methods section for tooth identification numbers). Table 10 provides a summary of relative intensities of elements detected for this tooth type. Figures 25, 26, and 27 depict examples of isotopic detection and distribution for this tooth type.

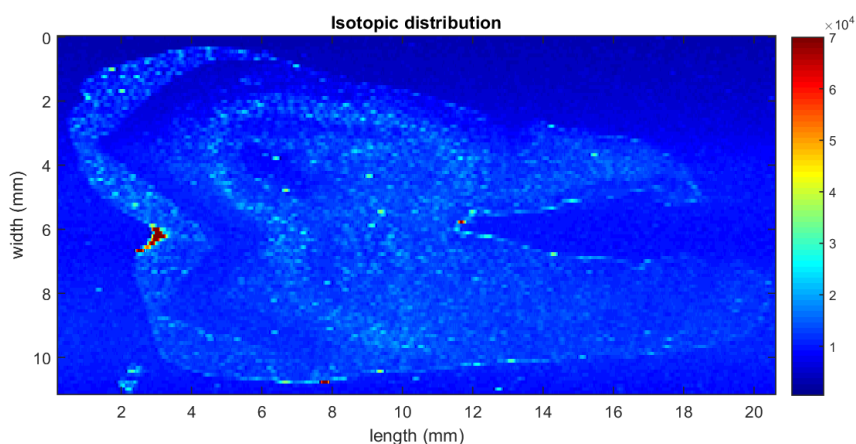


Figure 25: Example of low or poor isotopic detection (^{47}Ti) within UPM1 sample.

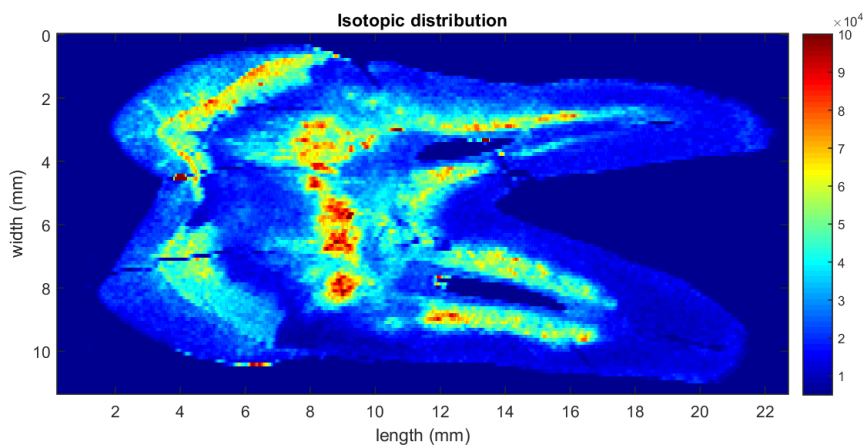


Figure 26: Example of moderate isotopic detection (^{24}Mg) within UPM1 sample.

Table 10: Summary of relative signal intensities of isotopes observed at each tooth location in the UPM1 sample (n=6).

Isotope	Enamel Surface	Inner Enamel	Inner Dentine	EDJ	DPB	Outer Root Border
¹³ C	LOW	LOW	LOW-MOD	N/A-MOD	LOW-MOD	LOW-HIGH
²⁴ Mg	LOW-MOD	LOW-MOD	MOD-HIGH	LOW-MOD	LOW-HIGH	LOW
²⁷ Al	LOW	N/A	N/A	N/A	N/A-MOD	LOW-MOD
³¹ P	LOW-MOD	LOW-MOD	MOD	LOW-MOD	LOW-MOD	MOD
⁴⁴ Ca	LOW-MOD	LOW-MOD	MOD-HIGH	LOW-MOD	LOW-MOD	MOD
⁴⁷ Ti	N/A-MOD	LOW-MOD	LOW-MOD	N/A-LOW	N/A-LOW	LOW-MOD
⁵² Cr	LOW	LOW	LOW-MOD	N/A-LOW	LOW-MOD	LOW-MOD
⁵⁵ Mn	LOW	N/A-LOW	N/A-LOW	N/A	N/A	LOW-HIGH
⁵⁶ Fe	LOW	N/A	N/A-LOW	N/A	LOW-HIGH	MOD-HIGH
⁶⁶ Zn	LOW-MOD	N/A	LOW-MOD	N/A-LOW	LOW-MOD	LOW-MOD
⁸⁸ Sr	LOW	LOW	MOD-HIGH	LOW-MOD	LOW-MOD	MOD
¹³⁸ Ba	N/A-LOW	N/A	MOD-HIGH	N/A-MOD	LOW-MOD	MOD-HIGH
²⁰⁸ Pb	LOW-MOD	N/A	N/A-LOW	N/A-LOW	LOW-HIGH	LOW-HIGH

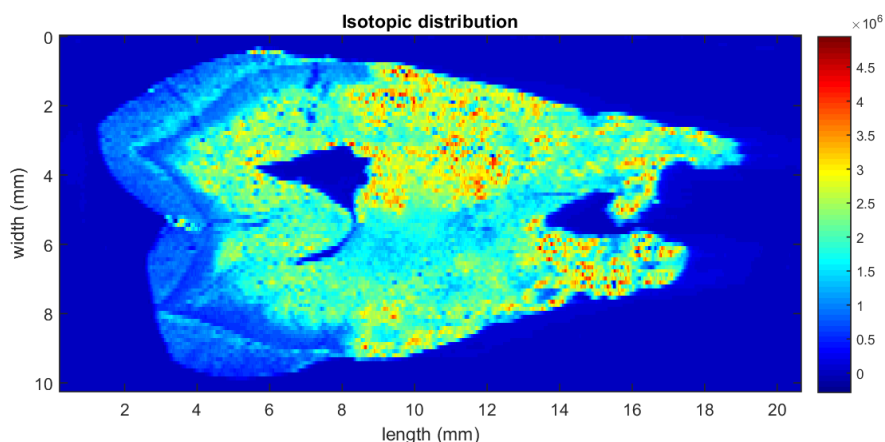


Figure 27: Example of high or good isotopic detection (^{88}Sr) within UPM1 sample.

Carbon (^{13}C)

The relative intensity of isotope ^{13}C varied within the UPM1 sample, depending on the tooth location (Table 10). Both the enamel surface and within the inner enamel exhibited low intensity of ^{13}C detection. The inner dentine exhibited low-to-moderate intensity of ^{13}C detection. The EDJ exhibited a range of no detection for the presence of ^{13}C up to moderate intensity of ^{13}C detection, depending on the individual tooth scale. The DPB exhibited low-to-moderate intensity of ^{13}C detection. And the outer root border exhibited low-to-high intensity of ^{13}C detection, depending on the individual tooth scale. Overall, the dentine surrounding the pulp border (i.e. near the DPB) and the outer root border exhibited the highest relative intensity of ^{13}C detection, whereas the enamel exhibited the lowest relative intensity of ^{13}C detection for this tooth type.

Magnesium (^{24}Mg)

The relative intensity of ^{24}Mg varied within the UPM1 sample, depending on the tooth location (Table 10, Figure 26). The enamel surface and the inner enamel exhibited low-to-moderate intensity of ^{24}Mg detection. The inner dentine exhibited moderate-to-high intensity of ^{24}Mg detection. The EDJ low-to-moderate intensity of ^{24}Mg detection. The DPB exhibited low-to-high intensity of ^{24}Mg detection, depending on the individual tooth scale. And the outer root border exhibited low intensity of ^{24}Mg detection. Overall, the dentine space near and surrounding the pulp border (i.e. the DPB) exhibited the highest relative intensity of ^{24}Mg detection, whereas the outer root border exhibited the lowest relative intensity of ^{24}Mg detection for this tooth type.

Aluminum (^{27}Al)

The relative intensity of ^{27}Al varied within the UPM1 sample, depending on the tooth location (Table 10). The enamel surface exhibited low intensity of ^{27}Al detection. The inner enamel, the inner dentine, and the EDJ exhibited no detection for the presence of ^{27}Al . The DPB exhibited a range of no detection for the presence of ^{27}Al up to moderate intensity of ^{27}Al detection, depending on the individual tooth scale. And the outer root border exhibited low-to-moderate intensity of ^{27}Al detection. Overall, the outer root border exhibited the highest relative intensity of ^{27}Al detection for this tooth type.

Phosphorus (^{31}P)

The relative intensity of ^{31}P varied within the UPM1 sample, depending on the tooth location (Table 10). The enamel surface and the inner enamel exhibited low-to-

moderate intensity of ^{31}P detection. The inner dentine exhibited moderate intensity of ^{31}P detection. The EDJ and the DPB exhibited low-to-moderate intensity of ^{31}P detection. And the outer root border exhibited moderate intensity of ^{31}P detection. Overall, the dentine space surrounding the pulp border (i.e. near the DPB) and some dentine closer to the root apex exhibited the highest relative intensity of ^{31}P detection, whereas the dentine space near or at the EDJ exhibited the lowest relative intensity of ^{31}P detection for this tooth type.

Calcium (^{44}Ca)

The relative intensity of ^{44}Ca varied within the UPM1 sample, depending on the tooth location (Table 10). The enamel surface and the inner enamel exhibited low-to-moderate intensity of ^{44}Ca detection. The inner dentine exhibited moderate-to-high intensity of ^{44}Ca detection. The EDJ and the DPB exhibited low-to-moderate intensity of ^{44}Ca detection. And the outer root border exhibited moderate intensity of ^{44}Ca detection. Overall, the dentine space surrounding the pulp border (i.e. near the DPB) and some dentine closer to the root apex exhibited the highest relative intensity of ^{44}Ca detection, whereas the dentine space near or at the EDJ exhibited the lowest relative intensity of ^{44}Ca detection for this tooth type.

Titanium (^{47}Ti)

When detected, the relative intensity of isotope titanium-47 (^{47}Ti) remained at a generally consistent level of intensity within each tooth in the UPM1 sample (Table 10, Figure 25). The enamel surface exhibited a range of no detection for the presence of ^{47}Ti

up to moderate intensity of ^{47}Ti detection. The inner enamel and the inner dentine exhibited low-to-moderate intensity of ^{47}Ti detection. Both the EDJ and the DPB exhibited either no detection for the presence of ^{47}Ti or low intensity of ^{47}Ti detection, depending on the individual tooth scale. And the outer root border exhibited low-to-moderate intensity of ^{47}Ti detection for this tooth type.

Chromium (^{52}Cr)

The relative intensity of ^{52}Cr within the UPM1 sample, depending on the tooth location (Table 10). The enamel surface and inner enamel exhibited low intensity of ^{52}Cr detection. The inner dentine exhibited low-to-moderate intensity of ^{52}Cr detection. The EDJ exhibited either no detection for the presence of ^{52}Cr or low intensity of ^{52}Cr detection, depending on the individual tooth scale. Both the DPB and the outer root border exhibited low-to-moderate intensity of ^{52}Cr detection. Overall, the dentine space near the root apex exhibited the highest relative intensity of ^{52}Cr detection, whereas the enamel exhibited the lowest relative intensity of ^{52}Cr detection for this tooth type.

Manganese (^{55}Mn)

The relative intensity of ^{55}Mn varied within the UPM1 sample, depending on the tooth location (Table 10). The enamel surface exhibited low intensity of ^{55}Mn detection. Both the inner enamel and the inner dentine exhibited either no detection for the presence of ^{55}Mn or low intensity of ^{55}Mn detection, depending on the individual tooth scale. The EDJ and the DPB exhibited no detection for the presence of ^{55}Mn . And the outer root border exhibited low-to-high intensity of ^{55}Mn detection, depending on the individual

tooth scale. Overall, the outer root border exhibited the highest relative intensity of ^{55}Mn detection for this tooth type.

Iron (^{56}Fe)

The relative intensity of ^{56}Fe varied within the UPM1 sample, depending on the tooth location (Table 10). The enamel surface exhibited low intensity of ^{56}Fe detection. The inner enamel exhibited no detection for the presence of ^{56}Fe . The inner dentine exhibited either no detection for the presence of ^{56}Fe or low intensity of ^{56}Fe detection, depending on the individual tooth scale. The EDJ exhibited no detection for the presence of ^{56}Fe . The DPB exhibited low-to-high intensity of ^{56}Fe detection, depending on the individual tooth scale. And the outer exhibited moderate-to-high intensity of ^{56}Fe detection for this tooth type.

Zinc (^{66}Zn)

The relative intensity of ^{66}Zn varied within the UPM1 sample, depending on the tooth location (Table 10). The enamel surface exhibited low-to-moderate intensity of ^{66}Zn detection. The inner enamel exhibited no detection for the presence of ^{66}Zn . The inner dentine exhibited low-to-moderate intensity of ^{66}Zn detection. The EDJ exhibited either no detection for the presence of ^{66}Zn or low intensity of ^{66}Zn detection, depending on the individual tooth scale. Both the DPB and the outer root border exhibited low-to-moderate intensity of ^{66}Zn detection. Overall, dentine space surrounding near and at the DPB exhibited the highest relative intensity of ^{66}Zn detection for this tooth type

Strontium (^{88}Sr)

The relative intensity of ^{88}Sr varied within the UPM1 sample, depending on the tooth location (Table 10, Figure 27). The enamel surface and inner enamel exhibited low intensity of ^{88}Sr detection. The inner dentine exhibited moderate-to-high intensity of ^{88}Sr detection. The EDJ and the DPB exhibited low-to-moderate intensity of ^{88}Sr detection. And the outer root border exhibited moderate intensity of ^{88}Sr detection. Overall, the dentine space surrounding the pulp border (i.e. near the DPB) and some dentine closer to the root apex exhibited the highest relative intensity of ^{88}Sr detection, whereas the enamel exhibited the lowest relative intensity of ^{88}Sr detection for this tooth type.

Barium (^{138}Ba)

The relative intensity of ^{138}Ba varied within the UPM1 sample, depending on the tooth location (Table 10). The enamel surface exhibited either no detection for the presence ^{138}Ba or low intensity of ^{138}Ba detection, depending on the individual tooth scale. The inner enamel exhibited no detection for the presence of ^{138}Ba . The inner dentine exhibited moderate-to-high intensity of ^{138}Ba detection. The EDJ exhibited a range of either no detection for the presence ^{138}Ba up to moderate intensity of ^{138}Ba detection, depending on the individual tooth scale. The EDJ exhibited low-to-moderate intensity of ^{138}Ba detection. And the outer root border exhibited moderate-to-high intensity of ^{138}Ba detection. Overall, the dentine space surrounding the pulp border (i.e. near the DPB) and the outer root border exhibited the highest relative intensity of ^{138}Ba detection, whereas the enamel exhibited the lowest relative intensity of ^{138}Ba detection for this tooth type.

Lead (^{208}Pb)

The relative intensity of ^{208}Pb varied within the UPM1 sample, depending on the tooth location (Table 10). The enamel surface exhibited low-to-moderate intensity of ^{208}Pb detection. The inner enamel exhibited no detection for the presence of ^{208}Pb . Both the inner dentine and the EDJ exhibited either no detection for the presence ^{208}Pb or low intensity of ^{208}Pb detection, depending on the individual tooth scale. And both the DPB and the outer root border exhibited low-to-high intensity of ^{208}Pb detection, depending on the individual tooth scale. Overall, the outer root border highest relative intensity of ^{208}Pb detection, whereas the inner enamel exhibited the lowest relative intensity of ^{208}Pb detection for this tooth type.

Upper Second Premolar

All thirteen elements were observed at various locations and in varying relative intensities in the UPM2 sample (n=7, refer to Table 2 in Materials and Methods section for tooth identification numbers). Table 11 provides a summary of relative intensities of elements detected for this tooth type. Figures 28, 29, and 30 depict examples of isotopic detection and distribution for this tooth type.

Carbon (^{13}C)

The relative intensity of ^{13}C varied within the UPM2 sample, depending on the tooth location (Table 11). Both the enamel surface and within the inner enamel exhibited low intensity of ^{13}C detection. The inner dentine exhibited low-to-moderate intensity of ^{13}C detection. The EDJ exhibited either no detection for the presence of ^{13}C or low

intensity of ^{13}C detection, depending on the individual tooth scale. The DPB exhibited low-to-moderate intensity of ^{13}C detection. And the outer root border exhibited low-to-high intensity of ^{13}C detection, depending on the individual tooth scale. Overall, the dentine surrounding the pulp border (i.e. near the DPB) and the dentine near the root apex exhibited the highest relative intensity of ^{13}C detection, whereas the enamel exhibited the lowest relative intensity of ^{13}C detection for this tooth type.

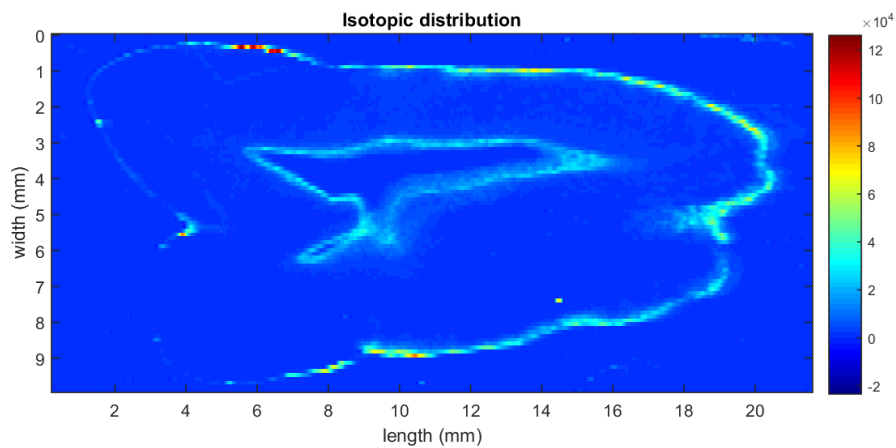


Figure 28: Example of low or poor isotopic detection (^{208}Pb) within UPM2 sample.

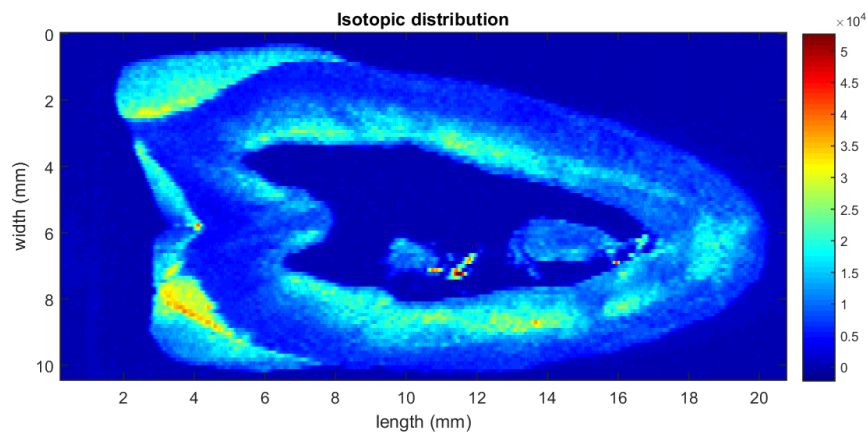


Figure 29: Example of moderate isotopic detection (^{24}Mg) within UPM2 sample.

Table 11: Summary of relative signal intensities of isotopes observed at each tooth location in the UPM2 sample (n=7).

Isotope	Enamel Surface	Inner Enamel	Inner Dentine	EDJ	DPB	Outer Root Border
¹³ C	LOW	LOW	LOW-MOD	N/A-LOW	LOW-MOD	LOW-HIGH
²⁴ Mg	LOW-MOD	LOW-MOD	LOW-MOD	LOW-HIGH	LOW-HIGH	N/A-LOW
²⁷ Al	LOW	N/A	N/A-LOW	N/A	LOW-MOD	LOW-HIGH
³¹ P	LOW-MOD	LOW-MOD	MOD-HIGH	N/A-MOD	MOD	LOW-MOD
⁴⁴ Ca	LOW-MOD	LOW-HIGH	MOD-HIGH	LOW-MOD	LOW-HIGH	MOD
⁴⁷ Ti	LOW	N/A-LOW	N/A-LOW	N/A-LOW	N/A-LOW	LOW
⁵² Cr	LOW	LOW	N/A-LOW	N/A-LOW	N/A-LOW	LOW-MOD
⁵⁵ Mn	LOW-HIGH	N/A-LOW	N/A-LOW	N/A-LOW	N/A-LOW	MOD-HIGH
⁵⁶ Fe	LOW-HIGH	N/A	N/A-LOW	N/A	LOW-HIGH	MOD-HIGH
⁶⁶ Zn	MOD-HIGH	N/A	LOW-MOD	N/A-LOW	LOW-HIGH	LOW-MOD
⁸⁸ Sr	N/A-LOW	N/A-LOW	MOD-HIGH	LOW-MOD	MOD	MOD
¹³⁸ Ba	N/A-LOW	N/A	MOD-HIGH	N/A-MOD	MOD	MOD
²⁰⁸ Pb	LOW-MOD	N/A	N/A-LOW	N/A-LOW	LOW-HIGH	MOD-HIGH

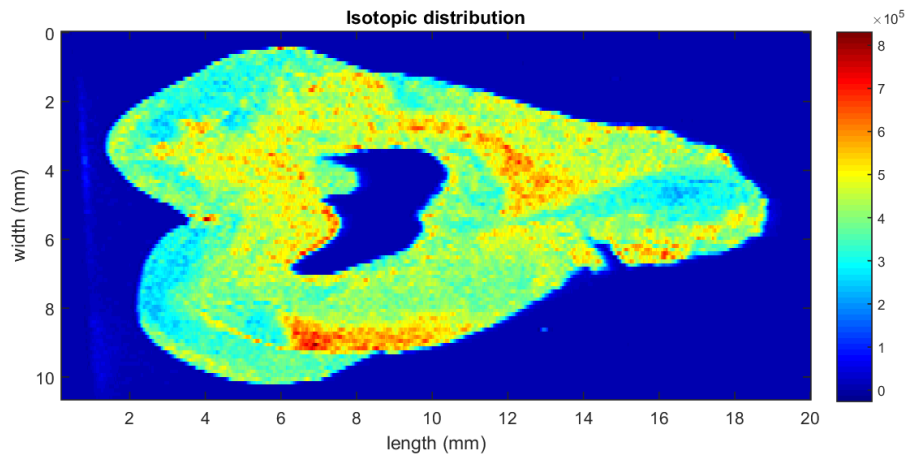


Figure 30: Example of high or good isotopic detection (^{44}Ca) within UPM2 sample.

Magnesium (^{24}Mg)

The relative intensity of ^{24}Mg varied within the UPM2 sample, depending on the tooth location (Table 11, Figure 29). The enamel surface, the inner enamel, and the inner dentine exhibited low-to-moderate intensity of ^{24}Mg detection. Both the EDJ and the DPB exhibited low-to-high intensity ^{24}Mg detection, depending on the individual tooth scale. And the outer root border exhibited either no detection for the presence of ^{24}Mg or low intensity of ^{24}Mg detection, depending on the individual tooth scale. Overall, the dentine space surrounding the pulp border (i.e. near the DPB, but not the DPB itself) exhibited the highest relative intensity of ^{24}Mg detection, whereas the outer root border exhibited the lowest relative intensity of ^{24}Mg detection for this tooth type.

Aluminum (^{27}Al)

The relative intensity of ^{27}Al varied within the UPM2 sample, depending on the tooth location (Table 11). The enamel surface exhibited low intensity of ^{27}Al detection.

The inner enamel exhibited no detection for the presence of ^{27}Al . The inner dentine exhibited either no detection for the presence of ^{27}Al or low intensity of ^{27}Al detection, depending on the individual tooth scale. The EDJ also exhibited no detection for the presence of ^{27}Al . The DPB exhibited low-to-moderate intensity of ^{27}Al detection. And the outer root border exhibited low-to-high intensity of ^{27}Al detection, depending on the individual tooth scale. Overall, the outer root border exhibited the highest relative intensity of ^{27}Al detection for this tooth type.

Phosphorus (^{31}P)

The relative intensity of ^{31}P varied within the UPM2 sample, depending on the tooth location (Table 11). The enamel surface and the inner enamel exhibited low-to-moderate intensity of ^{31}P detection. The inner dentine exhibited moderate-to-high intensity of ^{31}P detection. The EDJ exhibited a range from no detection for the presence of ^{31}P to moderate intensity of ^{31}P detection, depending on the individual tooth scale. The DPB exhibited moderate intensity of ^{31}P detection. And the outer root border exhibited low-to-moderate intensity of ^{31}P detection. Overall, the dentine space surrounding the pulp border (i.e. near the DPB) and some dentine closer to the root apex exhibited the highest relative intensity of ^{31}P detection, whereas the dentine space near or at the EDJ exhibited the lowest relative intensity of ^{31}P detection for this tooth type.

Calcium (^{44}Ca)

The relative intensity of ^{44}Ca varied within the UPM2 sample, depending on the tooth location (Table 11, Figure 30). The enamel surface exhibited low-to-moderate

intensity of ^{44}Ca detection. The inner enamel exhibited low-to-high intensity of ^{44}Ca detection, depending on the individual tooth scale. The inner dentine exhibited moderate-to-high intensity of ^{44}Ca detection. The EDJ exhibited low-to-moderate intensity of ^{44}Ca detection. The DPB exhibited low-to-high intensity of ^{44}Ca detection, depending on the individual tooth scale. And the outer root border exhibited moderate intensity of ^{44}Ca detection. Overall, the dentine space surrounding the pulp border (i.e. near the DPB) and some dentine closer to the root apex exhibited the highest relative intensity of ^{44}Ca detection, whereas the dentine space near or at the EDJ exhibited the lowest relative intensity of ^{44}Ca detection for this tooth type.

Titanium (^{47}Ti)

When detected, the relative intensity of ^{47}Ti remained at a generally consistent level of intensity within each tooth in the UPM2 sample (Table 11). The enamel surface exhibited low intensity of ^{47}Ti detection. The inner enamel, the inner dentine, the EDJ, and the DPB all exhibited either no detection for the presence of ^{47}Ti or low intensity of ^{47}Ti detection, depending on the individual tooth scale. And the outer root border exhibited low intensity of ^{47}Ti detection for this tooth type.

Chromium (^{52}Cr)

The relative intensity of ^{52}Cr within the UPM2 sample, depending on the tooth location (Table 11). The enamel surface and inner enamel exhibited low intensity of ^{52}Cr detection. The inner dentine, the EDJ, and the DPB exhibited either no detection for the presence of ^{52}Cr or low intensity of ^{52}Cr detection, depending on the individual tooth

scale. And the outer root border exhibited low-to-moderate intensity of ^{52}Cr detection. Overall, the dentine space near the root apex exhibited the highest relative intensity of ^{52}Cr detection, whereas the enamel exhibited the lowest relative intensity of ^{52}Cr detection for this tooth type.

Manganese (^{55}Mn)

The relative intensity of ^{55}Mn varied within the UPM2 sample, depending on the tooth location (Table 11). The enamel surface exhibited low-to-high intensity of ^{55}Mn detection, depending on the individual tooth scale. The inner enamel, the inner dentine, the EDJ, and the DPB all exhibited either no detection for the presence of ^{55}Mn or low intensity of ^{55}Mn detection, depending on the individual tooth scale. And the outer root border exhibited moderate-to-high intensity of ^{55}Mn detection. Overall, the outer root border exhibited the highest relative intensity of ^{55}Mn detection for this tooth type.

Iron (^{56}Fe)

The relative intensity of ^{56}Fe varied within the UPM2 sample, depending on the tooth location (Table 11). The enamel surface exhibited low-to-high intensity of ^{56}Fe detection, depending on the individual tooth scale. The inner enamel exhibited no detection for the presence of ^{56}Fe . The inner dentine exhibited either no detection for the presence of ^{56}Fe or low intensity of ^{56}Fe detection, depending on the individual tooth scale. The EDJ exhibited no detection for the presence of ^{56}Fe . The DPB exhibited low-to-high intensity of ^{56}Fe detection, depending on the individual tooth scale. And the outer exhibited moderate-to-high intensity of ^{56}Fe detection for this tooth type.

Zinc (^{66}Zn)

The relative intensity of ^{66}Zn varied within the UPM2 sample, depending on the tooth location (Table 11). The enamel surface exhibited moderate-to-high intensity of ^{66}Zn detection. The inner enamel exhibited no detection for the presence of ^{66}Zn . The inner dentine exhibited low-to-moderate intensity of ^{66}Zn detection. The EDJ exhibited either no detection for the presence of ^{66}Zn or low intensity of ^{66}Zn detection, depending on the individual tooth scale. The DPB exhibited low-to-high intensity of ^{66}Zn detection, depending on the individual tooth scale. And the outer root border exhibited low-to-moderate intensity of ^{66}Zn detection. Overall, dentine space surrounding near and at the DPB exhibited the highest relative intensity of ^{66}Zn detection for this tooth type

Strontium (^{88}Sr)

The relative intensity of ^{88}Sr varied within the UPM2 sample, depending on the tooth location (Table 11). The enamel surface and inner enamel exhibited either no detection for the presence of ^{88}Sr or low intensity of ^{88}Sr detection, depending on the individual tooth scale. The inner dentine exhibited moderate-to-high intensity of ^{88}Sr detection. The EDJ exhibited low-to-moderate intensity of ^{88}Sr detection. Both the DPB and the outer root border exhibited moderate intensity of ^{88}Sr detection. Overall, the dentine space surrounding the pulp border (i.e. near the DPB) and some dentine closer to the root apex exhibited the highest relative intensity of ^{88}Sr detection, whereas the enamel exhibited the lowest relative intensity of ^{88}Sr detection for this tooth type.

Barium (^{138}Ba)

The relative intensity of ^{138}Ba varied within the UPM2 sample, depending on the tooth location (Table 11). The enamel surface exhibited either no detection for the presence ^{138}Ba or low intensity of ^{138}Ba detection, depending on the individual tooth scale. The inner enamel exhibited no detection for the presence of ^{138}Ba . The inner dentine exhibited moderate-to-high intensity of ^{138}Ba detection. The EDJ exhibited a range of either no detection for the presence ^{138}Ba up to moderate intensity of ^{138}Ba detection, depending on the individual tooth scale. Both the EDJ and the outer root border exhibited moderate intensity of ^{138}Ba detection. Overall, the dentine space surrounding the pulp border (i.e. near the DPB) and some dentine closer to the root apex exhibited the highest relative intensity of ^{138}Ba detection, whereas the enamel exhibited the lowest relative intensity of ^{138}Ba detection for this tooth type.

Lead (^{208}Pb)

The relative intensity of ^{208}Pb varied within the UPM2 sample, depending on the tooth location (Table 11, Figure 28). The enamel surface exhibited low-to-moderate intensity of ^{208}Pb detection. The inner enamel exhibited no detection for the presence of ^{208}Pb . The inner dentine and the EDJ exhibited either no detection for the presence ^{208}Pb or low intensity of ^{208}Pb detection, depending on the individual tooth scale. The DPB exhibited low-to-high intensity of ^{208}Pb detection, depending on the individual tooth scale. And the outer root border exhibited moderate-to-high intensity of ^{208}Pb detection. Overall, the outer root border highest relative intensity of ^{208}Pb detection, whereas the inner enamel exhibited the lowest relative intensity of ^{208}Pb detection for this tooth type.

Frequency of Detection by Tooth Type

The relative frequencies of certain isotopes detected were similar in frequency across all tooth types, with other isotopes exhibited some variations based on tooth type in the sample group (Figures 31 and 32). Relative frequencies of isotopes detected at low, moderate, and high intensities were calculated and are presented in Figure 31. In addition, averages and ranges of frequencies of low, moderate, and high intensity detection across all tooth types were calculated, and the results are presented in Table 12.

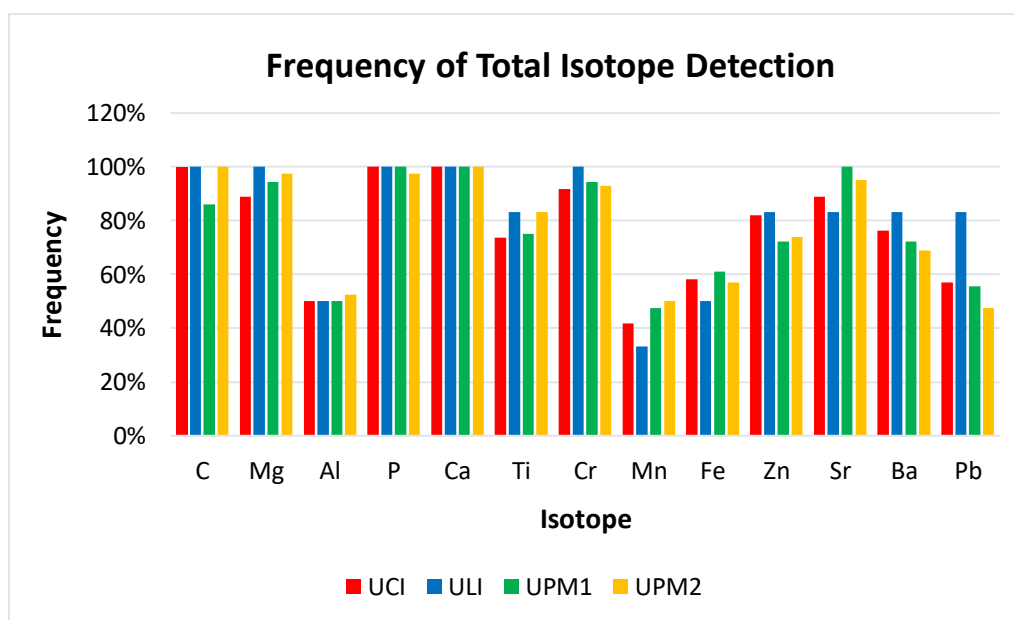


Figure 31: Total frequency of all isotopes detected based on tooth type. This included detection of low, moderate, and high intensities per tooth.

For low, moderate, and high intensities of ^{13}C detection, the UCI, ULI and UPM2 samples all had a maximum frequency of detection at 100%, whereas the UPM1 sample had 86% frequency of detection. For ^{24}Mg , UCI had 89% frequency of detection, and ULI had the highest frequency at 100% frequency of detection. UPM1 had 94%

frequency of detection, and UPM2 had 98% frequency of detection for ^{24}Mg . For ^{27}Al , UCI, ULI, and UPM1 all had 50% frequency of detection, and UPM2 had the highest frequency at 52% frequency of detection. For ^{31}P , UCI, ULI, and UPM1 all had 100% frequency of detection, whereas UPM2 had the lowest frequency at 98% frequency of detection. For ^{44}Ca , all tooth types had 100% frequency of detection.

For ^{47}Ti , UCI had the lowest frequency at 74% frequency of detection, and UPM1 had 75% frequency of detection; ULI and UPM2 had the highest frequency at 83% frequency of detection for ^{47}Ti . For ^{52}Cr , UCI had the lowest frequency at 92% frequency of detection, and ULI had the highest frequency at 100% frequency of detection. UPM1 had 94% frequency of detection, and UPM2 had 93% frequency of detection for ^{52}Cr . For ^{55}Mn , UCI had 42% frequency of detection, ULI had the lowest frequency at 33% frequency of detection, UPM1 had 48% frequency of detection, and UPM2 had the highest frequency at 50% frequency of detection.

For ^{56}Fe , UCI had 58% frequency of detection, ULI had the lowest frequency at 50% frequency of detection, UPM1 had the highest frequency at 61% frequency of detection, and UPM2 had 57% frequency of detection. For ^{66}Zn , UCI had 82% frequency of detection, ULI had the highest frequency at 83% frequency of detection, UPM1 had the lowest frequency at 72% frequency detection, and UPM2 had 74% frequency of detection. For ^{88}Sr , UCI had 89% frequency of detection, ULI had the lowest frequency at 83% frequency of detection, UPM1 had the highest frequency at 100% frequency of detection, and UPM2 had 95% frequency of detection. For ^{138}Ba , UCI had 76% frequency of detection, ULI had the highest frequency at 83% frequency of detection, UPM1 had 72% frequency of detection, and UPM2 had the lowest frequency at 69%

frequency of detection. For ^{208}Pb , UCI had 57% frequency of detection, ULI had the highest frequency at 83% frequency of detection, UPM1 had 56% frequency of detection, and UPM2 had the lowest frequency at 48% frequency of detection.

Table 12: Calculated averages and ranges of frequencies of isotope detection across all teeth (N=26) for low, moderate, and high intensities.

Isotope	Average	Maximum	Minimum	Range
^{13}C	97%	100%	86%	14%
^{24}Mg	95%	100%	94%	6%
^{27}Al	51%	52%	50%	2%
^{31}P	99%	100%	98%	2%
^{44}Ca	100%	100%	100%	0%
^{47}Ti	79%	83%	75%	8%
^{52}Cr	95%	100%	93%	7%
^{55}Mn	43%	50%	33%	17%
^{56}Fe	57%	61%	50%	11%
^{66}Zn	78%	83%	72%	11%
^{88}Sr	92%	100%	83%	17%
^{138}Ba	75%	83%	69%	14%
^{208}Pb	61%	83%	48%	36%

Relative frequencies of isotopes detected at only moderate and high intensities were also calculated and are presented in Figure 32. Averages and ranges of frequencies of moderate and high intensity detection across all tooth types were calculated, with results presented in Table 13. In addition, a summary of tooth types exhibiting the highest frequency of detection of each isotope at each intensity is also presented in Table 14.

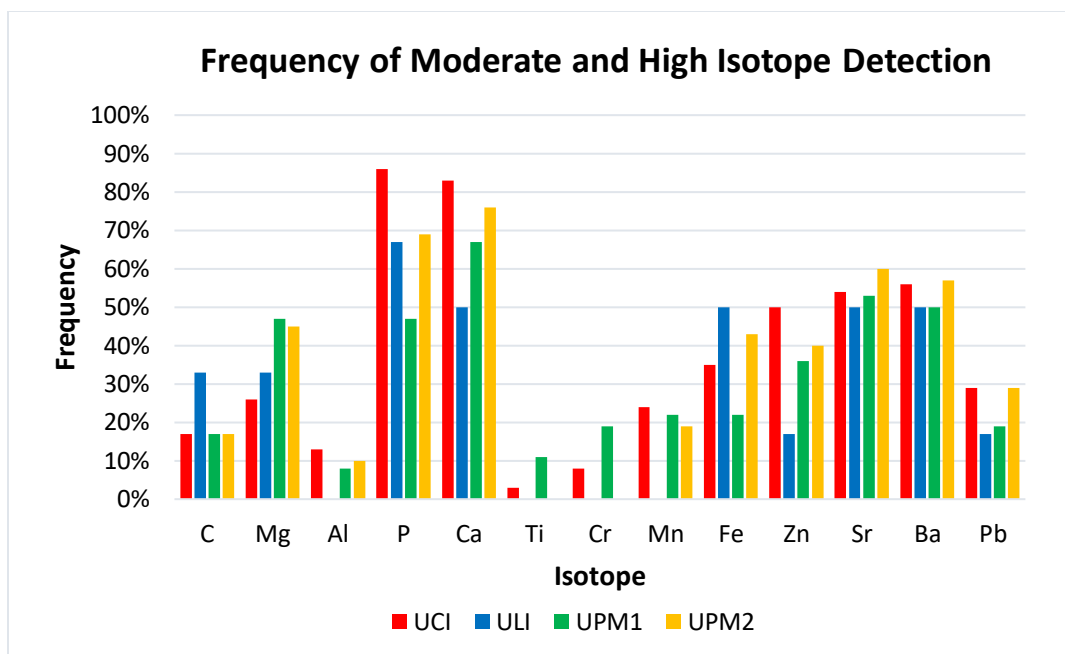


Figure 32: Frequency of all isotopes detected based on tooth type. This included detection of only moderate and high intensities per tooth.

For moderate-to-high detection of ^{13}C , the UCI, UPM1, and UPM2 samples all had 17% frequency of detection, whereas the ULI sample had the highest frequency at 33% frequency of detection. For ^{24}Mg , UCI had the least amount of detection with 26% frequency of detection, ULI had 33% frequency of detection, UPM1 had the highest frequency at 47% frequency of detection, and UPM2 had 45% frequency of detection. For ^{27}Al , UCI had the highest frequency at 13% frequency of detection, while ULI had a no moderate-to-high detection of ^{27}Al . UPM1 had 8% frequency of detection, and UPM2 had 10% frequency of detection for ^{27}Al . For ^{31}P , UCI had the highest frequency at 86% frequency of detection, ULI had 67% frequency of detection, UPM1 had the lowest frequency at 47% frequency of detection, and UPM2 had 69% frequency of detection. For ^{44}Ca , UCI had the highest frequency at 83% frequency of detection, and ULI had the

lowest frequency at 50% frequency of detection. UPM1 had 67% frequency of detection, and UPM2 had 76% frequency of detection for ^{44}Ca .

For ^{47}Ti , UCI had 3% frequency of detection, and UPM1 had the highest frequency at 11% frequency of detection. Both ULI and UPM2 had no moderate-to-high detection of ^{47}Ti . For ^{52}Cr , UCI had 8% frequency of detection, and UPM1 had the highest frequency at 19% frequency of detection. Both ULI and UPM2 had no moderate-to-high detection of ^{52}Cr . For ^{55}Mn , UCI had the highest frequency at 24% frequency of detection, while ULI had a no moderate-to-high detection of ^{55}Mn . UPM1 had 22% frequency of detection, and UPM2 had 19% frequency of detection for ^{55}Mn .

For ^{56}Fe , UCI had 35% frequency of detection, ULI had the highest frequency at 50% frequency of detection, UPM1 had the lowest frequency at 22% frequency of detection, and UPM2 had 43% frequency of detection. For ^{66}Zn , UCI had the highest frequency at 50% frequency of detection, while ULI had the lowest frequency at 17% frequency of detection. UPM1 had 36% frequency of detection, and UPM2 had 40% frequency of detection for ^{66}Zn .

For ^{88}Sr , UCI had 54% frequency of detection, ULI had the lowest frequency at 50% frequency of detection, UPM1 had 53% frequency of detection, and UPM2 had the highest frequency at 60% frequency of detection. For ^{138}Ba , UCI had 56% frequency of detection, ULI and UPM1 both had the lowest frequency at 50% frequency of detection, and UPM2 had the highest frequency at 57% frequency of detection. For ^{208}Pb , UCI and UPM2 both had the highest frequency at 29% frequency of detection. ULI had the lowest frequency at 17% frequency of detection, and UPM1 had 19% frequency of detection for ^{208}Pb .

Table 13: Calculated averages and ranges of frequencies of isotope detection across all teeth (N=26) for moderate and high intensities only.

Isotope	Average	Maximum	Minimum	Range
¹³ C	21%	33%	17%	16%
²⁴ Mg	28%	47%	33%	14%
²⁷ Al	8%	13%	0%	13%
³¹ P	67%	86%	47%	39%
⁴⁴ Ca	69%	83%	50%	33%
⁴⁷ Ti	4%	11%	0%	11%
⁵² Cr	7%	19%	0%	19%
⁵⁵ Mn	16%	24%	0%	24%
⁵⁶ Fe	38%	50%	22%	28%
⁶⁶ Zn	36%	50%	17%	33%
⁸⁸ Sr	54%	60%	50%	10%
¹³⁸ Ba	53%	57%	50%	7%
²⁰⁸ Pb	24%	29%	17%	12%

Table 14: Summary of tooth types exhibiting the highest frequency of detection of each isotope. **Bold text** indicates that this tooth type had the highest frequency of detection of the isotope in both categories

Isotope	Highest Frequency of Detection of Low, Moderate, and High Intensities	Highest Frequency of Detection of Moderate and High Intensities Only
¹³ C	UCI, ULI , UPM2	ULI
²⁴ Mg	ULI	UPM2
²⁷ Al	UPM2	UCI
³¹ P	UCI , ULI, UPM1	UCI
⁴⁴ Ca	UCI , ULI, UPM1, UPM2	UCI
⁴⁷ Ti	ULI	UPM1
⁵² Cr	ULI	UPM1
⁵⁵ Mn	UPM2	UCI
⁵⁶ Fe	UPM1	ULI
⁶⁶ Zn	ULI	UCI
⁸⁸ Sr	UPM1	UPM2
¹³⁸ Ba	ULI	UPM2
²⁰⁸ Pb	ULI	UCI, UPM2

CHAPTER FIVE: DISCUSSION

Because tooth enamel and dentine have different chemical and structural makeups, it is expected that maps produced would exhibit heterogeneous distribution and relative intensities of isotopes within the tooth. In addition, due to differences in isotope bioavailability and dental tissue physiology, some variation in isotope detection was expected across all teeth samples. Factors and implications of detected isotopic variations are discussed in the following sections.

Relative Intensities of Isotopes by Tooth Location

All isotopes were generally detected at a minimum of low intensity for all teeth. By focusing on only moderate and high intensities, the variations between teeth become clearer. This allows for better characterization of the teeth and more precise interpretation of any disparities exhibited in the presence and distribution of these trace isotopes.

Results of analysis and maps produced demonstrate that overall the most common areas in the tooth exhibiting the highest intensity of isotopic detection (i.e. moderate-to-high intensity) are in the inner dentine and at the outer root border (Table 6 and Table 7). In general, selected isotopes were detected at the highest intensity (i.e. moderate to high only) and in the greatest total frequency at the following tooth locations in descending order: outer root border > DPB > inner dentine > enamel surface > EDJ > inner enamel (Figure 33). There is a similar relationship between the moderate and high detections, with the outer root border being the most common area of moderate to high intensity. In comparison, the inner enamel and EDJ had the least amount of moderate to high intensity

detection, as these instead were areas containing low intensity detection for the majority of isotopes (Figure 33).

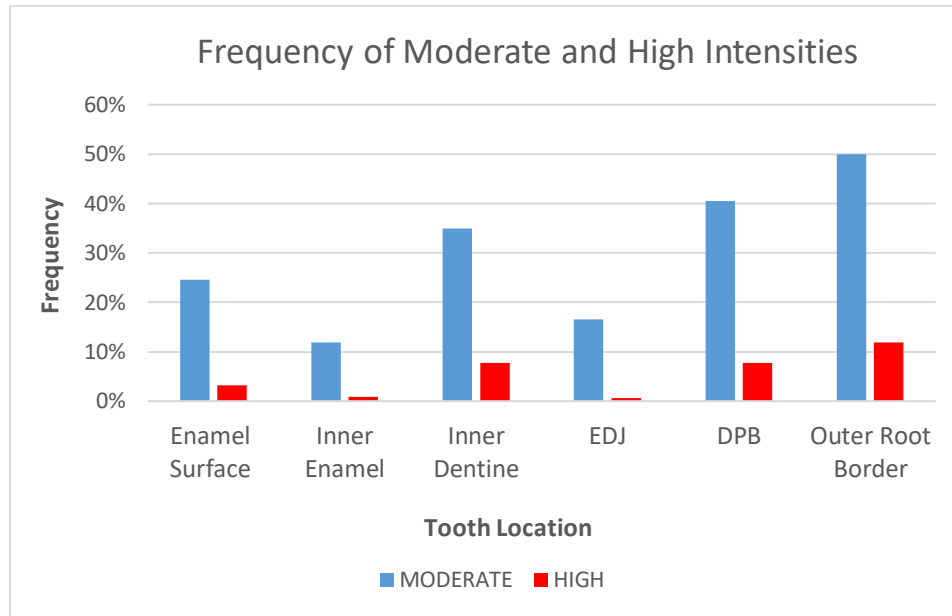


Figure 33: Frequencies of isotopes detected at only moderate and high intensities at each tooth location across entire sample (N=26).

In general, the overall relative intensity and frequency of detection increases from the anatomically outer portion of the tooth (i.e. enamel surface) to the inner portion (i.e. inner dentine and root border), which is in agreement with previous bioarchaeological and dentistry literature (Farell et al., 2013 Guede et al., 2017; Hanć et al., 2013) (Figure 33). The exception to this is ^{66}Zn , which shows a less consistent distribution, with its overall detection occurring at the following locations in descending order: enamel surface > DPB > outer root border > inner dentine > inner enamel / EDJ (Figure 33).

Overall, nonessential isotope ^{138}Ba had the smallest range of frequency detection for moderate to high intensities (range of 50-57%, Table 13), whereas major and essential

isotope ^{31}P had the greatest range of frequency detection for moderate to high intensities (range of 47-86%, Table 13).

Most isotopes, whether essential or nonessential, were detected at moderate to high intensities the most at the inner dentine and the outer root border, according to their individual biochemical properties (Asaduzzaman et al., 2017) (Table 7, Figure 34). Essential isotopes ^{24}Mg , ^{31}P , and ^{44}Ca were detected the most in the inner dentine, while essential isotopes ^{55}Mn and ^{56}Fe were detected the most at the outer root border. ^{13}C was detected in equal frequency at the inner dentine and outer root border. In comparison, nonessential isotopes ^{27}Al , ^{47}Ti , ^{52}Cr , and ^{208}Pb were detected the most at the outer root border, while ^{88}Sr and ^{138}Ba were detected in equal frequency at the inner dentine and outer root border. As mentioned above, the exception to this pattern of detection is ^{66}Zn , which was the only isotope to have most moderate and high intensity detection occurring at the enamel surface, in comparison to the inner parts of the tooth (Table 7, Figure 35).

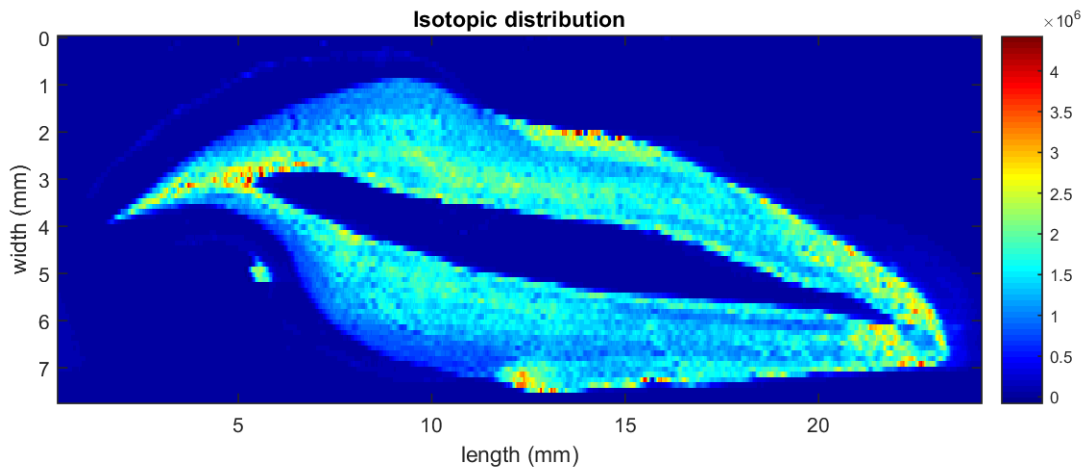


Figure 34: Example of ^{138}Ba distribution in the tooth (sample N10-4/46C Large UCI), showing highest relative intensity occurring at the inner dentine and outer root border.

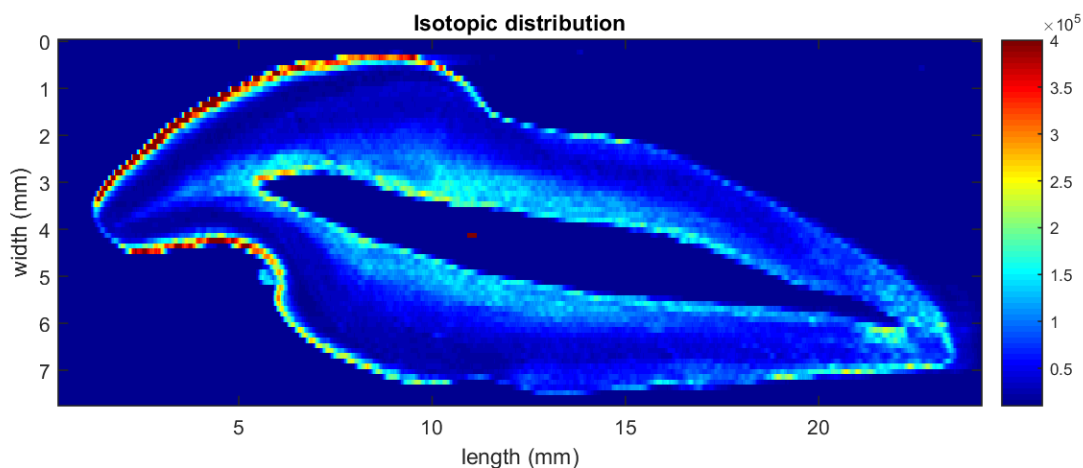


Figure 35: Example of ^{66}Zn distribution in the tooth (sample N10-4/46C Large UCI), showing highest relative intensity occurring at the enamel surface.

Overall, the enamel surface had the highest frequency of low intensity detection of all isotopes across all teeth (N=26) (Figure 13). In general, most nonessential isotopes (i.e. isotopes of nonessential trace elements analyzed in this study) were detected at lower intensities, while essential isotopes were detected at higher intensities at the enamel surface. For example, nonessential isotopes ^{27}Al , ^{52}Cr , ^{88}Sr , ^{138}Ba were all detected at low intensity. In comparison, most essential isotopes ^{31}P , ^{44}Ca , ^{55}Mn , ^{56}Fe , and ^{66}Zn all exhibited a range of low to high intensity detection at the enamel surface, with ^{56}Fe and ^{66}Zn having the greatest frequency of high intensity detection. The exceptions to this are essential isotopes ^{13}C and ^{24}Mg , both of which mostly had low detection at the enamel surface, with less than five teeth each exhibiting moderate detection (Figure 13). In addition, ^{47}Ti and ^{208}Pb , both nonessential isotopes, exhibited a range of low to moderate intensities at the enamel surface.

Overall, the inner enamel exhibited the least frequency of detection of all isotopes in the tooth, as compared to the other five defined tooth locations (Table 6 and Figure 14). In the inner enamel, the intensities of isotopes detected was not necessarily consistently divided based on whether the isotope was essential or nonessential. For example, both essential isotope ^{56}Fe and nonessential isotopes ^{27}Al and ^{138}Ba were not detected at all in the inner enamel. In addition, both essential isotopes ^{13}C and ^{66}Zn and nonessential isotopes ^{52}Cr and ^{208}Pb were detected at low intensity in the inner enamel. However, while ^{13}C and ^{52}Cr were detected at low intensity for either most or the entire sample Figure 13, in comparison ^{66}Zn and ^{208}Pb were mostly undetected in the inner enamel, with the exception of one tooth each showing low intensity (Figure 14). In addition, both essential isotopes ^{24}Mg and ^{55}Mn and nonessential isotopes ^{47}Ti and ^{88}Sr had a range of low to moderate intensity detection. Only essential isotopes ^{31}P and ^{44}Ca , which form the matrix, exhibited a range of low to high intensity detection.

Overall, the inner dentine had substantial variation of isotopic detection (Figure 15). The nonessential isotope ^{27}Al had the least amount of detection, with only two teeth exhibiting low detection in the inner dentine, followed by the essential isotope ^{55}Mn , with two teeth exhibiting low detection and one tooth exhibiting moderate detection in the inner dentine. Essential isotopes ^{24}Mg , ^{31}P , and ^{44}Ca exhibited moderate to high detection overall, while nonessential isotopes ^{88}Sr and ^{138}Ba also exhibited moderate to high detection. The similarity of intensity of ^{88}Sr and ^{138}Ba with one another and with ^{44}Ca in the inner dentine has been demonstrated in previous microchemical literature (Guede et al., 2017; Reynard and Balter, 2014).

Overall, the EDJ had some variation of isotopic detection (Figure 16). The nonessential isotope ^{27}Al was not detected at all at the EDJ, with essential isotope ^{55}Mn exhibiting low detection for only one tooth and moderate detection for two teeth out of the total sample group (N=26). The essential isotopes ^{31}P and ^{44}Ca were split between low and moderate detection at the EDJ, with half of the group sample exhibiting low detection for both isotopes and the other half exhibiting moderate detection for both isotopes (Figure 16).

Overall, the DPB had extensive variation of isotopic detection (Figure 17). The nonessential isotope ^{57}Ti was detected the least at the DPB, with 17 teeth detected at low intensity and the other nine teeth having no detection for ^{57}Ti . In comparison, essential isotope ^{56}Fe had the highest frequency for high detection at the DPB, which is to be expected since this location borders the remnants of the pulp cavity. During the life, the pulp cavity is filled with a blood supply; and since Fe is the key element associated with red blood cell production, the high presence of ^{56}Fe detected at this location is reflective of that previous blood supply in the tooth (Fraga, 2005).

Overall, the outer root border had extensive variation and exhibited the highest frequency of detection of all isotopes across all teeth (N=26) (Figure 18). The nonessential isotopes ^{57}Ti and ^{52}Cr were detected at low to moderate intensities, while essential isotopes ^{24}Mg and ^{66}Zn were detected at low to moderate intensities. In addition, nonessential ^{208}Pb had a range from low to high intensity detection, while essential isotopes ^{55}Mn and ^{56}Fe had a range from low to high intensity detection. ^{55}Mn and ^{56}Fe exhibited the greatest frequency of high intensity detection specifically at the outer root border for essential isotopes; in comparison, ^{208}Pb exhibited the greatest frequency of

high intensity detection specifically at the outer root border for nonessential isotopes (Figure 18). The overall moderate intensity of ^{56}Fe at the DPB and high intensity of ^{56}Fe concurs with the general consensus that areas previously containing blood supply equate to higher ^{56}Fe content (Hare et al., 2015); thus, specific areas in the teeth where blood used to be present are reflected in the higher intensities of ^{56}Fe at the DPB and outer root border detected in this study.

Results of this study show that the detection of major isotopes (generally ones associated with tooth structure, e.g. ^{31}P and ^{44}Ca) is similar in both spatial locations within the tooth and in relative intensity. In comparison, the detection of the remaining trace isotopes, while often similar in spatial locations in the tooth, do tend to vary in relative intensity.

Relative Intensities Compared to Other Studies

It is important to consider the results of this study fit within the context of broader knowledge, specifically previous clinical, forensic, and bioarchaeological research. The results of this study (isotope intensities based on tooth location and tooth type) and the results of previous studies are summarized in Tables 15 and 16. In this study, major isotopes ^{13}C and ^{24}Mg were detected the most at the inner dentine, which concurs with previous findings (Arnold and Gaengler, 2007; de Dios Teruel et al., 2015). The overall higher presence of biologically essential isotope ^{66}Zn detected at the enamel surface also concurs with previous findings (Farell et al., 2013). Additionally, the UCI sample had a higher frequency of detection for ^{66}Zn in this study, which also agrees with previous studies showing higher concentrations of ^{66}Zn in incisors, as compared to premolars

(Asaduzzaman et al., 2017). Interestingly, the highest frequency of detection for nonessential isotope ^{138}Ba occurred at primarily dentine locations (e.g. inner dentine and DPB), which has also been shown in previous research (Austin et al., 2013; Guede et al., 2017). Overall, in this study, the highest frequency of detection occurred in the UPM2 sample, which also concurs with previous findings demonstrating higher concentrations of Ba in premolars as compared to incisors (Asaduzzaman et al., 2017).

Table 15: Biologically essential isotope intensities by tooth location and tooth type in comparison with previous studies.

Isotope	Higher Detection	Previous Findings	Sources
$^{13}\text{C}/^{24}\text{Mg}$	Inner Dentine	Dentine > Enamel	-Arnold and Gaengler, 2007 -de Dios Teruel et al., 2015 -Guede et al., 2017 -Kang et al., 2004
$^{31}\text{P}/^{44}\text{Ca}$	Inner Dentine	Enamel > Dentine	-Arnold and Gaengler, 2007 -de Dios Teruel et al., 2015
^{55}Mn	Outer Root Border > DPB Dentine = Enamel	↑DPB Dentine/Enamel varies	-Arora et al., 2011 -Asaduzzaman et al., 2017 -Guede et al., 2017
	UCI	Incisor = Premolar	
^{56}Fe	Outer Root Border; DPB > EDJ/Dentine/Enamel	Enamel > Dentine DPB > EDJ	-de Dios Teruel et al., 2015 -Kang et al., 2004
^{66}Zn	Enamel Surface DPB > Dentine > Enamel	Enamel Surface ↑DPB; Dentine/Enamel varies	-Asaduzzaman et al., 2017 -Farell et al., 2013 -Hare et al., 2011 -Kang et al., 2004
	UCI	Incisor > Premolar	

*↑ denotes high and ↓ denotes low

Table 16: Nonessential isotope intensities by tooth location and tooth type in comparison with previous studies.

Isotope	Higher Detection	Previous Findings	Sources
²⁷ Al	Dentine = Enamel	Enamel > Dentine	-Asaduzzaman et al., 2017 -Guede et al., 2017
	UCI	Premolar > Incisor	-Tanaka et al., 2004
⁴⁷ Ti	Dentine = Enamel	Dentine > Enamel	-Guede et al., 2017
⁵² Cr	Dentine > Enamel	Enamel > Dentine	-Asaduzzaman et al., 2017 -Guede et al., 2017
	UPM1	Premolar > Incisor	
¹³⁸ Ba	Inner Dentine DPB > EDJ > Enamel	Dentine > Enamel DPB > EDJ > Enamel	-Asaduzzaman et al., 2017 -Austin et al., 2013 -Guede et al., 2017
	UPM2	Premolar > Incisor	
²⁰⁸ Pb	↑Outer Root Border Dentine > DPB > EDJ > Enamel	↑Enamel Surface DPB > EDJ DPB > Dentine & Enamel	-Arora et al., 2004 -Asaduzzaman et al., 2017 -Budd et al., 1998 -de Souza Guerra et al., 2010 -Farell et al., 2013
	UCI/UPM2	Incisor > Premolar	-Hare et al., 2011 -Kang et al., 2004

*↑ denotes high and ↓ denotes low

However, the detection and distribution of the remaining trace isotopes analyzed in this study vary in their relationship to previous findings (Tables 15 and 16). These differences demonstrate the natural variation of biological processes and highlight the impact of local environment and exposure on the individual. For example, ³¹P and ⁴⁴Ca (the matrix of the tooth) exhibited higher frequency of detection in the dentine over the enamel, which is contrary to what previous studies have shown (Arnold and Gaengler, 2007; de Dios Teruel et al., 2015). ⁵⁵Mn was detected in higher frequency and intensity at

the outer root border in this study, whereas previous research has noted higher concentrations of Mn at the DPB (Arora et al., 2011). Additionally, the distributions of ^{27}Al , ^{47}Ti , and ^{52}Cr are different than what has been shown in previous studies regarding individuals from different periods in history and different regions of the world (Asaduzzaman et al., 2017; Guede et al., 2017; Tanaka et al., 2004). While there was some detection of ^{208}Pb in the teeth in this study, the overall detection appears lower than Pb found in modern teeth (Arora et al., 2004; Budd et al., 1998; Hare et al., 2011).

Previous bioarchaeological literature has focused heavily on the importance of essential elements Mn and Zn and the nonessential elements Sr, Ba, and Pb, as these elements specifically have been used to discuss the biocultural environmental exposure and archaeological processes, such as biopurification and diagenesis (Asaduzzaman et al., 2017; Budd et al., 1998; Dolphin and Goodman, 2009; Ezzo, 1994; Farell et al., 2013; Reynard and Balter, 2014; Shepherd et al., 2012).

Overall, results of isotope distribution observed in this study are comparable with previous research mapping the distribution of trace elements in teeth. For example, two recent LA-ICP-MS studies utilizing archaeological teeth samples (one involving Chilean mummies and the other involving medieval Spanish skeletal remains) have noted a heterogeneous distribution of Zn based on the type of dental tissue, with higher concentrations of Zn occurring at the outer enamel relative to the inner dentine (Farell et al., 2013; Guede et al., 2017). In addition, Farell et al. (2013) also noted that Zn around the pulp of the tooth is higher than the Zn found in the remaining dentine tissue, which agrees with the overall results of this study, as depicted in Figure 34. Farell et al. (2013) also found that, within the ancient Chilean mummies sample, there was a higher

concentration of Zn in the pulp relative to the enamel. In this study, for the majority of teeth, the DPB exhibited either lower or equal relative intensity as compared to the enamel surface. The only exceptions to this trend are individual samples N10-1/01 UCI and N10-4/33 UPM2 (see Appendix for figures and tables). In addition, the results for ^{66}Zn distribution in this study are comparable with contemporary dental analyses from Egypt and Malaysia (Asaduzzaman et al., 2017; Farell et al., 2013). Both of these studies using modern tooth samples also noted higher Zn concentration at the enamel than in the inner dentine. In particular, the study by Asaduzzaman et al. (2017) notes unusually low concentrations of Zn and an accumulation of Zn at the enamel surface, which is comparable with the overall high intensity detection of ^{66}Zn noted at the enamel surface for most teeth in this study (Figure 34).

Additionally, while previous literature has demonstrated the presence of high Mn concentration in close vicinity to the DPB (Arora et al., 2011), a moderate or high intensity of ^{55}Mn was not observed in this study. Rather, the highest intensity of ^{55}Mn could be observed at the outer root border. The presence of Mn at the outer root border is has not been documented, although Mn is generally higher in the dentine than at the enamel (Arora et al., 2011). Depending on the individual map and relative intensity scale, a low to moderate intensity of ^{55}Mn was also observed along the enamel surface, though this intensity was never as high as the outer root border intensity by comparison. According to a previous study (Arora et al., 2011), a high(er) detection of Mn along the enamel surface could be the result of natural enamel mineralization, in which the surface of the enamel becomes hypermineralized over the inner enamel tissues.

Previous bioarchaeological literature has also noted that Sr is usually higher in concentration in the inner dentine than in the inner enamel (Farell et al., 2013; Guede et al., 2017; Lugli and Cipriani, 2017), and results of this study are comparable in that ^{88}Sr is detected in moderate to high intensities at the inner dentine, while ^{88}Sr is detected in low to moderate intensities at the inner enamel (Figures 14, 15 and 27). In comparison, one study of a modern dental sample from Egypt found that there was no disparity in Sr concentration between dentine and enamel (Farell et al., 2013).

Previous bioarchaeological studies examining the distribution of Ba in teeth have also noted that the concentration of Ba is higher within the inner dentine as compared to the enamel (Asaduzzaman et al., 2017; Amr, 2011; Austin et al., 2013; Guede et al., 2017). The results of this study are comparable with these previous studies, as ^{138}Ba was detected at much high intensities throughout the inner dentine, in very low intensities at the enamel surface, and exhibiting no detection within the inner enamel (Figure 35). Guede et al. (2017) has also observed that there are significant positive correlations between the presence of Zn, Ba, and Sr in enamel and in dentine respectively ($p < 0.01$ for both tissue types).

There has been extensive research on the distribution of Pb in teeth, both in bioarchaeology and clinical-based literature, particularly in geographic locations that are known to be predisposed to natural environmental and industrial pollution lead exposure (Asaduzzaman et al., 2017; Budd et al., 1998; Farell et al., 2013; Guede et al., 2017; Shepherd et al., 2012). In previous LA-ICP-MS studies, Pb concentrations are generally higher in the inner dentine relative to the inner enamel, especially near the DPB (Asaduzzaman et al., 2017; Budd et al., 1998; Shepherd et al., 2012); these studies are

comparable with the results of this study, as ^{208}Pb was detected in higher intensity at the DPB and at the outer root border in comparison to other tooth locations (Figure 28). The enrichment of Pb close to the pulp cavity has been reported in previous contemporary studies as well (Arora et al., 2011; Hare et al., 2011; Kang et al., 2004; Shepherd et al., 2012). It has been suggested that Pb enrichment near the DPB, in particular, may be due to the close interaction and thus high rate of exchange between blood vessels in the pulp with the odontoblasts in the inner dentine (Shepherd et al., 2012). However, previous studies analyzing Pb exposure do not discuss in detail the concentration of Pb at the outer root border.

The variations in spatial distribution and intensity of these trace isotopes can infer interindividual variation within this sample population. Differences in intensity and spatial distribution could be attributed to differences in diet during early life, differences in how food sources were prepared or processed, and/or natural differences in the developmental and metabolic processes of each individual. In the field of bioarchaeology, these differences observed in the elemental maps can be useful for illuminating the timing and extent of dietary changes during the early life of the individual, as compared to the population, as has been done in previous studies (Austin et al., 2013; Dolphin and Goodman, 2009; Humphrey et al. 2016).

In the field of forensics, the specific ratio of certain isotopes to one another (e.g. Sr and Pb), in combination with stable isotope analyses, could be used to link unidentified human remains with a specific area or region, as has been done in previous studies (Font et al., 2015; Kamenov and Curtis, 2017; Kumagai et al., 2012). In addition, as modern populations have become exposed to the byproducts of industry and pollution

it may also be possible to determine whether human remains are contemporary or ancient, based on the relatively intensity of isotopes present that are associated with pollution (e.g. Pb, Ti and Cr) (Brown et al., 2004; Shepherd et al., 2012). Thus, mapping of isotopes may be useful for determining whether or not human remains have forensic significance.

Relative Intensities of Isotopes by Tooth Type

The results of this study also show that the spatial distribution of each isotope is generally consistent, regardless of tooth type. However, the frequency that each isotope is detected can vary based on tooth type in this sample (Figures 31 and 32).

Overall, the frequency of detection of moderate and high intensities of each isotope showed some variability depending on the isotope being detected (Figure 32). In this study, all tooth types show low frequency of detection of both nonessential and essential isotopes, including ^{27}Al , ^{55}Mn and ^{56}Fe (Figure 33). In comparison, all tooth types show high frequency of detection of essential isotopes, including ^{24}Mg , ^{31}P , and ^{44}Ca (Figure 32). However, there are a few isotope frequencies associated with a specific tooth type that do not follow the general trends. For example, the ULI sample has a higher detection of ^{52}Cr , ^{138}Ba , and in particular ^{208}Pb than the other tooth types. However, due to the ULI sample only being one tooth, it is difficult to say whether the subtle differences observed within isotope frequencies for the ULI sample are specific to its tooth type or specific to the individual. The UPM1 sample has the least frequency detection of ^{13}C as compared to the other tooth types, but as the highest frequency detection of ^{88}Sr as compared to the other tooth types.

In addition, when considering only moderate to high intensity detection, the UCI sample showed the highest detection of the fundamental matrix elements ^{31}P and ^{44}Ca , while the ULI sample showed the highest detection of major isotope ^{13}C (Table 14). In particular, the distribution of trace isotopes ^{66}Zn , ^{88}Sr , ^{138}Ba , and ^{208}Pb follows a similar pattern across all tooth types (Figure 32). Both the UCI and UPM2 samples exhibited higher detections of ^{66}Zn , ^{88}Sr , ^{138}Ba , and ^{208}Pb as compared to the ULI and UPM1 samples. For example, UCI and UPM2 had an average of 50% and 40% detection of moderate to high ^{66}Zn intensity respectively, whereas ULI and UPM1 had an average of 17% and 36% detection of moderate to high ^{66}Zn intensity respectively. UCI and UPM2 had an average of 54% and 60% detection of moderate to high ^{88}Sr intensity respectively, whereas ULI and UPM1 had an average of 50% and 53% detection of moderate to high ^{88}Sr intensity respectively. In addition, UCI and UPM2 had an average of 56% and 57% detection of moderate to high ^{138}Ba intensity respectively, whereas ULI and UPM1 both had an average of 50% detection of moderate to high ^{138}Ba intensity. And finally, both UCI and UPM2 had an average of 29% detection of moderate to high ^{208}Pb intensity respectively, whereas ULI and UPM1 had an average of 17% and 19% detection of moderate to high ^{208}Pb intensity respectively.

In order to consider the results of this study in context with previous clinical, forensic, and bioarchaeological research, a summary table comparing the results of this study (isotope intensities based on tooth type) and results of previous studies are available in Tables 15 and 16 in the previous section. Consistencies in isotope frequencies detected across all tooth types may reflect similar environmental influences throughout the development of these teeth, whereas major differences in detection (e.g.

^{66}Zn , Figure 31) may reflect differences in bioavailability or exposure during specific points of growth in this sample group (Dolphin et al., 2005).

Regarding the importance of tooth type, previous studies of contemporary populations have found higher concentrations of Pb, Sr, and Zn present within incisors over other tooth types (Asaduzzaman et al., 2017). These data are comparable with this study for the UCI sample but are not in agreement with the ULI sample. It is important to note that since the ULI sample had the smallest sample size ($n=1$) of all four tooth types present in this study, the results of the ULI analysis may be skewed. In addition, Asaduzzaman et al. (2017) found that premolars had higher concentrations of nonessential elements Cr, Al, and Ba. This previous information is somewhat comparable to this present study. For example, UPM1 had a higher frequency of moderate and high intensity detection of ^{52}Cr than UCI; however, neither ULI nor UPM2 were detected at moderate or high intensity for ^{52}Cr (Figure 32). Both UPM1 and UPM2 had higher frequency of moderate and high intensity detection of ^{27}Al than ULI; however, UCI had the highest overall frequency of moderate to high detection for ^{27}Al (Figure 32). And only UPM2 had a slightly higher frequency of moderate and high intensity detection of ^{138}Ba than the other tooth types, though ULI and UPM1 exhibited the same frequency of detection for ^{138}Ba (Figures 32 and 33).

However, Asaduzzaman et al. (2017) do not specify which incisors or premolars were utilized in their study or from which bone (i.e. maxilla or mandible) these teeth were acquired. Thus, although the tooth eruption of maxillary and mandibular premolars is similar, there is about a year's difference in the timing of maxillary versus mandibular central and lateral incisors (Hillson, 2005). Additionally, a study by Fischer et al. (2009)

found that both permanent and deciduous maxillary (upper) teeth exhibited higher concentrations of heavy metal elements than those of their corresponding mandibular (lower) teeth, thus suggesting that there is natural variation between maxillary and mandibular teeth in their ability to bind to certain elements. In considering the natural variation that may exist between upper and lower teeth, it may be problematic to make direct comparisons between elemental analyses that use teeth from different regions of the mouth.

At the same time, spatial distribution and intensity variations of these trace isotopes across different tooth types can infer interindividual and intraindividual variation within this sample population. Differences in intensity and spatial distribution between incisors and premolars (particularly within the same individual) could be attributed to change in diet during early life, a change in how food sources were prepared or processed, and/or natural differences in the growth and development process. Since the four tooth types analyzed in this form at different intervals during life (Hillson, 2005), one possible reason for the variation seen between tooth types is a change in diet during the time each tooth type was forming. In addition, variation between tooth types may also be attributed to the natural growth and development processes and bioavailability of nutrients at each growth stage. Thus, in bioarchaeology research, mapping of elemental distribution can be useful for correlating changes in relative intensities at specific tooth locations across tooth types with time intervals of the individual, in order to inform biocultural behaviors during an early life history.

In forensic research, mapping of elemental distribution has the potential to be useful for individual identification and interpreting manner of death (e.g. Fortes et al.,

2015). The subtle differences in relative intensity and spatial location of specific isotopes may be useful for sorting remains (e.g. sorting upper from lower teeth), estimating the minimum number of individuals present, determining sex and age, and discriminating between individuals in cases containing mass burials.

Relative Intensities Through Time

In this study, there were eight individuals with two different tooth types (UCI and UPM1/2). Thus, it is possible to examine the differences in isotopes across time within the same individual, by noting how average intensities of certain isotope varied from the UCI to the UPM1 or UPM2 (Figures 36-43).

For individual N10-1/02, isotopes ^{24}Mg , ^{138}Ba , and ^{208}Pb exhibited an increase in relative intensity over time (Figure 36). The difference in ^{24}Mg could indicate a transition in how the body processes minerals during growth and development, while the increasing average relative intensity of all three isotopes over time could indicate an increased level of exposure due to a change in dietary resources or food processing.

For individual N10-2/20A or B, isotopes ^{47}Ti , ^{56}Fe , ^{66}Zn , and ^{138}Ba all exhibited a decrease in relative intensity over time (Figure 37). The differences in ^{56}Fe and ^{66}Zn could indicate a transition in how the body processes minerals during growth and development, while the decreasing average relative intensity of all four isotopes over time could indicate a decreased level of exposure due to a change in dietary resources or food processing.

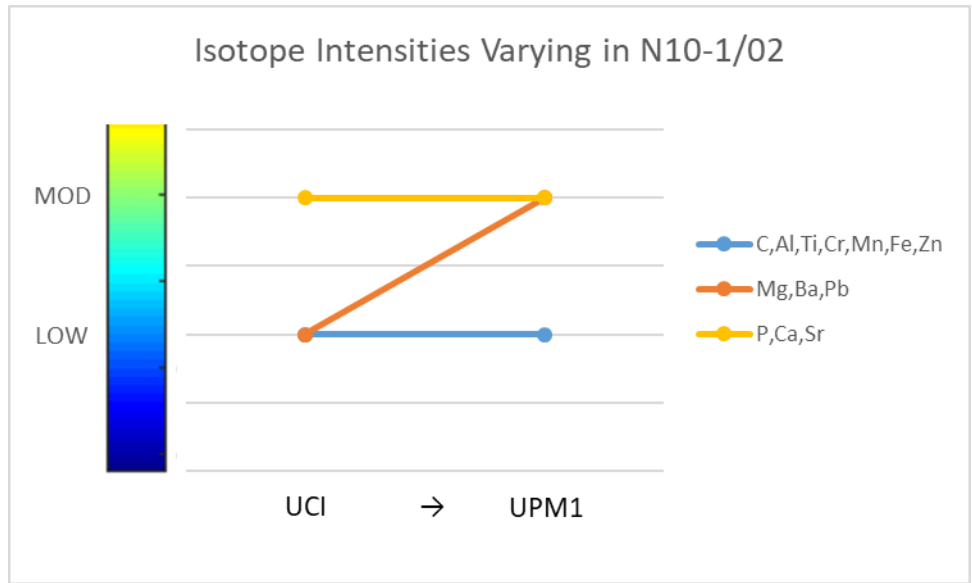


Figure 36: Average isotope intensities varying across time in individual N10-1/02.

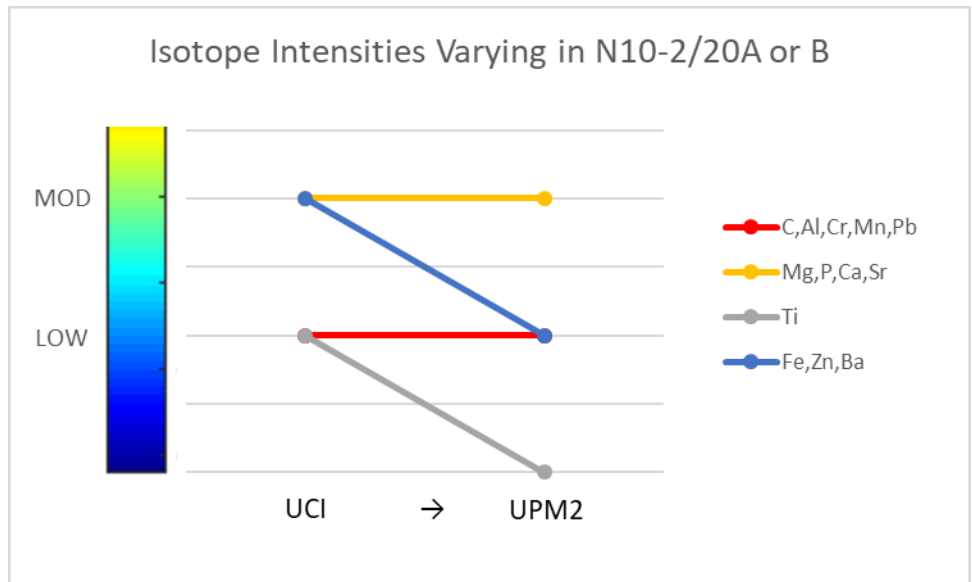


Figure 37: Average isotope intensities varying across time in individual N10-2/20A or B.

For individual N10-2/21, isotopes ^{13}C and ^{52}Cr exhibited a decrease in relative intensity over time, while isotopes ^{24}Mg , ^{55}Mn , ^{66}Zn , and ^{88}Sr exhibited an increase in

relative intensity over time (Figure 38). The differences in ^{24}Mg , ^{55}Mn , and ^{66}Zn could indicate a transition in how the body processes minerals during growth and development, while the changes in average relative intensity of all four isotopes could indicate a change in dietary resources or food processing over time.

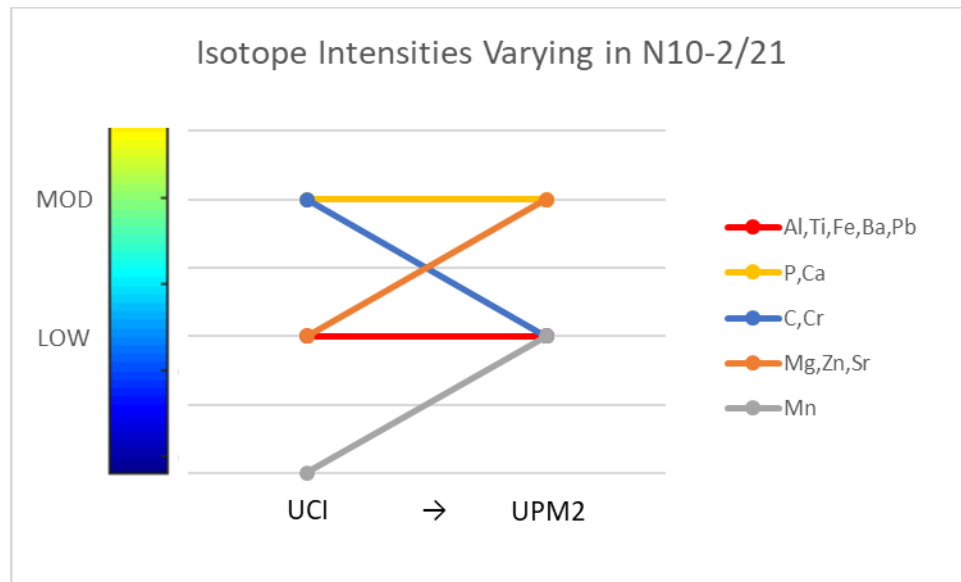


Figure 38: Average isotope intensities varying across time in individual N10-2/21.

For individual N10-2/21A, isotopes ^{31}P and ^{138}Ba exhibited a decrease in relative intensity over time, while isotope ^{55}Mn exhibited an increase in relative intensity over time (Figure 39). The differences in ^{31}P and ^{55}Mn could indicate a transition in how the body processes minerals during growth and development, while the changes in average relative intensity of all three isotopes could indicate a change in dietary resources or food processing over time.

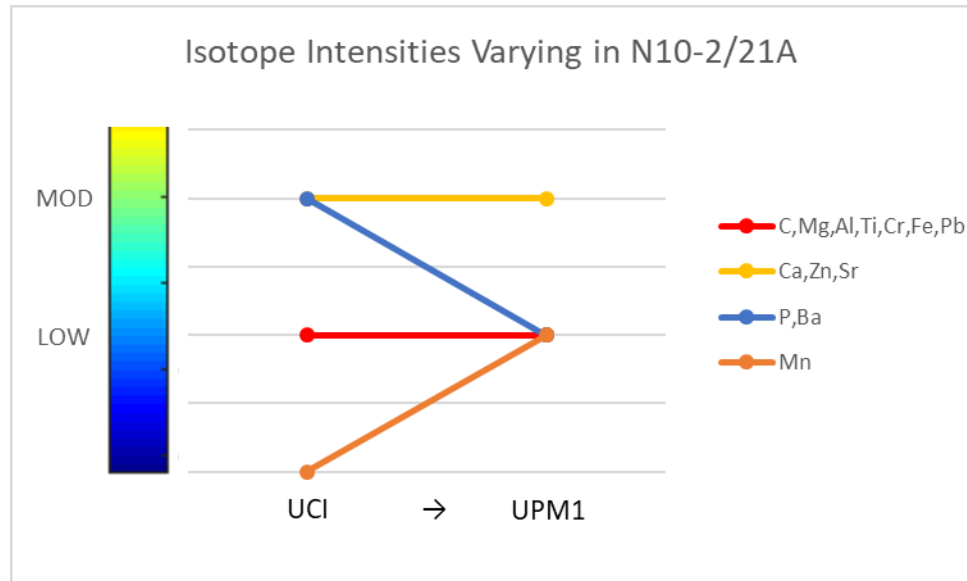


Figure 39: Average isotope intensities varying across time in individual N10-2/21A.

For individual N10-2/42B, isotopes ^{56}Fe , ^{88}Sr , and ^{138}Ba exhibited a decrease in relative intensity over time (Figure 40). The difference in ^{56}Fe could indicate a transition in how the body processes minerals during growth and development, while the decreasing average relative intensity of all three isotopes over time could indicate a decreased level of exposure due to a change in dietary resources or food processing.

For individual N10-4/01, isotope ^{13}C exhibited an increase in relative intensity over time, while isotope ^{66}Zn exhibited a decrease in relative intensity over time (Figure 41). The differences in these isotopes could indicate a transition in how the body processes minerals during growth and development, or these differences could indicate a change in dietary resources or food processing over time.

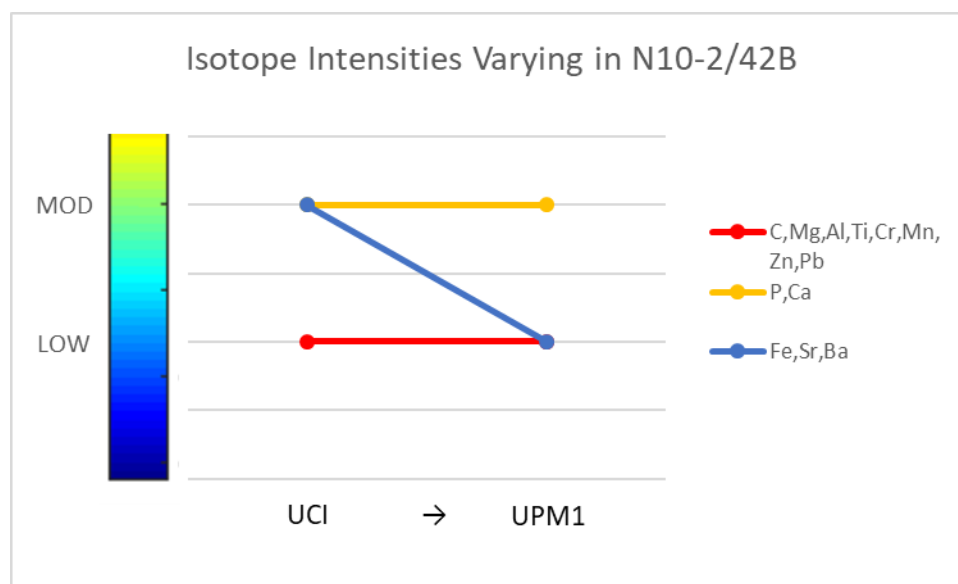


Figure 40: Average isotope intensities varying across time in individual N10-2/42B.

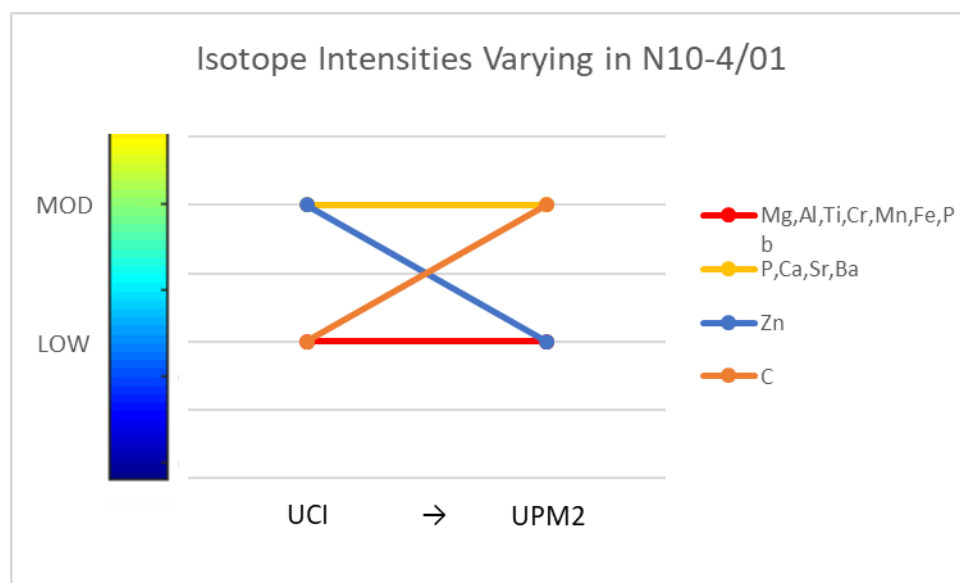


Figure 41: Average isotope intensities varying across time in individual N10-4/01.

For individual N10-4/43, isotopes ^{24}Mg and ^{55}Mn exhibited an increase in relative intensity over time, while isotopes ^{13}C , ^{31}P , and ^{138}Ba exhibited an increase in relative

intensity over time (Figure 42). The differences in ^{13}C , ^{31}P , ^{24}Mg , and ^{55}Mn could indicate a transition in how the body processes minerals during growth and development, while the changes in average relative intensity of all five isotopes could indicate a change in dietary resources or food processing over time.

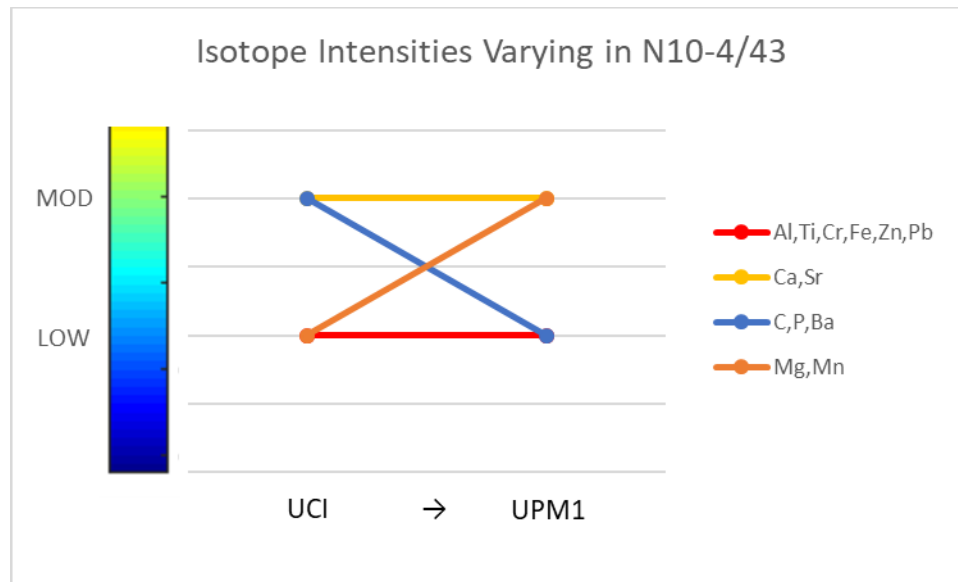


Figure 42: Average isotope intensities varying across time in individual N10-4/43.

For individual N10-4/4C Large, isotopes ^{44}Ca and ^{31}P exhibited a drastic decrease in relative intensity over time, while isotopes ^{24}Mg and ^{56}Fe exhibited an increase in relative intensity over time (Figure 43). These differences could indicate a transition in how the body processes minerals during growth and development, or these differences could indicate a change in dietary resources or food processing over time.

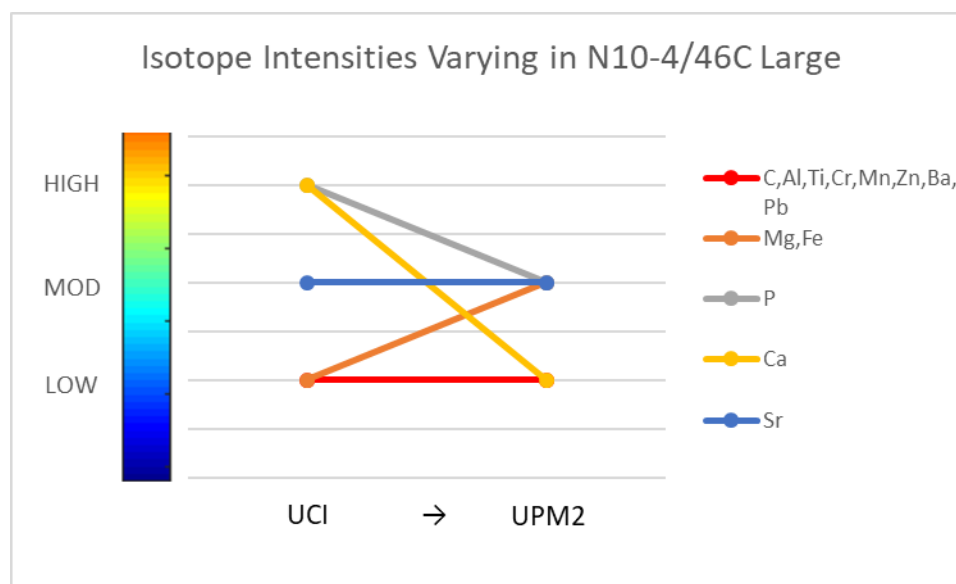


Figure 43: Average isotope intensities varying across time in individual N10-4/46C Large.

Based on these charts, the two isotopes that exhibited a change across time (i.e. variation from incisor to premolar) the most were ^{138}Ba and ^{55}Mg . The intensity of ^{138}Ba (functionally nonessential) varied between incisor and premolar for five out of eight individuals (63%), while the intensity of ^{55}Mg (functionally essential) varied between incisor and premolar for four out of eight individuals (50%). Overall, the information generated through these charts further demonstrates the dynamicity of early growth and development and provides insight into the timeframe in between each tooth formation (approximately a two-year gap). This information may also illuminate how nutrients are absorbed and expressed and can vary within the same individual, which may reflect changes in diet during the early life history of these individuals.

Intentionally Modified Teeth

In this study, six upper central incisors out of the entire sample group also exhibited intentional dental modification of the enamel crown, a cultural action that has been documented in much of the bioarchaeological literature and may have served as a representation of high status in the Postclassic Maya community (Williams and White, 2006) (see Table 2 in Materials and Methods section for individual sample numbers). In this case, because four of these incisors also came from the same individual as four premolars (G1, Table 3), a total of 10 teeth (6 UCI, 2 UPM1 and 2 UPM2) can be associated with possibly more elite individuals from among this sample group. In general, all samples containing or associated modified central incisors (n=10) had higher frequency of moderate and high intensity detection of most isotopes, as compared to unmodified samples (n=16) (Figure 44). The exceptions to this trend are found at the detections of ^{13}C , ^{24}Mg , ^{47}Ti , and ^{52}Cr , which exhibited higher frequency of detection for unmodified samples as compared to modified ones.

One possible explanation for the higher presence of ^{52}Cr in unmodified teeth would be a difference in diet. Cr is present in maize (Fairweather-Tait and Hurrell, 1996), and previous stable isotope research on Postclassic Lamanai individuals has indicated that there was a social stratification of food, in which members of the social elite had greater access to freshwater and marine foods and were less reliant on maize as a resource as the commoners (Coyston, 1995). Thus, a higher presence of ^{52}Cr in unmodified teeth would indicate more reliance on maize in the diet, while an overall lower presence of ^{52}Cr in modified teeth would indicate less reliance on maize in the diet. Previous studies also suggest individuals from Postclassic Lamanai with intentionally

modified teeth were members of an even more elite social class than those with unmodified teeth (Williams and White, 2006).

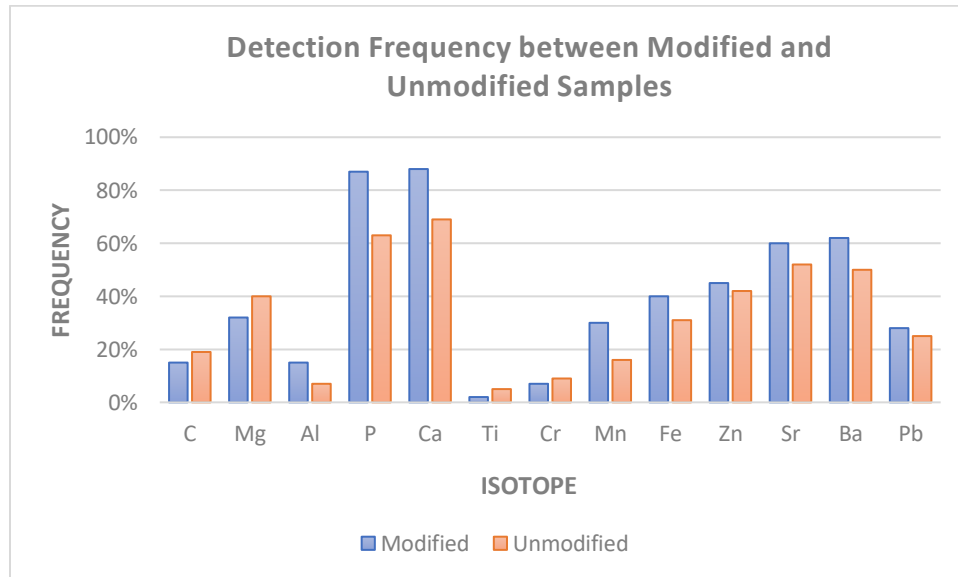


Figure 44: Frequency of detection of moderate and high intensities between all teeth associated with modified UCI (n=10) and all teeth associated with unmodified UCI (n=16).

Unique Tooth

There was also one unique sample (individual N10-2/21 UCI) that emerged through this study. This individual had a small piece of jade (chemical formula $\text{NaAlSi}_2\text{O}_6$) lodged inside where the pulp cavity would be (Figure 45). This individual did not show any signs of intentional dental modification, nor were there any signs of intentional or unintentional cracking noted on the external surface of the tooth. In addition, the internal cross-sectional area of the tooth did not show any internal signs of cracking as to indicate how this piece of jade became lodged inside.

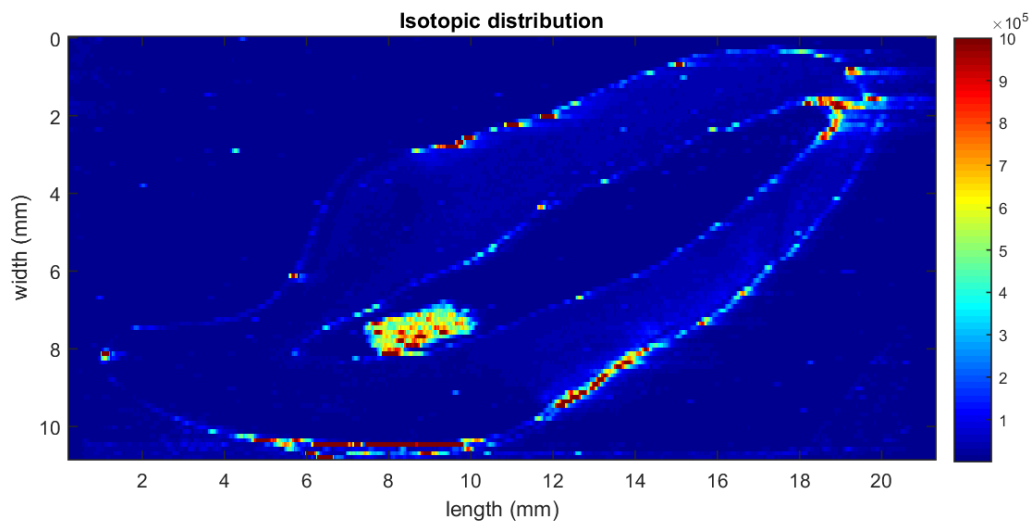


Figure 45: Example of ^{27}Al distribution in tooth sample N10-2/21 UCI. Note the high intensity of ^{27}Al outlining where the jade piece is located.

There are two possible reasons for the presence of this jade piece inside the pulp cavity of the tooth. One possibility is that this piece of jade was embedded within the alveolar bone of the individual prior to the adult crown formation, and the tooth was able to form around the piece. An alternative possibility is that, during development, this piece was small enough to be able to enter into the main cavity of the tooth through the hole at the apical root end, before the apical end became completely developed (no longer visible in Figure 45). At the Lamanai site, many recovered burials and objects contained jade, including burials from the N10-2 structures (Pendergast, 1981a). The presence of this jade piece further does confirm the high social status of this individual, as jade was considered to be an important symbol of rulership and a major component of Maya ritual (Taube, 2005).

Exposure and Bioavailability

During life, the external environment can influence the internal biological environment, in which long-term exposure to elements available within a specific geographic location, trophic level, and/or diet change the elemental characterization signatures found in the inorganic tissues of teeth (Asaduzzaman et al., 2017; Kang et al., 2004; Kohn et al., 2013). In this way, human biology and, in this case, chemistry can be influenced and even altered by cultural activities and processes (Martin et al., 2013). Thus, in bioarchaeology and forensic anthropology studies, not only is the presence and distribution of certain trace elements relevant to the discussion of environmental exposure, but it is also important to consider holistically the relative spectral intensities of certain essential and nonessential elements in relationship to one another.

The incorporation of heavy metals and toxins into the body due to exposure has been well-documented in both clinical and bioarchaeological literature. There are many biological processes that can influence the external oral environment surrounding the teeth and the internal environment from within the tooth structure. For example, over time, the internal crystalline structure of teeth containing hydroxyapatite may become modified through numerous cationic substitutions replacing Ca^{2+} , including Mn^{2+} , Cu^{2+} , Mg^{2+} , and Zn^{2+} (de Dios Teruel et al., 2015; Wolinsky and Altchuler, 1983). These ions may then become incorporated into the dentine and enamel of the tooth, particularly near the EDJ (Curzon and Featherstone, 1983; de Dios Teruel et al., 2015).

In addition, the intake of food and water from a specific geographic source can also influence the oral and metabolic environment within a body, indirectly influencing the ratio of trace elements to one another and indirectly or directly influencing other

chemical processes related to teeth. Teeth in particular have the potential to serve as a useful biomarker of chronic, long-term exposure of dietary nutrients and environmental toxins (Arruda-Neto et al., 2010; Shepherd et al., 2012). There are multiple factors (both internal and external) that can influence and alter the overall detection of certain trace elements in teeth (Figure 46). These factors include geological sources of exposure, water exposure, dietary influences, bioavailability, and natural biological processes (Asaduzzaman et al., 2017; Brown et al., 2004), also summarized in Table 17.

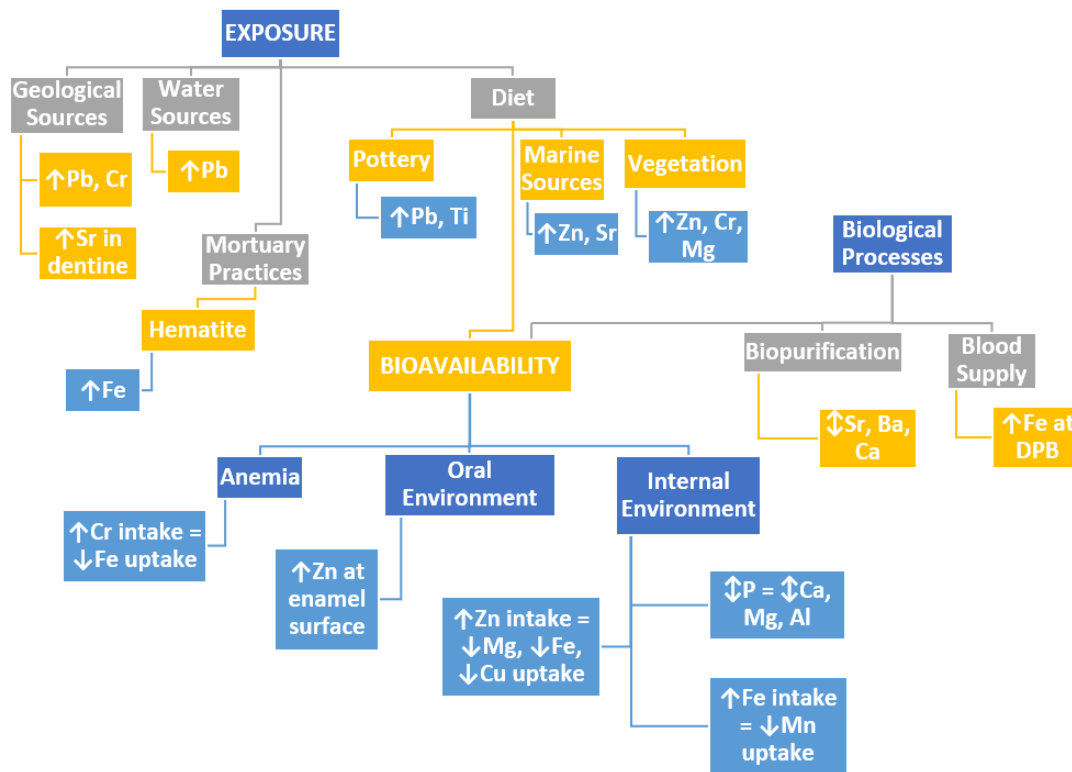


Figure 46: Possible external sources of exposure and internal bioavailability influencing the presence of certain trace elements in teeth.

Table 17: Summary of observed isotope intensities in relationship to one another and possible bioavailability and exposure influences.

Isotope Intensities	Exposure during Life	Sources
$^{88}\text{Sr} > ^{66}\text{Zn} > ^{24}\text{Mg}$ - ^{88}Sr in dentine	-Herbivore-based diet (grain/vegetables) -Marine foods (fish) -Accidental soil consumption - $\uparrow\text{Zn} = \downarrow\text{Mg}$	-Brown et al., 2004 -Comar et al., 1957 -Reynard and Balter, 2014 -Shepherd et al., 2012 -Spencer et al., 1994
- $\uparrow^{66}\text{Zn}$ at enamel surface - ^{66}Zn at DPB & inner dentine - $^{44}\text{Ca} > ^{66}\text{Zn}$	-Surface enrichment from enzyme interaction -Protein/Seafood/Phylates = $\uparrow\text{Zn}$ absorption - $\uparrow\text{Ca}$ in diet = $\downarrow\text{Zn}$ absorption	-Asaduzzaman et al., 2017 -Farell et al., 2013 -Fraga, 2005 -Freeland-Graves et al., 2015 -Krebs, 2013 -Sandström, 2001
- $^{44}\text{Ca} > ^{138}\text{Ba}$ - ^{44}Ca in dentine > enamel	-Biopurification -Accidental soil consumption - \uparrow fiber intake = $\downarrow\text{Ca}$ retention	-Lamb et al., 2013 -Reynard and Balter, 2014 -Zhu and Prince, 2012
-Low ^{52}Cr	-Soil residual exposure -Maize consumption -Anemia - $\uparrow\text{Cr}$ intake = $\downarrow\text{Fe}$ absorption	-Asaduzzaman et al., 2017 -Brown et al., 2004 -Coyston, 1995 -Nowak and Kozlowski, 1998
- $\uparrow^{56}\text{Fe}$ at DPB/root border - ^{56}Fe at enamel surface - $^{56}\text{Fe} > ^{55}\text{Mn}$	-Blood vessel exchange -Protective colloidal layer on enamel - $\uparrow\text{Fe}$ intake = $\downarrow\text{Mn}$ uptake -Hematite	-Ávila et al., 2014 -Freeland-Graves et al., 2015 -Lynch, 1997 -Sandström, 2001
- $\downarrow^{55}\text{Mn}$ at outer root border & enamel surface	-Soil residual exposure -Aquatic food chain - $\uparrow\text{Cr}$ or $\text{Pb} = \downarrow\text{Mn}$ uptake	-Asaduzzaman et al., 2017 -Freeland-Graves et al., 2015 -Nowak and Kozlowski, 1998 -Sandström, 2001
- $\downarrow^{208}\text{Pb}$ at DPB, outer root border, & enamel surface	-Biogenic tissue formation -Blood vessel exchange -Natural geological/water sources -Pottery	-Brown et al., 2004 -Budd et al., 1998 -Farell et al., 2013 -LeCount et al., 2016 -Shepherd et al., 2012

* \uparrow denotes high and \downarrow denotes low

For the individuals in this study, possible sources of exposure include geological sources, water sources, and diet. Geological sources can influence the presence of Pb, Cr and Sr found in living tissues including teeth (Asaduzzaman et al., 2017; Brown et al., 2004; Reynard and Balter, 2014). The presence of ^{208}Pb is of particular interest, because very low quantities of Pb could still be indicator of toxic level of exposure (Brown et al., 2004). Although Pb was detected in a low amount in the teeth in this study, literature has suggested that water sources can contribute to Pb in various living tissues. Exposure to Pb can occur through smelting and mining activities (Rieuwerts et al., 2000). In studies involving contemporary populations, Pb is a heavy metal toxicant that is commonly associated with environmental pollution. In this case, Pb exposure in this sample population may be attributed to mining, glazing, and painting associated with the production of ceramics, pottery, and other structures (Asaduzzaman et al., 2017; LeCount et al., 2016; Little et al., 2004).

Additionally, the higher presence of ^{208}Pb at the DPB, as noted in this study, may be due the rate of exchange between the nearby blood supply and dentine during life, as some studies have suggested that Pb may become part of the blood vessel exchange in the same way that Fe does (Shepherd et al., 2012). It is important to note that ^{56}Fe in this study was also detected at the DPB and outer root border, just like ^{208}Pb . Other research suggests that high intensities of ^{208}Pb and ^{66}Zn seen at the enamel surface may also reflect *in vivo* chemical exposure during enamel maturation (Budd et al., 1998).

Dietary exposure is a major influence as well. For example, the presence of vegetative life in the local environment and regular consumption of specific vegetables (including maize) can influence levels of ^{66}Zn , ^{52}Cr , and ^{24}Mg (Asaduzzaman et al., 2017;

Fairweather-Tait and Hurrell, 1996). In addition, more marine-based resources within the diet may also be a source of ^{66}Zn and ^{88}Sr . In particular, plants contain more natural Sr than animals, and thus more herbivore-based diets lead to a greater presence of Sr within teeth (Asaduzzaman et al., 2017; Webb et al., 2005). Fish and fish products (e.g. shellfish) are major sources of Sr for the human body, accumulating in various tissues other than bones, although there is less scientific clarity regarding possible influencers on Sr accumulation in enamel and dentine (Asaduzzaman et al., 2017; Krueger, 2016).

In this case, the presence and variation of ^{66}Zn , ^{52}Cr , ^{24}Mg , and ^{88}Sr in the enamel and dentine across all teeth may be attributed to diversity and changes within the diet. Overall, there was a generally high presence of ^{88}Sr detected in the dentine of teeth (average 54% frequency detection in the moderate to high intensity range, Table 7). In this study, ^{88}Sr had the highest frequency of detection of all nonessential isotopes analyzed and could indicate an enrichment of ^{88}Sr in this sample group. While maize has been noted as a staple food for the Postclassic Maya, paleobotanical records have also demonstrated that these individuals likely had access to and utilized a wide variety of other plants (such as beans and squash) and semi-domestic animals (Coyston, 1995; Emery, 1999). Research also suggests that freshwater aquatic resources, including fish, turtles, and mollusks, became more widespread during the early Postclassic Maya (Coyston, 1995). Previous stable isotope studies on bone collagen and apatite also confirm that the inhabitants at Lamanai likely consumed less maize and had a more diverse, carnivore-based diet than inhabitants occupying the lowlands further inland (Coyston, 1995; Coyston et al., 1999).

In addition to direct food consumption, other indirect sources of exposure include the types of paints, pottery, and other structures. For example, Maya pottery from the Postclassic period has been found to contain trace elements Pb and Ti, as well as other functionally and nutritionally nonessential trace elements (Jadot et al., 2016; LeCount et al., 2016; Little et al., 2004). Thus, the overall low presence of ^{47}Ti and ^{208}Pb observed within teeth in this study may be due to exposure to these isotopes during the preparation and consumption of foods.

Diet also influences bioavailability within the individual, as the mere presence of certain isotopes can influence or disrupt the activity of other isotopes. For example, Sr is unregulated in the body (Shepherd et al., 2012). Thus, chronic or excessive exposure to Sr can lead to metabolic dysfunction and other health issues, including osseous mineralization issues, as excessive Sr ingestion can diminish the Ca content in bone and possibly in teeth (Asaduzzaman et al., 2017). Thus, one possible reason for overall moderate intensity of ^{88}Sr and ^{138}Ba , in combination with moderate intensity of ^{66}Zn and ^{24}Mg , in dentine is exposure to marine resources, which would concur with previous Postclassic Lamanai studies.

In comparison, Zn is homeostatically regulated (Shepherd et al., 2012). Thus, while in paleodiet and bioarchaeology research, Zn has been assumed to be a useful indicator of trophic level, recent studies do not demonstrate a relationship between animal and plant sources and Zn content in teeth (Dolphin and Goodman, 2009; Ezzo, 1994). According to Asaduzzaman et al. (2017), one possible reason that Zn levels accumulate in higher degree along the enamel surface is due to the surface enamel coming into direct contact with saliva in the mouth. This information may explain why

the teeth in this study all exhibited relatively high intensity of ^{66}Zn at the enamel surface. Prolonged, higher exposure to Zn can also inhibit the uptake of other biologically essential elements, such as Cu and Fe (Asaduzzaman et al., 2017). In addition, the consumption of Ca-rich foods can potentially impact Zn intake and absorption, inhibiting these processes (Asaduzzaman et al., 2017).

In addition to diet and other types of exposure, natural biological processes influence the bioavailability of isotopes in the individual. For example, in this study, ^{88}Sr intensity in comparison to ^{44}Ca intensity may also be indicative of what is referred to as the biopurification processes. In this naturally occurring phenomenon, divalent cations (Ba and Sr) interact and replace isovalent Ca sites within the hydroxyapatite of bone and teeth (Asaduzzaman et al., 2017; Webb et al., 2005). Through biopurification, Ba and Sr substitute for Ca in the crystal lattice of the tooth (Asaduzzaman et al., 2017); thus, it is expected that levels of Sr and Ba will be similar within the tooth and concentrated more at the dentine than in the enamel.

Regarding the high presence of ^{56}Fe detected at the DPB, while the most likely contributing factor is the fact that the pulp cavity contained a large blood supply during life. However, a heavy dependence on maize could also explain why the detection of ^{56}Fe in this case is not higher. Previous research has noted that maize consumption leads to ^{56}Fe deficiency, as increased Cr intake causes decreased Fe absorption (Coyston, 1995; Lynch, 1997). In this study, the presence of ^{52}Cr was detected in similar areas as ^{56}Fe (e.g. near the DPB and outer root border). Thus, the presence of ^{52}Cr may have disrupted ^{56}Fe activity in this sample. These results also concur with previous findings that suggest this sample population from Postclassic Lamanai were anemic (Coyston, 1995).

Other sources of exposure influencing the isotopic presence and spatial distribution within this sample of teeth involves contact with artifacts involved in the mortuary practices of the ancient Maya. Inhabitants of Postclassic Maya engaged in many methods of body processing to prepare the individual for burial. One such method involved a mummification-like ritual, in which the individual was smeared with cinnabar or hematite (a red pigmented mixture containing a high presence of Fe) (Ávila et al., 2014; Weiss-Krejci et al., 2003). In particular, cinnabar often denoted high social status for the Maya (Ávila et al., 2014), and thus it would make sense for this mineral to influence the level of ^{56}Fe observed in this study, as this sample only included individuals of presumed higher social status.

CHAPTER SIX: CONCLUSION

The detection of major, structural isotopes is similar in both spatial locations within the tooth and in relative intensity. In comparison, the detection of trace isotopes, while often similar in spatial locations in the tooth, do tend to vary in relative intensity. Additionally, spatial distribution of each isotope is generally consistent, regardless of tooth type. However, the frequency that each isotope is detected can vary based on tooth type. Elemental maps show the frequency of moderate-to-high isotope detection occurred in the following descending order: $^{44}\text{Ca} > ^{31}\text{P} > ^{88}\text{Sr} > ^{138}\text{Ba} > ^{56}\text{Fe} > ^{66}\text{Zn} > ^{24}\text{Mg} > ^{208}\text{Pb} > ^{13}\text{C} > ^{55}\text{Mn} > ^{27}\text{Al} > ^{52}\text{Cr} > ^{47}\text{Ti}$. Maps also show that the following tooth locations exhibited the highest intensity of isotope detection in descending order: Outer Root Border > Dentine-Pulp Border > Inner Dentine > Enamel Surface > Enamel-Dentine Junction > Inner Enamel. Thus, frequency and intensity of detection increased from the anatomically outer portion (enamel surface) to the anatomically inner portion (outer root border) of the tooth.

Implications

The results of this study demonstrate that teeth serve as storehouses of trace elements beyond those needed for merely maintaining growth and structure. The degree of presence and spatial distribution of these elements within teeth are influenced by biological processes and cultural activities. Thus, this study also illuminates possible sources of exposure within this Postclassic Lamanai sample population.

Another possible implication in the use of LA-ICP-MS on enamel and dentine is to lend insight into possible exposure and other health issues for the sample population

from Lamanai, Belize. One way that this method can be useful in bioarchaeological research is to increase interdisciplinary understanding of the potential health effects of low-level exposure to functionally nonessential and potentially toxic elements (e.g. Ba and Pb) and to expose hidden heterogeneity. According to the Osteological Paradox, the macroscopic presence of pathological lesions in a skeleton does not necessarily reflect accurately the prevalence of a disease in that individual or within the population the individual belongs to, and this may also be applied to teeth (Wood et al., 1992; DeWitte and Stojanowski, 2015). It is possible that population-level health and disease trends may not be noticeable through gross morphological methods of analysis in anthropology (Wood et al., 1992). Thus, while the teeth examined in this study exhibited an overall healthy external appearance, these teeth may nevertheless serve to illuminate health conditions detectable at the biochemical level.

Another phenomenon that could impact the presence and distribution of metals in teeth is diagenesis. Diagenesis is an intricate postmortem process between buried skeletal remains and the surrounding soil environment, in which the chemical components of the skeleton become gradually altered via interaction and exchange with the soil (Burton et al., 2003; López-Costas et al., 2016). Thus, skeletal material becomes more and more inorganic over time, leading to fossilization or degradation. Although teeth have been shown to be less susceptible to the impact of diagenesis due to their higher mineralization (Hollund et al., 2015; Galiová et al., 2013), diagenesis can still impact chemical components of teeth. For example, the phosphate component of teeth is generally resistant to chemical alteration, but the hydroxyl component can become extensively altered (Kohn et al., 1999; Kohn et al., 2013).

Limitations

As a limitation, the LA-ICP-MS protocol in this study did not involve the use of an internal standard (e.g., commonly ^{43}Ca) or external matrix-matched standards in order to determine exact concentrations of isotopes detected and to further quantify data.

Future Directions

Future directions utilizing this sample of 18 individuals, as well as other samples from the Lamanai, Belize collection, would be to quantify these isotopic data by using external matrix-matched standards. Quantified characterization of isotopes would make this study more comparable with other elemental mapping studies. In particular, results of this preliminary study and additional trace element analyses may be compared with previous stable isotope research of Postclassic Lamanai individuals. This collaboration would allow researchers to draw more holistic interpretations about biocultural influences on the physiology of trace elements present and distributed within the different dental tissues of individuals analyzed in this study.

In order to generate a more accurate and complete picture of the plausible dietary and other environmental influences on this Postclassic Lamanai population, additional research is needed. In particular, it may be useful to examine the role of geographical location on the influence of trace elements exhibited and individual exposure to the environment, comparing trace elements between ancient and contemporary populations, as well as comparing differences in trace element intensities across global communities, as previous bioarchaeological research has attempted (e.g., Budd et al., 1998). Quantified data from this study may serve as a baseline of geographic information, which could then

be compared to trace elements analyses on individuals from various regions of the world. This information would be useful for more accurately comparing trace element data with previous and current bioarchaeological literature, as well as informing the place of origin of unknown remains in forensic research. Additionally, quantified data from this study would be useful for understanding where Postclassic Lamanai environmental exposure fits within human history of exposure.

A similar study that includes more trace elements or isotopes would also be useful. The examination of additional trace elements detected (e.g. biologically essential element Cu) may lend further insight into the bioavailability and exposure of this sample group from the Postclassic period.

A similar study also involving a larger sample size from this site and extending to incorporated a wider time period may be useful to more thoroughly and accurately interpret the subtle influences of exposure and bioavailability in this sample population and to perform more rigorous statistical analyses. A larger sample size should include a larger selection of upper lateral incisors (ULI), as well as an inclusion of all other tooth types from the maxilla (including canines and all three molars). Mapping the spatial distributions and relative intensities of trace isotopes for all eight tooth types would be useful for plotting isotopic variation across time, from the earliest tooth formation to the latest tooth formation. Similar mapping studies should also expand to include both upper and lower teeth, in order to compare how exposure and bioavailability manifests differently within the same individual.

Since this was a preliminary study, there was not demographic information of each tooth for the entire group sample. Thus, traditional bioarchaeological research

questions regarding the similarities and differences between different sexes and ages could not be explored in this study. Thus, a larger sample size that includes more substantial demographic information would also bolster bioarchaeological interpretations of this Postclassic Lamanai population, such as examining similarities and differences in isotopic distribution between biological males and females and younger and older individuals. For example, isotope intensities and concentrations may change with age (i.e. with time) and demonstrate prolonged exposure (Shepherd et al., 2012). In addition, any similarities or differences noted in diet-related isotopes between men and women could infer whether or not there was a sexual division of labor or further social status divisions within this sample population (Guede et al., 2017; Martin et al., 2013).

Additional studies using different tooth types from this same sample population may also broaden our understanding of environmental influences on intraindividual and interindividual variation. In particular, it may be useful to conduct a similar trace elemental analysis on the first molar, as this tooth type has been used in previous research for analyzing the prenatal and postnatal enamel regions in order to draw conclusions about dietary changes and health in the early life history of an individual (Dolphin et al., 2005; Dolphin and Goodman, 2009). Furthermore, comparative studies involving contemporary teeth or archaeological teeth with known dietary history and health conditions may serve as a useful control for better interpreting the results of this study.

In regards to the individual with a piece of jade lodged within the pulp cavity area (individual N10-2/21 UCI), it may be possible to use this initial finding to explore other avenues of the interaction of mortuary artifacts, containing jade or other valuable minerals such as hematite and cinnabar, with the physiology of human remains,

particularly among past or ancient populations known to incorporate these kinds of stones into their lifestyle. Although there were no distinctly unusual frequencies of isotopes associated with this individual sample, the interaction of jade with tooth chemical properties is an avenue worth exploring for further understanding exposure. In particular, futures studies should also include elemental mapping of mercury (Hg) detected in teeth recovered from Postclassic Lamanai, as this element is also a component of cinnabar. Research has shown that extreme heat can cause increased ionization of Hg (LeCount et al., 2016), and the location of the archaeological Lamanai site is conducive to generating this type of reaction. Thus, it would be useful to analyze the relative intensity and distribution of Hg in comparison to any cinnabar possibly recovered from the site.

In addition, soil sample collected from the Lamanai site (in particular each N10 structural location) could lend more insight into the role and extent of diagenesis on the teeth assess in this study, in comparison to the possible sources of exposure influencing the elemental distributions observed in this study. There have been many forensic and bioarchaeological studies that have considered the impact of diagenesis on human remains using LA-ICP-MS (Kohn et al., 2013; Martin et al., 2007; Willmes et al., 2016). This preliminary study could be a useful baseline for evaluating more directly the impact of diagenesis on dental remains.

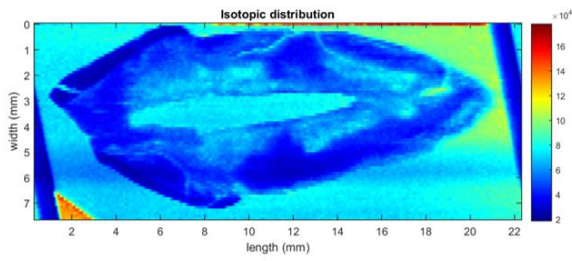
Mapping the trace elemental distribution in teeth using LA-ICP-MS has the potential to be applied in various avenues of study. For example, the distribution of essential isotopes in teeth, such as ^{13}C , may be useful in informing stable isotope research, which involves the use of dental enamel in effort to reconstruct paleodiet, as has been previously suggested in a trace elemental study by Dolphin et al. (2005). Trace

element maps created using LA-ICP-MS may serve to fill in missing gaps of information in anthropological study and allow for more precise interpretations of stable isotope data, as this method is nondestructive to the sample, whereas stable isotope analyses are destructive (Dolphin et al., 2005).

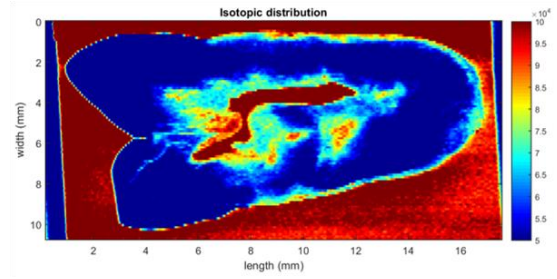
The continued application of LA-ICP-MS to map the distribution of elements in teeth warrants further forensic inquiry, for the potential to discriminate between species, sexes, or individuals (Castro et al., 2010; Kumagai et al., 2012; Nganvongpanit et al., 2017). Information gleaned from this study could provide deeper insight regarding the relationship between intraindividual variation and interindividual variation of this sample group. This study also serves as a baseline for standardizing trace elements' disruptions at specific tooth locations across tooth types and individuals. For example, although Ti has not been commonly analyzed in archaeological teeth, the examination of ^{47}Ti distribution in teeth in this study may be a useful reference for evaluating teeth in forensic and health-related research, as titanium-alloy dental implants have become more prominent and have been shown to impact the oral cavity environment through wear and corrosive processes (Sajnog et al., 2016; Souza et al., 2015).

Thus, elemental mapping of an entire cross-section of a tooth using LA-ICP-MS provides more nuanced information than is currently available through traditional bulk elemental analyses. This method has the potential to generate more precise discrimination between individuals and more refined evaluation of biocultural effects on teeth.

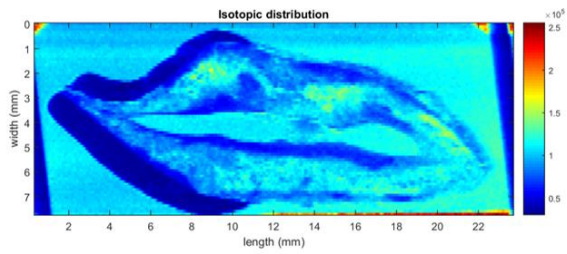
APPENDIX A: ELEMENTAL MAPS



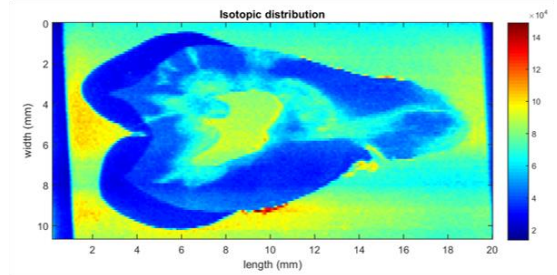
¹³C distribution (N10-1/02 UCI)



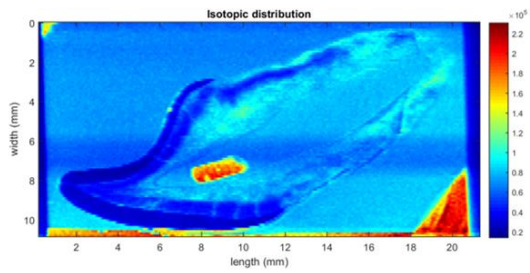
¹³C distribution (N10-1/02 UPM1)



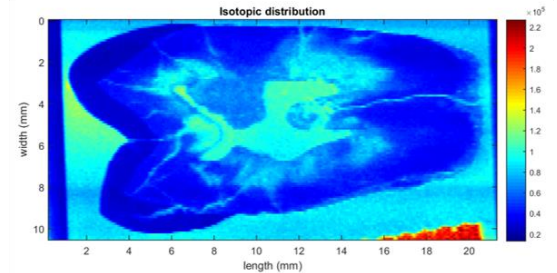
¹³C distribution (N10-2/20A or B UCI)



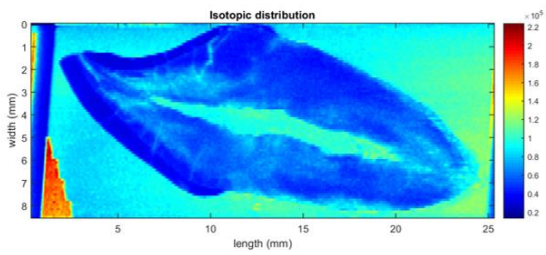
¹³C distribution (N10-2/20A or B UPM2)



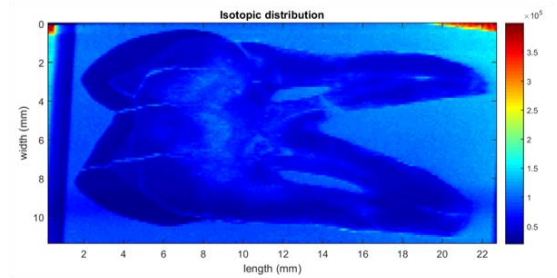
¹³C distribution (N10-2/21 UCI)



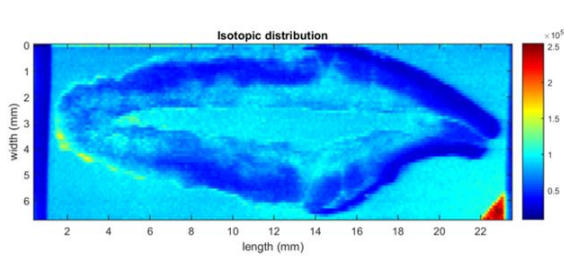
¹³C distribution (N10-2/21 UPM2)



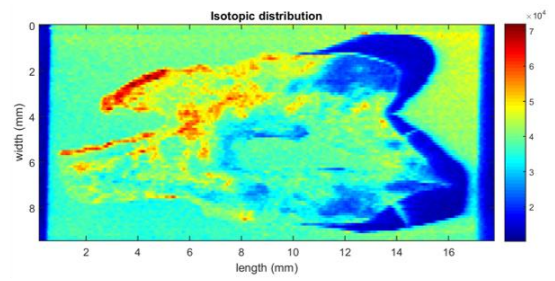
¹³C distribution (N10-2/21A UCI)



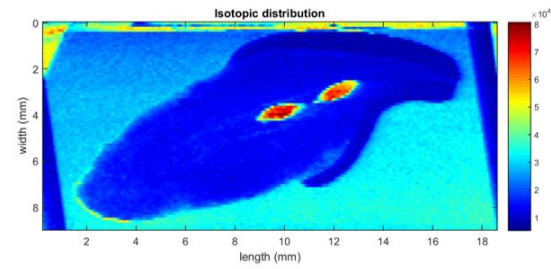
¹³C distribution (N10-2/21A UPM1)



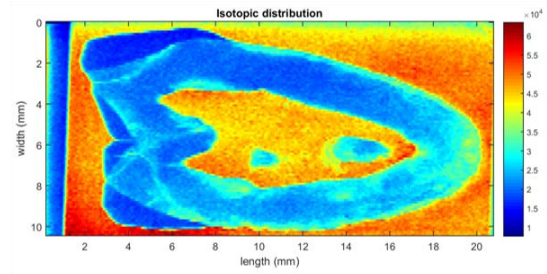
^{13}C distribution (N10-2/42B UCI)



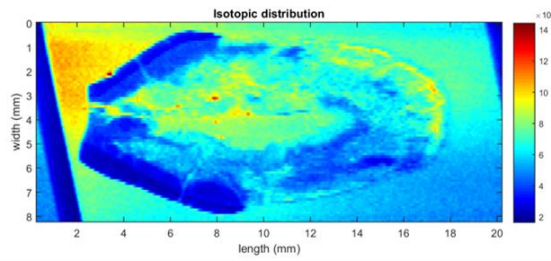
^{13}C distribution (N10-2/42B UPM1)



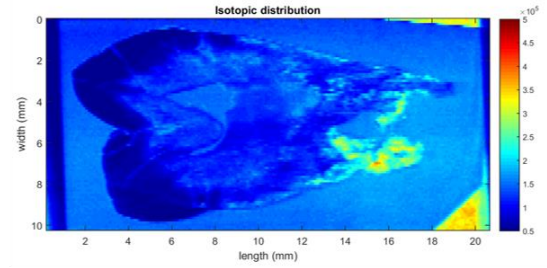
^{13}C distribution (N10-4/01 UCI)



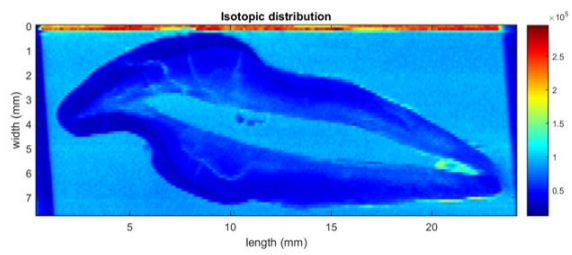
^{13}C distribution (N10-4/01 UPM2)



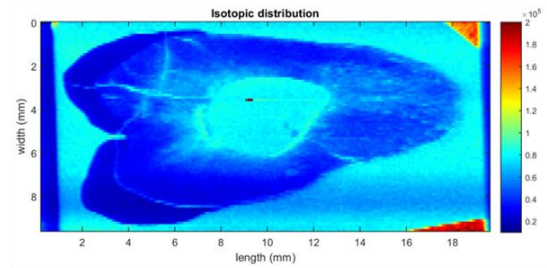
^{13}C distribution (N10-4/43 UCI)



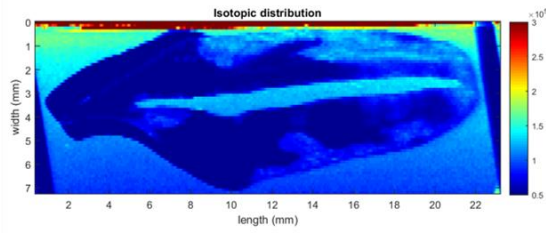
^{13}C distribution (N10-4/43 UPM1)



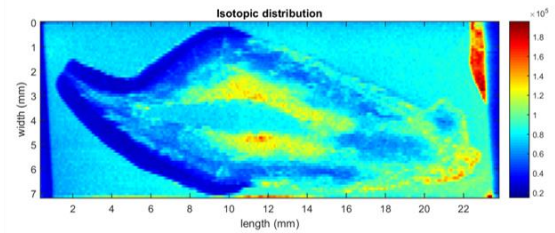
^{13}C distribution (N10-4/46C Large UCI)



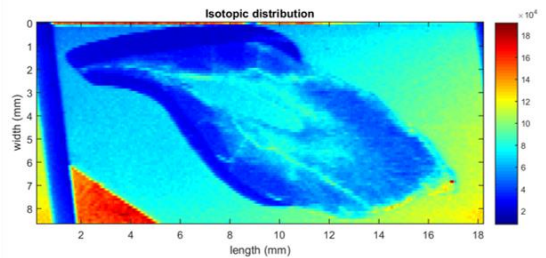
^{13}C distribution (N10-4/46C Large UPM2)



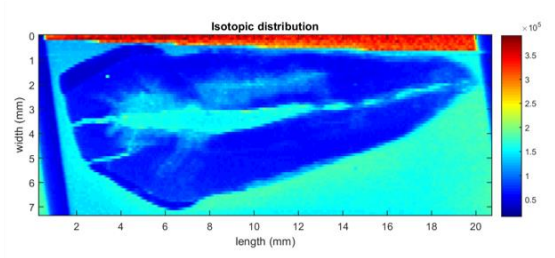
¹³C distribution (N10-4/19 UCI)



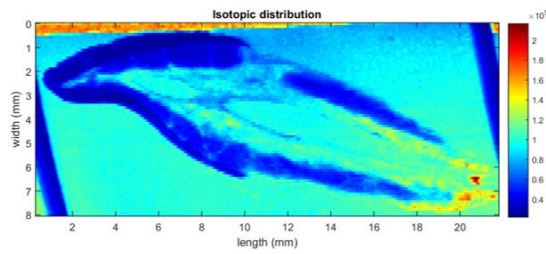
¹³C distribution (N10-4/31 UCI)



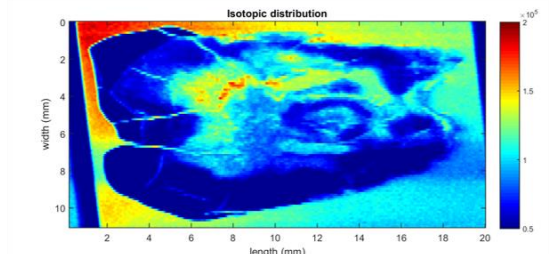
¹³C distribution (N10-4/35 UCI)



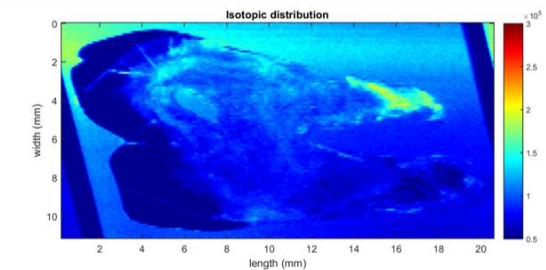
¹³C distribution (N10-4/46A UCI)



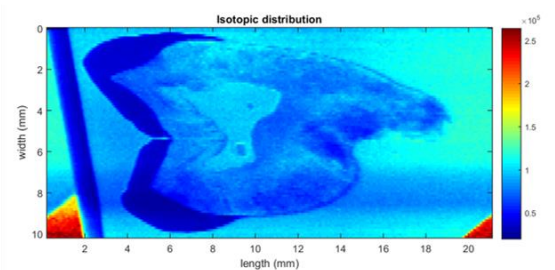
¹³C distribution (N10-2/49 ULI)



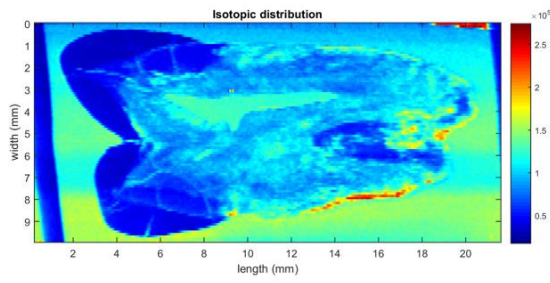
¹³C distribution (N10-2/22 UPM1)



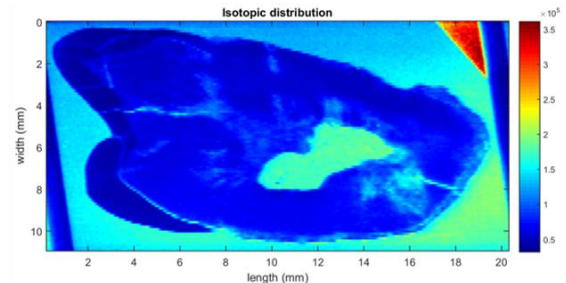
¹³C distribution (N10-2/40 UPM1)



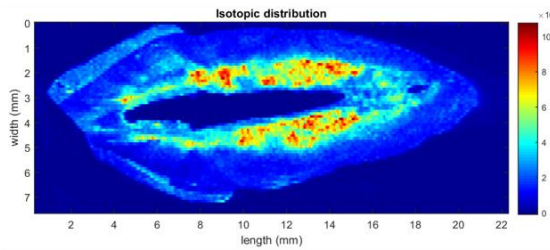
¹³C distribution (N10-4/10 UPM2)



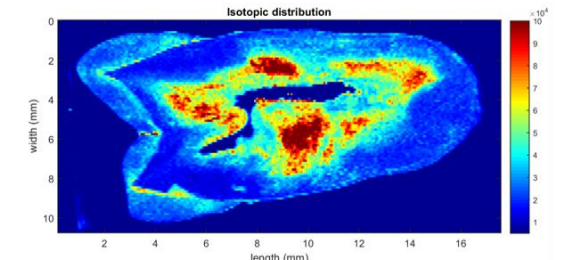
^{13}C distribution (N10-4/33 UPM2)



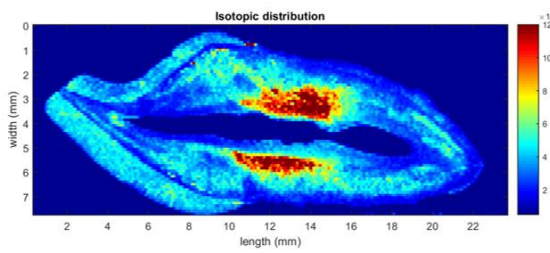
^{13}C distribution (N10-4/46C Small UPM2)



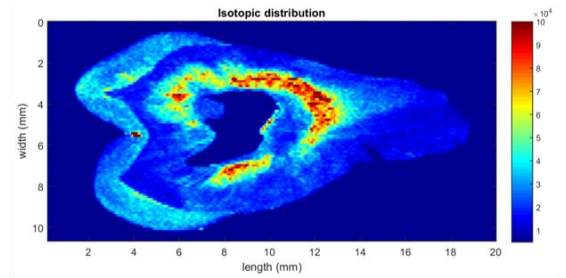
^{24}Mg distribution (N10-1/02 UCI)



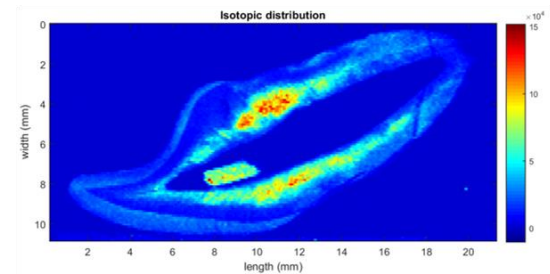
^{24}Mg distribution (N10-1/02 UPM1)



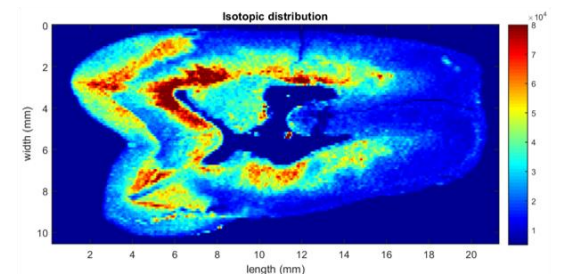
^{24}Mg distribution (N10-2/20A or B UCI)



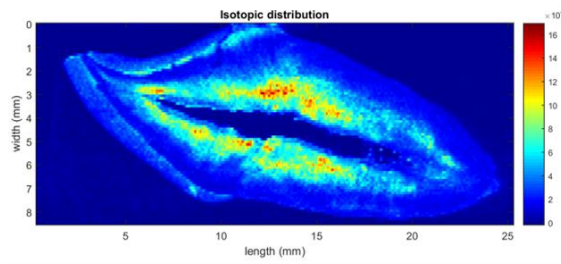
^{24}Mg distribution (N10-2/20A or B UPM2)



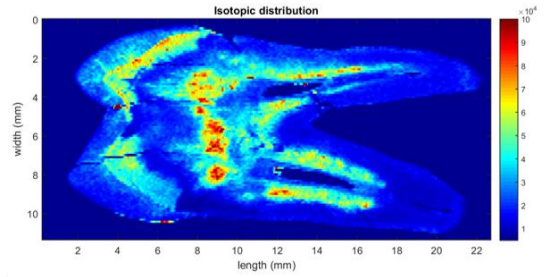
^{24}Mg distribution (N10-2/21 UCI)



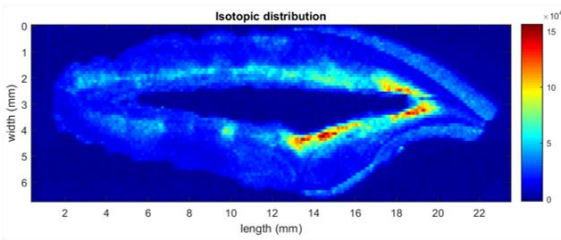
^{24}Mg distribution (N10-2/21 UPM2)



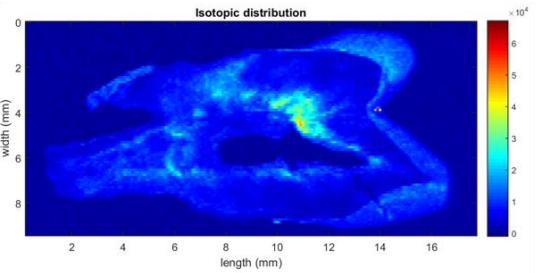
²⁴Mg distribution (N10-2/21A UCI)



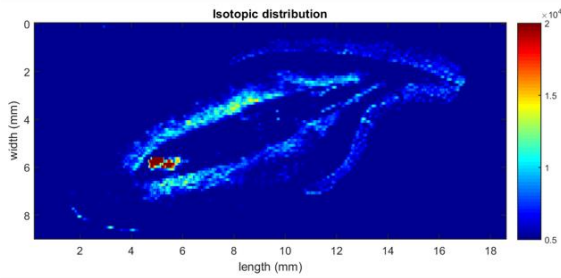
²⁴Mg distribution (N10-2/21A UPM1)



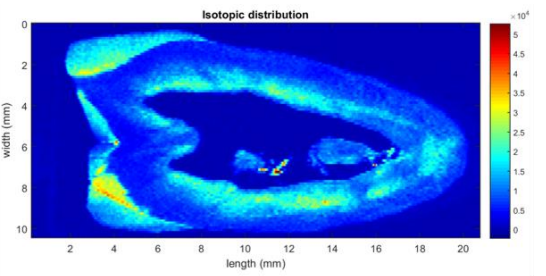
²⁴Mg distribution (N10-2/42B UCI)



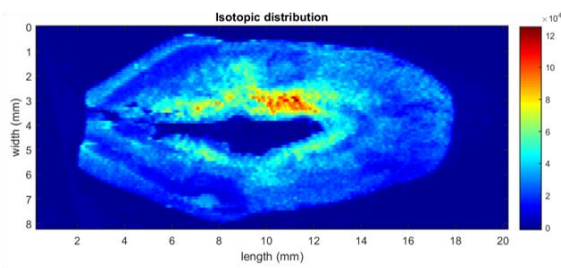
²⁴Mg distribution (N10-2/42B UPM1)



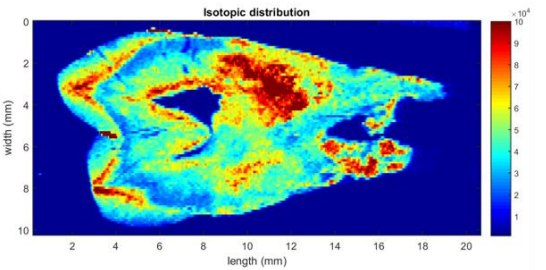
²⁴Mg distribution (N10-4/01 UCI)



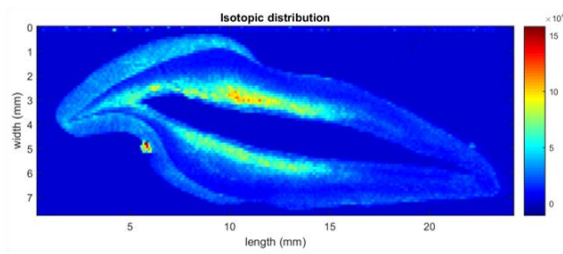
²⁴Mg distribution (N10-4/01 UPM2)



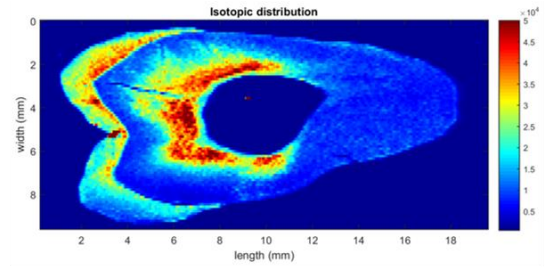
²⁴Mg distribution (N10-4/43 UCI)



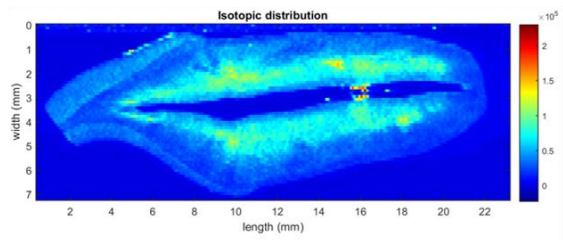
²⁴Mg distribution (N10-4/43 UPM1)



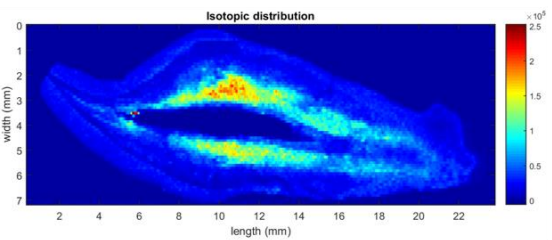
²⁴Mg distribution (N10-4/46C Large UCI)



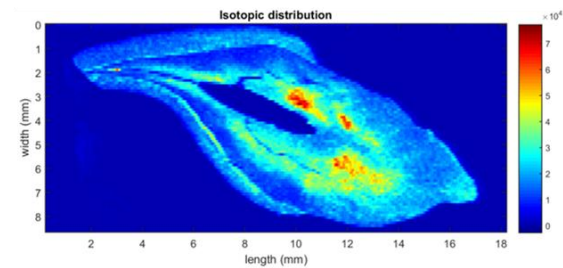
²⁴Mg distribution (N10-4/46C Large UPM2)



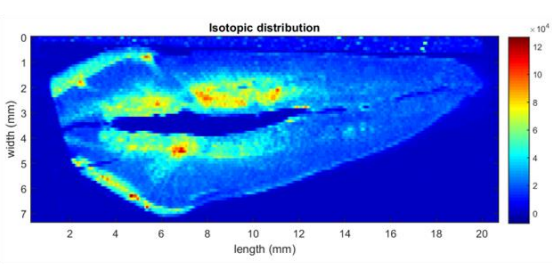
²⁴Mg distribution (N10-4/19 UCI)



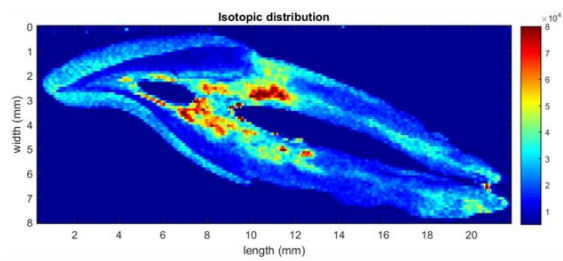
²⁴Mg distribution (N10-4/31 UCI)



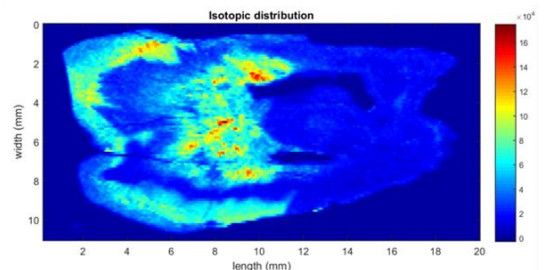
²⁴Mg distribution (N10-4/35 UCI)



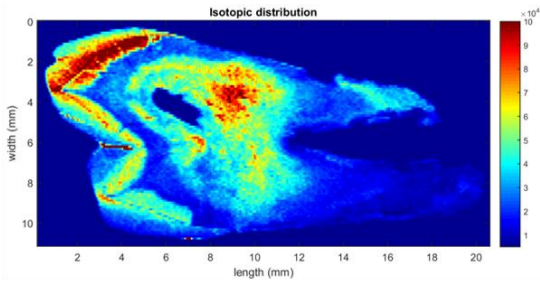
²⁴Mg distribution (N10-4/46A UCI)



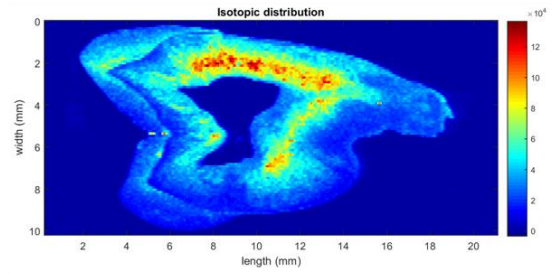
²⁴Mg distribution (N10-2/49 ULI)



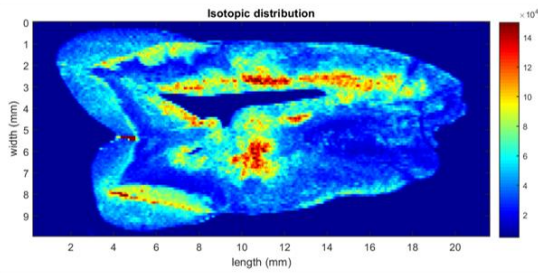
²⁴Mg distribution (N10-2/22 UPM1)



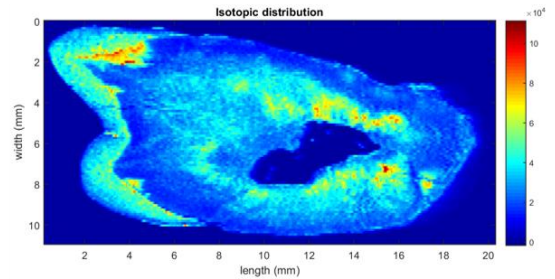
^{24}Mg distribution (N10-2/40 UPM1)



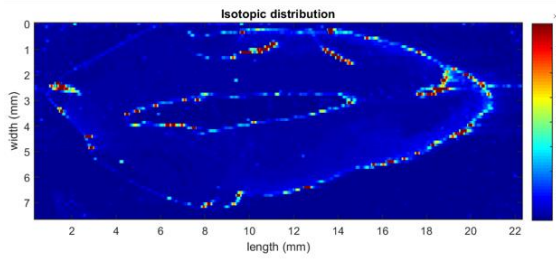
^{24}Mg distribution (N10-4/10 UPM2)



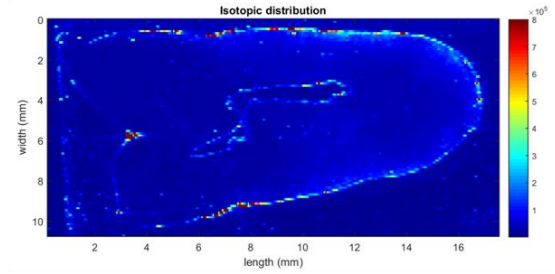
^{24}Mg distribution (N10-4/33 UPM2)



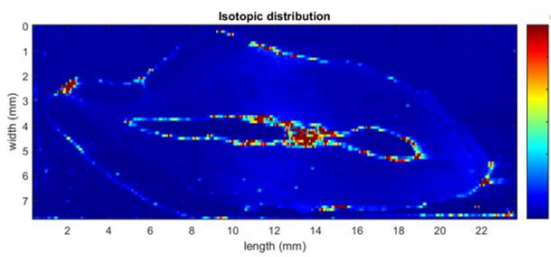
^{24}Mg distribution (N10-4/46C Small UPM2)



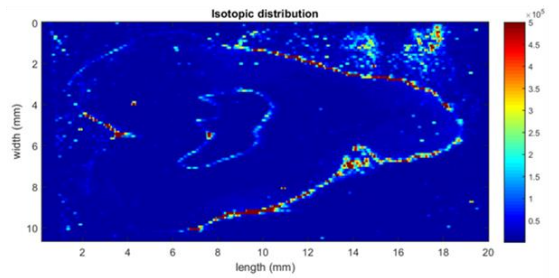
^{27}Al distribution (N10-1/02 UCI)



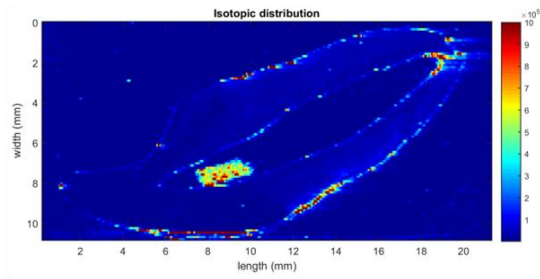
^{27}Al distribution (N10-1/02 UPM1)



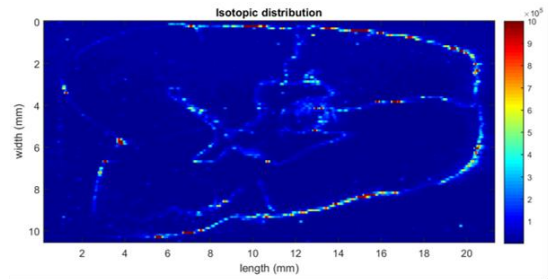
^{27}Al distribution (N10-2/20A or B UCI)



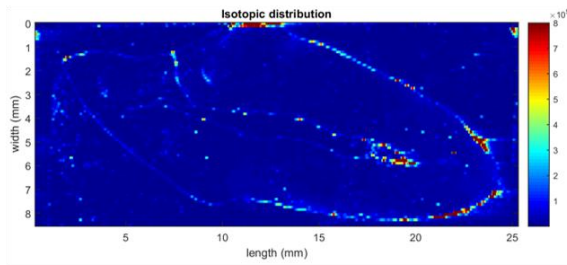
^{27}Al distribution (N10-2/20A or B UPM2)



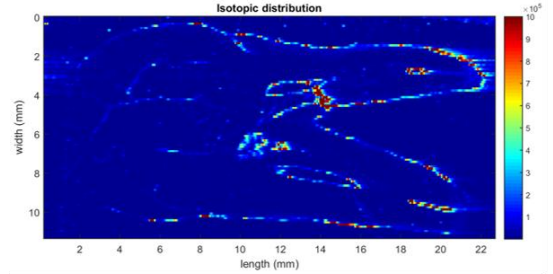
^{27}Al distribution (N10-2/21 UCI)



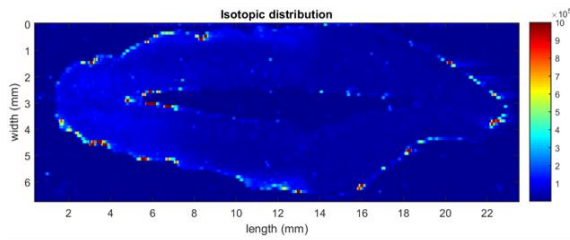
^{27}Al distribution (N10-2/21 UPM2)



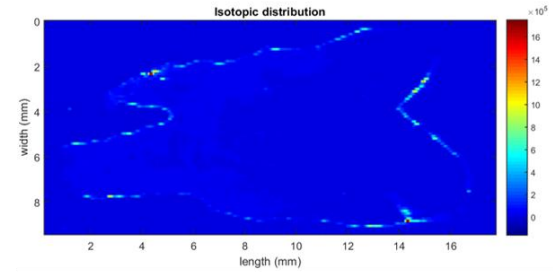
^{27}Al distribution (N10-2/21A UCI)



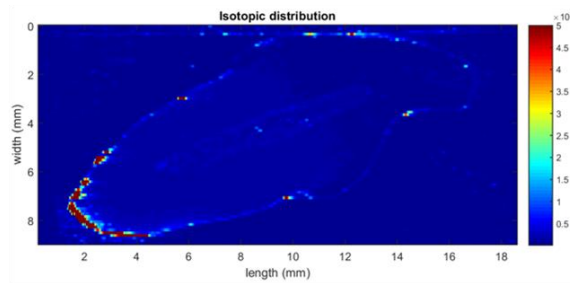
^{27}Al distribution (N10-2/21A UPM1)



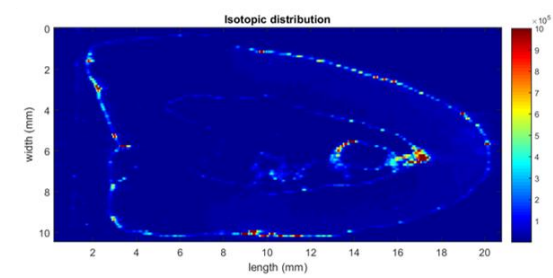
^{27}Al distribution (N10-2/42B UCI)



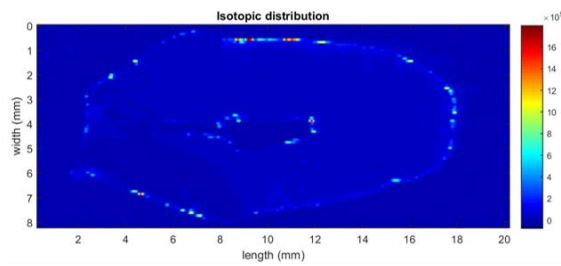
^{27}Al distribution (N10-2/42B UPM1)



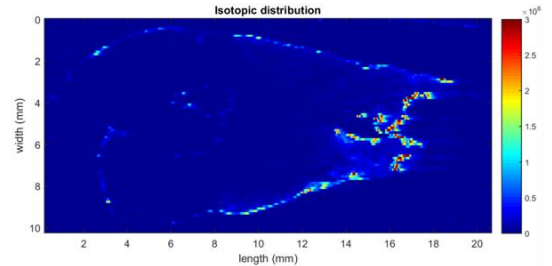
^{27}Al distribution (N10-4/01 UCI)



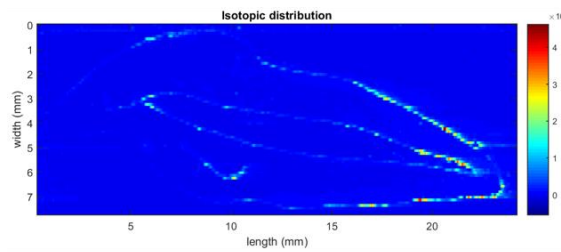
^{27}Al distribution (N10-4/01 UPM2)



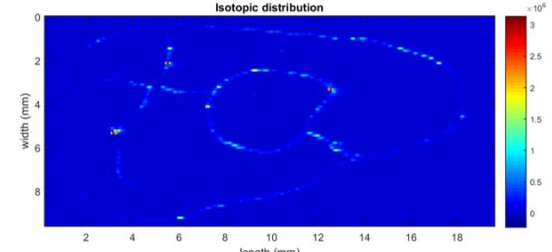
²⁷Al distribution (N10-4/43 UCI)



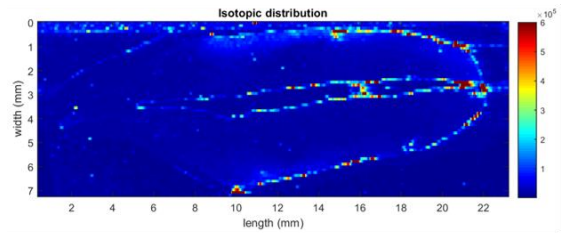
²⁷Al distribution (N10-4/43 UPM1)



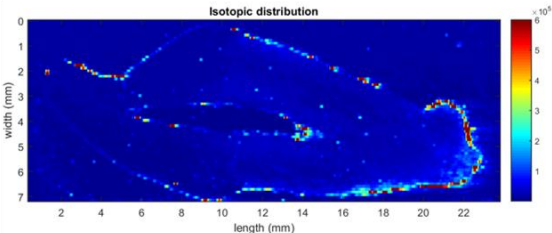
²⁷Al distribution (N10-4/46C Large UCI)



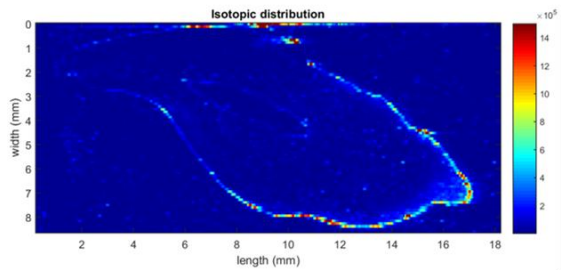
²⁷Al distribution (N10-4/46C Large UPM2)



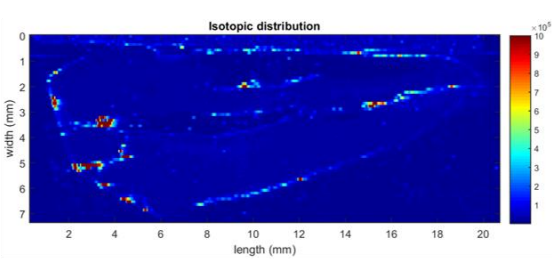
²⁷Al distribution (N10-4/19 UCI)



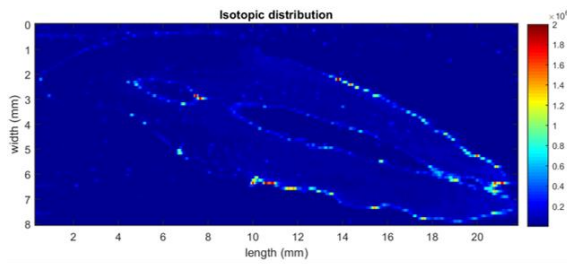
²⁷Al distribution (N10-4/31 UCI)



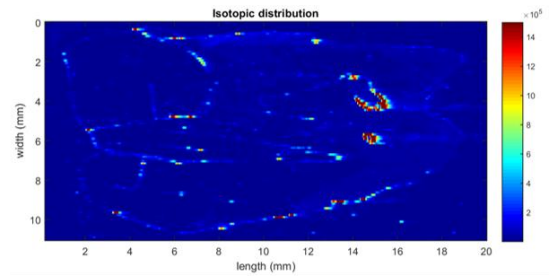
²⁷Al distribution (N10-4/35 UCI)



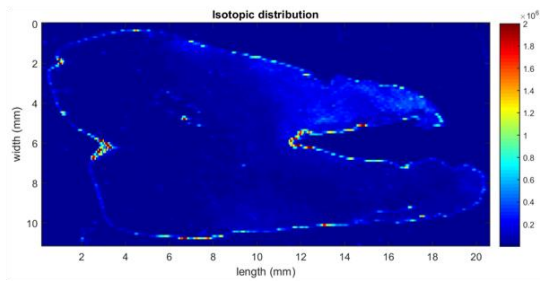
²⁷Al distribution (N10-4/46A UCI)



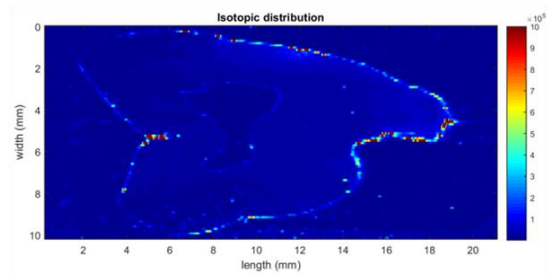
²⁷Al distribution (N10-2/49 ULI)



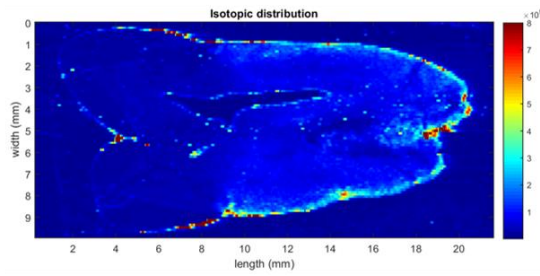
²⁷Al distribution (N10-2/22 UPM1)



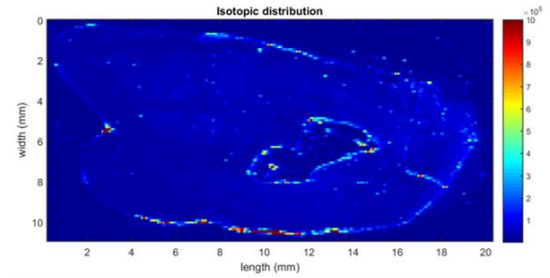
²⁷Al distribution (N10-2/40 UPM1)



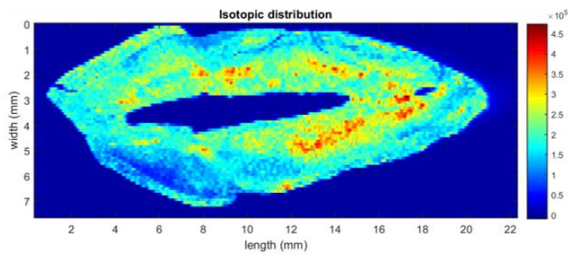
²⁷Al distribution (N10-4/10 UPM2)



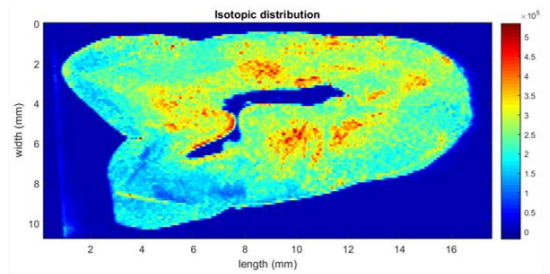
²⁷Al distribution (N10-4/33 UPM2)



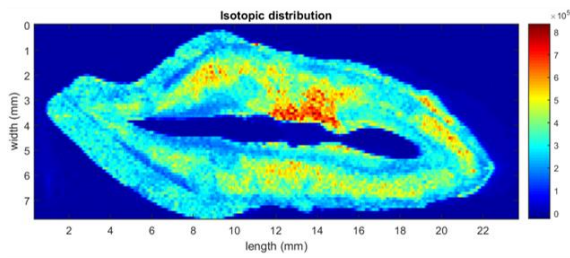
²⁷Al distribution (N10-4/46C Small UPM2)



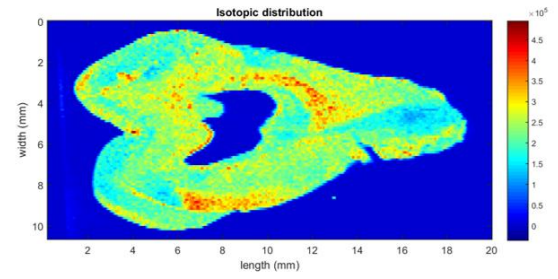
³¹P distribution (N10-1/02 UCI)



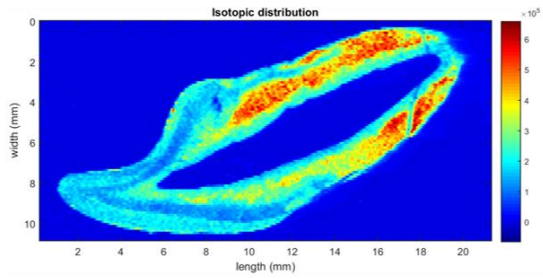
³¹P distribution (N10-1/02 UPM1)



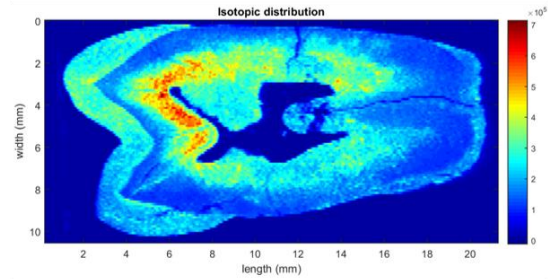
^{31}P distribution (N10-2/20A or B UCI)



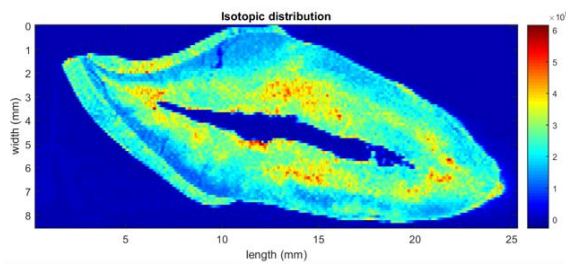
^{31}P distribution (N10-2/20A or B UPM2)



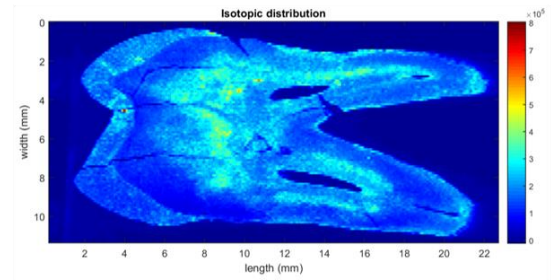
^{31}P distribution (N10-2/21 UCI)



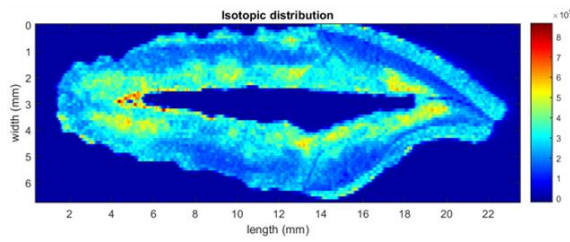
^{31}P distribution (N10-2/21 UPM2)



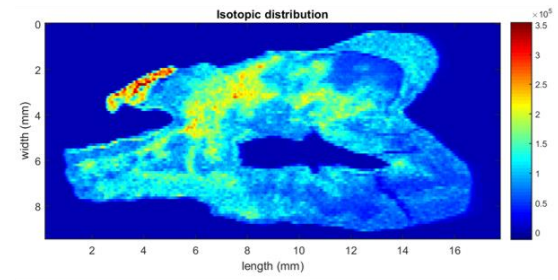
^{31}P distribution (N10-2/21A UCI)



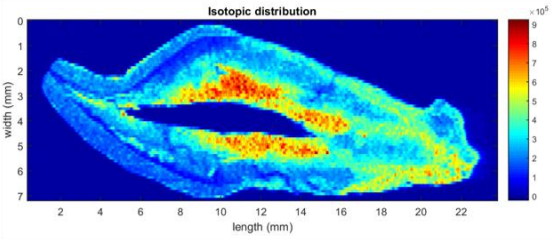
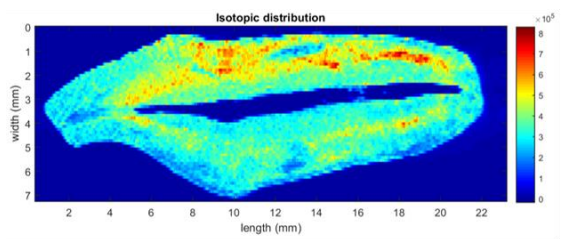
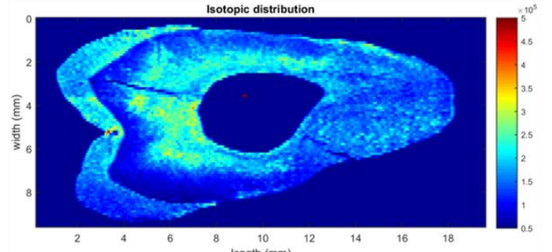
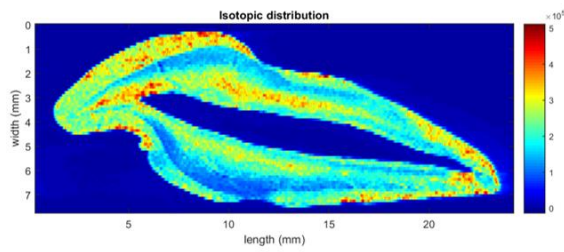
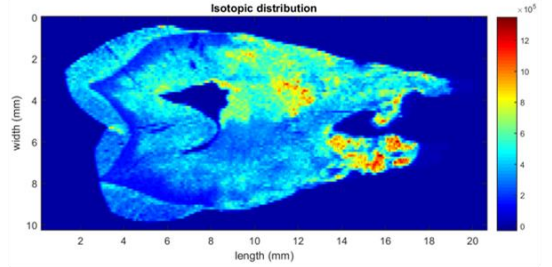
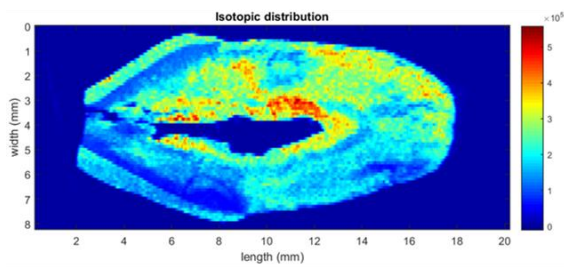
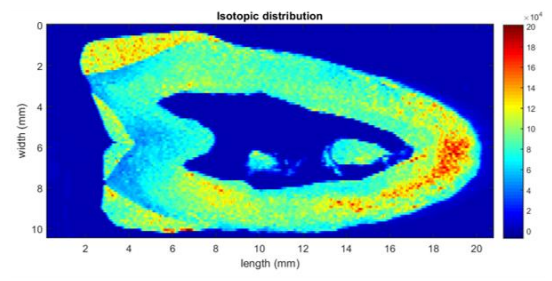
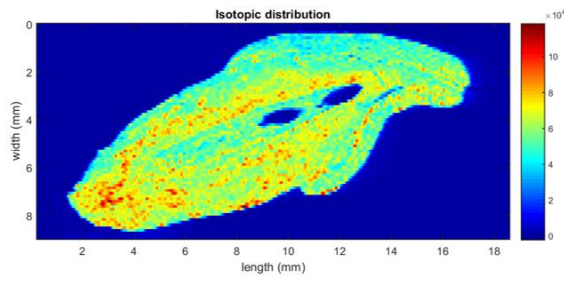
^{31}P distribution (N10-2/21A UPM1)

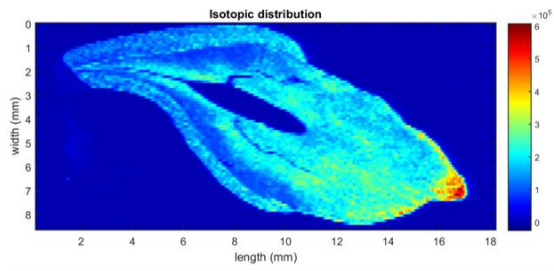


^{31}P distribution (N10-2/42B UCI)

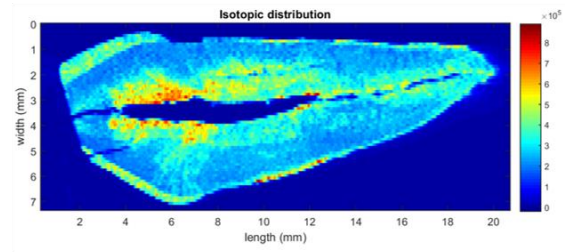


^{31}P distribution (N10-2/42B UPM1)

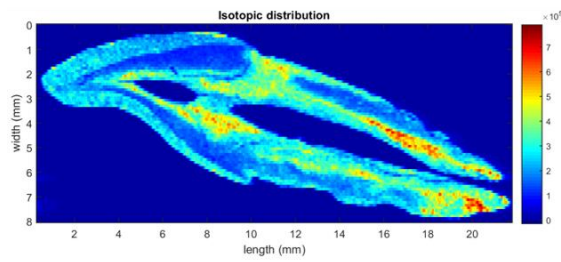




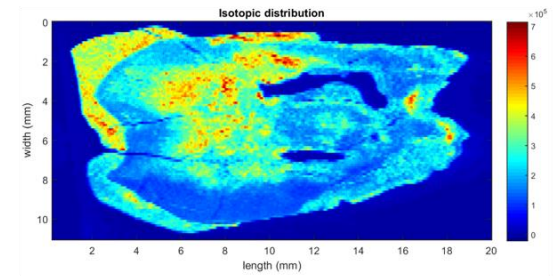
³¹P distribution (N10-4/35 UCI)



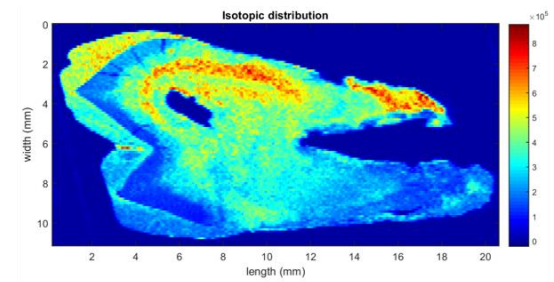
³¹P distribution (N10-4/46A UCI)



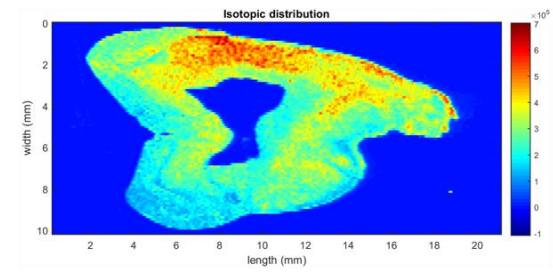
³¹P distribution (N10-2/49 ULI)



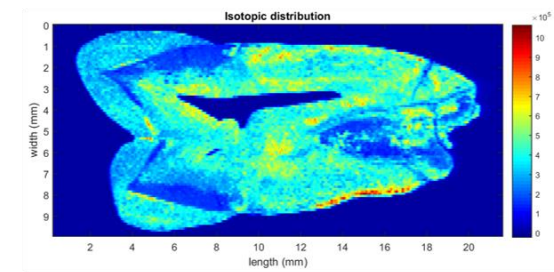
³¹P distribution (N10-2/22 UPM1)



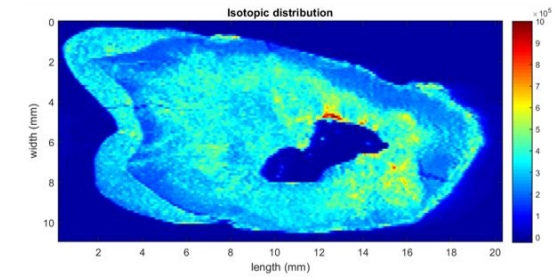
³¹P distribution (N10-2/40 UPM1)



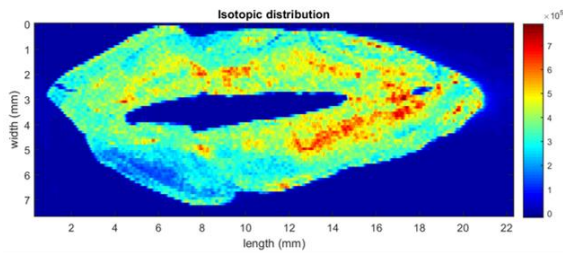
³¹P distribution (N10-4/10 UPM2)



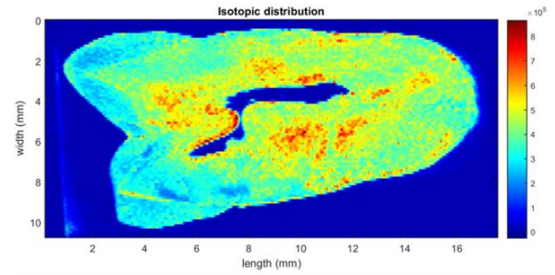
³¹P distribution (N10-4/33 UPM2)



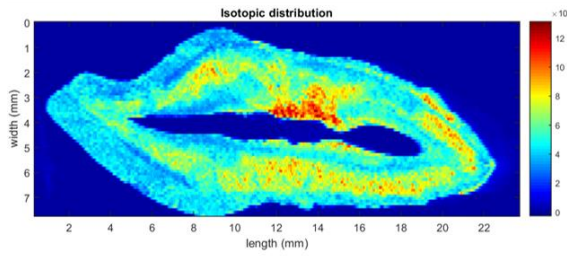
³¹P distribution (N10-4/46C Small UPM2)



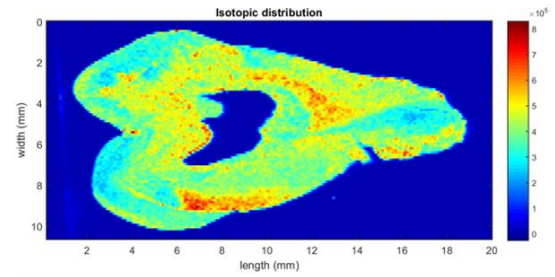
⁴⁴Ca distribution (N10-1/02 UCI)



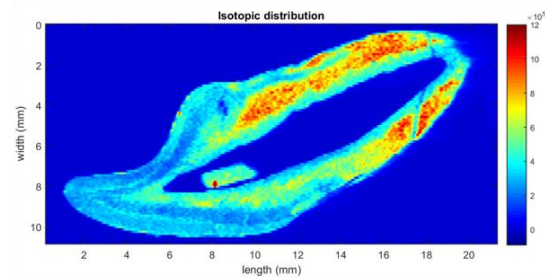
⁴⁴Ca distribution (N10-1/02 UPM1)



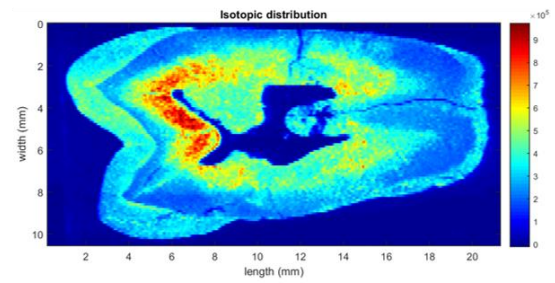
⁴⁴Ca distribution (N10-2/20A or B UCI)



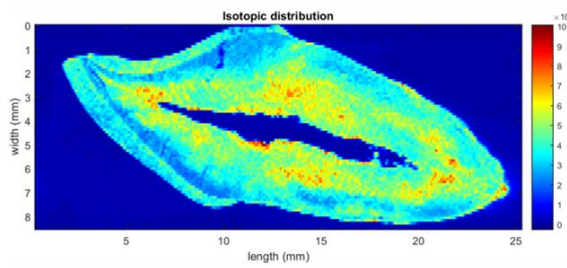
⁴⁴Ca distribution (N10-2/20A or B UPM2)



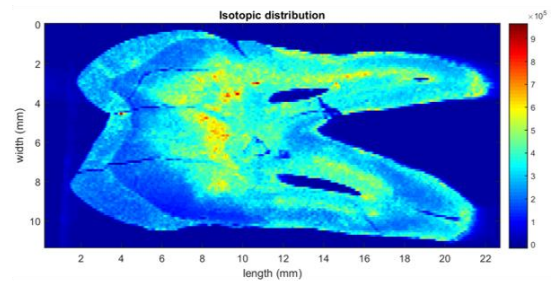
⁴⁴Ca distribution (N10-2/21 UCI)



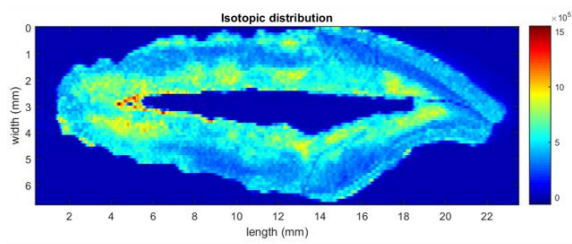
⁴⁴Ca distribution (N10-2/21 UPM2)



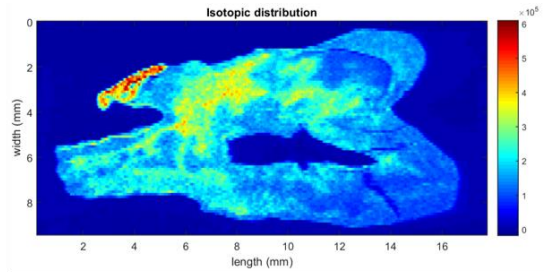
⁴⁴Ca distribution (N10-2/21A UCI)



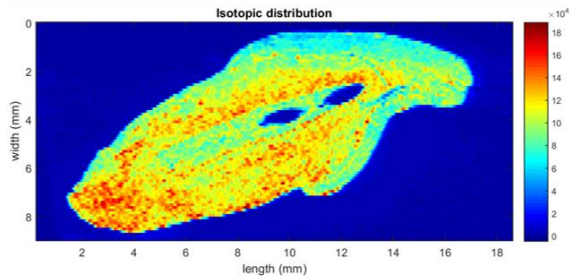
⁴⁴Ca distribution (N10-2/21A UPM1)



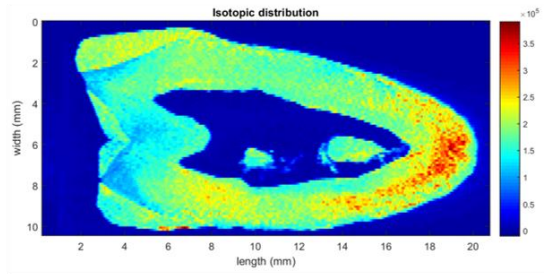
⁴⁴Ca distribution (N10-2/42B UCI)



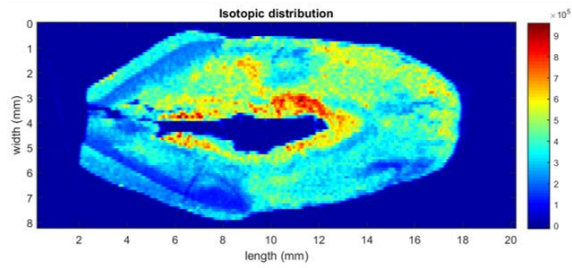
⁴⁴Ca distribution (N10-2/42B UPM1)



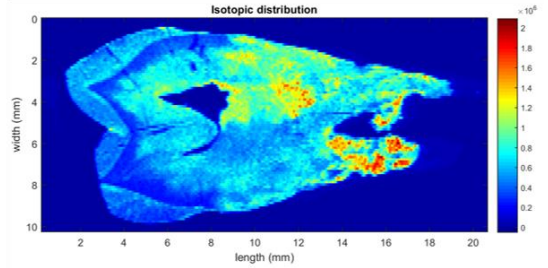
⁴⁴Ca distribution (N10-4/01 UCI)



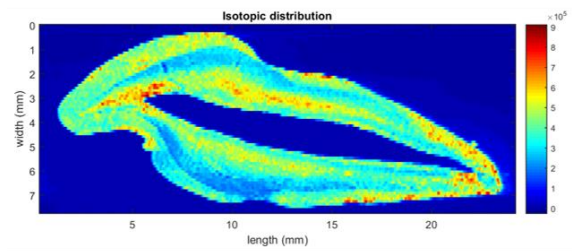
⁴⁴Ca distribution (N10-4/01 UPM2)



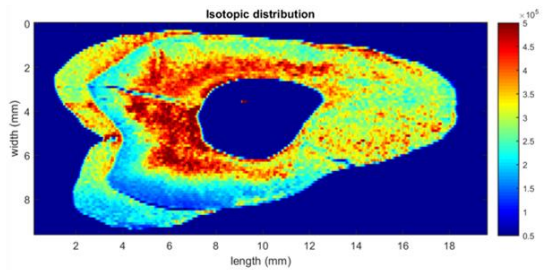
⁴⁴Ca distribution (N10-4/43 UCI)



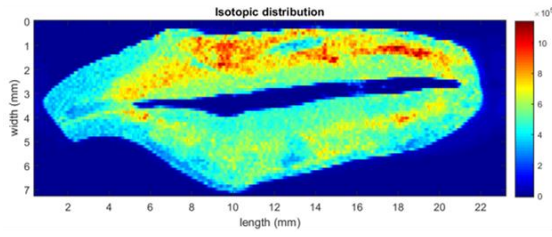
⁴⁴Ca distribution (N10-4/43 UPM1)



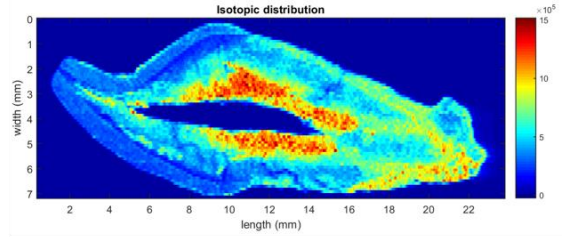
⁴⁴Ca distribution (N10-4/46C Large UCI)



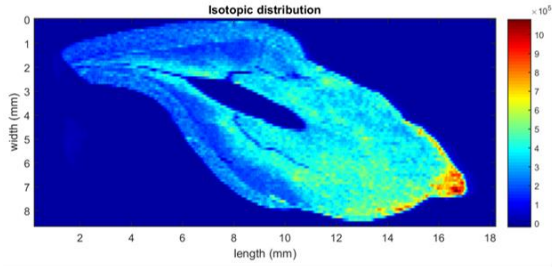
⁴⁴Ca distribution (N10-4/46C Large UPM2)



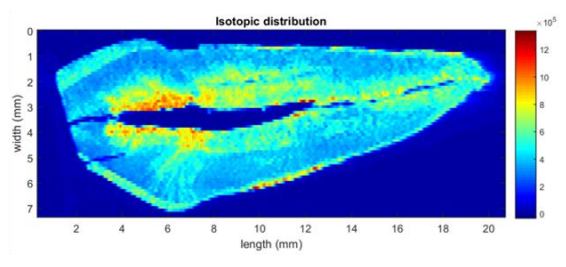
⁴⁴Ca distribution (N10-4/19 UCI)



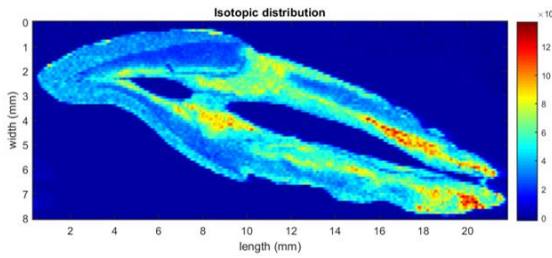
⁴⁴Ca distribution (N10-4/31 UCI)



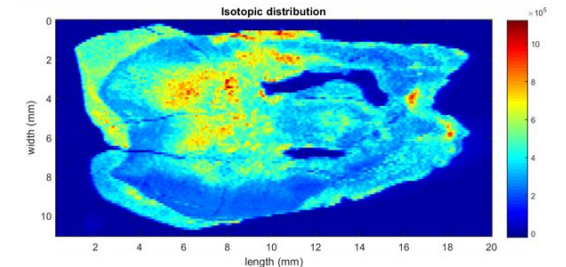
⁴⁴Ca distribution (N10-4/35 UCI)



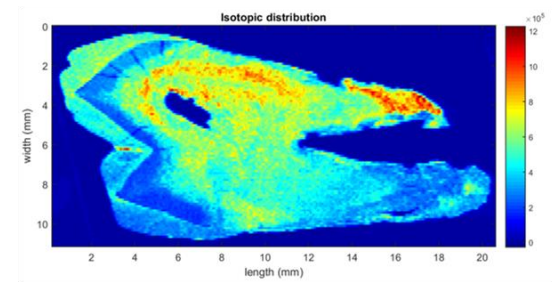
⁴⁴Ca distribution (N10-4/46A UCI)



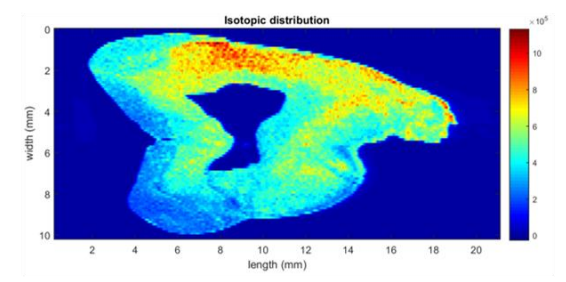
⁴⁴Ca distribution (N10-2/49 ULI)



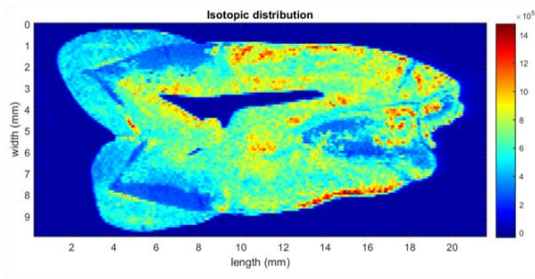
⁴⁴Ca distribution (N10-2/22 UPM1)



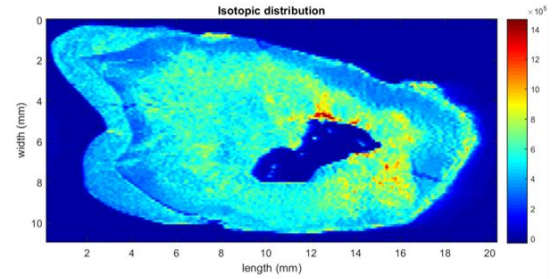
⁴⁴Ca distribution (N10-2/40 UPM1)



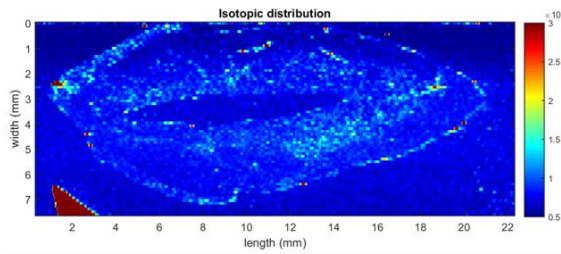
⁴⁴Ca distribution (N10-4/10 UPM2)



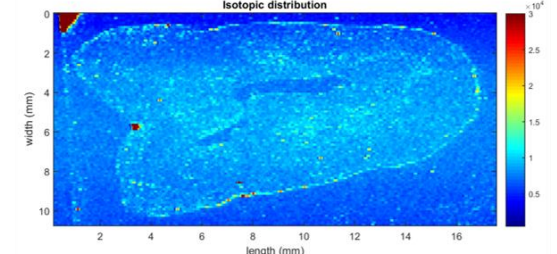
⁴⁴Ca distribution (N10-4/33 UPM2)



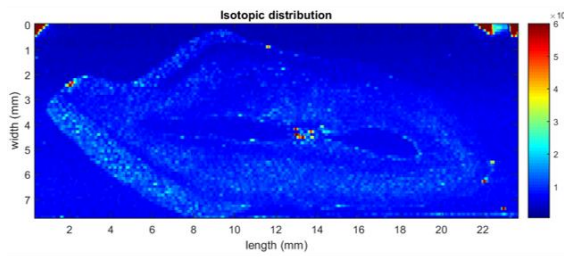
⁴⁴Ca distribution (N10-4/46C Small UPM2)



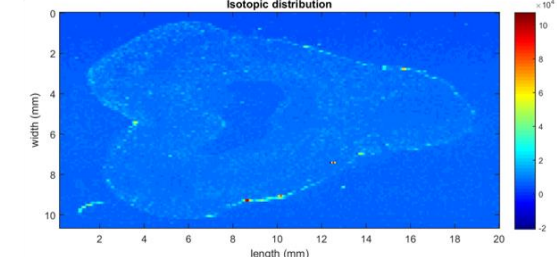
⁴⁷Ti distribution (N10-1/02 UCI)



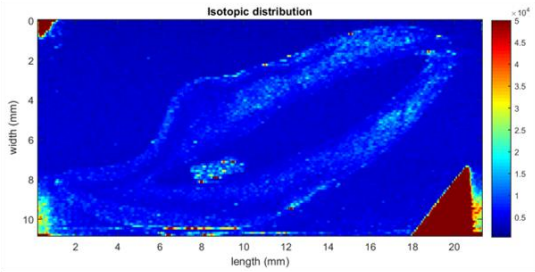
⁴⁷Ti distribution (N10-1/02 UPM1)



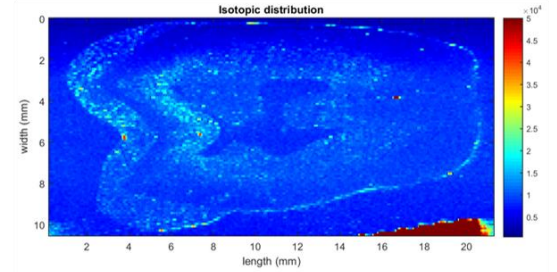
⁴⁷Ti distribution (N10-2/20A or B UCI)



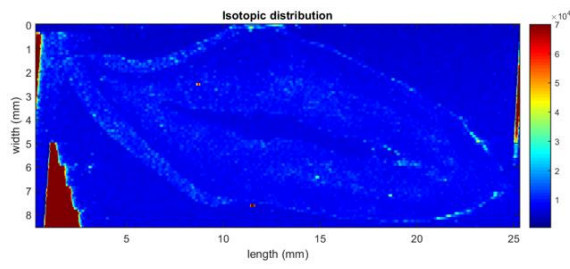
⁴⁷Ti distribution (N10-2/20A or B UPM2)



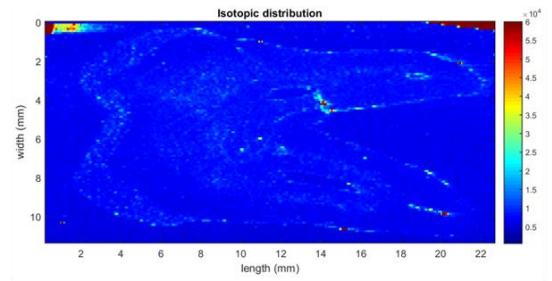
⁴⁷Ti distribution (N10-2/21 UCI)



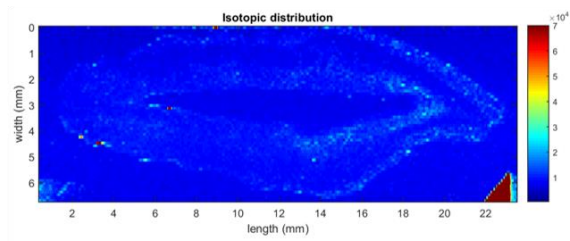
⁴⁷Ti distribution (N10-2/21 UPM2)



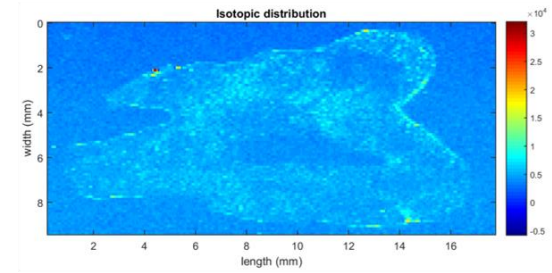
^{47}Ti distribution (N10-2/21A UCI)



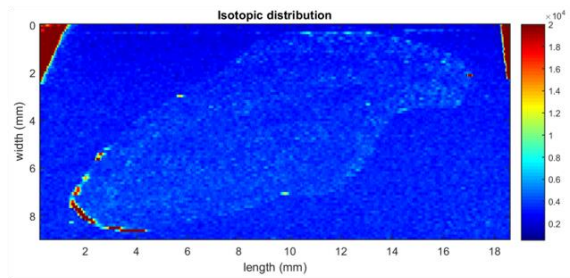
^{47}Ti distribution (N10-2/21A UPM1)



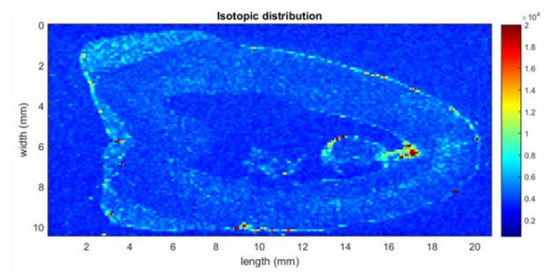
^{47}Ti distribution (N10-2/42B UCI)



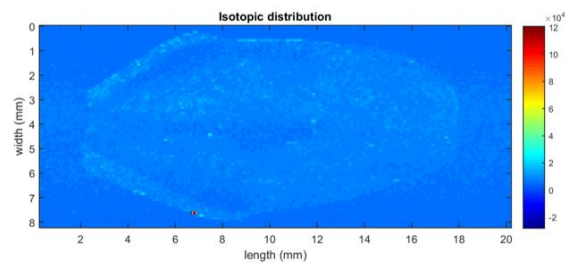
^{47}Ti distribution (N10-2/42B UPM1)



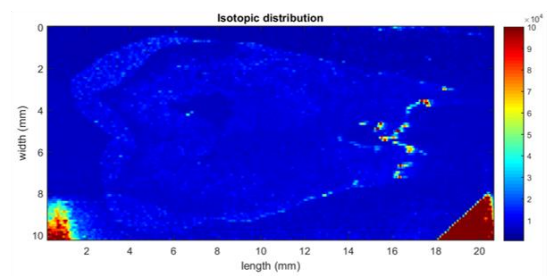
^{47}Ti distribution (N10-4/01 UCI)



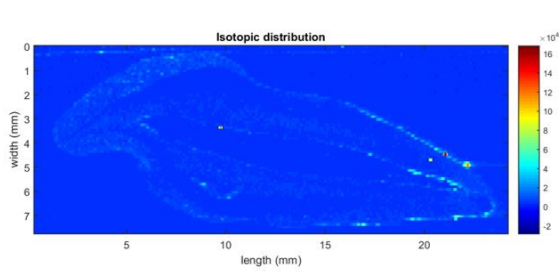
^{47}Ti distribution (N10-4/01 UPM2)



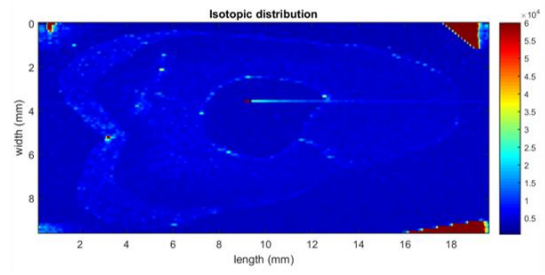
^{47}Ti distribution (N10-4/43 UCI)



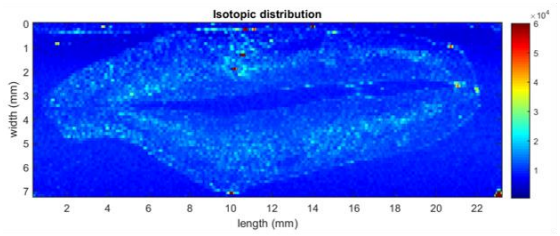
^{47}Ti distribution (N10-4/43 UPM1)



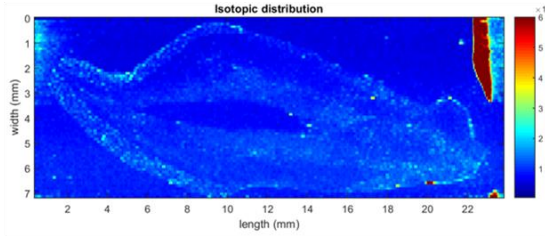
^{47}Ti distribution (N10-4/46C Large UCI)



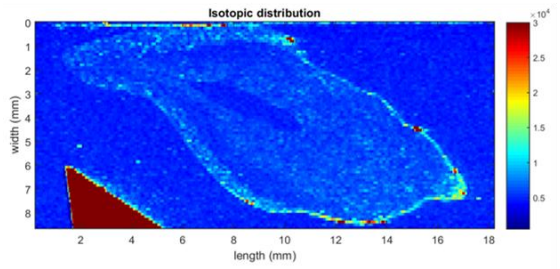
^{47}Ti distribution (N10-4/46C Large UPM2)



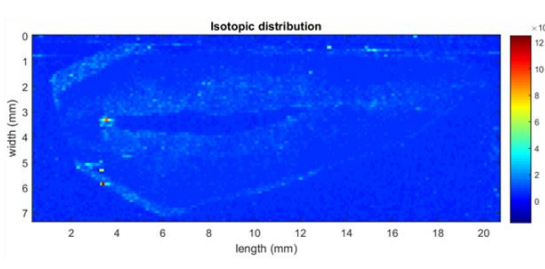
^{47}Ti distribution (N10-4/19 UCI)



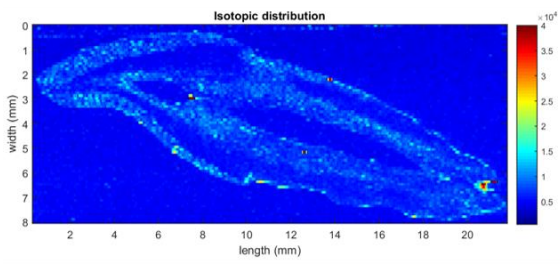
^{47}Ti distribution (N10-4/31 UCI)



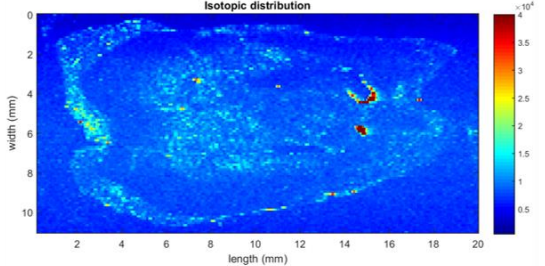
^{47}Ti distribution (N10-4/35 UCI)



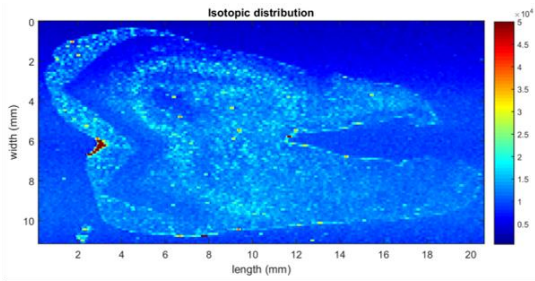
^{47}Ti distribution (N10-4/46A UCI)



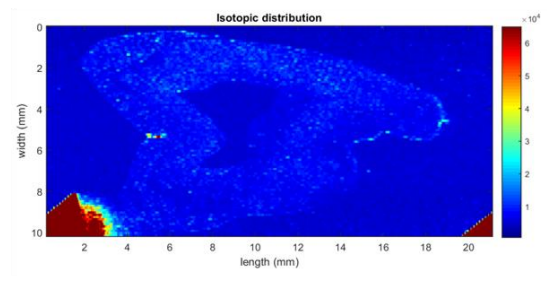
^{47}Ti distribution (N10-2/49 ULI)



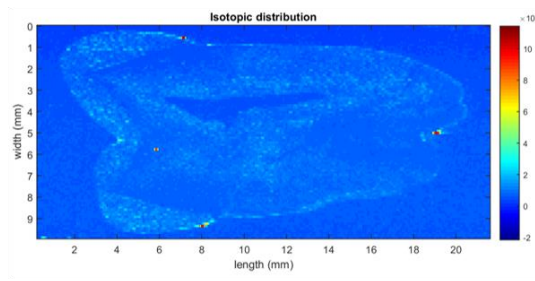
^{47}Ti distribution (N10-2/22 UPM1)



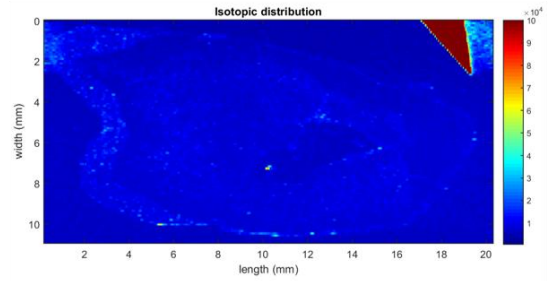
^{47}Ti distribution (N10-2/40 UPM1)



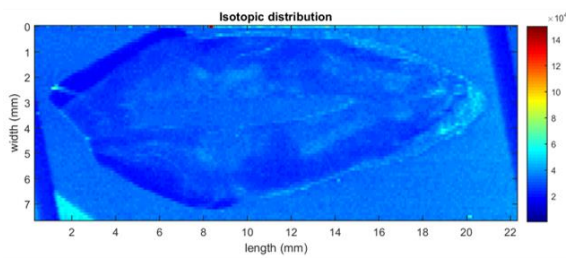
^{47}Ti distribution (N10-4/10 UPM2)



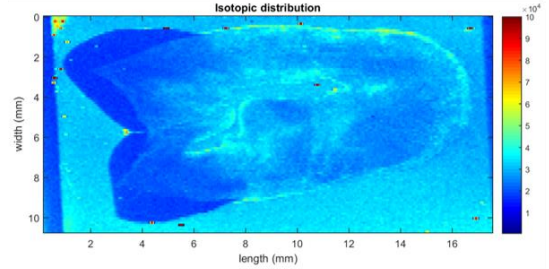
^{47}Ti distribution (N10-4/33 UPM2)



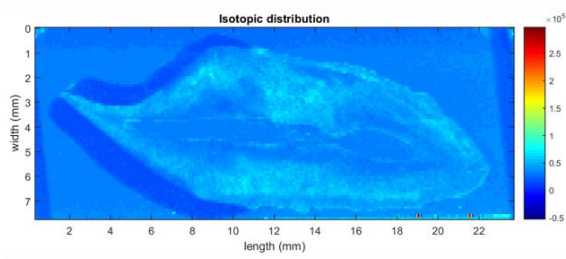
^{47}Ti distribution (N10-4/46C Small UPM2)



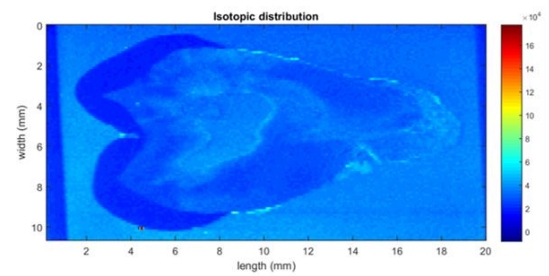
^{52}Cr distribution (N10-1/02 UCI)



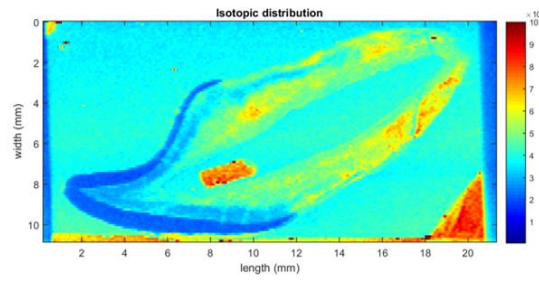
^{52}Cr distribution (N10-1/02 UPM1)



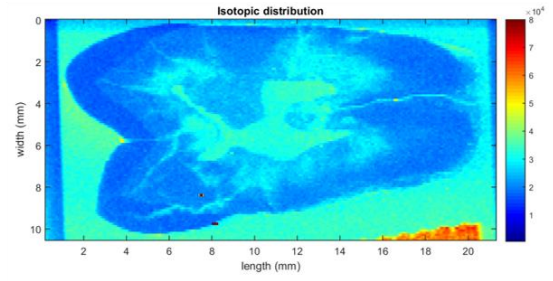
^{52}Cr distribution (N10-2/20A or B UCI)



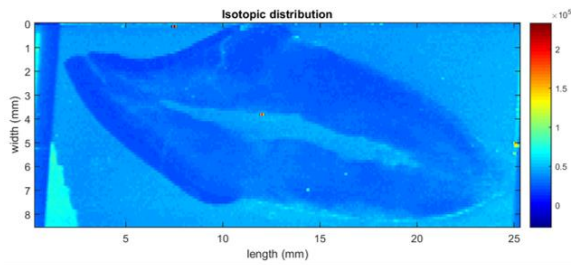
^{52}Cr distribution (N10-2/20A or B UPM2)



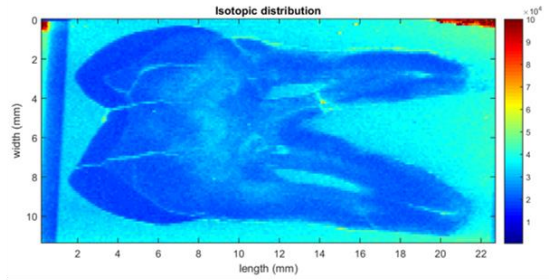
^{52}Cr distribution (N10-2/21 UCI)



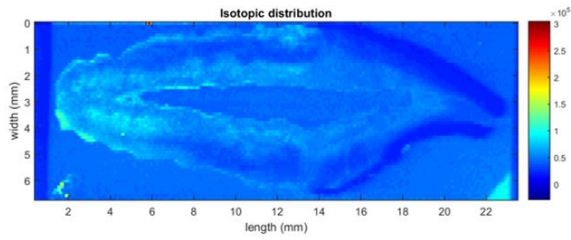
^{52}Cr distribution (N10-2/21 UPM2)



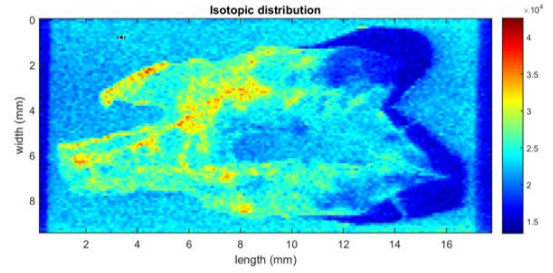
^{52}Cr distribution (N10-2/21A UCI)



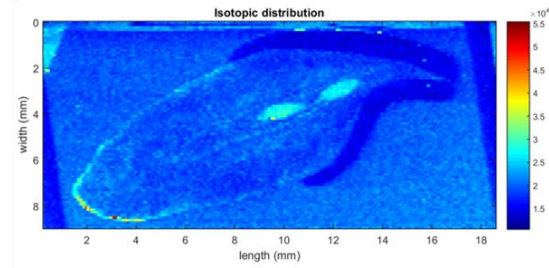
^{52}Cr distribution (N10-2/21A UPM1)



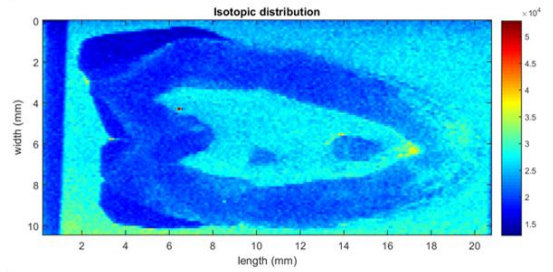
^{52}Cr distribution (N10-2/42B UCI)



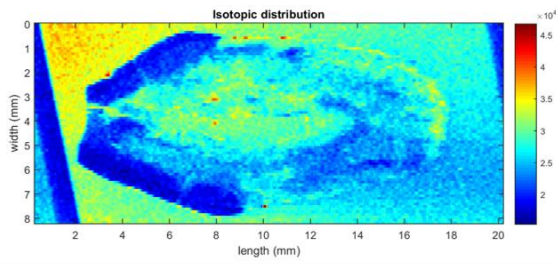
^{52}Cr distribution (N10-2/42B UPM1)



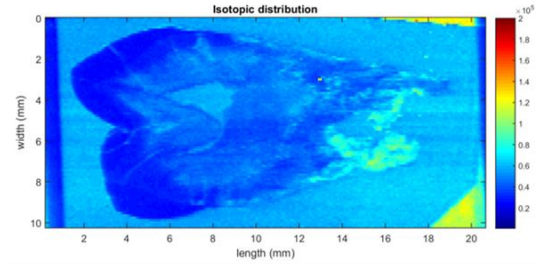
^{52}Cr distribution (N10-4/01 UCI)



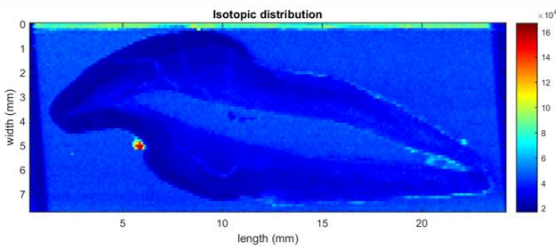
^{52}Cr distribution (N10-4/01 UPM2)



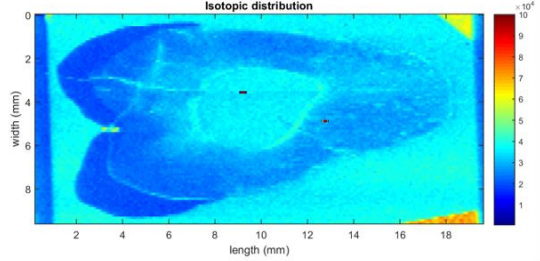
^{52}Cr distribution (N10-4/43 UCI)



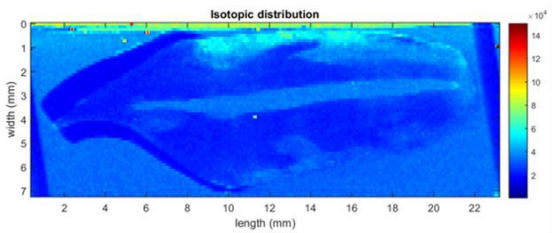
^{52}Cr distribution (N10-4/43 UPM1)



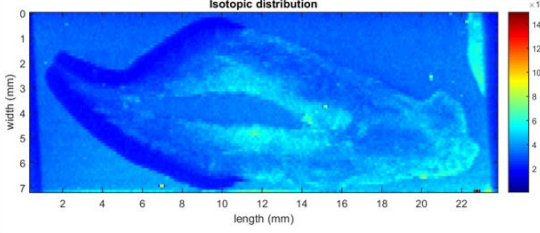
^{52}Cr distribution (N10-4/46C Large UCI)



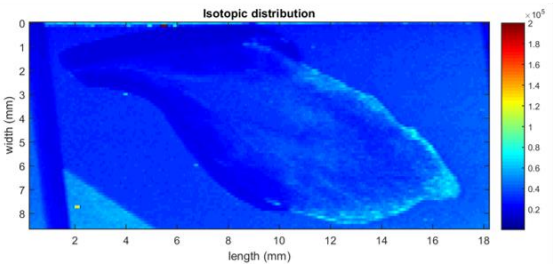
^{52}Cr distribution (N10-4/46C Large UPM2)



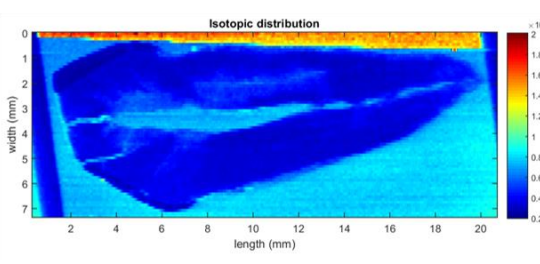
^{52}Cr distribution (N10-4/19 UCI)



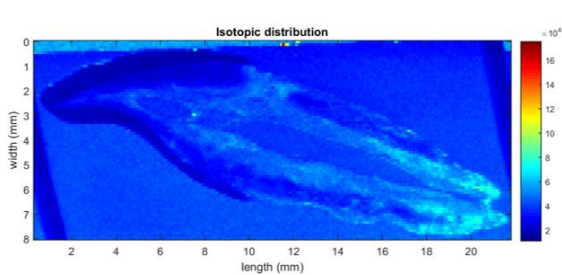
^{52}Cr distribution (N10-4/31 UCI)



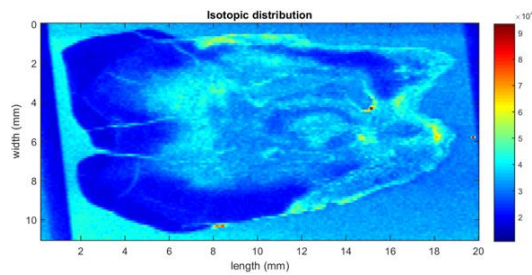
^{52}Cr distribution (N10-4/35 UCI)



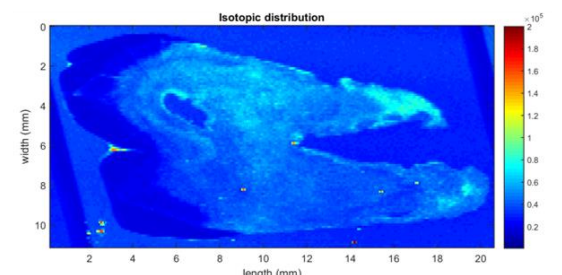
^{52}Cr distribution (N10-4/46A UCI)



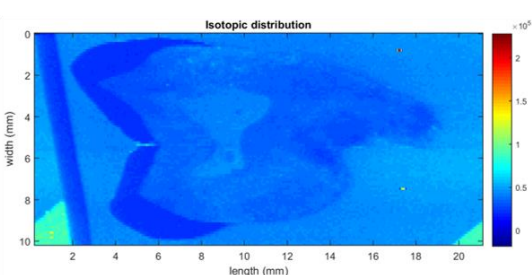
^{52}Cr distribution (N10-2/49 ULI)



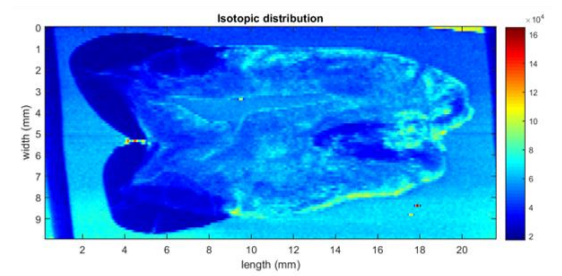
^{52}Cr distribution (N10-2/22 UPM1)



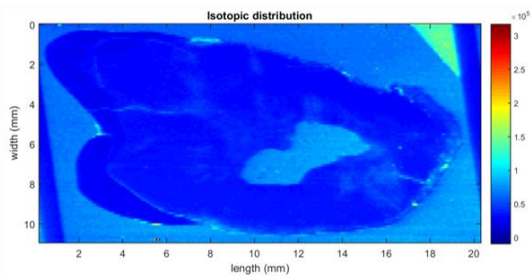
^{52}Cr distribution (N10-2/40 UPM1)



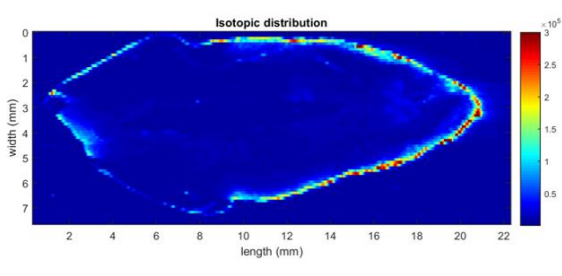
^{52}Cr distribution (N10-4/10 UPM2)



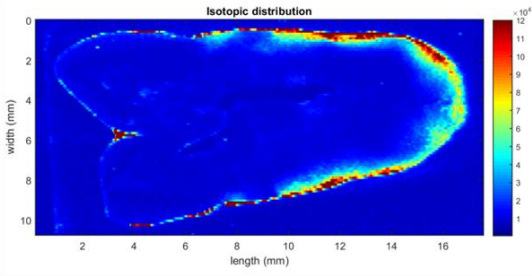
^{52}Cr distribution (N10-4/33 UPM2)



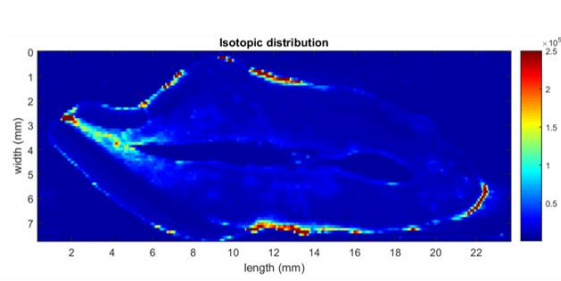
^{52}Cr distribution (N10-4/46C Small UPM2)



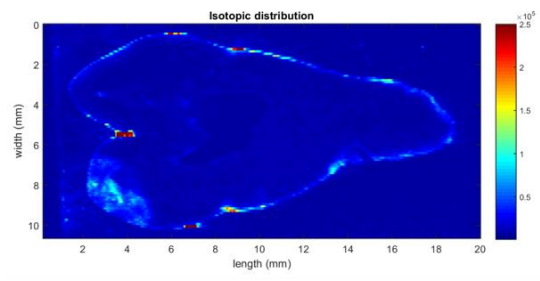
^{55}Mn distribution (N10-1/02 UCI)



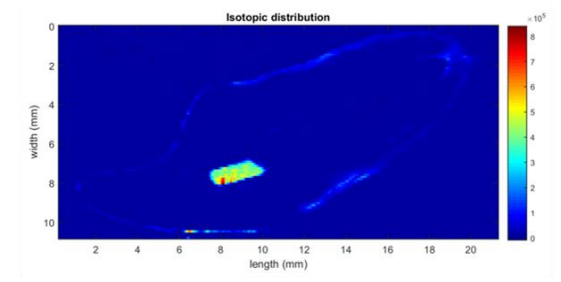
^{55}Mn distribution (N10-1/02 UPM1)



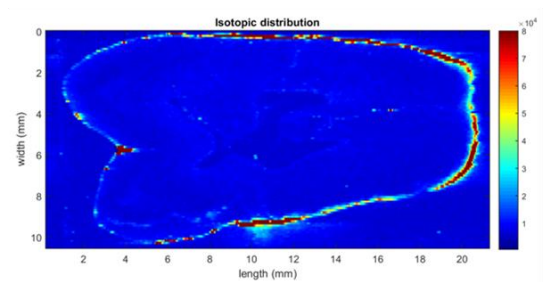
^{55}Mn distribution (N10-2/20A or B UCI)



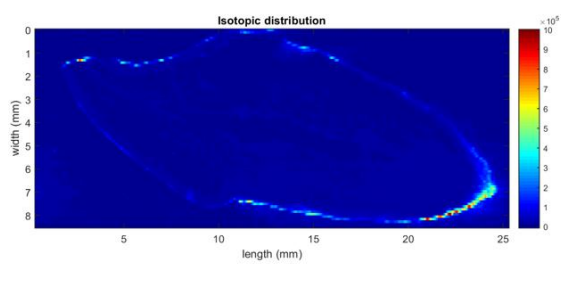
^{55}Mn distribution (N10-2/20A or B UPM2)



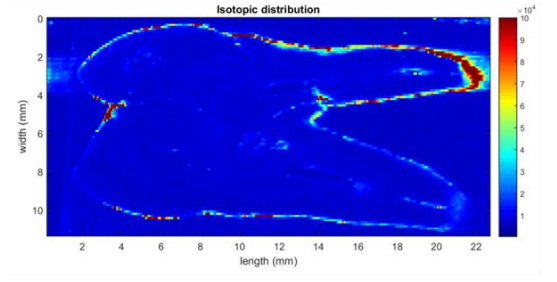
^{55}Mn distribution (N10-2/21 UCI)



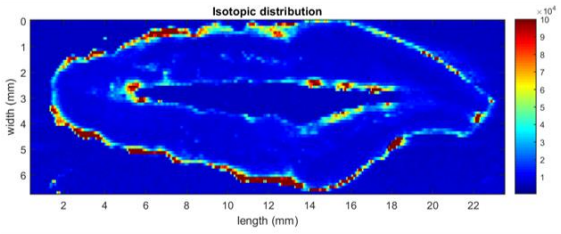
^{55}Mn distribution (N10-2/21 UPM2)



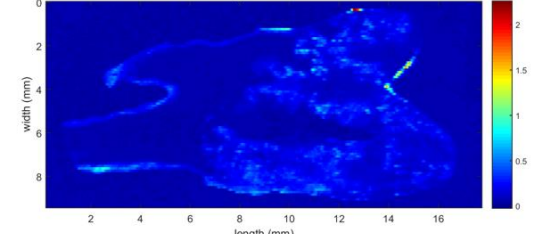
^{55}Mn distribution (N10-2/21A UCI)



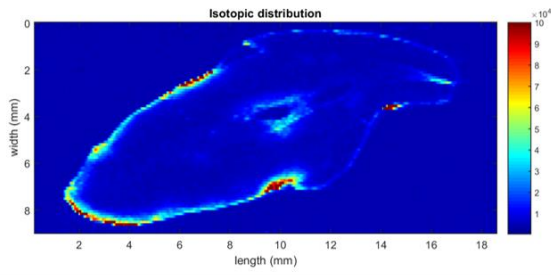
^{55}Mn distribution (N10-2/21A UPM1)



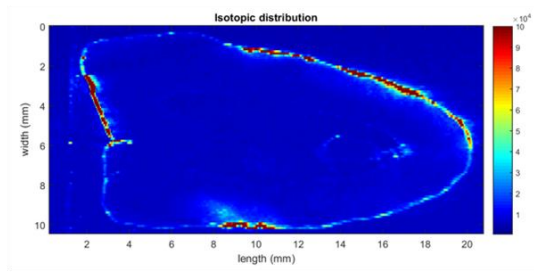
^{55}Mn distribution (N10-2/42B UCI)



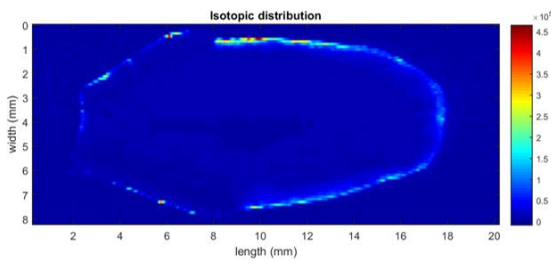
^{55}Mn distribution (N10-2/42B UPM1)



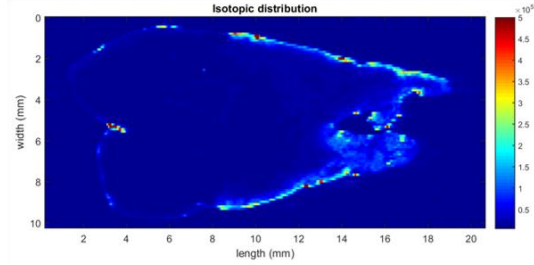
⁵⁵Mn distribution (N10-4/01 UCI)



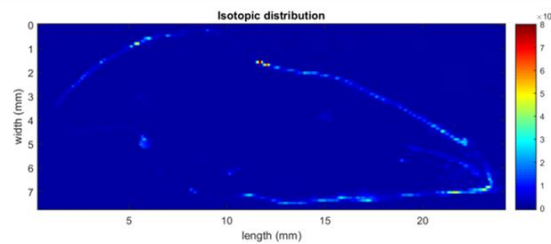
⁵⁵Mn distribution (N10-4/01 UPM2)



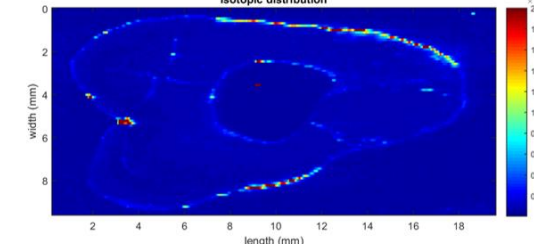
⁵⁵Mn distribution (N10-4/43 UCI)



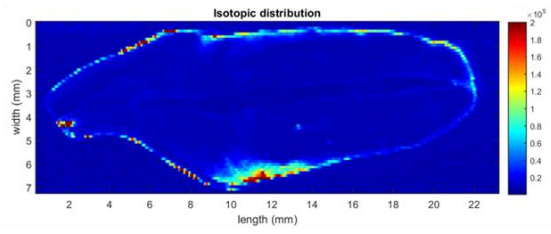
⁵⁵Mn distribution (N10-4/43 UPM1)



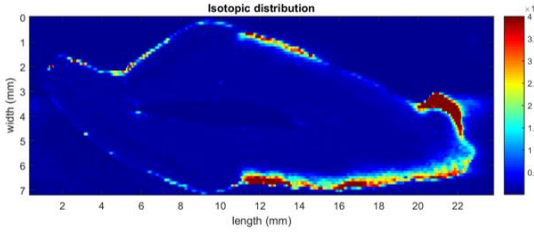
⁵⁵Mn distribution (N10-4/46C Large UCI)



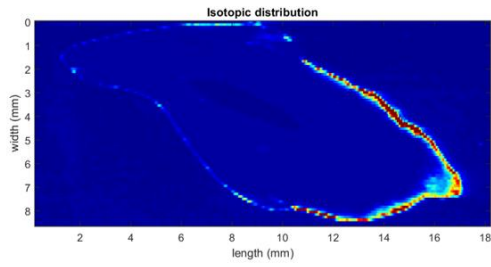
⁵⁵Mn distribution (N10-4/46C Large UPM2)



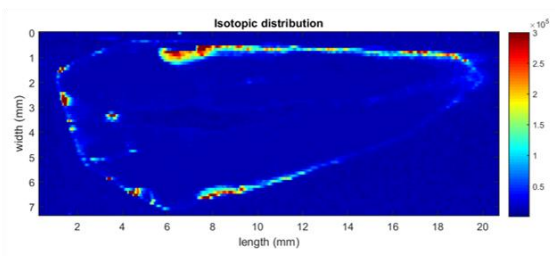
⁵⁵Mn distribution (N10-4/19 UCI)



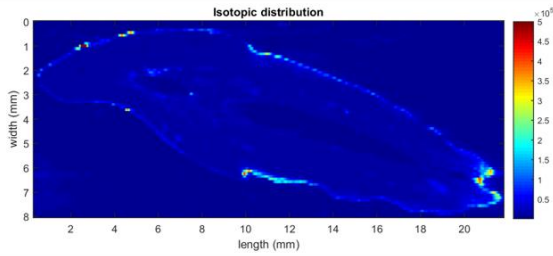
⁵⁵Mn distribution (N10-4/31 UCI)



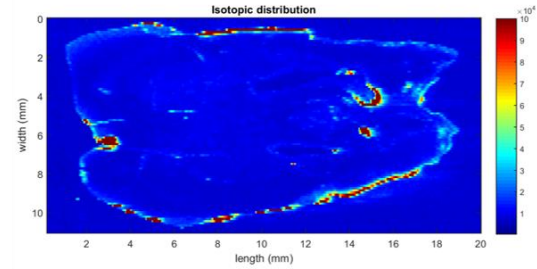
⁵⁵Mn distribution (N10-4/35 UCI)



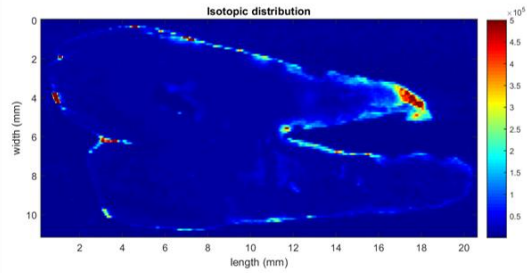
⁵⁵Mn distribution (N10-4/46A UCI)



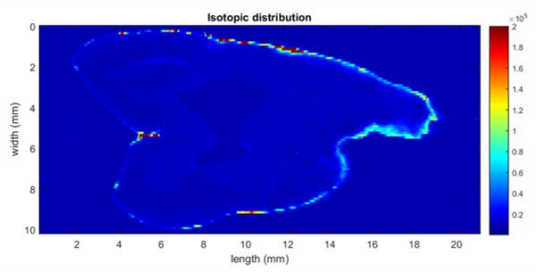
⁵⁵Mn distribution (N10-2/49 ULI)



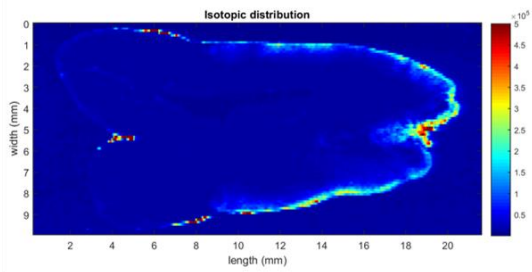
⁵⁵Mn distribution (N10-2/22 UPM1)



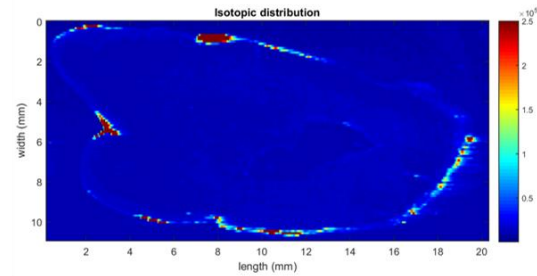
⁵⁵Mn distribution (N10-2/40 UPM1)



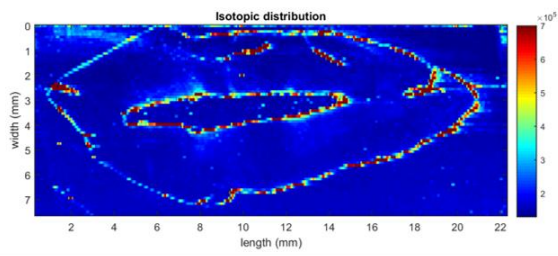
⁵⁵Mn distribution (N10-4/10 UPM2)



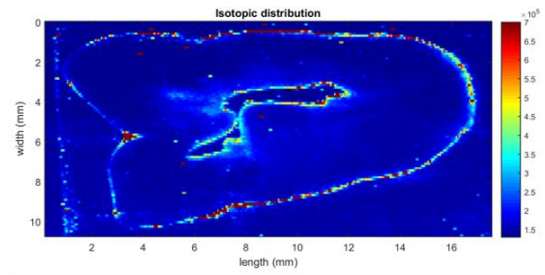
⁵⁵Mn distribution (N10-4/33 UPM2)



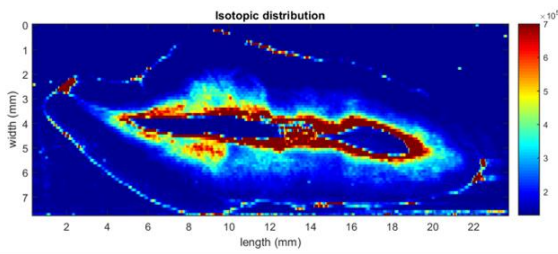
⁵⁵Mn distribution (N10-4/46C Small UPM2)



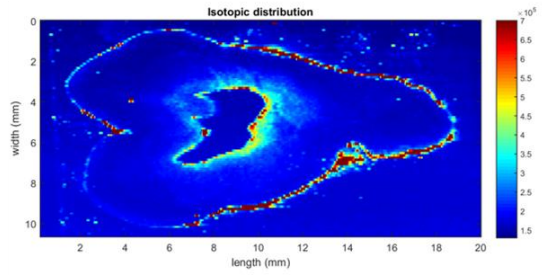
^{56}Fe distribution (N10-1/02 UCI)



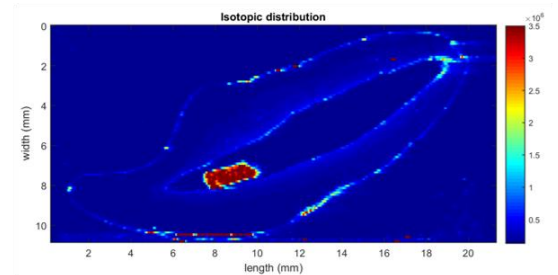
^{56}Fe distribution (N10-1/02 UPM1)



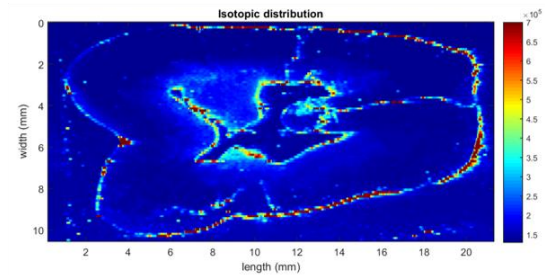
^{56}Fe distribution (N10-2/20A or B UCI)



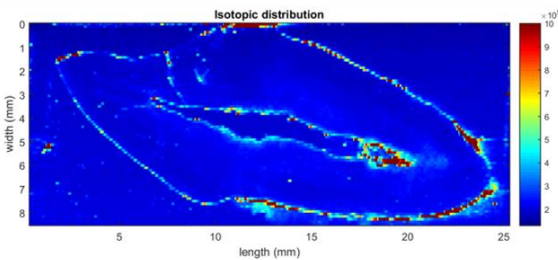
^{56}Fe distribution (N10-2/20A or B UPM2)



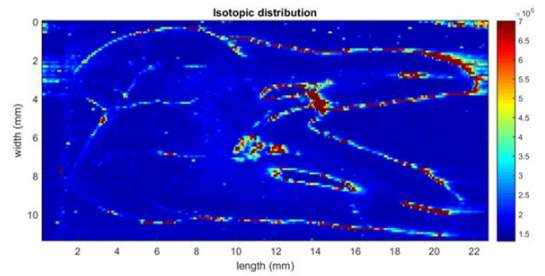
^{56}Fe distribution (N10-2/21 UCI)



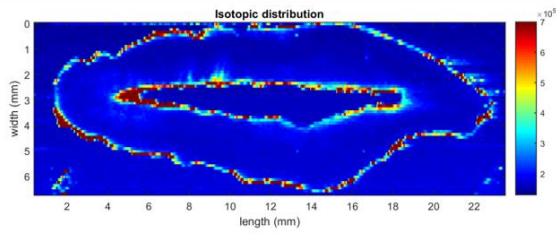
^{56}Fe distribution (N10-2/21 UPM2)



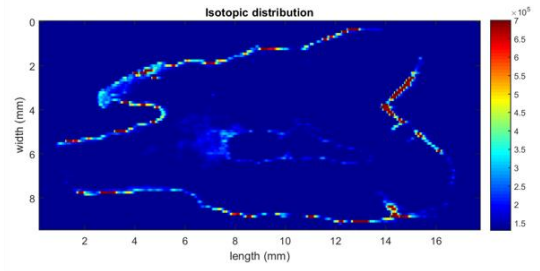
^{56}Fe distribution (N10-2/21A UCI)



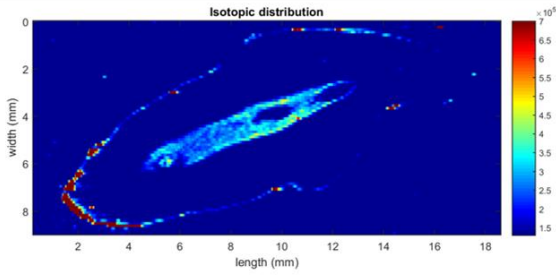
^{56}Fe distribution (N10-2/21A UPM1)



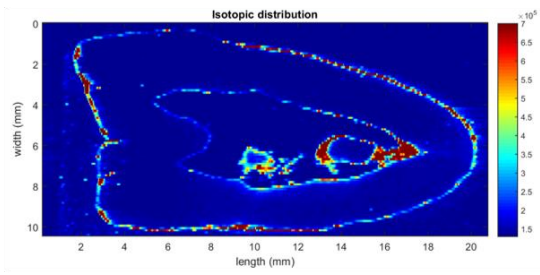
⁵⁶Fe distribution (N10-2/42B UCI)



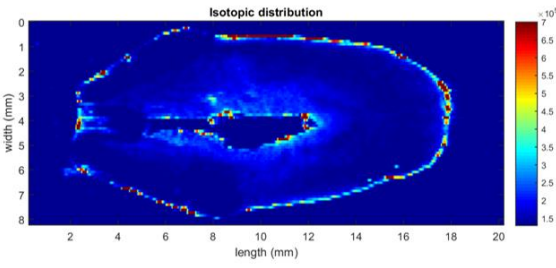
⁵⁶Fe distribution (N10-2/42B UPM1)



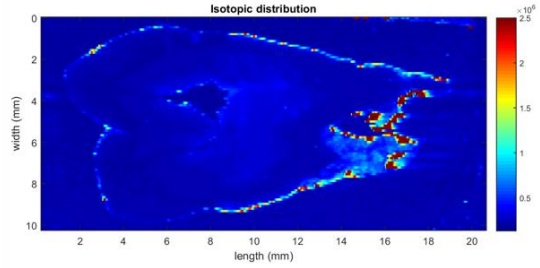
⁵⁶Fe distribution (N10-4/01 UCI)



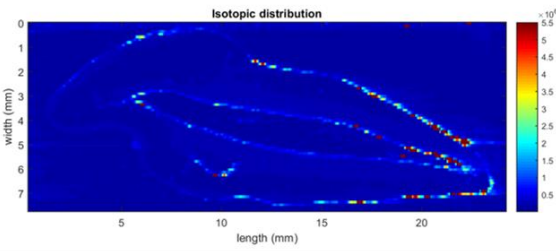
⁵⁶Fe distribution (N10-4/01 UPM2)



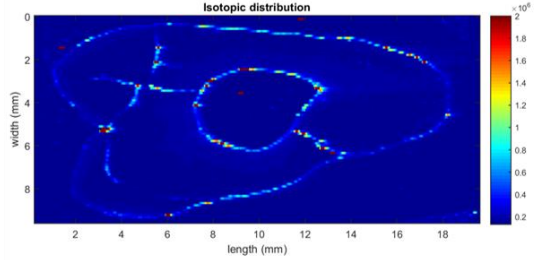
⁵⁶Fe distribution (N10-4/43 UCI)



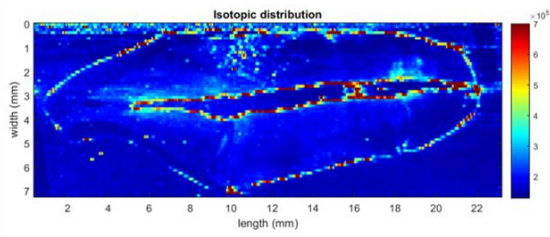
⁵⁶Fe distribution (N10-4/43 UPM1)



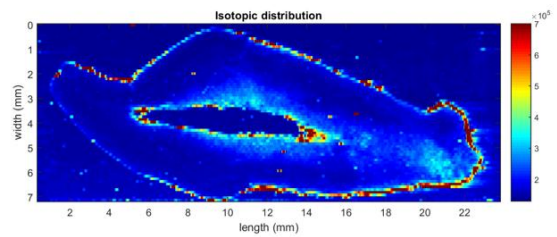
⁵⁶Fe distribution (N10-4/46C Large UCI)



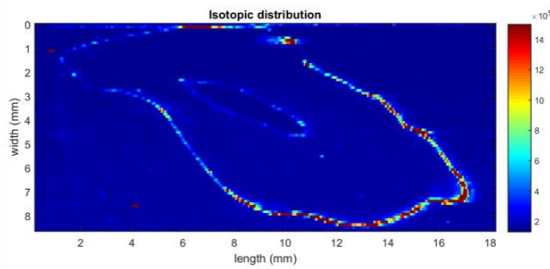
⁵⁶Fe distribution (N10-4/46C Large UPM2)



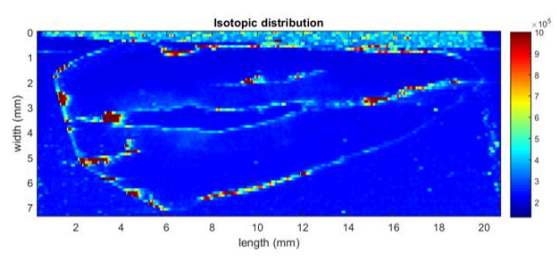
^{56}Fe distribution (N10-4/19 UCI)



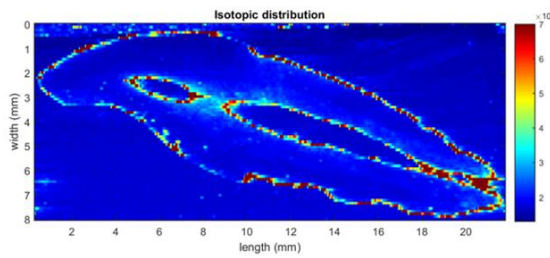
^{56}Fe distribution (N10-4/31 UCI)



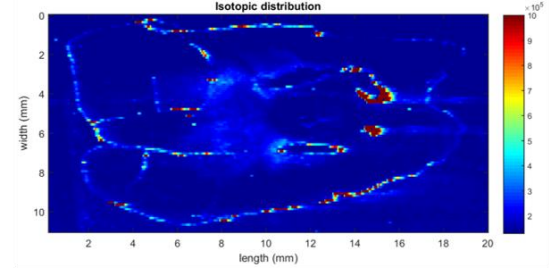
^{56}Fe distribution (N10-4/35 UCI)



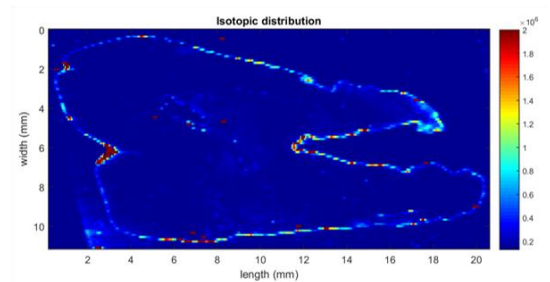
^{56}Fe distribution (N10-4/46A UCI)



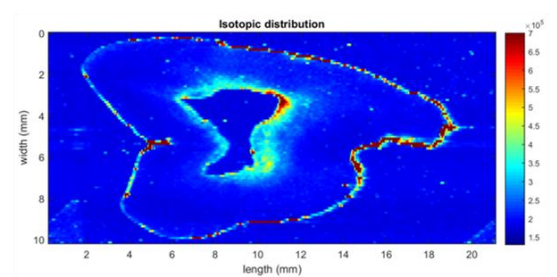
^{56}Fe distribution (N10-2/49 ULI)



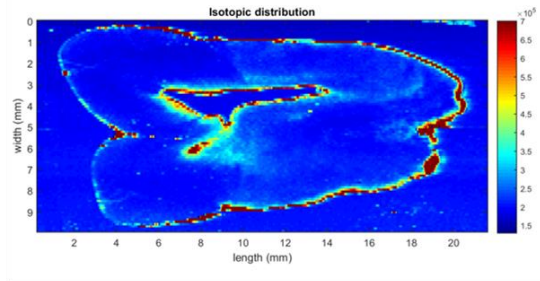
^{56}Fe distribution (N10-2/22 UPM1)



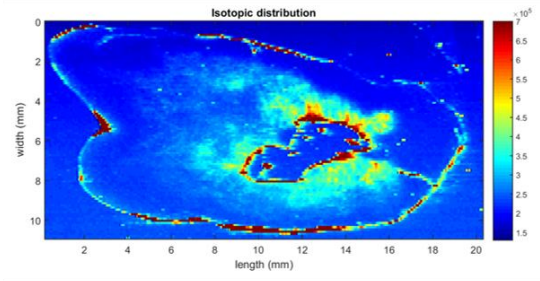
^{56}Fe distribution (N10-2/40 UPM1)



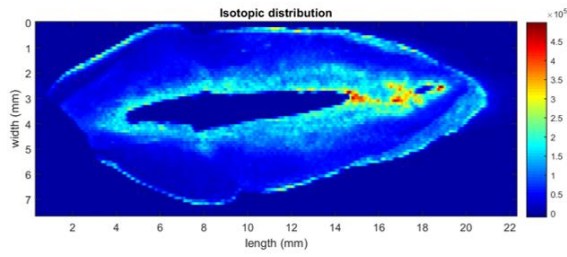
^{56}Fe distribution (N10-4/10 UPM2)



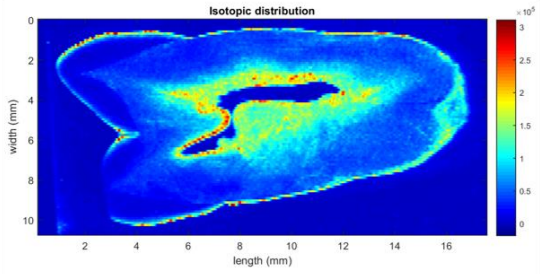
^{56}Fe distribution (N10-4/33 UPM2)



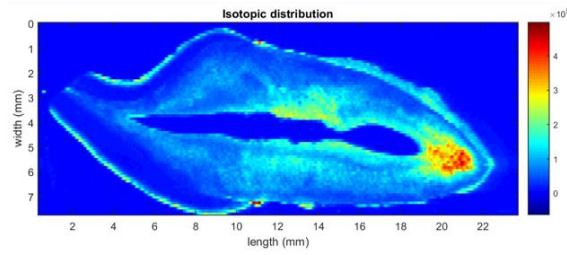
^{56}Fe distribution (N10-4/46C Small UPM2)



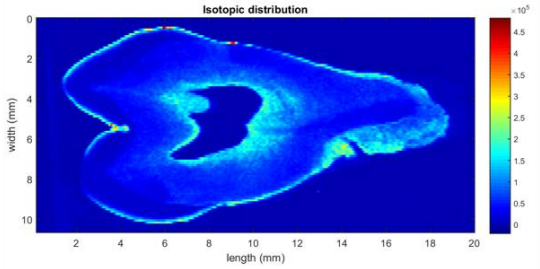
^{66}Zn distribution (N10-1/02 UCI)



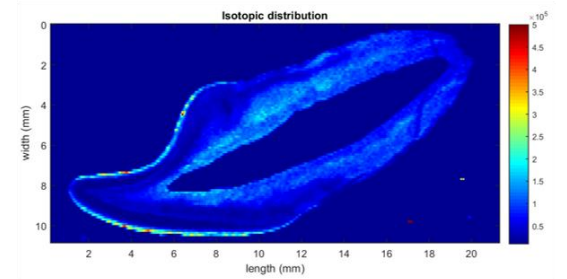
^{66}Zn distribution (N10-1/02 UPM1)



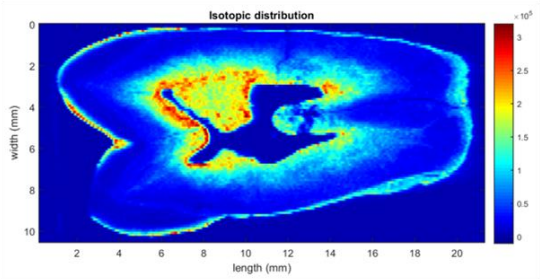
^{66}Zn distribution (N10-2/20A or B UCI)



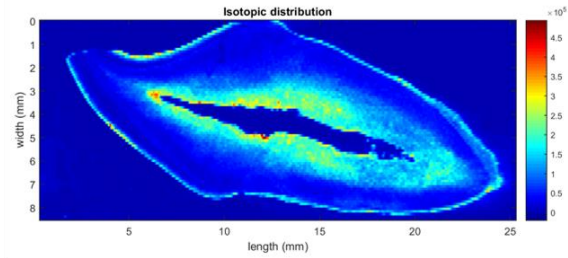
^{66}Zn distribution (N10-2/20A or B UPM2)



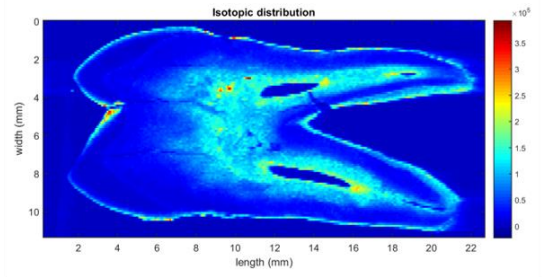
^{66}Zn distribution (N10-2/21 UCI)



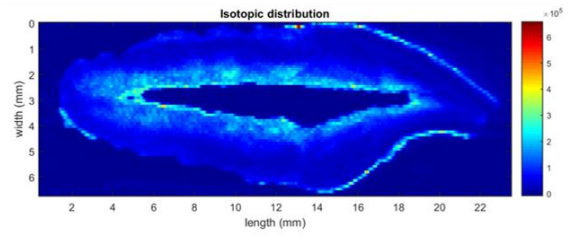
^{66}Zn distribution (N10-2/21 UPM2)



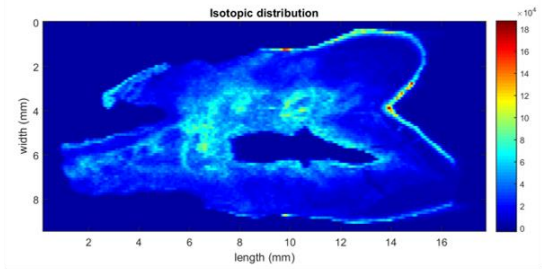
^{66}Zn distribution (N10-2/21A UCI)



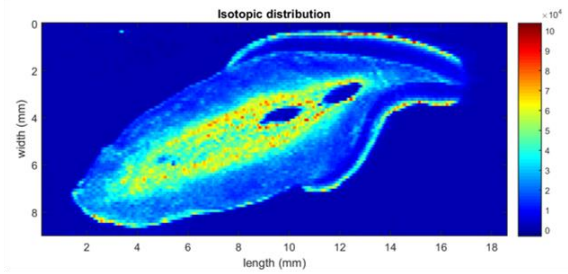
^{66}Zn distribution (N10-2/21A UPM1)



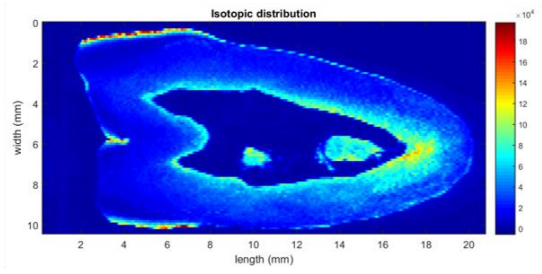
^{66}Zn distribution (N10-2/42B UCI)



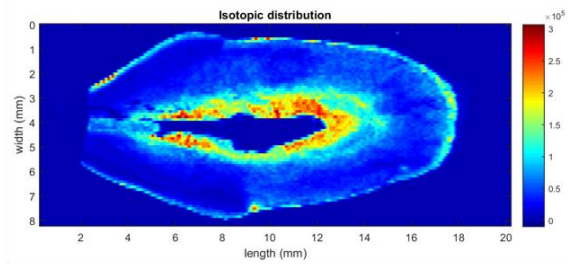
^{66}Zn distribution (N10-2/42B UPM1)



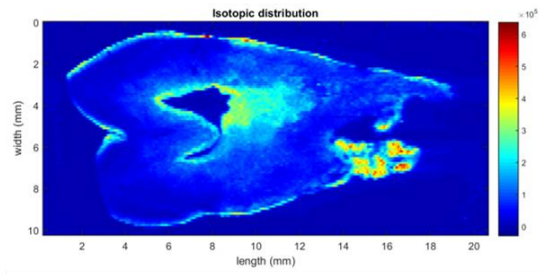
^{66}Zn distribution (N10-4/01 UCI)



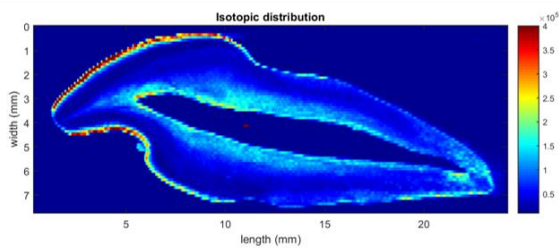
^{66}Zn distribution (N10-4/01 UPM2)



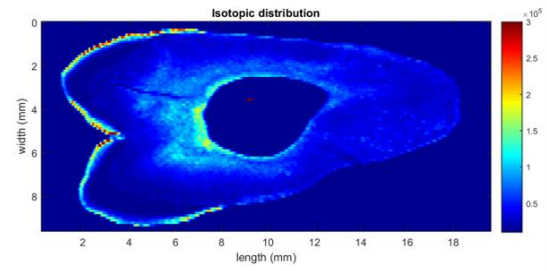
^{66}Zn distribution (N10-4/43 UCI)



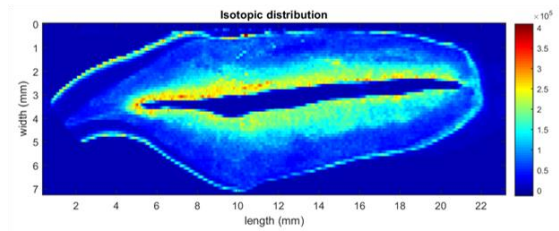
^{66}Zn distribution (N10-4/43 UPM1)



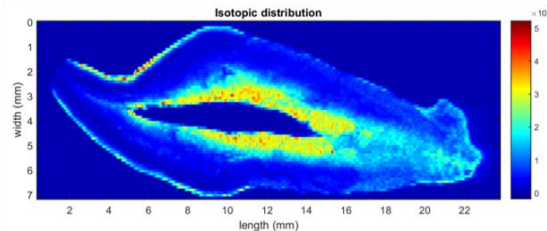
^{66}Zn distribution (N10-4/46C Large UCI)



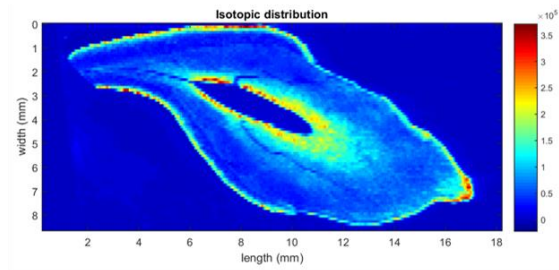
^{66}Zn distribution (N10-4/46C Large UPM2)



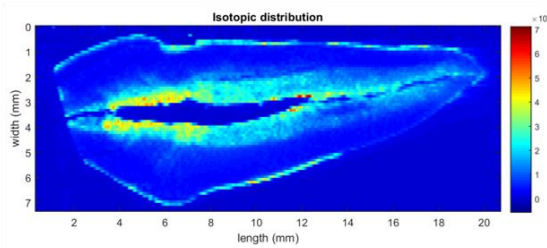
^{66}Zn distribution (N10-4/19 UCI)



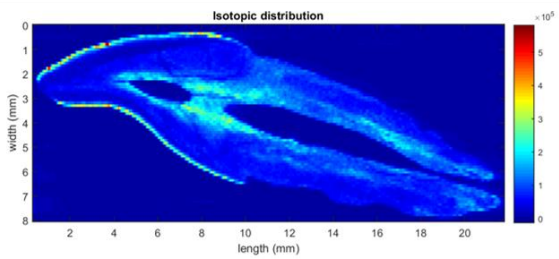
^{66}Zn distribution (N10-4/31 UCI)



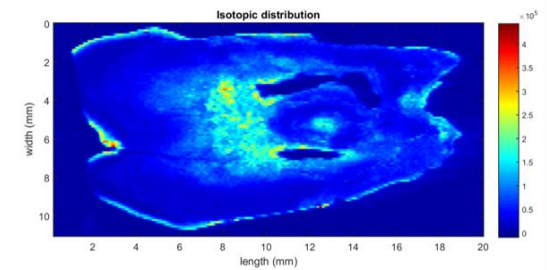
^{66}Zn distribution (N10-4/35 UCI)



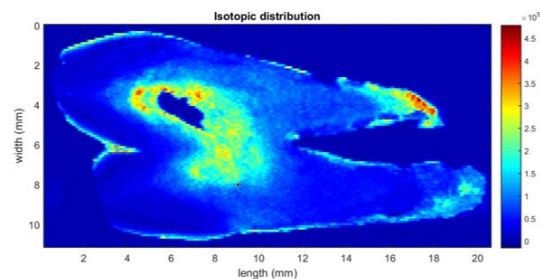
^{66}Zn distribution (N10-4/46A UCI)



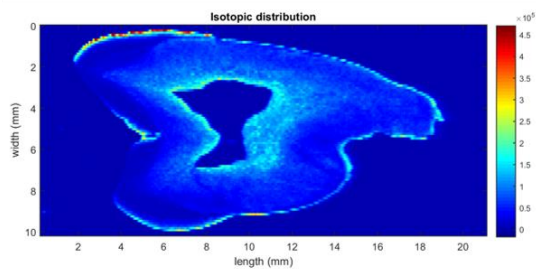
^{66}Zn distribution (N10-2/49 ULI)



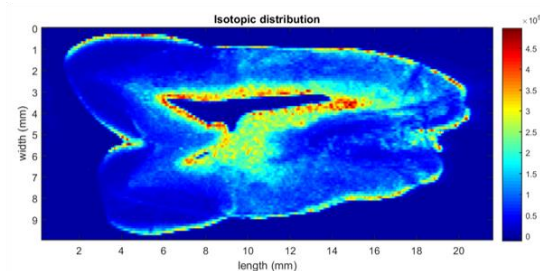
^{66}Zn distribution (N10-2/22 UPM1)



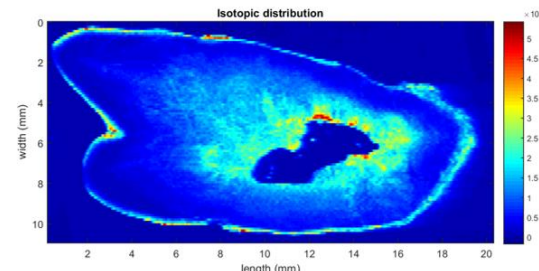
^{66}Zn distribution (N10-2/40 UPM1)



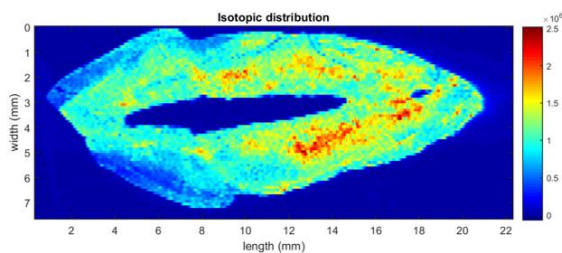
^{66}Zn distribution (N10-4/10 UPM2)



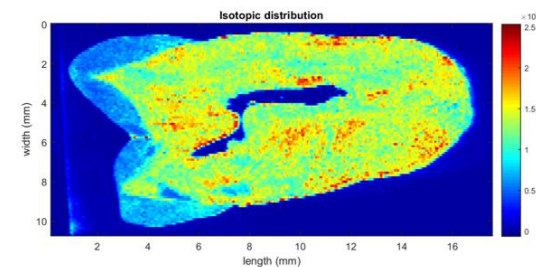
^{66}Zn distribution (N10-4/33 UPM2)



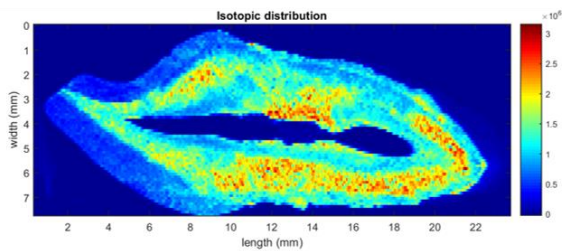
^{66}Zn distribution (N10-4/46C Small UPM2)



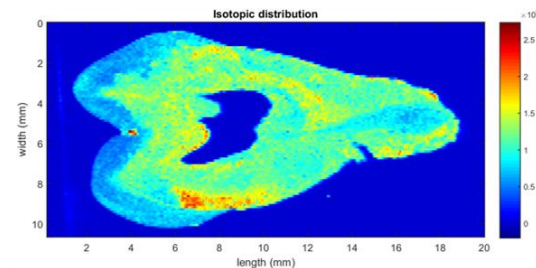
^{88}Sr distribution (N10-1/02 UCI)



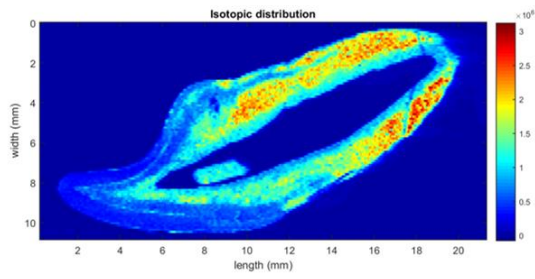
^{88}Sr distribution (N10-1/02 UPM1)



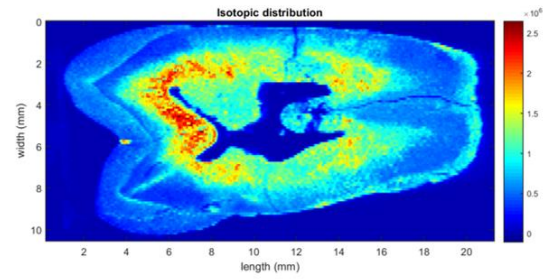
^{88}Sr distribution (N10-2/20A or B UCI)



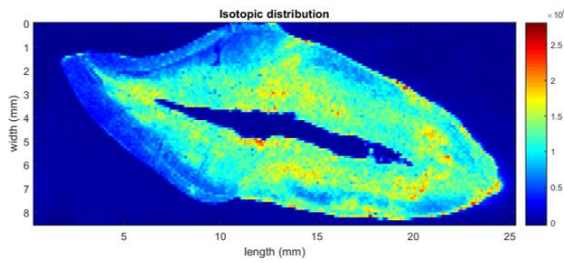
^{88}Sr distribution (N10-2/20A or B UPM2)



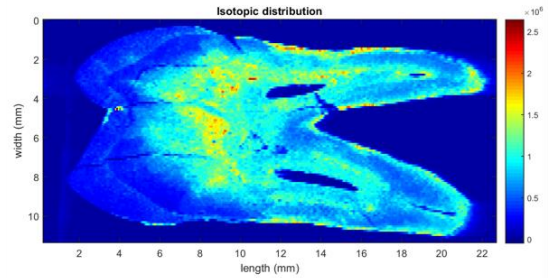
^{88}Sr distribution (N10-2/21 UCI)



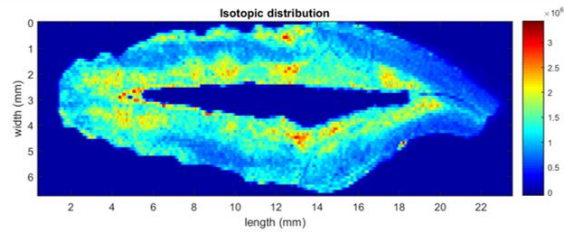
^{88}Sr distribution (N10-2/21 UPM2)



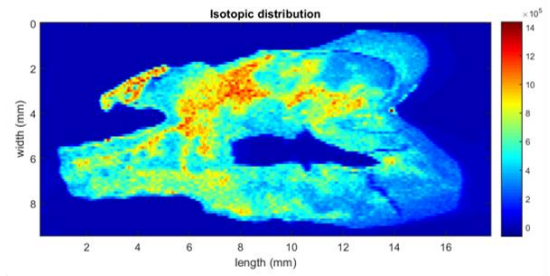
^{88}Sr distribution (N10-2/21A UCI)



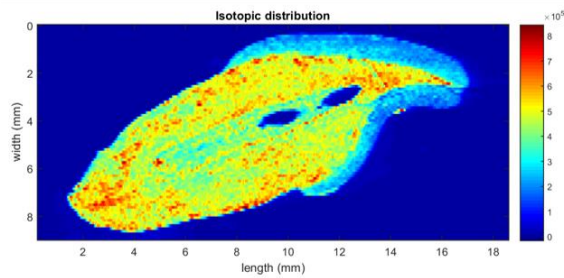
^{88}Sr distribution (N10-2/21A UPM1)



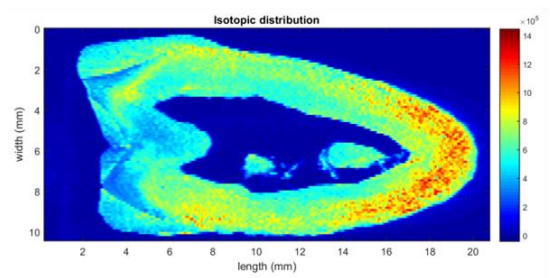
^{88}Sr distribution (N10-2/42B UCI)



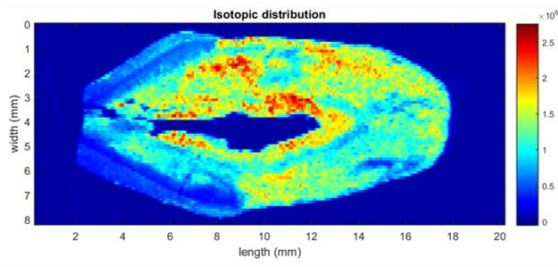
^{88}Sr distribution (N10-2/42B UPM1)



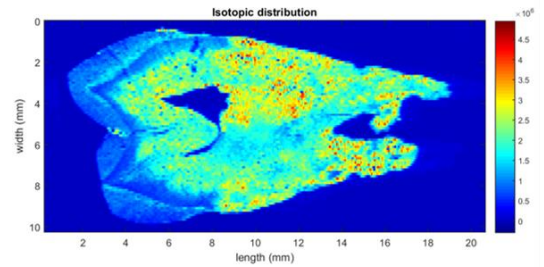
^{88}Sr distribution (N10-4/01 UCI)



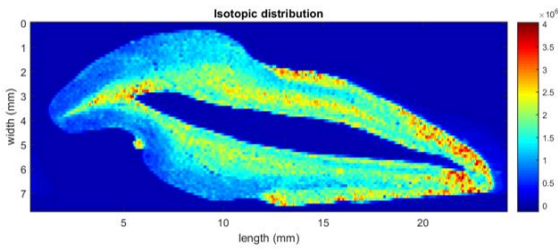
^{88}Sr distribution (N10-4/01 UPM2)



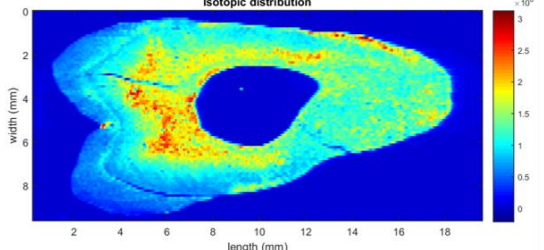
^{88}Sr distribution (N10-4/43 UCI)



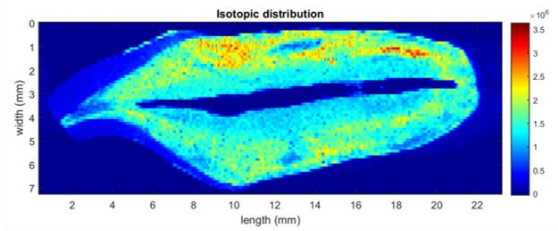
^{88}Sr distribution (N10-4/43 UPM1)



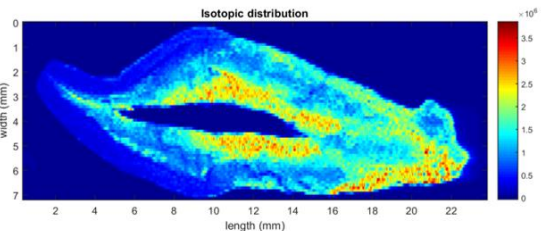
^{88}Sr distribution (N10-4/46C Large UCI)



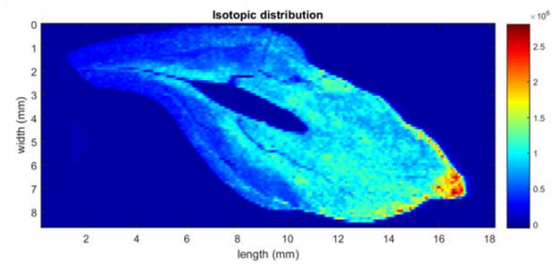
^{88}Sr distribution (N10-4/46C Large UPM2)



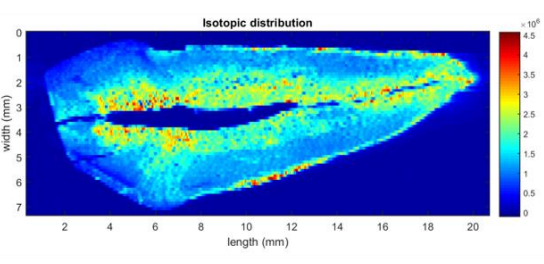
^{88}Sr distribution (N10-4/19 UCI)



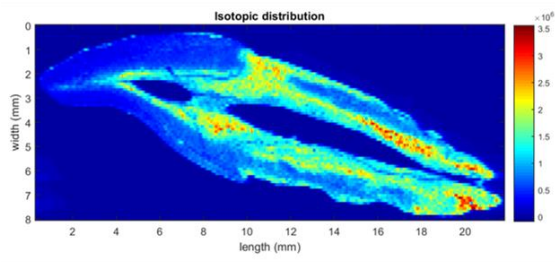
^{88}Sr distribution (N10-4/31 UCI)



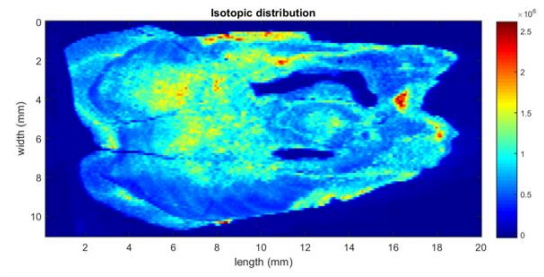
^{88}Sr distribution (N10-4/35 UCI)



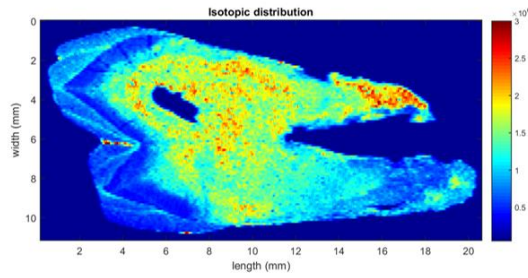
^{88}Sr distribution (N10-4/46A UCI)



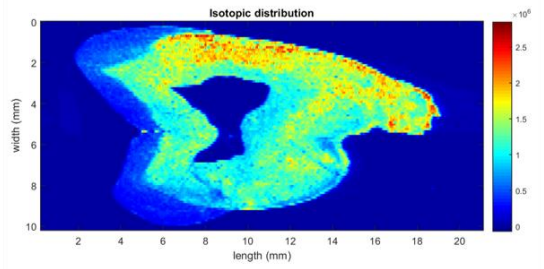
^{88}Sr distribution (N10-2/49 ULI)



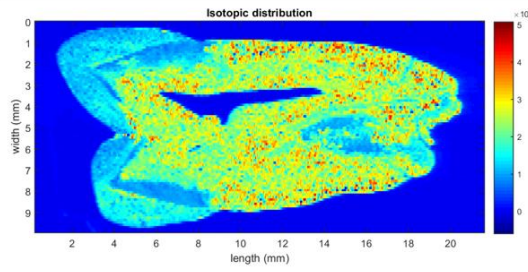
^{88}Sr distribution (N10-2/22 UPM1)



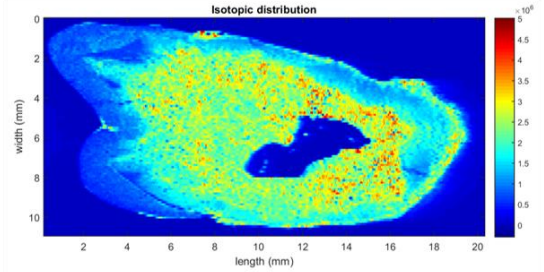
^{88}Sr distribution (N10-2/40 UPM1)



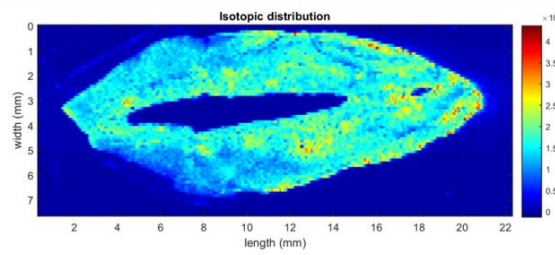
^{88}Sr distribution (N10-4/10 UPM2)



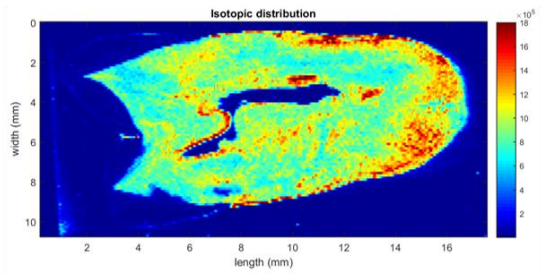
^{88}Sr distribution (N10-4/33 UPM2)



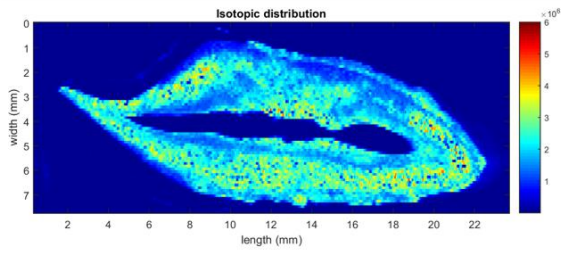
^{88}Sr distribution (N10-4/46C Small UPM2)



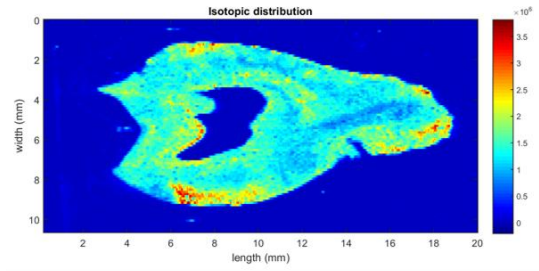
^{138}Ba distribution (N10-1/02 UCI)



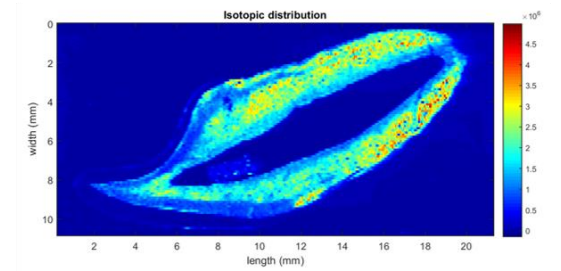
^{138}Ba distribution (N10-1/02 UPM1)



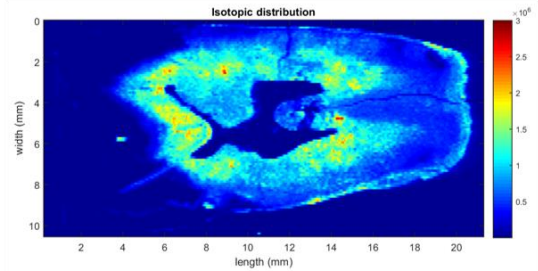
^{138}Ba distribution (N10-2/20A or B UCI)



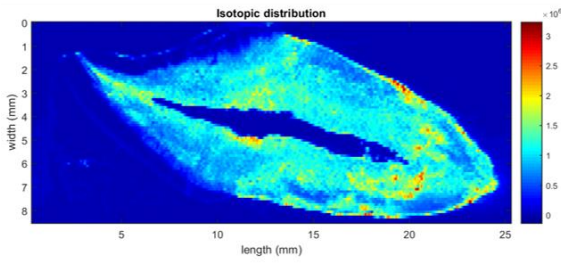
^{138}Ba distribution (N10-2/20A or B UPM2)



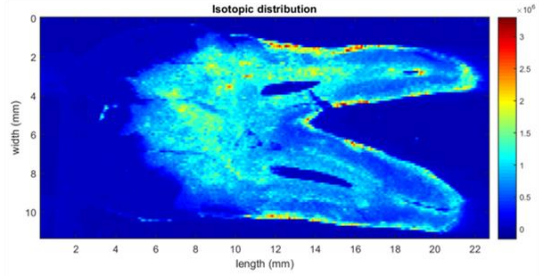
^{138}Ba distribution (N10-2/21 UCI)



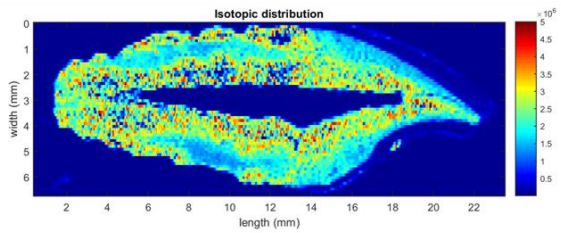
^{138}Ba distribution (N10-2/21 UPM2)



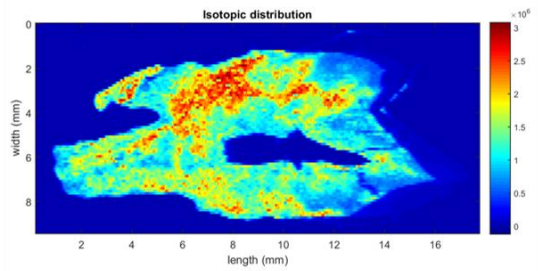
^{138}Ba distribution (N10-2/21A UCI)



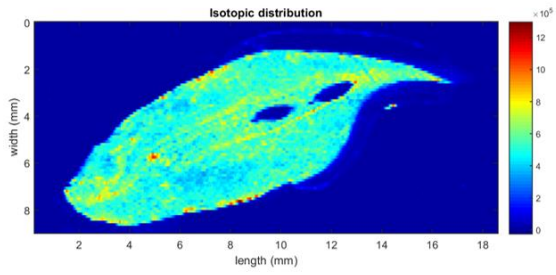
^{138}Ba distribution (N10-2/21A UPM1)



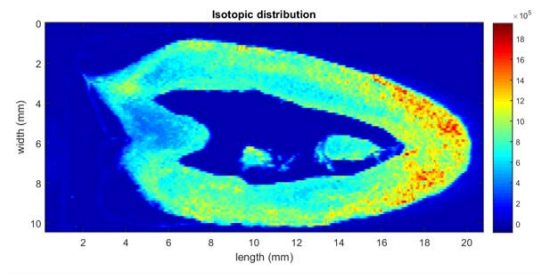
^{138}Ba distribution (N10-2/42B UCI)



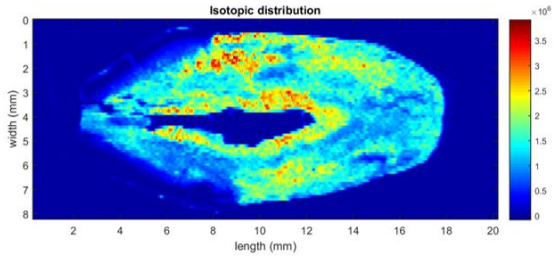
^{138}Ba distribution (N10-2/42B UPM1)



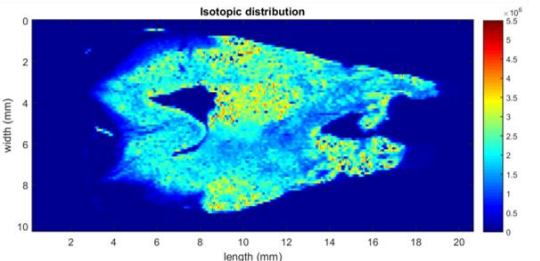
^{138}Ba distribution (N10-4/01 UCI)



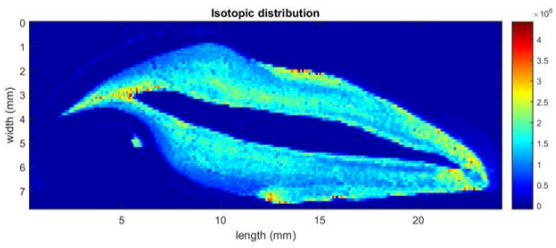
^{138}Ba distribution (N10-4/01 UPM2)



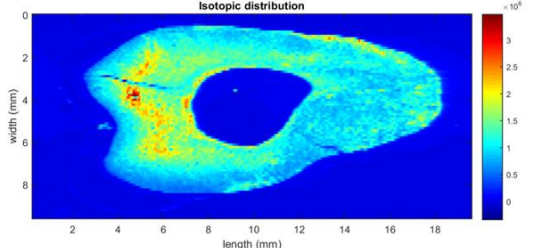
^{138}Ba distribution (N10-4/43 UCI)



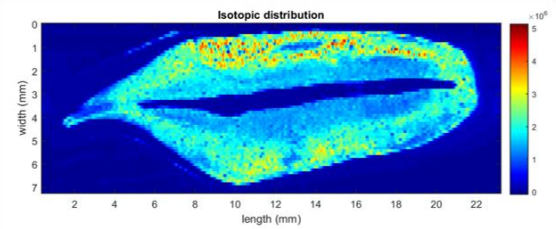
^{138}Ba distribution (N10-4/43 UPM1)



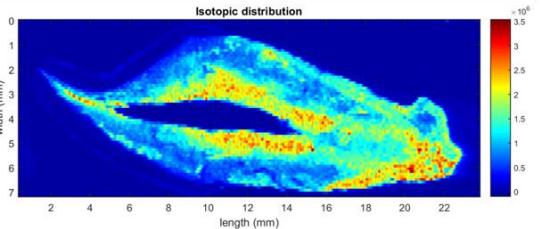
^{138}Ba distribution (N10-4/46C Large UCI)



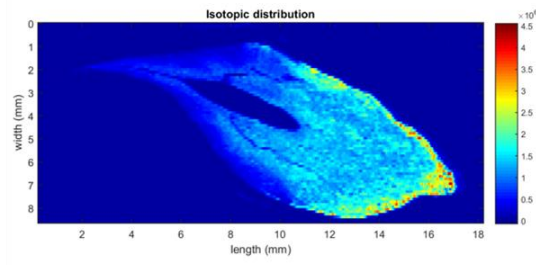
^{138}Ba distribution (N10-4/46C Large UPM2)



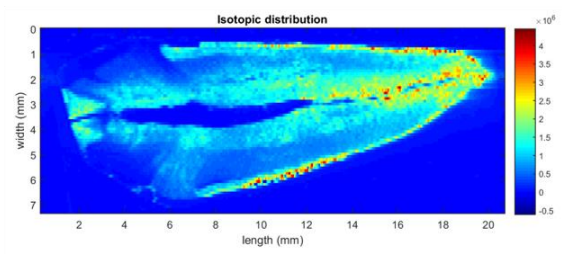
^{138}Ba distribution (N10-4/19 UCI)



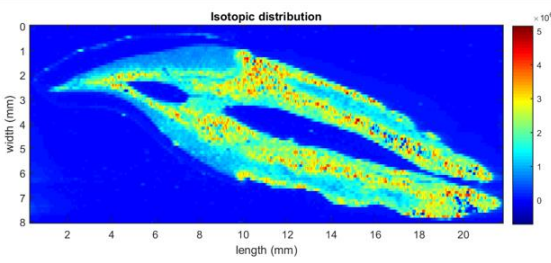
^{138}Ba distribution (N10-4/31 UCI)



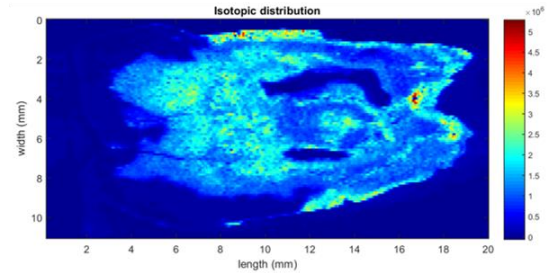
^{138}Ba distribution (N10-4/35 UCI)



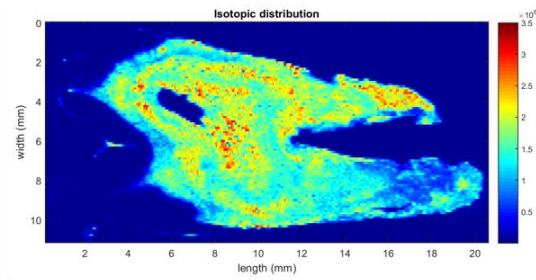
^{138}Ba distribution (N10-4/46A UCI)



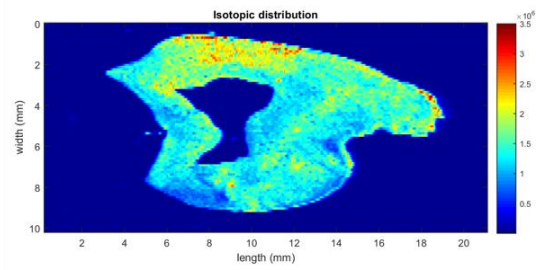
^{138}Ba distribution (N10-2/49 ULI)



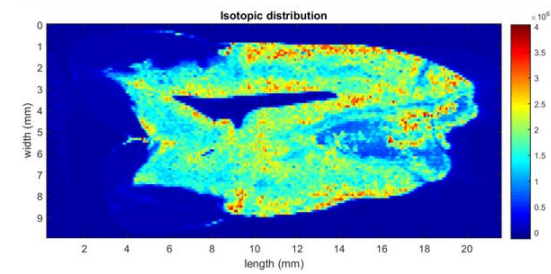
^{138}Ba distribution (N10-2/22 UPM1)



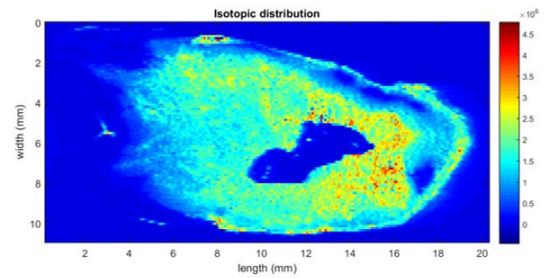
^{138}Ba distribution (N10-2/40 UPM1)



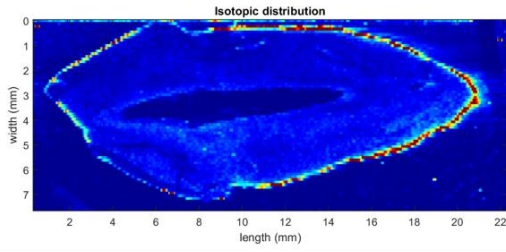
^{138}Ba distribution (N10-4/10 UPM2)



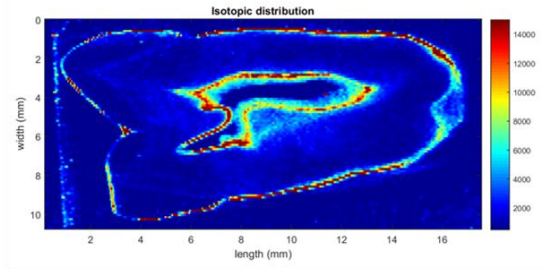
^{138}Ba distribution (N10-4/33 UPM2)



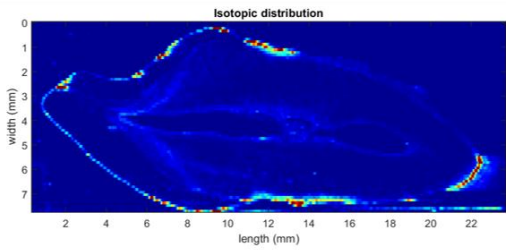
^{138}Ba distribution (N10-4/46C Small UPM2)



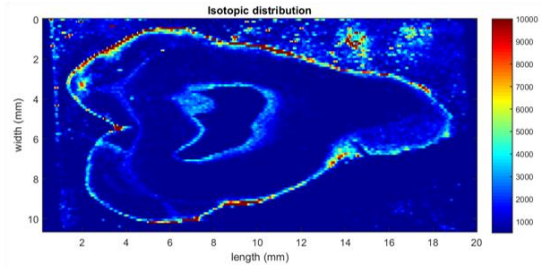
^{208}Pb distribution (N10-1/02 UCI)



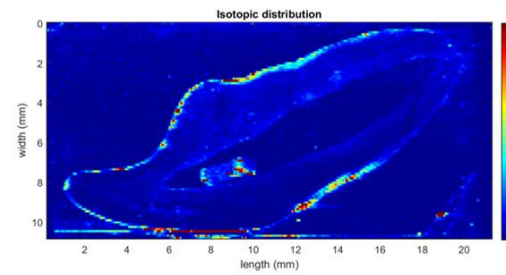
^{208}Pb distribution (N10-1/02 UPM1)



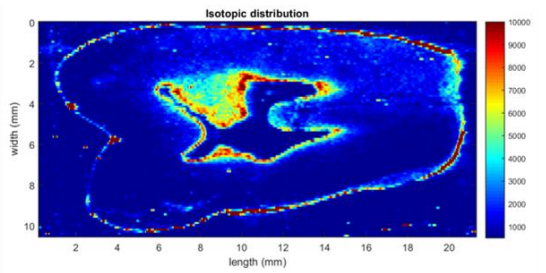
^{208}Pb distribution (N10-2/20A or B UCI)



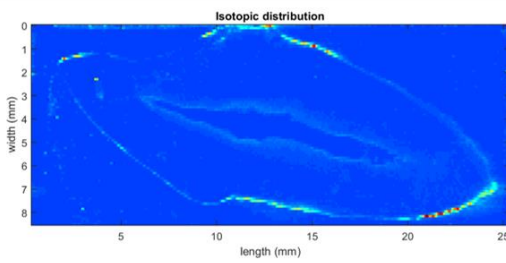
^{208}Pb distribution (N10-2/20A or B UPM2)



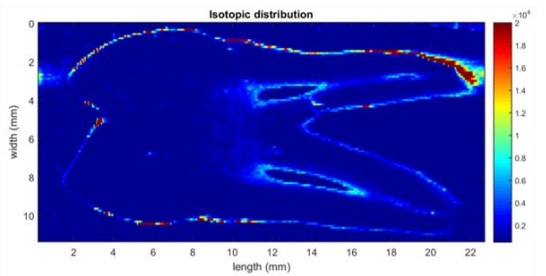
^{208}Pb distribution (N10-2/21 UCI)



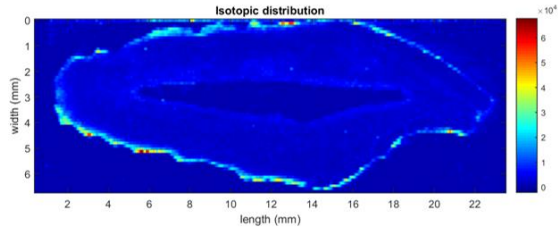
^{208}Pb distribution (N10-2/21 UPM2)



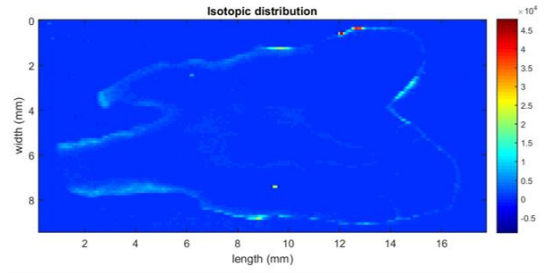
^{208}Pb distribution (N10-2/21A UCI)



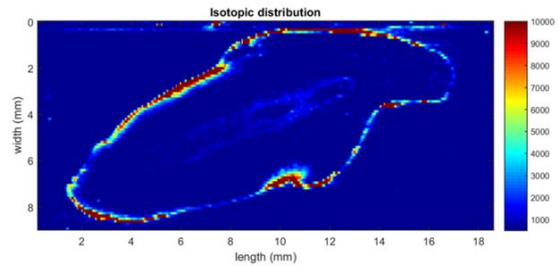
^{208}Pb distribution (N10-2/21A UPM1)



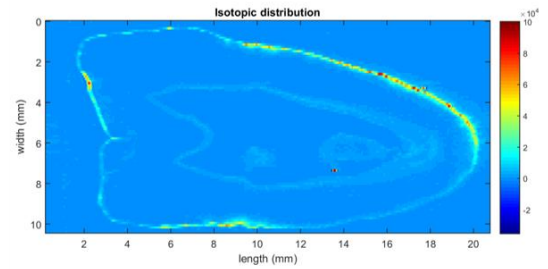
^{208}Pb distribution (N10-2/42B UCI)



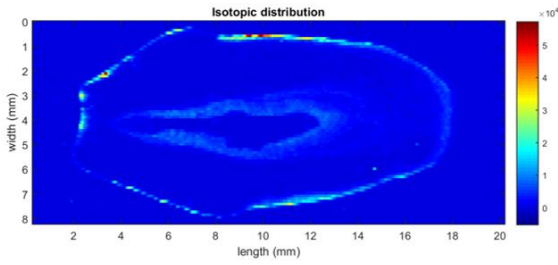
^{208}Pb distribution (N10-2/42B UPM1)



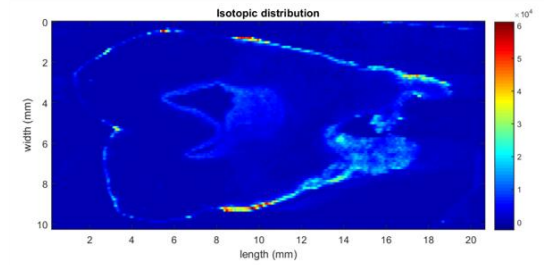
^{208}Pb distribution (N10-4/01 UCI)



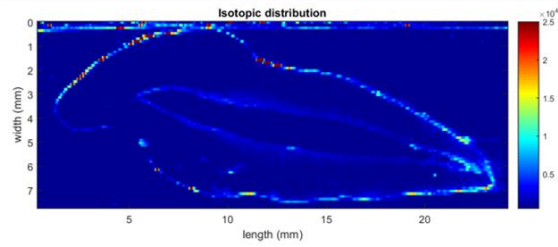
^{208}Pb distribution (N10-4/01 UPM2)



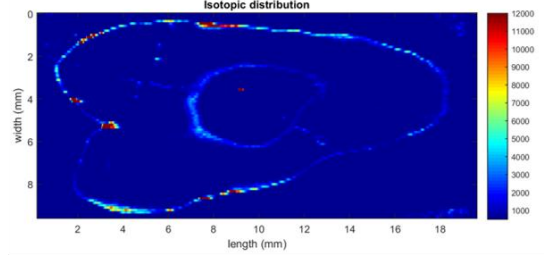
^{208}Pb distribution (N10-4/43 UCI)



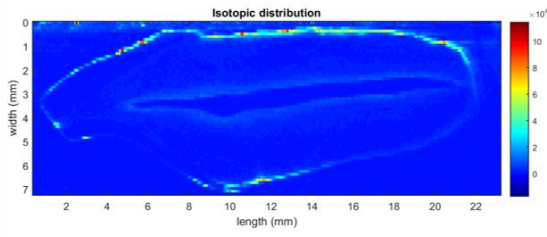
^{208}Pb distribution (N10-4/43 UPM1)



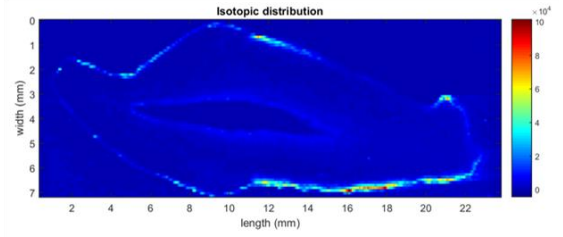
^{208}Pb distribution (N10-4/46C Large UCI)



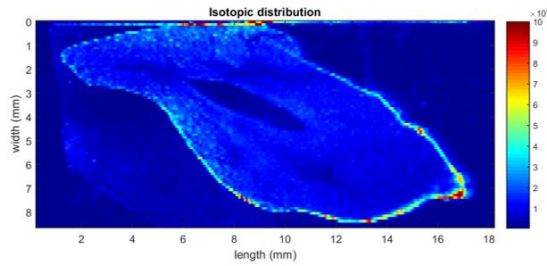
^{208}Pb distribution (N10-4/46C Large UPM2)



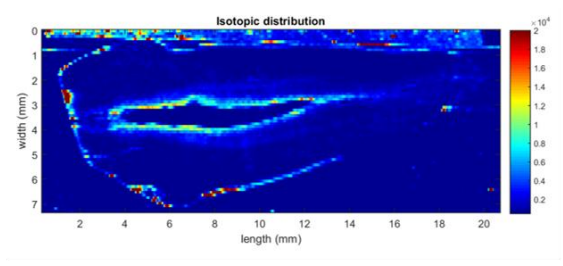
^{208}Pb distribution (N10-4/19 UCI)



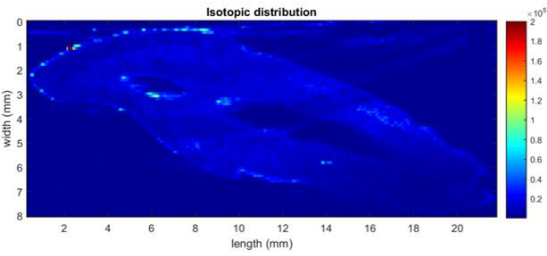
^{208}Pb distribution (N10-4/31 UCI)



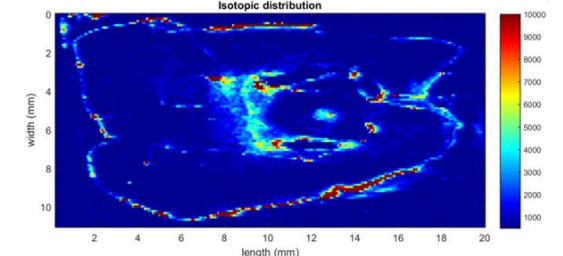
^{208}Pb distribution (N10-4/35 UCI)



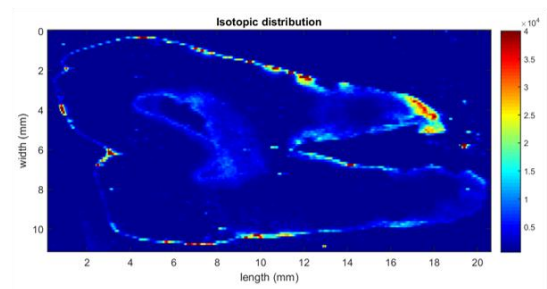
^{208}Pb distribution (N10-4/46A UCI)



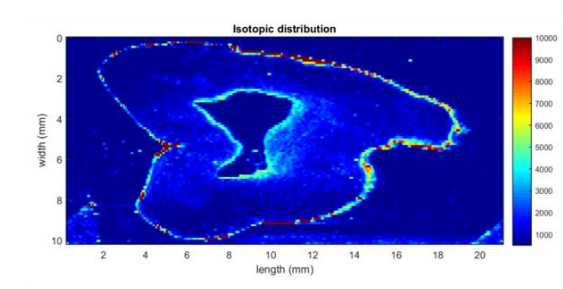
^{208}Pb distribution (N10-2/49 ULI)



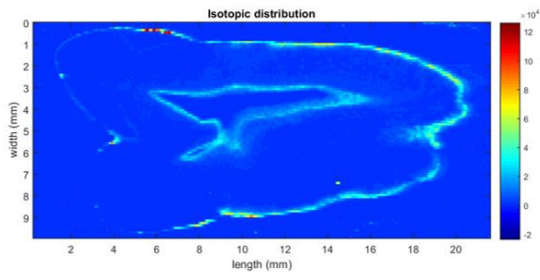
^{208}Pb distribution (N10-2/22 UPM1)



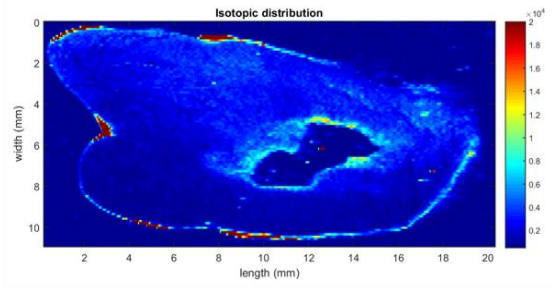
^{208}Pb distribution (N10-2/40 UPM1)



^{208}Pb distribution (N10-4/10 UPM2)



^{208}Pb distribution (N10-4/33 UPM2)



^{208}Pb distribution (N10-4/46C Small UPM2)

APPENDIX B: RELATIVE INTENSITY DATA TABLES

Table 18: Relative intensities of isotopes observed in N10-1/02 UCI at each tooth location.

Isotope	Enamel Surface	Inner Enamel	Inner Dentine	EDJ	DPB	Outer Root Border
¹³ C	LOW	LOW	LOW-MOD	LOW	LOW-MOD	LOW
²⁴ Mg	N/A	LOW	MOD-HIGH	N/A	MOD	N/A
²⁷ Al	LOW	N/A	N/A	N/A	MOD	MOD
³¹ P	MOD	MOD	HIGH	MOD	MOD	MOD
⁴⁴ Ca	MOD	MOD	HIGH	MOD	MOD	MOD
⁴⁷ Ti	LOW	LOW	LOW	N/A	N/A	LOW
⁵² Cr	LOW	LOW	LOW	LOW	LOW	LOW
⁵⁵ Mn	MOD	N/A	N/A	N/A	N/A	HIGH
⁵⁶ Fe	LOW	N/A	N/A	N/A	HIGH	HIGH
⁶⁶ Zn	MOD	N/A	LOW-MOD	LOW	MOD	MOD
⁸⁸ Sr	LOW	LOW	MOD-HIGH	MOD	MOD	MOD
¹³⁸ Ba	N/A	N/A	MOD	MOD	MOD	MOD
²⁰⁸ Pb	MOD	N/A	LOW	LOW	LOW	HIGH

Table 19: Relative intensities of isotopes observed in N10-1/02 UPM1 at each tooth location.

Isotope	Enamel Surface	Inner Enamel	Inner Dentine	EDJ	DPB	Outer Root Border
¹³ C	LOW	N/A	LOW-MOD	N/A	MOD-HIGH	MOD-HIGH
²⁴ Mg	LOW	LOW	MOD-HIGH	MOD	MOD-HIGH	LOW
²⁷ Al	LOW	N/A	N/A	N/A	LOW	MOD-HIGH
³¹ P	MOD	MOD	MOD-HIGH	MOD	MOD-HIGH	MOD
⁴⁴ Ca	MOD	MOD	MOD-HIGH	MOD	MOD-HIGH	MOD
⁴⁷ Ti	LOW	LOW	LOW	N/A	LOW	LOW
⁵² Cr	LOW	LOW	LOW-MOD	LOW	MOD	MOD
⁵⁵ Mn	LOW	N/A	N/A	N/A	N/A	HIGH
⁵⁶ Fe	LOW	N/A	LOW	N/A	MOD-HIGH	HIGH
⁶⁶ Zn	LOW-MOD	N/A	LOW-MOD	LOW	MOD-HIGH	MOD
⁸⁸ Sr	LOW	LOW	MOD-HIGH	MOD	MOD-HIGH	MOD
¹³⁸ Ba	LOW	N/A	HIGH	MOD	MOD-HIGH	MOD-HIGH
²⁰⁸ Pb	MOD	N/A	LOW	LOW	HIGH	HIGH

Table 20: Relative intensities of isotopes observed in N10-2/20A or B UCI at each tooth location.

Isotope	Enamel Surface	Inner Enamel	Inner Dentine	EDJ	DPB	Outer Root Border
¹³ C	LOW	LOW	MOD	LOW	LOW	LOW-MOD
²⁴ Mg	MOD	MOD	HIGH	LOW	MOD	LOW
²⁷ Al	LOW	N/A	N/A	N/A	MOD	LOW
³¹ P	MOD	MOD	HIGH	MOD	HIGH	MOD
⁴⁴ Ca	MOD	MOD	HIGH	MOD	HIGH	MOD
⁴⁷ Ti	LOW	LOW	N/A	N/A	LOW	N/A
⁵² Cr	LOW	LOW	LOW	LOW	LOW	LOW
⁵⁵ Mn	MOD	N/A	LOW	MOD	LOW	MOD
⁵⁶ Fe	MOD	N/A	LOW-MOD	LOW	HIGH	MOD
⁶⁶ Zn	MOD	LOW	MOD	LOW	MOD	MOD
⁸⁸ Sr	LOW	LOW	HIGH	MOD	MOD	MOD
¹³⁸ Ba	N/A	N/A	HIGH	HIGH	HIGH	MOD
²⁰⁸ Pb	N/A	N/A	N/A	LOW	LOW	MOD

Table 21: Relative intensities of isotopes observed in N10-2/20A or B UPM2 at each tooth location.

Isotope	Enamel Surface	Inner Enamel	Inner Dentine	EDJ	DPB	Outer Root Border
¹³ C	LOW	LOW	LOW-MOD	LOW	MOD	LOW-MOD
²⁴ Mg	MOD	MOD	MOD-HIGH	LOW	LOW	LOW
²⁷ Al	LOW	N/A	N/A	N/A	MOD	MOD-HIGH
³¹ P	MOD	MOD	HIGH	MOD-HIGH	MOD	MOD
⁴⁴ Ca	MOD	MOD	MOD-HIGH	MOD	MOD	MOD
⁴⁷ Ti	LOW	N/A	N/A	N/A	N/A	LOW
⁵² Cr	LOW	LOW	LOW	LOW	LOW	LOW
⁵⁵ Mn	LOW	LOW	N/A	N/A	N/A	LOW-MOD
⁵⁶ Fe	LOW	N/A	LOW	N/A	MOD	HIGH
⁶⁶ Zn	MOD	N/A	LOW	LOW	MOD	MOD
⁸⁸ Sr	LOW	LOW	MOD-HIGH	MOD	MOD	MOD
¹³⁸ Ba	N/A	N/A	MOD-HIGH	MOD	MOD-HIGH	MOD-HIGH
²⁰⁸ Pb	MOD	N/A	N/A	LOW	LOW	HIGH

Table 22: Relative intensities of isotopes observed in N10-2/21 UCI at each tooth location.

Isotope	Enamel Surface	Inner Enamel	Inner Dentine	EDJ	DPB	Outer Root Border
¹³ C	LOW	LOW	MOD	LOW	MOD	MOD
²⁴ Mg	LOW	LOW	MOD	LOW	N/A	N/A
²⁷ Al	LOW	N/A	N/A	N/A	LOW	LOW-MOD
³¹ P	MOD	MOD	HIGH	MOD	MOD	MOD-HIGH
⁴⁴ Ca	MOD	MOD	HIGH	MOD	MOD	MOD-HIGH
⁴⁷ Ti	LOW	LOW	LOW	LOW	LOW	LOW
⁵² Cr	N/A	N/A	MOD	LOW	MOD	MOD
⁵⁵ Mn	LOW	N/A	N/A	N/A	N/A	LOW
⁵⁶ Fe	LOW	N/A	N/A	N/A	LOW	MOD
⁶⁶ Zn	MOD	N/A	LOW	LOW	LOW	LOW
⁸⁸ Sr	LOW	N/A	MOD-HIGH	LOW	MOD	MOD
¹³⁸ Ba	LOW	N/A	MOD	LOW	MOD	MOD
²⁰⁸ Pb	MOD	N/A	LOW	LOW	LOW	MOD

Table 23: Relative intensities of isotopes observed in N10-2/21 UPM2 at each tooth location.

Isotope	Enamel Surface	Inner Enamel	Inner Dentine	EDJ	DPB	Outer Root Border
¹³ C	LOW	LOW	LOW	LOW	LOW	N/A
²⁴ Mg	LOW	MOD-HIGH	LOW-MOD	HIGH	HIGH	LOW
²⁷ Al	LOW	N/A	N/A	N/A	LOW	MOD
³¹ P	MOD	MOD	MOD	LOW	MOD	LOW
⁴⁴ Ca	MOD	MOD	MOD	LOW	MOD-HIGH	MOD
⁴⁷ Ti	N/A	LOW	LOW	N/A	LOW	LOW
⁵² Cr	LOW	LOW	LOW	LOW	LOW	LOW
⁵⁵ Mn	LOW	N/A	N/A	N/A	LOW	HIGH
⁵⁶ Fe	LOW	N/A	N/A	N/A	HIGH	HIGH
⁶⁶ Zn	MOD	N/A	LOW-MOD	LOW	HIGH	MOD
⁸⁸ Sr	LOW	MOD	MOD-HIGH	LOW	MOD	MOD
¹³⁸ Ba	N/A	N/A	MOD	LOW	MOD	MOD
²⁰⁸ Pb	LOW	N/A	N/A	N/A	HIGH	HIGH

Table 24: Relative intensities of isotopes observed in N10-2/21A UCI at each tooth location.

Isotope	Enamel Surface	Inner Enamel	Inner Dentine	EDJ	DPB	Outer Root Border
¹³ C	LOW	LOW	LOW	LOW	LOW	LOW
²⁴ Mg	LOW	LOW	MOD	LOW	MOD	LOW
²⁷ Al	LOW	N/A	N/A	N/A	LOW	MOD
³¹ P	MOD	MOD	MOD-HIGH	MOD	MOD	MOD
⁴⁴ Ca	MOD	MOD	MOD-HIGH	MOD	MOD-HIGH	MOD
⁴⁷ Ti	LOW	LOW	N/A	N/A	N/A	LOW
⁵² Cr	N/A	N/A	LOW	N/A	LOW	LOW
⁵⁵ Mn	LOW	N/A	N/A	N/A	MOD	HIGH
⁵⁶ Fe	LOW	N/A	N/A	N/A	N/A	LOW-MOD
⁶⁶ Zn	MOD	N/A	MOD	LOW	MOD	MOD
⁸⁸ Sr	LOW	LOW	MOD	LOW	MOD	MOD
¹³⁸ Ba	LOW	N/A	MOD-HIGH	MOD	MOD	MOD
²⁰⁸ Pb	LOW	N/A	N/A	N/A	LOW	MOD

Table 25: Relative intensities of isotopes observed in N10-2/21A UPM1 at each tooth location.

Isotope	Enamel Surface	Inner Enamel	Inner Dentine	EDJ	DPB	Outer Root Border
¹³ C	LOW	LOW	LOW	LOW	LOW	LOW
²⁴ Mg	LOW	LOW-MOD	MOD-HIGH	MOD	LOW	LOW
²⁷ Al	LOW	N/A	N/A	N/A	LOW-MOD	MOD
³¹ P	LOW	LOW	LOW-MOD	LOW	LOW	LOW-MOD
⁴⁴ Ca	LOW	LOW-MOD	MOD	LOW	MOD	MOD
⁴⁷ Ti	N/A	LOW	LOW	N/A	N/A	LOW
⁵² Cr	LOW	LOW	LOW	LOW	LOW	LOW-MOD
⁵⁵ Mn	LOW-MOD	N/A	N/A	N/A	N/A	HIGH
⁵⁶ Fe	LOW	N/A	LOW	N/A	HIGH	HIGH
⁶⁶ Zn	MOD	N/A	MOD	LOW	MOD	MOD
⁸⁸ Sr	LOW	LOW	MOD-HIGH	LOW	MOD	MOD-HIGH
¹³⁸ Ba	LOW	N/A	MOD	N/A	LOW	MOD
²⁰⁸ Pb	MOD	N/A	LOW	N/A	LOW	MOD-HIGH

Table 26: Relative intensities of isotopes observed in N10-2/42B UCI at each tooth location.

Isotope	Enamel Surface	Inner Enamel	Inner Dentine	EDJ	DPB	Outer Root Border
¹³ C	LOW	LOW	LOW	LOW	LOW	LOW
²⁴ Mg	LOW	LOW	MOD	N/A	LOW-MOD	N/A
²⁷ Al	LOW	N/A	N/A	N/A	LOW	LOW
³¹ P	LOW	LOW	MOD	LOW	MOD	MOD
⁴⁴ Ca	LOW	LOW	MOD	LOW	MOD	MOD
⁴⁷ Ti	LOW	LOW	N/A	N/A	LOW	LOW
⁵² Cr	N/A	N/A	LOW	LOW	LOW	LOW
⁵⁵ Mn	MOD	N/A	N/A	N/A	MOD	HIGH
⁵⁶ Fe	HIGH	N/A	N/A	N/A	HIGH	HIGH
⁶⁶ Zn	MOD	N/A	LOW	LOW	LOW	LOW
⁸⁸ Sr	LOW	LOW	MOD	LOW	MOD	MOD
¹³⁸ Ba	LOW	N/A	MOD	MOD	MOD	MOD
²⁰⁸ Pb	MOD	N/A	LOW	N/A	N/A	MOD

Table 27: Relative intensities of isotopes observed in N10-2/42B UPM1 at each tooth location.

Isotope	Enamel Surface	Inner Enamel	Inner Dentine	EDJ	DPB	Outer Root Border
¹³ C	LOW	LOW	HIGH	MOD	LOW	HIGH
²⁴ Mg	N/A	LOW	LOW-MOD	LOW	LOW	LOW
²⁷ Al	LOW	N/A	N/A	N/A	N/A	LOW
³¹ P	LOW	LOW	MOD	LOW	MOD	MOD
⁴⁴ Ca	LOW	LOW	MOD	LOW	LOW	MOD
⁴⁷ Ti	LOW	LOW	LOW	N/A	N/A	LOW
⁵² Cr	N/A	N/A	MOD	LOW	MOD	MOD
⁵⁵ Mn	LOW	LOW	LOW	LOW	LOW	LOW
⁵⁶ Fe	MOD	N/A	N/A	N/A	LOW	HIGH
⁶⁶ Zn	MOD	N/A	LOW-MOD	N/A	LOW	LOW
⁸⁸ Sr	LOW	LOW	MOD	LOW	MOD	MOD
¹³⁸ Ba	LOW	N/A	MOD-HIGH	LOW	MOD	MOD
²⁰⁸ Pb	LOW	N/A	N/A	N/A	LOW	LOW

Table 28: Relative intensities of isotopes observed in N10-4/01 UCI at each tooth location.

Isotope	Enamel Surface	Inner Enamel	Inner Dentine	EDJ	DPB	Outer Root Border
¹³ C	LOW	LOW	LOW	LOW	N/A	LOW
²⁴ Mg	LOW	LOW	LOW-MOD	N/A	LOW	LOW
²⁷ Al	LOW	N/A	N/A	N/A	LOW	HIGH
³¹ P	MOD	MOD	HIGH	MOD	HIGH	MOD-HIGH
⁴⁴ Ca	MOD	MOD	HIGH	MOD	HIGH	MOD-HIGH
⁴⁷ Ti	LOW	LOW	LOW	N/A	N/A	MOD
⁵² Cr	N/A	N/A	LOW	LOW	LOW	LOW
⁵⁵ Mn	LOW	N/A	N/A	LOW	LOW	HIGH
⁵⁶ Fe	LOW	N/A	N/A	N/A	MOD	HIGH
⁶⁶ Zn	MOD	N/A	MOD	LOW	MOD	MOD
⁸⁸ Sr	LOW	LOW	HIGH	HIGH	HIGH	HIGH
¹³⁸ Ba	LOW	N/A	MOD	MOD	MOD	MOD
²⁰⁸ Pb	MOD	N/A	N/A	N/A	LOW	HIGH

Table 29: Relative intensities of isotopes observed in N10-4/01 UPM2 at each tooth location.

Isotope	Enamel Surface	Inner Enamel	Inner Dentine	EDJ	DPB	Outer Root Border
¹³ C	MOD	LOW	MOD	LOW	LOW	MOD
²⁴ Mg	LOW	MOD	MOD	LOW	LOW	N/A
²⁷ Al	LOW	N/A	N/A	N/A	LOW	LOW
³¹ P	MOD	MOD	HIGH	MOD	MOD	MOD
⁴⁴ Ca	MOD	MOD	HIGH	MOD	MOD	MOD
⁴⁷ Ti	LOW	LOW	LOW	N/A	LOW	LOW
⁵² Cr	N/A	N/A	LOW	LOW	LOW	LOW
⁵⁵ Mn	HIGH	N/A	N/A	N/A	N/A	HIGH
⁵⁶ Fe	HIGH	N/A	N/A	N/A	MOD	HIGH
⁶⁶ Zn	MOD	N/A	LOW	N/A	MOD	LOW
⁸⁸ Sr	LOW	LOW	HIGH	MOD	MOD	MOD
¹³⁸ Ba	LOW	N/A	HIGH	MOD	MOD	MOD
²⁰⁸ Pb	MOD	N/A	N/A	N/A	LOW	MOD

Table 30: Relative intensities of isotopes observed in N10-4/43 UCI at each tooth location.

Isotope	Enamel Surface	Inner Enamel	Inner Dentine	EDJ	DPB	Outer Root Border
¹³ C	LOW	N/A	MOD	LOW	MOD	MOD
²⁴ Mg	LOW	LOW	MOD	LOW	LOW	LOW
²⁷ Al	LOW	N/A	N/A	N/A	LOW	LOW
³¹ P	MOD	MOD	MOD-HIGH	LOW-MOD	MOD	MOD
⁴⁴ Ca	MOD	MOD	MOD-HIGH	LOW	MOD-HIGH	MOD
⁴⁷ Ti	LOW	LOW	N/A	LOW	N/A	N/A
⁵² Cr	N/A	N/A	MOD	N/A	MOD	MOD
⁵⁵ Mn	LOW	N/A	N/A	N/A	N/A	MOD
⁵⁶ Fe	LOW	N/A	N/A	N/A	MOD	HIGH
⁶⁶ Zn	MOD	N/A	MOD	N/A	MOD-HIGH	MOD
⁸⁸ Sr	LOW	LOW	HIGH	LOW	HIGH	MOD
¹³⁸ Ba	LOW	N/A	MOD-HIGH	MOD	MOD	MOD
²⁰⁸ Pb	MOD	N/A	N/A	N/A	LOW	MOD

Table 31: Relative intensities of isotopes observed in N10-4/43 UPM1 at each tooth location.

Isotope	Enamel Surface	Inner Enamel	Inner Dentine	EDJ	DPB	Outer Root Border
¹³ C	LOW	N/A	LOW	LOW	LOW	LOW-MOD
²⁴ Mg	MOD	MOD-HIGH	HIGH	MOD	HIGH	MOD
²⁷ Al	LOW	N/A	N/A	N/A	LOW	MOD
³¹ P	LOW	LOW	MOD	LOW	MOD	MOD
⁴⁴ Ca	LOW	LOW	MOD	LOW	MOD	MOD
⁴⁷ Ti	LOW	LOW	LOW	N/A	N/A	LOW-MOD
⁵² Cr	N/A	N/A	LOW	N/A	LOW	LOW-MOD
⁵⁵ Mn	LOW	N/A	N/A	N/A	N/A	MOD
⁵⁶ Fe	LOW	N/A	LOW	N/A	LOW	MOD-HIGH
⁶⁶ Zn	MOD	N/A	LOW-MOD	N/A	MOD	MOD
⁸⁸ Sr	LOW	LOW	MOD	LOW	MOD	MOD
¹³⁸ Ba	LOW	N/A	MOD	N/A-LOW	MOD	MOD
²⁰⁸ Pb	LOW	N/A	N/A	N/A	LOW	MOD

Table 32: Relative intensities of isotopes observed in N10-4/4C Large UCI at each tooth location.

Isotope	Enamel Surface	Inner Enamel	Inner Dentine	EDJ	DPB	Outer Root Border
¹³ C	LOW	LOW	LOW	LOW	LOW	MOD
²⁴ Mg	LOW	LOW	MOD	LOW	LOW	LOW
²⁷ Al	LOW	N/A	N/A	N/A	LOW	MOD
³¹ P	HIGH	HIGH	HIGH	MOD	MOD-HIGH	MOD
⁴⁴ Ca	HIGH	HIGH	HIGH	MOD	HIGH	HIGH
⁴⁷ Ti	LOW	LOW	LOW	N/A	LOW	LOW
⁵² Cr	N/A	N/A	LOW	N/A	LOW	LOW
⁵⁵ Mn	LOW	N/A	N/A	N/A	N/A	MOD
⁵⁶ Fe	LOW	N/A	N/A	N/A	LOW	MOD
⁶⁶ Zn	HIGH	N/A	LOW-MOD	LOW	MOD	LOW
⁸⁸ Sr	LOW	LOW	MOD-HIGH	MOD	MOD	MOD-HIGH
¹³⁸ Ba	LOW	N/A	MOD	LOW	MOD	MOD
²⁰⁸ Pb	MOD	N/A	N/A	N/A	LOW	MOD

Table 33: Relative intensities of isotopes observed in N10-4/4C Large UPM2 at each tooth location.

Isotope	Enamel Surface	Inner Enamel	Inner Dentine	EDJ	DPB	Outer Root Border
¹³ C	LOW	LOW	LOW	LOW	LOW	LOW
²⁴ Mg	LOW	MOD-HIGH	MOD-HIGH	MOD	MOD	LOW
²⁷ Al	LOW	N/A	N/A	N/A	LOW	LOW
³¹ P	LOW	LOW-MOD	LOW-MOD	LOW	MOD	LOW
⁴⁴ Ca	MOD	HIGH	HIGH	MOD	HIGH	MOD
⁴⁷ Ti	LOW	LOW	LOW	N/A	LOW	LOW
⁵² Cr	N/A	N/A	LOW	LOW	LOW-MOD	LOW-MOD
⁵⁵ Mn	LOW	N/A	N/A	N/A	LOW	MOD
⁵⁶ Fe	LOW	N/A	N/A	N/A	MOD	MOD
⁶⁶ Zn	HIGH	N/A	LOW-MOD	N/A	LOW-MOD	LOW
⁸⁸ Sr	LOW	LOW	MOD-HIGH	LOW	MOD	MOD
¹³⁸ Ba	LOW	N/A	MOD-HIGH	LOW-MOD	MOD	MOD
²⁰⁸ Pb	LOW-MOD	N/A	N/A	N/A	LOW	LOW-MOD

Table 34: Relative intensities of isotopes observed in N10-4/19 UCI at each tooth location.

Isotope	Enamel Surface	Inner Enamel	Inner Dentine	EDJ	DPB	Outer Root Border
¹³ C	LOW	LOW	LOW	LOW	LOW	LOW
²⁴ Mg	LOW	LOW	MOD	LOW	LOW	LOW
²⁷ Al	LOW	N/A	N/A	N/A	MOD	MOD-HIGH
³¹ P	MOD	MOD	MOD-HIGH	MOD	MOD	MOD
⁴⁴ Ca	LOW	LOW	MOD-HIGH	MOD	MOD	MOD
⁴⁷ Ti	LOW	LOW	LOW	N/A	LOW	LOW
⁵² Cr	N/A	N/A	LOW	LOW	LOW	LOW-MOD
⁵⁵ Mn	MOD	N/A	N/A	N/A	N/A	MOD-HIGH
⁵⁶ Fe	MOD	N/A	LOW	LOW	HIGH	HIGH
⁶⁶ Zn	MOD	N/A	MOD	LOW	MOD	MOD
⁸⁸ Sr	N/A	N/A	MOD-HIGH	MOD	LOW	MOD
¹³⁸ Ba	LOW	N/A	MOD	LOW	LOW	MOD
²⁰⁸ Pb	LOW-MOD	N/A	N/A	N/A	LOW	LOW-MOD

Table 35: Relative intensities of isotopes observed in N10-4/31 UCI at each tooth location.

Isotope	Enamel Surface	Inner Enamel	Inner Dentine	EDJ	DPB	Outer Root Border
¹³ C	LOW	LOW	LOW	LOW	LOW	LOW
²⁴ Mg	LOW	LOW	MOD	LOW	LOW	LOW
²⁷ Al	LOW-MOD	N/A	N/A	N/A	LOW	LOW-MOD
³¹ P	MOD	LOW	MOD-HIGH	LOW	HIGH	MOD
⁴⁴ Ca	MOD	LOW	MOD-HIGH	LOW	MOD-HIGH	MOD
⁴⁷ Ti	LOW	LOW	LOW	N/A	LOW	LOW
⁵² Cr	N/A	N/A	LOW	LOW	LOW	MOD
⁵⁵ Mn	MOD	N/A	N/A	N/A	N/A	HIGH
⁵⁶ Fe	MOD	N/A	LOW	N/A	MOD-HIGH	HIGH
⁶⁶ Zn	HIGH	N/A	MOD	LOW	MOD	LOW
⁸⁸ Sr	N/A	N/A	MOD	LOW	MOD	MOD
¹³⁸ Ba	LOW	N/A	MOD-HIGH	MOD	MOD-HIGH	MOD
²⁰⁸ Pb	LOW	N/A	N/A	N/A	LOW	MOD

Table 36: Relative intensities of isotopes observed in N10-4/35 UCI at each tooth location.

Isotope	Enamel Surface	Inner Enamel	Inner Dentine	EDJ	DPB	Outer Root Border
¹³ C	LOW	LOW	LOW	LOW	LOW	LOW-MOD
²⁴ Mg	LOW	LOW	MOD	LOW	LOW	LOW
²⁷ Al	LOW	N/A	N/A	N/A	LOW	MOD-HIGH
³¹ P	LOW	LOW	MOD	LOW	LOW	MOD
⁴⁴ Ca	LOW	LOW	MOD	LOW	LOW	MOD
⁴⁷ Ti	LOW	LOW	LOW	N/A	LOW	MOD
⁵² Cr	N/A	N/A	LOW	N/A	N/A	LOW
⁵⁵ Mn	LOW	N/A	N/A	N/A	N/A	HIGH
⁵⁶ Fe	LOW	N/A	N/A	N/A	LOW	HIGH
⁶⁶ Zn	HIGH	N/A	LOW	LOW	MOD	MOD
⁸⁸ Sr	N/A	LOW	MOD	N/A	LOW	MOD
¹³⁸ Ba	N/A	N/A	MOD	LOW	LOW	MOD
²⁰⁸ Pb	LOW	LOW	N/A	N/A	N/A	MOD

Table 37: Relative intensities of isotopes observed in N10-4/46A UCI at each tooth location.

Isotope	Enamel Surface	Inner Enamel	Inner Dentine	EDJ	DPB	Outer Root Border
¹³ C	LOW	LOW	LOW	N/A	LOW	LOW
²⁴ Mg	MOD	MOD	LOW-MOD	MOD	MOD	LOW
²⁷ Al	LOW-MOD	N/A	N/A	N/A	LOW	LOW
³¹ P	MOD	MOD	MOD	MOD	HIGH	MOD
⁴⁴ Ca	MOD	MOD	MOD	LOW	MOD-HIGH	MOD
⁴⁷ Ti	LOW	LOW	LOW	LOW	LOW	LOW
⁵² Cr	N/A	N/A	LOW	N/A	LOW	LOW
⁵⁵ Mn	LOW	N/A	N/A	N/A	N/A	HIGH
⁵⁶ Fe	HIGH	N/A	N/A	N/A	LOW	MOD-HIGH
⁶⁶ Zn	MOD	N/A	LOW-MOD	N/A	MOD	MOD
⁸⁸ Sr	LOW	LOW	MOD	N/A	MOD	MOD-HIGH
¹³⁸ Ba	N/A	N/A	MOD	N/A	LOW	MOD-HIGH
²⁰⁸ Pb	MOD	N/A	N/A	LOW	MOD	MOD

Table 38: Relative intensities of isotopes observed in N10-2/49 ULI at each tooth location.

Isotope	Enamel Surface	Inner Enamel	Inner Dentine	EDJ	DPB	Outer Root Border
¹³ C	LOW	LOW	MOD	LOW	MOD	LOW-MOD
²⁴ Mg	LOW	LOW	MOD	LOW	LOW	LOW
²⁷ Al	LOW	N/A	N/A	N/A	LOW	LOW-MOD
³¹ P	LOW	MOD	MOD	LOW	MOD	MOD
⁴⁴ Ca	LOW	LOW	MOD	LOW	MOD	MOD
⁴⁷ Ti	LOW	LOW	LOW	N/A	LOW	LOW
⁵² Cr	N/A	N/A	LOW	LOW	LOW	LOW
⁵⁵ Mn	LOW	N/A	N/A	N/A	LOW	LOW
⁵⁶ Fe	HIGH	N/A	N/A	N/A	HIGH	HIGH
⁶⁶ Zn	MOD	N/A	LOW	LOW	LOW	LOW
⁸⁸ Sr	N/A	N/A	MOD	N/A	MOD	MOD
¹³⁸ Ba	LOW	N/A	MOD-HIGH	LOW	MOD	MOD
²⁰⁸ Pb	MOD	N/A	LOW	N/A	LOW	LOW

Table 39: Relative intensities of isotopes observed in N10-2/22 UPM1 at each tooth location.

Isotope	Enamel Surface	Inner Enamel	Inner Dentine	EDJ	DPB	Outer Root Border
¹³ C	LOW	LOW	LOW	N/A	LOW	LOW
²⁴ Mg	LOW	MOD	MOD	LOW	N/A	N/A
²⁷ Al	LOW	N/A	N/A	N/A	LOW	LOW
³¹ P	MOD	MOD-HIGH	MOD	LOW	LOW	MOD
⁴⁴ Ca	MOD	MOD	MOD	LOW	LOW	MOD
⁴⁷ Ti	LOW	LOW	LOW	LOW	N/A	LOW
⁵² Cr	N/A	N/A	LOW	N/A	LOW	MOD
⁵⁵ Mn	LOW	N/A	N/A	N/A	N/A	HIGH
⁵⁶ Fe	LOW	N/A	LOW	N/A	MOD	LOW-MOD
⁶⁶ Zn	MOD	N/A	LOW	N/A	LOW	LOW-MOD
⁸⁸ Sr	LOW	LOW	MOD	LOW	LOW	MOD
¹³⁸ Ba	N/A-LOW	N/A	HIGH	N/A	MOD	MOD-HIGH
²⁰⁸ Pb	LOW	N/A	LOW	N/A	LOW	HIGH

Table 40: Relative intensities of isotopes observed in N10-2/40 UPM1 at each tooth location.

Isotope	Enamel Surface	Inner Enamel	Inner Dentine	EDJ	DPB	Outer Root Border
¹³ C	LOW	LOW	LOW	LOW	LOW	LOW
²⁴ Mg	LOW-MOD	MOD-HIGH	MOD	MOD	MOD	LOW
²⁷ Al	LOW	N/A	LOW	N/A	LOW	LOW-MOD
³¹ P	LOW-MOD	LOW-MOD	MOD-HIGH	LOW	MOD	LOW-MOD
⁴⁴ Ca	MOD	MOD	MOD-HIGH	LOW	MOD	LOW-MOD
⁴⁷ Ti	LOW	LOW	LOW	N/A	N/A	LOW
⁵² Cr	N/A	N/A	LOW	N/A	LOW	LOW
⁵⁵ Mn	LOW	N/A	N/A	N/A	LOW	LOW-MOD
⁵⁶ Fe	LOW	N/A	N/A	N/A	LOW	MOD
⁶⁶ Zn	MOD	N/A	LOW-MOD	N/A	MOD	LOW-MOD
⁸⁸ Sr	LOW	LOW	MOD	LOW	MOD	MOD
¹³⁸ Ba	N/A	N/A	MOD-HIGH	LOW	MOD	MOD
²⁰⁸ Pb	LOW	N/A	N/A	N/A	LOW	LOW-MOD

Table 41: Relative intensities of isotopes observed in N10-4/10 UPM2 at each tooth location.

Isotope	Enamel Surface	Inner Enamel	Inner Dentine	EDJ	DPB	Outer Root Border
¹³ C	LOW	LOW	LOW	LOW	LOW	LOW
²⁴ Mg	LOW	LOW	MOD	LOW	LOW	LOW
²⁷ Al	LOW	N/A	N/A	N/A	LOW	LOW-MOD
³¹ P	MOD	MOD	HIGH	MOD	MOD	MOD
⁴⁴ Ca	LOW	LOW	HIGH	MOD	MOD	MOD
⁴⁷ Ti	LOW	LOW	LOW	N/A	LOW	LOW
⁵² Cr	N/A	N/A	LOW	LOW	LOW	N/A
⁵⁵ Mn	LOW	N/A	N/A	N/A	N/A	MOD
⁵⁶ Fe	MOD	N/A	LOW	N/A	MOD	HIGH
⁶⁶ Zn	MOD	N/A	LOW	LOW	LOW	LOW
⁸⁸ Sr	N/A	N/A	MOD-HIGH	MOD	MOD	MOD
¹³⁸ Ba	N/A	N/A	MOD-HIGH	MOD	MOD	MOD
²⁰⁸ Pb	MOD	N/A	LOW	N/A	MOD	HIGH

Table 42: Relative intensities of isotopes observed in N10-4/33 UPM2 at each tooth location.

Isotope	Enamel Surface	Inner Enamel	Inner Dentine	EDJ	DPB	Outer Root Border
¹³ C	LOW	LOW	LOW	LOW	LOW	MOD
²⁴ Mg	LOW	LOW	MOD	MOD	MOD	LOW
²⁷ Al	LOW	N/A	LOW	N/A	LOW	MOD-HIGH
³¹ P	LOW	LOW	MOD	N/A	MOD	MOD
⁴⁴ Ca	LOW	LOW	MOD-HIGH	LOW	MOD	MOD
⁴⁷ Ti	LOW	LOW	LOW	N/A	LOW	LOW
⁵² Cr	N/A	N/A	LOW	LOW	LOW	MOD
⁵⁵ Mn	LOW	N/A	N/A	N/A	N/A	MOD
⁵⁶ Fe	MOD	N/A	N/A	N/A	HIGH	HIGH
⁶⁶ Zn	MOD	N/A	MOD	N/A	HIGH	MOD
⁸⁸ Sr	LOW	LOW	MOD-HIGH	LOW	MOD	MOD-HIGH
¹³⁸ Ba	LOW	N/A	MOD-HIGH	N/A	MOD	MOD
²⁰⁸ Pb	LOW	N/A	N/A	N/A	LOW	LOW-MOD

Table 43: Relative intensities of isotopes observed in N10-4/46C Small UPM2 at each tooth location.

Isotope	Enamel Surface	Inner Enamel	Inner Dentine	EDJ	DPB	Outer Root Border
¹³ C	LOW	LOW	LOW	LOW	LOW	LOW
²⁴ Mg	LOW	MOD	MOD	MOD	LOW	LOW
²⁷ Al	LOW	N/A	N/A	N/A	LOW	LOW-MOD
³¹ P	LOW	LOW	MOD	LOW	MOD	MOD
⁴⁴ Ca	LOW	LOW	MOD	LOW	LOW	MOD
⁴⁷ Ti	LOW	LOW	LOW	LOW	LOW	LOW
⁵² Cr	N/A	N/A	N/A	LOW	N/A	LOW
⁵⁵ Mn	LOW	N/A	N/A	N/A	LOW	MOD
⁵⁶ Fe	MOD-HIGH	N/A	LOW	N/A	HIGH	HIGH
⁶⁶ Zn	MOD	N/A	LOW	N/A	MOD	MOD
⁸⁸ Sr	LOW	LOW	MOD-HIGH	LOW	MOD	MOD
¹³⁸ Ba	N/A	N/A	MOD	N/A	MOD	MOD
²⁰⁸ Pb	LOW-MOD	N/A	LOW	N/A	MOD	MOD

LIST OF REFERENCES

- Almirall JR, Trejos T. 2016. Applications of LA-ICP-MS to forensic science. *Elements* 12(5):335-340.
- Amr MA. 2011. Trace elements in Egyptian teeth. *Int J Phys Sci* 6(27):6241-6245.
- Anjos MJ, Barroso RC, Pérez CA, Braz D, Moreira S, Dias KRHC, Lopes RT. 2004. Elemental mapping of teeth using μ SRXRF. *Nucl Instr Meth Phys Res B* 213:569-573.
- Antoine D, Hillson S. 2016. Enamel structure and properties. In: Irish JD, Scott GR, editors. *A companion to dental anthropology*. Chichester, West Sussex: John Wiley & Sons, Inc., p 223-243.
- Arnold WH, Gaengler P. 2007. Quantitative analysis of the calcium and phosphorus content of developing and permanent human teeth. *Ann Anat* 189(2):183-190.
- Arora M, Chan SWY, Kennedy BJ, Sharma A, Crisante D, Walker DM. 2004. Spatial distribution of lead in the roots of human primary teeth. *J Trace Elem Med Biol* 18:135-139
- Arora M, Hare D, Austin C, Smith DR, Doble P. 2011. Spatial distribution of manganese in enamel and coronal dentine of human primary teeth. *Sci Total Environ* 409(7):1315-1319.
- Arruda-Neto JDT, Geraldo LP, Prado GR, Garcia F, Bittencourt-Oliveira MC, Sarkis JES, Martinez-Lusardo F, Lima-Cazorla L, Rosa-Medero D, Rodrigues TE, Genofre GC. 2010. Study of metals transfer from environment using teeth as biomonitor. *Environ Int* 36:243-246.
- Asaduzzaman K, Khandaker MU, Baharudin NAB, Amin YBM, Farook MS, Bradley DA, Mahmoud O. 2017. Heavy metals in human teeth dentine: a bio-indicator of metals exposure and environmental pollution. *Chemosphere* 176:221-230.
- Aschner M. 2000. Manganese: brain transport and emerging research needs. *Environ Health Perspect* 108(Suppl 3):429-432.
- Austin C, Smith TM, Bradman A, Hinde K, Joannes-Boyau R, Bishop D, Hare DJ, Doble P, Eskenazi B, Arora M. 2013. Barium distributions in teeth reveal early-life dietary transitions in primates. *Nature* 498(7453):216-219.
- Ávila A, Mansilla J, Bosch P, Pijoan C. 2014. Cinnabar in Mesoamerica: poisoning or mortuary ritual? *J Archaeol Sci* 49:48-56.

- Balasse M. 2002. Reconstructing dietary and environmental history from enamel isotopic analysis: time resolution of intra-tooth sequential sampling. *Int J Osteoarchaeol* 12(3):155-165.
- Beaumont J, Montgomery J, Buckberry J, Jay M. 2015. Infant mortality and isotopic complexity: new approaches to stress, maternal health, and weaning. *Am J Physical Anthropol* 157:441-157.
- Becker JS, Zoriy M, Matusch A, Wu B, Salber D, Palm C, Becker JS. 2010. Bioimaging of metals by laser ablation inductively coupled plasma mass spectrometry (LA-ICP-MS). *Mass Spectrom Rev* 29(1):156-175.
- Bosshardt DD, Chappuis V, Buser D. 2017. Osseointegration of titanium, titanium alloy and zirconia dental implants: current knowledge and open questions. *Periodontol* 2000 73(1):22-40.
- Brothwell DR. 1981. *Digging up bones*, 3rd edition. Ithaca, NY: Cornell University Press.
- Brown CJ, Chenery SRN, Smith B, Mason C, Tomkins A, Roberts GJ, Sserunjogi L, Tiberindwa JV. 2004. Environmental influences on the trace element content of teeth—implications for disease and nutritional status. *Arch Oral Biol* 49:705-717.
- Buchman AL. 2014. Manganese. In: Ross AC, Caballero B, Cousins RJ, Tucker KL, Ziegler TR. *Modern nutrition in health and disease*, eleventh edition. Philadelphia, PA: Lippincott Williams and Wilkins, p 238-244.
- Budd P, Montgomery J, Cox A, Krause P, Barreiro B, Thomas RG. 1998. The distribution of lead within ancient and modern human teeth: implications for long-term and historical exposure monitoring. *Sci Total Environ* 220(2):121-136.
- Buehler. 1992. Operation and maintenance instructions: ISOMET™ low speed saw. Lake Bluff, IL: Buehler Ltd.
- Burton JH, Price TD, Cahue L, Wright LE. 2003. The use of barium and strontium abundances in human skeletal tissues to determine their geographic origins. *Int J Osteoarchaeol* 13(1-2):88-95.
- Cashman KD. 2002. Calcium intake, calcium bioavailability and bone health. *Brit J Nutr* 82(2):S169-S177.
- Castro W, Hoogewerff J, Latkoczy C, Almirall JR. 2010. Application of laser ablation (LA-ICP-SF-MS) for the elemental analysis of bone and teeth samples for discrimination purposes. *Forensic Sci Int* 195(1):17-27.

- Christensen AM, Passalacqua NV, Bartelink EJ. 2014. Forensic anthropology: current methods and practice. San Diego, CA: Elsevier Inc.
- Comar CL, Russell RS, Wasserman RH. 1957. Strontium-calcium movement from soil to man. *Science* 126(3272):485-492.
- Coyston S. 1995. An application of carbon isotopic analysis of bone apatite to the study of Maya diets and subsistence at Pacbitun and Lamanai, Belize. Thesis. Trent University, Peterborough, ON.
- Coyston S, White CD, Schwarcz HP. 1999. Dietary carbonate analysis of bone and enamel for two sites in Belize. In: White CD, editor. *Reconstructing ancient Maya diet*. Salt Lake City, UT: The University of Utah Press, p 221-244.
- Cucina A, Dudgeon J, Neff H. 2007. Methodological strategy for the analysis of human dental enamel by LA-ICP-MS. *J Archaeol Sci* 34(11):1884-1888.
- Cucina A, Tiesler V, Sosa TS, Neff H. 2011. Trace-element evidence for foreigners at a Maya port in Northern Yucatan. *J Archaeol Sci* 38(8):1878-1885.
- Curzon MEJ, Featherstone JDB. 1983. Chemical composition of enamel. In: Lazzari EP, editor. *CRC handbook of experimental aspects of oral biochemistry*. Boca Raton, FL: CRC Press, p 123-135.
- de Dios Teruel J, Alcolea A, Hernández A, Ruiz AJO. 2015. Comparison of chemical composition of enamel and dentine in human, bovine, porcine and ovine teeth. *Arch Oral Biol* 60(5):768-775.
- Delmdahl R, von Oldershausen G. 2005. Quantitative solid sample analysis by ArF excimer laser ablation. *J Molecular Structure* 744:255-258.
- de Souza Guerra C, Gerlach RF, Pinto NGV, Cardoso SC, Moreira S, de Almeida AP, Peixoto ITA, Meloni CH, Mota CL, de Oliveira LF, Braz D, Barroso RC. 2010. X-ray fluorescence with synchrotron radiation to elemental analysis of lead and calcium content of primary teeth. *Appl Radiat Isot* 68(1):71-75.
- DeWitte SN, Stojanowski CM. 2015. The osteological paradox 20 years later: past perspectives, future directions. *J Archaeol Research* 23(4):397-450.
- Djingova R, Zlateva B, Kuleff I. 2004. On the possibilities of inductively coupled plasma mass spectrometry for analysis of archaeological bones for reconstruction of paleodiet. *Talanta* 63:785-789.

- Dolphin AE, Goodman AH. 2009. Maternal diets, nutritional status, and zinc in contemporary Mexican infants' teeth: Implications for reconstructing paleodiets. *Am J Phys Anthropol* 140(3):399-409.
- Dolphin AE, Goodman AH, Amarasiriwardena DD. 2005. Variation in elemental intensities among teeth and between pre-and postnatal regions of enamel. *Am J Phys Anthropol* 128(4):878-888.
- Dormon TM. 2007. Degenerative joint disease in the ancient Maya population of Lamanai, Belize. Thesis. Trent University, Peterborough, ON.
- Duval M, Aubert M, Hellstrom J, Grün R. 2011. High resolution LA-ICP-MS mapping of U and Th isotopes in an early Pleistocene equid tooth from Fuente Nueva-3 (Orce, Andalusia, Spain). *Quat Geochronol* 6(5):458-467.
- Emery KF. 1999. Continuity and variability in Postclassic and Colonial animal use at Lamanai and Tipu, Belize. In: White CD, editor. *Reconstructing ancient Maya diet*. Salt Lake City, UT: The University of Utah Press, p 61-82.
- Ezzo JA. 1994. Zinc as a paleodietary indicator: an issue of theoretical validity in bone-chemistry analysis. *Am Ant* 59(4):606-621.
- Fairweather-Tait S, Hurrell RF. 1996. Bioavailability of minerals and trace elements. *Nutr Res Rev* 9:295-324.
- Farell J, Amarasiriwardena D, Goodman AH, Arriaza B. 2013. Bioimaging of trace metals in ancient Chilean mummies and contemporary Egyptian teeth by laser ablation-inductively coupled plasma-mass spectrometry (LA-ICP-MS). *Microchem J* 106:340-346.
- Fischer A, Wiechula D, Postek-Stefańska L, Kwapuliński J. 2009. Concentrations of metals in maxilla and mandible deciduous and permanent human teeth. *Biol Trace Elem Res* 132(1-3):19-26.
- Font L, Jonker G, van Aalderen PA, Schiltmans EF, Davies GR. 2015. Provenancing of unidentified World War II casualties: Application of strontium and oxygen isotope analysis in tooth enamel. *Sci Justic* 55(1):10-17.
- Fortes FJ, Perez-Carceles MD, Sibon A, Luna A, Laserna JJ. 2015. Spatial distribution analysis of strontium in human teeth by laser-induced breakdown spectroscopy: application to diagnosis of seawater drowning. *Int J Legal Med* 129(4):807-813.
- Fraga CG. 2005. Relevance, essentiality and toxicity of trace elements in human health. *Mol Aspects Med* 26(4):235-244.

- Freeland-Graves JH, Sanjeevi N, Lee JJ. 2015. Global perspectives on trace element requirements. *J Trace Elem Med Biol* 31:135-141.
- Fricker MB, Günther D. 2016. Instrumentation, fundamentals, and application of laser ablation-inductively coupled plasma-mass spectrometry. In: Dussubieux L, Golitko M, Gratuze B, editors. *Recent advances in laser ablation ICP-MS for archaeology*. Berlin: Springer. p 1-19.
- Galiová MV, Fišáková MN, Kynický J, Prokeš L, Neff H, Mason AZ, Gadas P, Kosler J, Kanický V. 2013. Elemental mapping in fossil tooth root section of *Ursus arctos* by laser ablation inductively coupled plasma mass spectrometry (LA-ICP-MS). *Talanta* 105:235-243.
- Guatelli-Steinberg D. 2016. Dental stress indicators from micro- to macroscopic. In: Irish JD, Scott GR, editors. *A companion to dental anthropology*. Chichester, West Sussex: John Wiley & Sons, Inc., p 450-464.
- Guede I., Zuluaga MC, Ortega LA, Alonso-Olazabal A, Murelaga X, Pina M, Gutierrez FJ. 2017. Analyses of human dentine and tooth enamel by laser ablation-inductively coupled plasma-mass spectrometry (LA-ICP-MS) to study the diet of medieval Muslim individuals from Tauste (Spain). *Microchem J* 130:287-294.
- Hanć A, Olszewska A, Barańkiewicz D. 2013. Quantitative analysis of elements migration in human teeth with and without filling using LA-ICP-MS. *Microchem J* 110:61-69.
- Hare DJ, Arora M, Jenkins NL, Finkelstein DI, Doble PA, Bush AI. 2015. Is early-life iron exposure critical in neurodegeneration? *Nat Rev Neurol* 11(9):536-544.
- Hare D, Austin C, Doble P, Arora M. 2011. Elemental bio-imaging of trace elements in teeth using laser ablation-inductively coupled plasma-mass spectrometry. *J Dentistry* 39(5):397-403.
- Harris EF. 2016. Odontogenesis. In: Irish JD, Scott GR, editors. *A companion to dental anthropology*. Chichester, West Sussex: John Wiley & Sons, Inc., p 142-158.
- Hillson S. 2005. *Teeth*, 2nd edition. Cambridge, NY: Cambridge University Press.
- Hollund HI, Arts N, Jans MME, Kars H. 2015. Are teeth better? histological characterization of diagenesis in archaeological bone-tooth pairs and a discussion of the consequences for archaeometric sample selection and analyses. *Int J Osteoarchaeol* 25(6):901-911.

- Humphrey LT. 2016. Chemical and isotopic analyses of dental tissues. In: Irish JD, Scott GR, editors. *A companion to dental anthropology*. Chichester, West Sussex: John Wiley & Sons, Inc., p 499-513.
- Jadot E, Schiavon N, Manso M. 2016. The ceramics of Malpaís of Zacapu, Michoacán, Mexico, during the Early and Middle Postclassic periods (900–1450AD): Micro-chemical characterization of surface paintings. *Spectrochim Acta B* 119:10-16.
- Kamenov GD, Curtis JH. 2017. Using carbon, oxygen, strontium, and lead isotopes in modern human teeth for forensic investigations: a critical overview based on data from Bulgaria. *J Forensic Sci* doi:10.1111/1556-4029.13462.
- Kang D, Amarasiriwardena D, Goodman AH. 2004. Application of laser ablation–inductively coupled plasma–mass spectrometry (LA–ICP–MS) to investigate trace metal spatial distributions in human tooth enamel and dentine growth layers and pulp. *Anal Bioanal Chem* 378(6):1608-1615.
- Keen CI, Ensunsa JL, Watson MH, Baly DL, Donovan SM, Monaco MH, Clegg MS. 1999. Nutritional aspects of manganese from experimental studies. *NeuroToxicology* 20(2-3):213-224.
- King JC, Cousins RJ. 2014. Zinc. In: Ross AC, Caballero B, Cousins RJ, Tucker KL, Ziegler TR. *Modern nutrition in health and disease*, eleventh edition. Philadelphia, PA: Lippincott Williams and Wilkins, p 189-205.
- Kohn MJ, Morris J, Olin P. 2013. Trace element concentrations in teeth—a modern Idaho baseline with implications for archeometry, forensics, and palaeontology. *J Archaeol Sci* 40(4):1689-1699.
- Kohn MJ, Schoeninger MJ, Barker WW. 1999. Altered states: effects of diagenesis on fossil tooth chemistry. *Geochim Cosmochim Acta* 63(18):2737-2747.
- Kravchenko J, Darrah TH, Miller RK, Lyerly HK, Vengosh A. 2014. A review of the health impacts of barium from natural and anthropogenic exposure. *Environ Geochem Health* 36(4):797-814.
- Krebs NF. 2013. Update on zinc deficiency and excess in clinical pediatric practice. *Ann Nutr Metab* 62:19-29.
- Krueger KL. 2016. Dentition behavior, and diet determination. In: Irish JD, Scott GR, editors. *A companion to dental anthropology*. Chichester, West Sussex: John Wiley & Sons, Inc., p 396-411.
- Kumagai A, Fujita Y, Endo S, Itai K. 2012. Concentrations of trace element in human dentin by sex and age. *Forensic Sci Int* 219(1):29-32.

- Lang CA. 1990. The dental morphology of the Maya from Lamanai and Tipu. Thesis. Trent University, Peterborough, ON.
- LeCount LJ, Wells EC, Jamison TR, Mixer DW. 2016. Geochemical characterization of inorganic residues on plaster floors from a Maya palace complex at Actuncan, Belize. *J Archaeol Sci* 5:453-464.
- Legge SS, Hardin AM. 2016. The pulp cavity and its contents. In: Irish JD, Scott GR, editors. *A companion to dental anthropology*. Chichester, West Sussex: John Wiley & Sons, Inc., p 191-203.
- Lentz DL. 1999. Plant resources of the ancient Maya: the paleoethnobotanical evidence. In: White CD, editor. *Reconstructing ancient Maya diet*. Salt Lake City, UT: The University of Utah Press, p 3-18.
- Lieverse AR. 1999. Diet and aetiology of dental calculus. *Int J Osteoarchaeol* 9:219-232.
- Limbeck A, Galler P, Bonta M, Bauer G, Nischkauer W, Vanhaecke F. 2015. Recent advances in quantitative LA-ICP-MS analysis: challenges and solutions in the life sciences and environmental chemistry. *Ana Bioanal Chem* 407(22):6593-6617.
- Lin J, Liu Y, Yang Y, Hu Z. 2016. Calibration and correction of LA-ICP-MS and LA-MC-ICP-MS analyses for element contents and isotopic ratios. *Solid Earth Sciences* 1:5-27.
- Little N, Kosakowsky L, Speakman R, Glascock M, Lohse J. 2004. Characterization of Maya pottery by INAA and ICP-MS. *J Radioanal Nucl Chem* 262(1):103-110.
- Liu HY, Chao J, Chuang CY, Chiu HL, Yang CW, Sun YC. 2013. Study of P, Ca, Sr, Ba and Pb levels in enamel and dentine of human third molars for environmental and archaeological research. *Adv Anthropol* 13(2):71-77.
- Liversidge HM. 2016. Tooth eruption and timing. In: Irish JD, Scott GR, editors. *A companion to dental anthropology*. Chichester, West Sussex: John Wiley & Sons, Inc., p 159-171.
- Logan WHG, Kronfeld R. 1933. Development of the human jaws and surrounding structures from birth to the age of fifteen years*. *J Am Dent Assoc* 20(3):379-428.
- López-Costas O, Lantes-Suárez Ó, Cortizas AM. 2016. Chemical compositional changes in archaeological human bones due to diagenesis: Type of bone vs soil environment. *J Archaeol Sci* 67:43-51.

- Lugli F, Cipriani A. 2017. Commentary on “Analyses of human dentine and tooth enamel by laser ablation-inductively coupled plasma-mass spectrometry (LA-ICP-MS) to study the diet of medieval Muslim individuals from Tauste (Spain)” by Guede et al. 2017, *Microchemical Journal* 130, 287-294. *Microchem J* 133:67-69.
- Lynch SR. 1997. Interaction of iron with other nutrients. *Nutr Rev* 55(4):102-110.
- Martin DL, Harrod RP, Pérez VR. 2013. *Bioarchaeology: an integrated approach to working with human remains*. New York, NY: Springer.
- Martin RR, Naftel SJ, Nelson AJ, Feilen AB, Narvaez A. 2007. Metal distributions in the cementum rings of human teeth: possible depositional chronologies and diagenesis. *J Archaeol Sci* 34(6):936-945.
- Mertz W. 1981. The essential trace elements. *Science* 213(4514):1332-1338.
- Nganvongpanit K, Buddhachat K, Piboon P, Euppayo T, Mahakkanukrauh P. 2017. Variation in elemental composition of human teeth and its application for feasible species identification. *Forensic Sci Int* 271:33-42.
- Nowak B, Kozłowski H. 1998. Heavy metals in human hair and teeth: the correlation with metal concentration in the environment. *Biol Trace Elem Res* 62:213-228.
- O'Brien KO, Kerstetter JE, Insogna KL. 2014. Phosphorus. In: Ross AC, Caballero B, Cousins RJ, Tucker KL, Ziegler TR. *Modern nutrition in health and disease*, eleventh edition. Philadelphia, PA: Lippincott Williams and Wilkins, p 150-158.
- Pendergast DM. 1981a. Lamanai, Belize: summary of excavation results, 1974–1980. *J Field Archaeol* 8(1):29-53.
- Pendergast DM. 1981b. The 1980 excavations at Lamanai, Belize. *Mexicon* 2(6):96-99.
- Pendergast DM. 1984. Excavations at Lamanai, Belize, 1983. *Mexicon* 6(1):5-10.
- Pendergast DM. 1986. *Historic Lamanai: Royal Ontario Museum 1985 excavations at Lamanai, Belize*. *Mexicon* 8(1):9-13.
- Pozebon D, Scheffler GL, Dressler VL. 2017. Recent applications of laser ablation inductively coupled plasma mass spectrometry (LA-ICP-MS) for biological sample analysis: a follow-up review. *J Anal At Spectrom* 32:890-919.
- Reitznerová E, Amarasiriwardena D, Kopčáková M, Barnes RM. 2000. Determination of some trace elements in human tooth enamel. *Fresenius J Anal Chem* 367(8):748-754.

- Reynard B, Balter V. 2014. Trace elements and their isotopes in bones and teeth: diet, environments, diagenesis, and dating of archeological and paleontological samples. *Palaeogeogr Palaeoclimatol Palaeoecol* 416:4-16.
- Rieuwerts JS, Farago ME, Cikrt M, Bencko V. 2000. Differences in lead bioavailability between a smelting and a mining area. *Water Air Soil Pollut* 122:203-229.
- Rude RK. 2014. Magnesium. In: Ross AC, Caballero B, Cousins RJ, Tucker KL, Ziegler TR. *Modern nutrition in health and disease*, eleventh edition. Philadelphia, PA: Lippincott Williams and Wilkins, p 159-175.
- Sajnóg A, Hanć A, Makuch K, Koczorowski R, Barańkiewicz D. 2016. Study on quantitative analysis of Ti, Al and V in clinical soft tissues after placing the dental implants by laser ablation inductively coupled plasma mass spectrometry. *Spectrochim Acta B* 125:1-10.
- Sandström B. 2001. Micronutrient interactions: effect on absorption and bioavailability. *Br J Nutr* 85(Suppl 2):S181-S185.
- Scott GR. 2008. Dental morphology. In: Katzenberg MA, Saunders SR, editors. *Biological anthropology of the human skeleton*. Hoboken, NJ: John Wiley & Sons, Inc., p 265-298.
- Shepherd TJ, Dirks W, Manmee C, Hodgson S, Banks DA, Averley P, Pless-Mulloli T. 2012. Reconstructing the life-time lead exposure in children using dentine in deciduous teeth. *Sci Total Environ* 425:214-222.
- Simonetti A, Buzon MR, Creaser RA. 2008. In-situ elemental and Sr isotope investigation of human tooth enamel by Laser Ablation-(MC)-ICP-MS: successes and pitfalls. *Archaeometry* 50(2):371-385.
- Smith TM, Tafforeau P. 2008. New visions of dental tissue research: tooth development, chemistry, and structure. *Evol Anthropol* 17(5):213-226.
- Souza JC, Henriques M, Teughels W, Ponthiaux P, Celis JP, Rocha LA. 2015. Wear and corrosion interactions on titanium in oral environment: literature review. *J Bio Tribo Corros* 1(2):1-13.
- Speakman RJ, Neff H. 2005. The application of Laser Ablation-ICP-MS to the study of archaeological materials—an introduction. In: Speakman RJ, Neff H, editors. *Laser ablation-ICP-MS in archaeological research*. Albuquerque: University of New Mexico Press. p 1-16.
- Spencer H, Norris C, Williams D. 1994. Inhibitory effects of zinc on magnesium balance and magnesium absorption in man. *J Am Coll Nutr* 13(5):479-484.

- Stadlbauer C, Reiter C, Patzak B, Stinger G, Prohaska T. 2007. History of individuals of the 18th/19th centuries stored in bones, teeth, and hair analyzed by LA-ICP-MS—a step in attempts to confirm the authenticity of Mozart's skull. *Anal Bioanal Chem* 388(3):593-602.
- Stojanowski CM, Larsen CS, Tung TA, McEwan BG. 2007. Biological structure and health implications from tooth size at Mission San Luis de Apalachee. *Am J Phys Anthropol* 132(2):207-222.
- Tacail T, Kovačiková L, Brůžek J, Balter V. 2017. Spatial distribution of trace element Ca-normalized ratios in primary and permanent human tooth enamel. *Sci Total Environ* 603:308-318.
- Tanaka T, Maki K, Hayashida Y, Kimura M. 2004. Aluminum concentrations in human deciduous enamel and dentin related to dental caries. *J Trace Elem Med Biol* 18(2):149-154.
- Tang N, Le Cabec A, Antoine D. 2016. Dentine and cementum structure and properties. In: Irish JD, Scott GR, editors. *A companion to dental anthropology*. Chichester, West Sussex: John Wiley & Sons, Inc., p 204-222.
- Taube KA. 2005. The symbolism of jade in Classic Maya religion. *Ancient Mesoamerica* 16:23-50.
- Ubelaker 1989. *Human skeletal remains*, second edition. Washington, D.C.: Taraxacum Press.
- Weaver CM, Heaney RP. 2014. Calcium. In: Ross AC, Caballero B, Cousins RJ, Tucker KL, Ziegler TR. *Modern nutrition in health and disease*, eleventh edition. Philadelphia, PA: Lippincott Williams and Wilkins, p 133-149.
- Webb E, Amarasiriwardena D, Tauch S, Green EF, Jones J, Goodman AH. 2005. Inductively coupled plasma-mass (ICP-MS) and atomic emission spectrometry (ICP-AES): versatile analytical techniques to identify the archived elemental information in human teeth. *Microchem J* 81(2):201-208.
- Weiss-Krejci E. 2003. The Maya corpse: body processing from Preclassic to Postclassic times in the Maya highlands and lowlands. In: Colas PR, LeFort G, Persson BL, editors. *Jaws of the underworld: life, death and rebirth among the ancient Maya*. Möckmühl, DE: Verlag Anton Saurwein, p 71-97.
- Wessling-Resnick M. 2014. Iron. In: Ross AC, Caballero B, Cousins RJ, Tucker KL, Ziegler TR. *Modern nutrition in health and disease*, eleventh edition. Philadelphia, PA: Lippincott Williams and Wilkins, p 176-188.

- White CD. 1986. Paleodiet and nutrition of the ancient Maya at Lamanai, Belize: a study of trace elements, stable isotopes, nutritional and dental pathologies. Thesis. Trent University, Peterborough, ON.
- White TD, Folkens PA. 2005. The human bone manual. Burlington, MA: Elsevier Inc.
- Williams JS, White CD. 2006. Dental modification in the Postclassic population from Lamanai, Belize. *Ancient Mesoamerica* 17(1):139-151.
- Willmes M, Kinsley L, Moncel MH, Armstrong RA, Aubert M, Eggins S, Grün, R. 2016. Improvement of laser ablation in situ micro-analysis to identify diagenetic alteration and measure strontium isotope ratios in fossil human teeth. *J Archaeol Sci* 70:102-116.
- Wolinsky I, Alchuler SI. 1983. Calcium. In: Lazzari EP, editor. *CRC handbook of experimental aspects of oral biochemistry*. Boca Raton, FL: CRC Press, p 3-26.
- Wood JW, Milner GR, Harpending HC, Weiss KM. 1992. The osteological paradox: problems of inferring prehistoric health from skeletal samples [and comments and reply]. *Curr Anthropol* 33(4):343-370.
- Wright LE. 1999. The elements of Maya diets: alkaline earth baselines and paleodietary reconstruction in the Pasión region. In: White CD, editor. *Reconstructing ancient Maya diet*. Salt Lake City, UT: The University of Utah Press, p 197-220.
- Zhu K, Prince RL. 2012. Calcium and bone. *Clin Biochem* 45:936-942.
- Zilberman U, Smith P. 2001. Sex-and age-related differences in primary and secondary dentin formation. *Adv Dental Res* 15(1):42-45.